Open- and closed-loop aero-servo-elastic analysis with HAWCStab2

Hansen, Morten Hartvig; Sønderby, Ivan Bergquist

Published in:
Presentations from the Aeroelastic Workshop – latest results from AeroOpt

Publication date:
2011

Document Version
Publisher's PDF, also known as Version of record

Presentations from Aeroelastic Workshop 2 – latest results from AeroOpt

Risø-R-Report

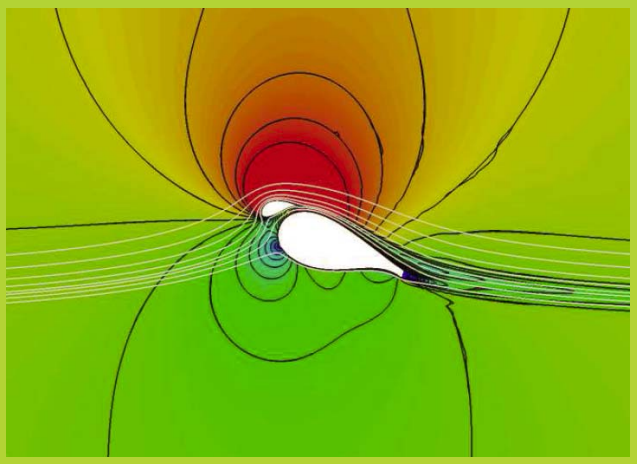

Morten Hartvig Hansen (Ed.)
Risø-R-1796(EN)
October 2011

Risø DTU
National Laboratory for Sustainable Energy

Author: Morten Hartvig Hansen (Ed.)
Title: Presentations from the Aeroelastic Workshop – latest results from AeroOpt
Division: Wind Energy Division

Risø-R-1796(EN)
October 2011

Abstract (max. 2000 char.):

This report contains the slides of the presentations at the Aeroelastic Workshop held at Risø-DTU for the wind energy industry in Denmark on October 27, 2011. The scientific part of the agenda at this workshop was

- Detailed and reduced models of dynamic mooring system (Anders M. Hansen)
- Bend-twist coupling investigation in HAWC2 (Taeseong Kim)
- Q^3UIC – A new aerodynamic airfoil tool including rotational effects (Néstor R. García)
- Influence of up-scaling on loads, control and aerodynamic modeling (Helge Aa. Madsen)
- Aerodynamic damping of lateral tower vibrations (Bjarne S. Kallesøe)
- Open- and closed-loop aeroservoelastic analysis with HAWCStab2 (Morten H. Hansen)
- Design and test of a thick, flatback, high-lift multi-element airfoil (Frederik Zahle)

The presented results are mainly obtained in the EUDP project "Aeroelastic Optimization of MW Wind Turbines (AeroOpt)" funded under contract no. 63011-0190.

ISSN 0106-2840
ISBN 978-87-550-3940-7

Contract no.:
EUDP 63011-0190

Group's own reg. no.:
1110073

Sponsorship:

Cover :

Pages:192
Tables: -
References: -

Information Service Department
Risø National Laboratory for Sustainable Energy
Technical University of Denmark
P.O.Box 49
DK-4000 Roskilde
Denmark
Telephone +45 46774005
bibl@risoe.dtu.dk
Fax +45 46774013
www.risoe.dtu.dk

Contents

Preface

This report contains the slides of the presentations at the Aeroelastic Workshop held at Risø-DTU for the wind energy industry in Denmark on October 27, 2011. The scientific part of the agenda at this workshop was

- Detailed and reduced models of dynamic mooring system (Anders M. Hansen)
- Bend-twist coupling investigation in HAWC2 (Taeseong Kim)
- Q^3UIC – A new aerodynamic airfoil tool including rotational effects (Néstor R. García)
- Influence of up-scaling on loads, control and aerodynamic modeling (Helge Aa. Madsen)
- Aerodynamic damping of lateral tower vibrations (Bjarne S. Kallesøe)
- Open- and closed-loop aeroservoelastic analysis with HAWCStab2 (Morten H. Hansen)
- Design and test of a thick, flatback, high-lift multi-element airfoil (Frederik Zahle)

The presented results are mainly obtained in the EUDP project "Aeroelastic Optimization of MW Wind Turbines (AeroOpt)" funded under contract no. 63011-0190.

1 Dynamic mooring systems

Detailed and reduced models of dynamic mooring system

Anders M. Hansen and Bjarne S. Kallesøe

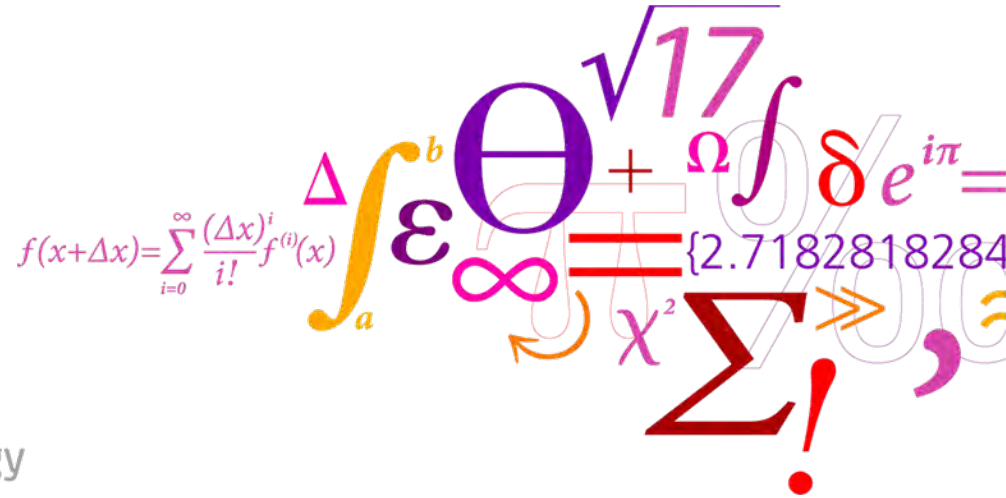

Risø DTU
National Laboratory for Sustainable Energy

Outline

- Introduction
- Full dynamic mooring model
- Load implications of using full model compared to existing QS on floating WT.
- Method to extract reduced ODE model.
- What's in it for You!

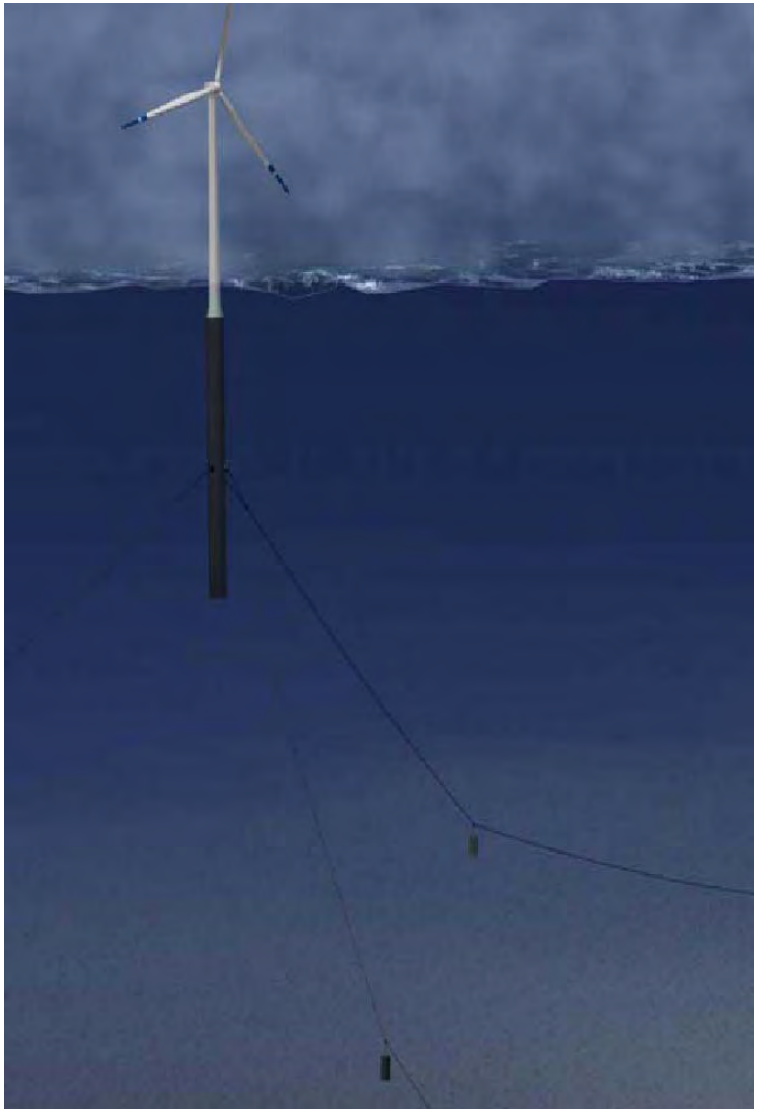

From: http://www.statoil.com/en/NewsAndMedia/News/2008/Downloads/StatoilHydro%20Hywind%20English%20presentation.pdf

Full dynamic model

- Element outline
  - Elastic bar, 3 DOFs/node
  - External forces from
    - Gravity
    - Buoyancy
    - Added mass
    - Damping (quadratic).
  - Non-linear node springs/dampers model bottom contact.
- Discrete mass/buoyancy element
- Constraints to couple it all together
- Implemented in external DLL HAWC2 format
- Wave/current forces missing

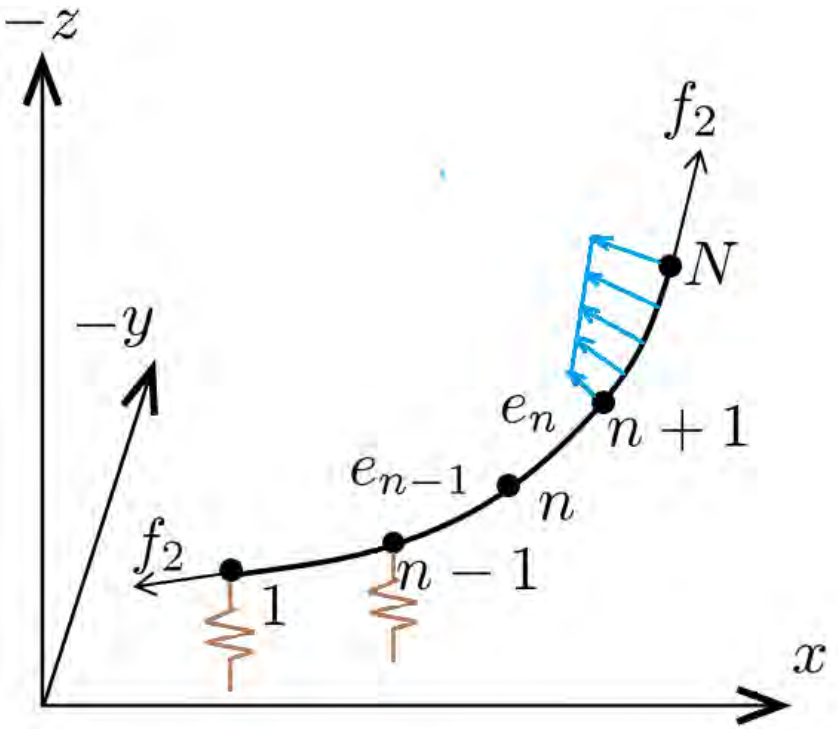

Line Animation

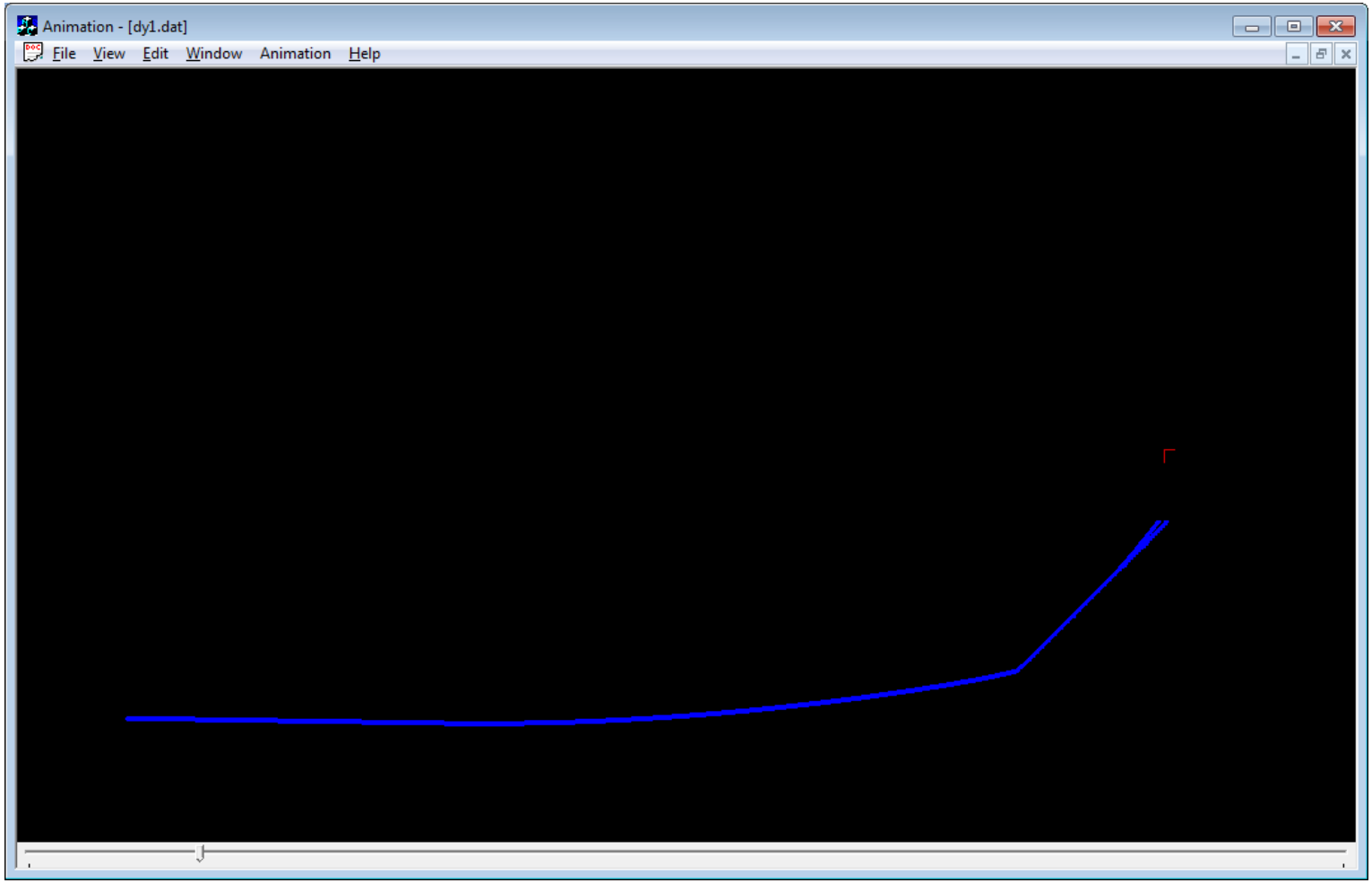

Load implications of using dynamic model compared to existing QS on floating WT.

- Compare extreme and fatigue loads for 3 different model complexities:
  - Q-S: Quasi-static model.
  - M1: Dynamic without delta lines.
  - M2: Dynamic with delta lines.
- Normal operation.
- 5 to 23 m/s in 2 m/s steps.

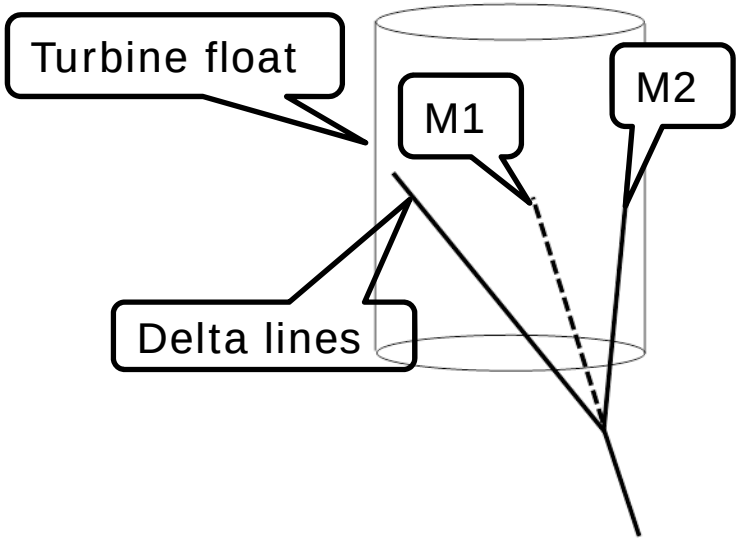

Ws	[m/s]	5	7	9	11	13	15	17	19	21	23
Ti	[-]	0.224	0.186	0.165	0.151	0.142	0.135	0.130	0.125	0.122	0.119
H_s	[m]	1.94	2.26	2.65	3.11	3.61	4.14	4.70	5.25	5.79	6.31
T_p	[s]	3.82	3.98	4.20	4.49	4.85	5.26	5.73	6.24	6.77	7.30
time	[h]	22460	26068	25102	23340	18958	14123	9708	6182	3657	2014

- 1200 seconds simulations, skip first 300 seconds for transients
- 6 different seeds for wind and waves for each wind speed.

Blade Loads

Extreme

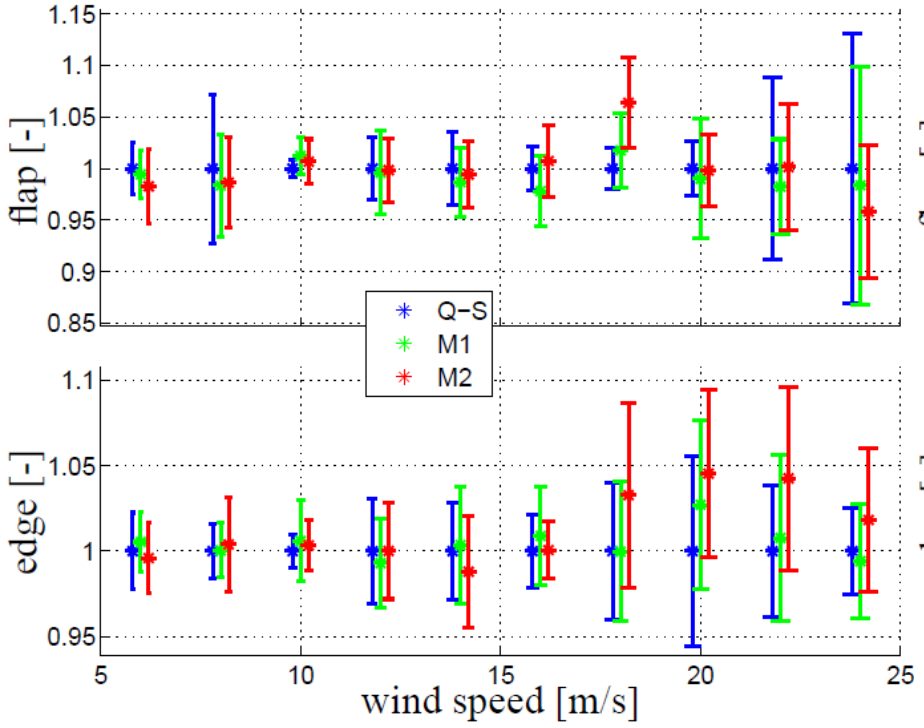

Fatigue

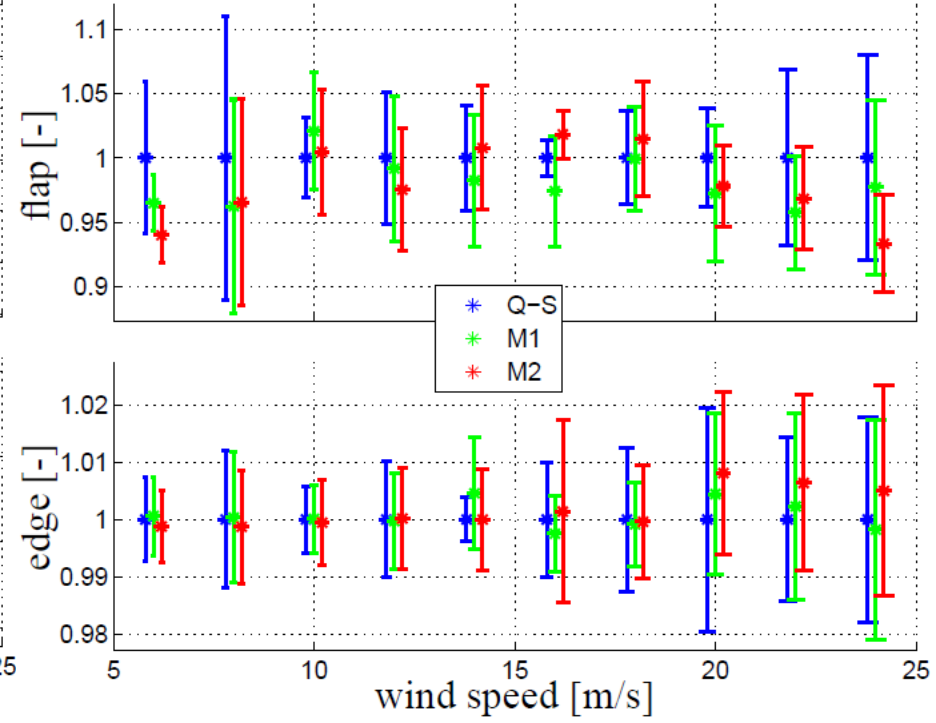

All loads are normalized with respect to the quasi-static result.

Tower Loads

Extreme

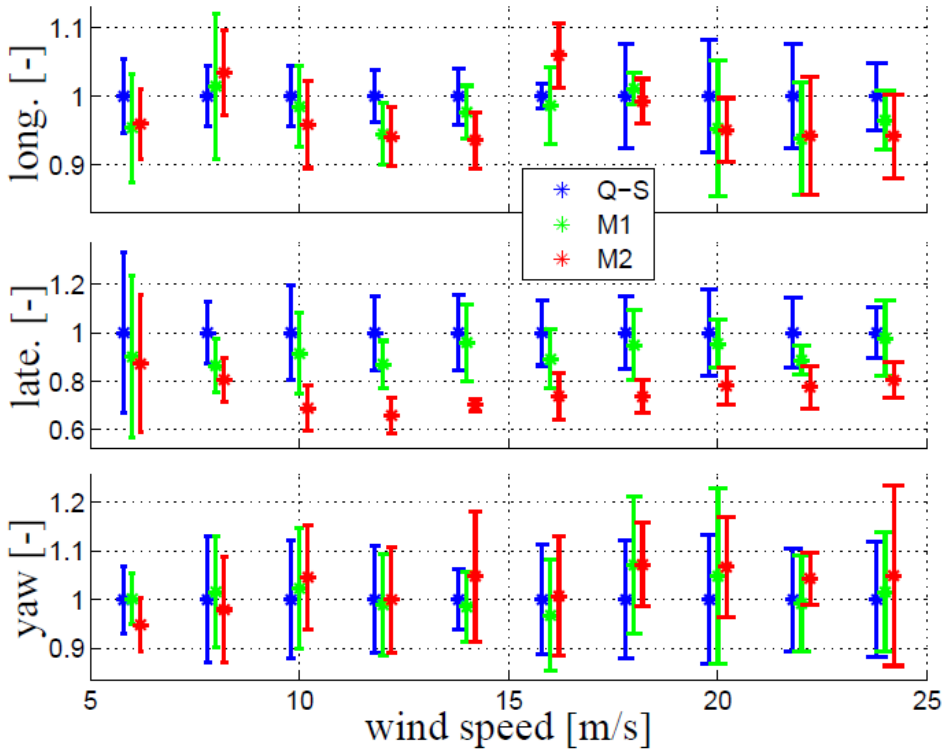

Fatigue

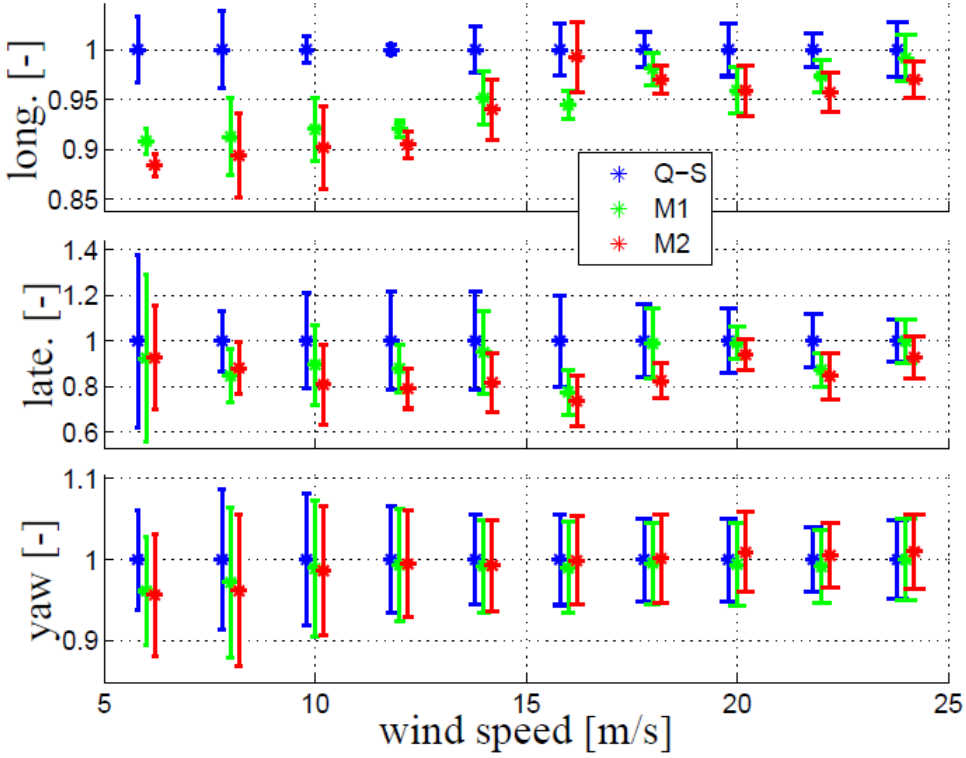

All loads are normalized with respect to the quasi-static result.

Reduction method

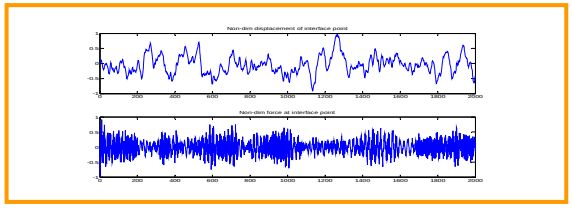

$$\mathbf{D_f}\dot{\alpha_f} - \mathbf{A_f}\alpha_f = \left\{ \begin{array}{c} \mathbf{u} \\ \mathbf{0} \end{array} \right\} \quad \alpha_f = \left\{ \begin{array}{c} \mathbf{y} \\ \vdots \end{array} \right\}$$

- What does it do and how/where can the result be used
  - Reduces (and linearises) the full model (with many DOFs) to a set of ODEs (with few DOFs), capturing only frequency response up to a user specified threshold. The ODEs can be used in, e.g.
    - Modal based methods, e.g. HAWCStab2
    - Distribution to external parties
    - Simulation models, e.g. HAWC2

Input/output relation derived from HAWC2 simulations

Mooring model in HAWC2

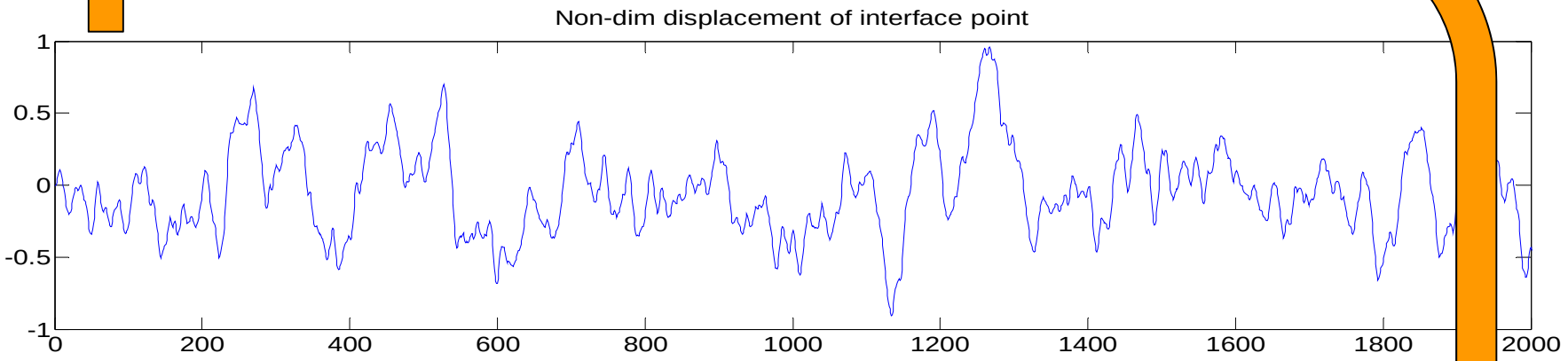

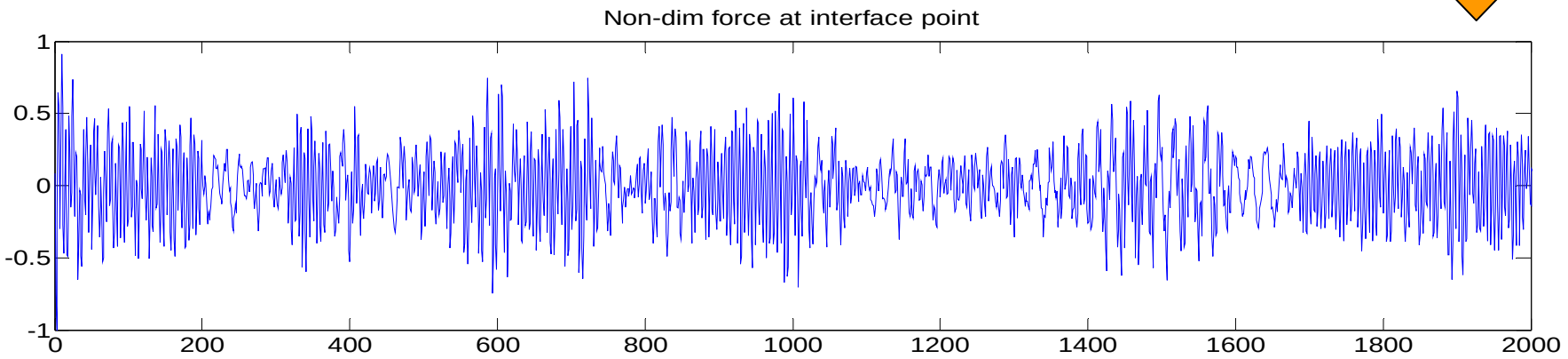

Step 0: Target FRF estimated directly from input/output relation.

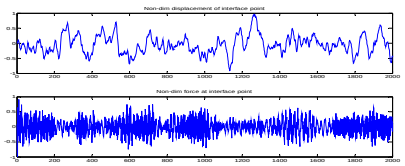

Impulse response function estimated by least square + FFT

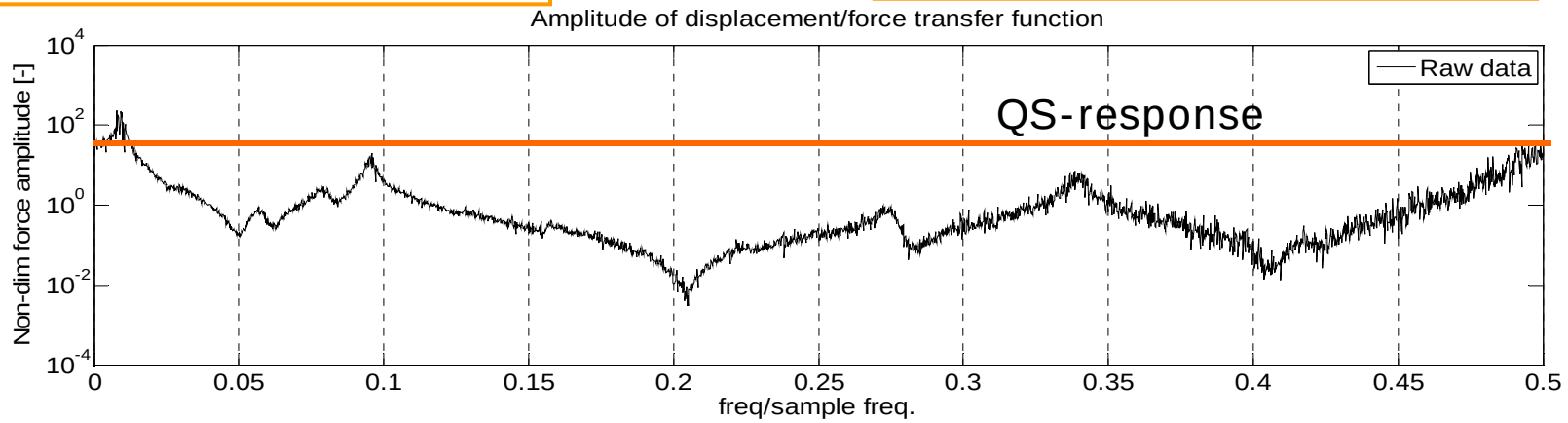

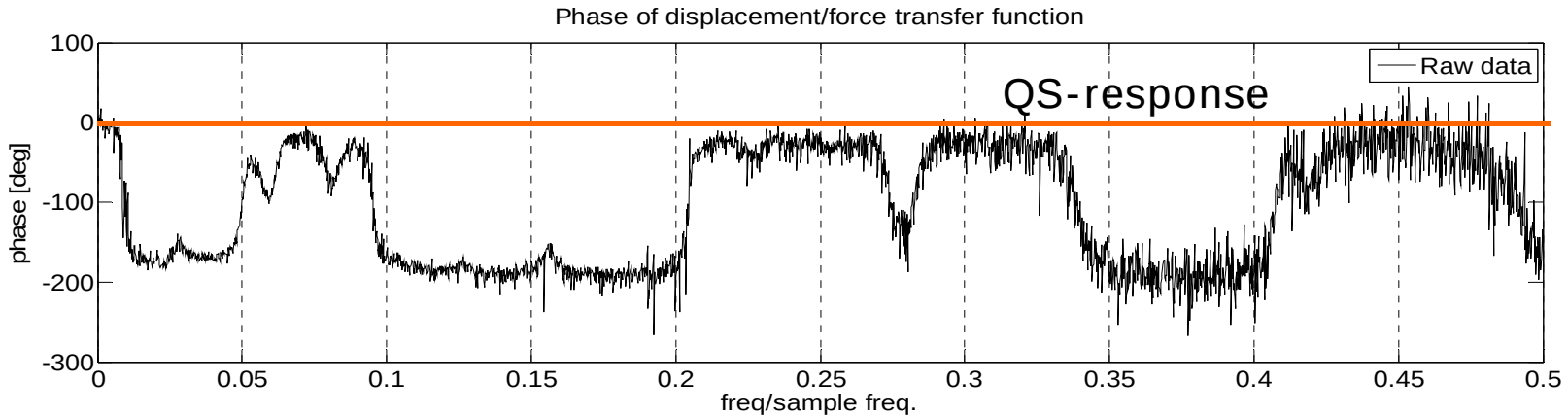

Step 1: ID of discrete state space model based on input/output relation.

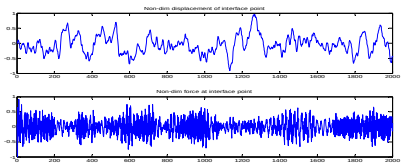

MATLAB, n4sid

$$\mathbf{x}_{n+1} = \mathbf{A}_D\mathbf{x}_n + \mathbf{B}_D\mathbf{u}_n$$
$$\mathbf{y}_n = \mathbf{C}_D\mathbf{x}_n$$

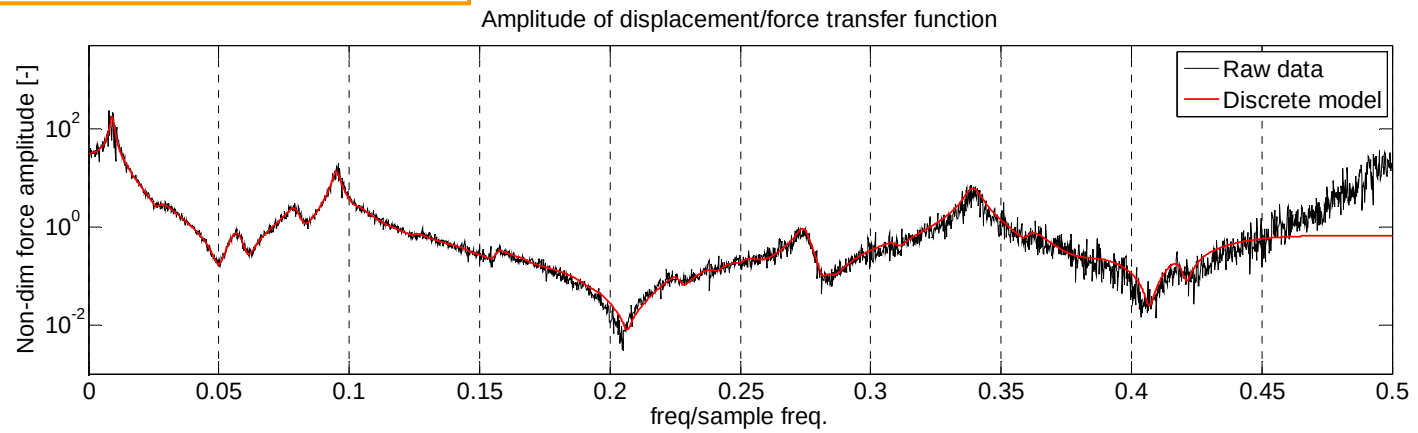

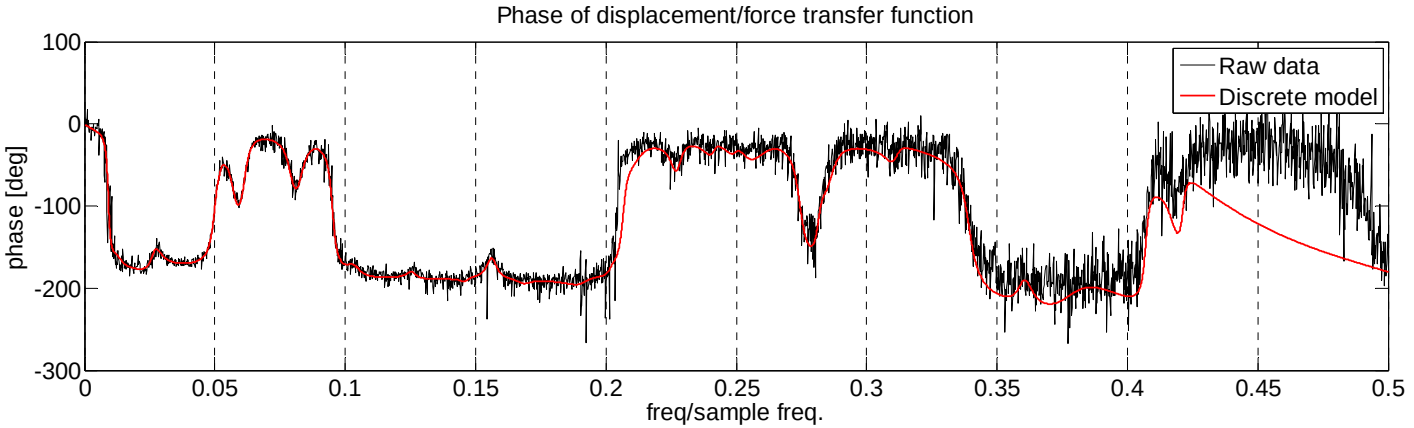

Step 2: Conversion from discrete state space to continous time.

$$\mathbf{x}_{n+1} = \mathbf{A}_D\mathbf{x}_n + \mathbf{B}_D\mathbf{u}_n$$
$$\mathbf{y}_n = \mathbf{C}_D\mathbf{x}_n$$

MATLAB, d2c

$$\dot{\mathbf{x}} = \mathbf{A}_C\mathbf{x} + \mathbf{B}_C\mathbf{u}$$
$$\mathbf{y} = \mathbf{C}_C\mathbf{x}$$

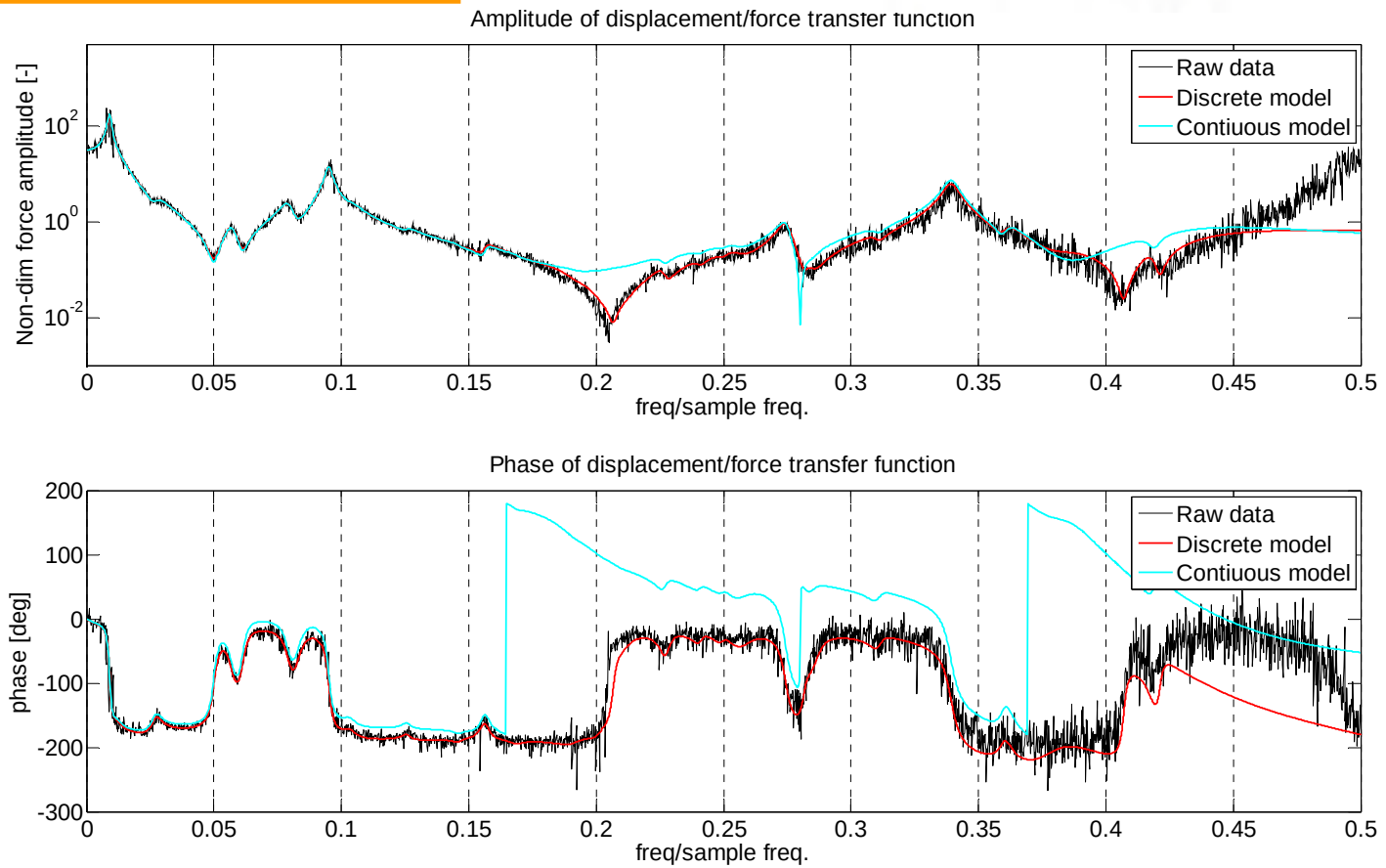

Step 3: Modal reduction of NOF states AND similarity transformation – Final form!

$$\dot{\mathbf{x}} = \mathbf{A}_C\mathbf{x} + \mathbf{B}_C\mathbf{u}$$
$$\mathbf{y} = \mathbf{C}_C\mathbf{x}$$

MAGIC

$$\mathbf{D}_\mathbf{f}\dot{\alpha}_\mathbf{f} - \mathbf{A}_\mathbf{f}\alpha_\mathbf{f} = \left\{ \begin{array}{c} \mathbf{u} \\ \mathbf{0} \end{array} \right\}; \quad \alpha_\mathbf{f} = \left\{ \begin{array}{c} \mathbf{y} \\ \vdots \end{array} \right\}$$

Amplitude of displacement/force transfer function

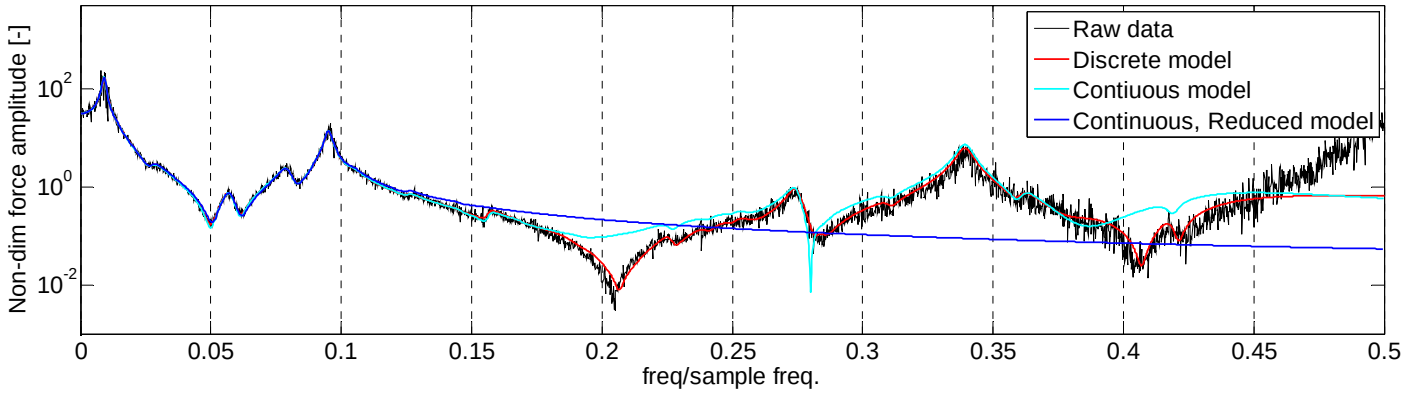

Phase of displacement/force transfer function

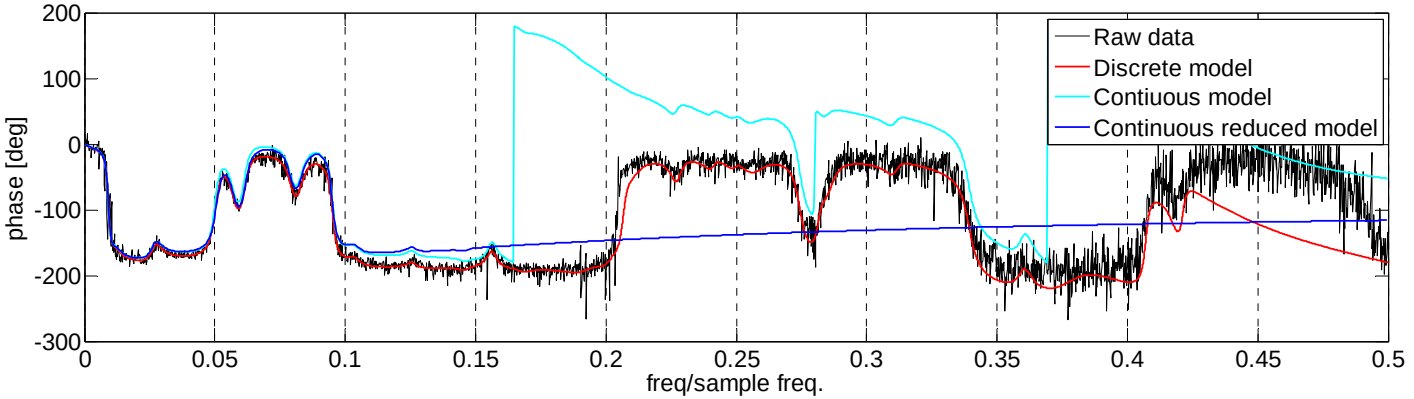

So, What's in it for You !

- The external mooring system DLL will be included in the HAWC2 distribution asap. Source code distribution is still an open issue.
- The reduction method (MATLAB m-file) can be forwarded on request – send an email to anmh@risoe.dtu.dk
- The reduction method is general and can be used for other systems than mooring systems – component models based on experiments, perhaps!?
- We can offer to make reduced models on commercial basis.

2 Bend-twist coupling investigation

A New Beam Element in HAWC2 for Investigating Blade Bending-Twist Coupling Effects

Taeseong Kim

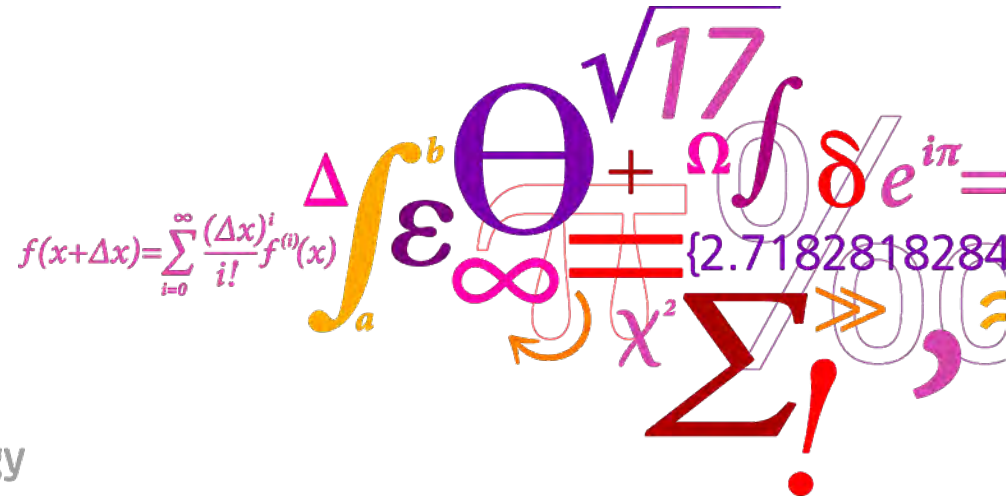

Risø DTU
National Laboratory for Sustainable Energy

Introduction

- All of composite blades have anisotropic material properties due to different layup angles.
  - It introduces addtional bending-bending and bending-twist couplings.

±45deg layup angle

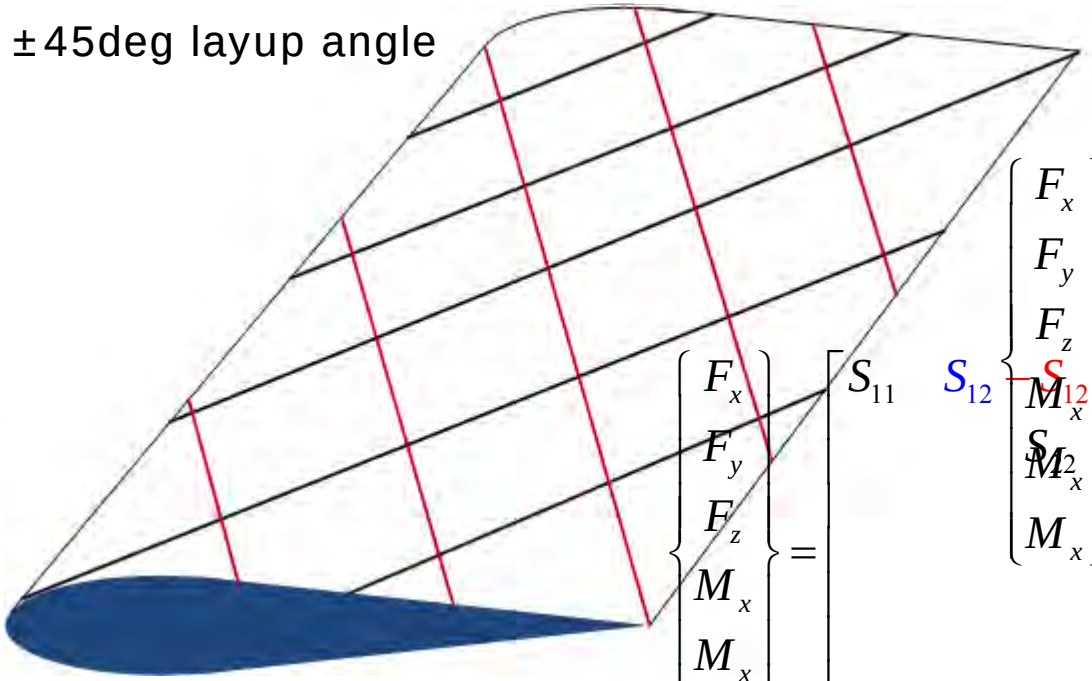

$$\begin{Bmatrix} F_x \\ F_y \\ F_z \\ M_x \\ M_x \\ M_x \end{Bmatrix} = \begin{bmatrix} S_{11} & S_{12} & S_{12} & S_{12} & S_{12} & S_{12} \\ & S_{22} & S_{23} & S_{23} & S_{23} & S_{23} \\ & & S_{33} & S_{23} & S_{23} & S_{23} \\ & & & S_{44} & S_{45} & S_{45} \\ & & & & S_{55} & S_{56} \\ & & & & & S_{66} \end{bmatrix} \begin{Bmatrix} \varepsilon_x \\ \varepsilon_y \\ \varepsilon_z \\ \kappa_x \\ \kappa_y \\ \kappa_z \end{Bmatrix}$$

$$\begin{Bmatrix} F_x \\ F_y \\ F_z \\ M_x \\ M_x \\ M_x \end{Bmatrix} = \begin{bmatrix} S_{11} & S_{12} & S_{12} & S_{12} & S_{12} & S_{12} \\ & S_{22} & S_{23} & S_{23} & S_{23} & S_{23} \\ & & S_{33} & S_{23} & S_{23} & S_{23} \\ & & & S_{44} & S_{45} & S_{45} \\ & & & & S_{55} & S_{56} \\ & & & & & S_{66} \end{bmatrix} \begin{Bmatrix} \varepsilon_x \\ \varepsilon_y \\ \varepsilon_z \\ \kappa_x \\ \kappa_y \\ \kappa_z \end{Bmatrix}$$

$$S_{12} - S_{12} = 0 \qquad S_{45} - S_{45} = 0$$

Couplings

- A classical Timoshenko beam model (HAWC2)
  - Geometric couplings
    - The offset between elastic axis and shear center
    - Sweep blade

❑ Structural coupling

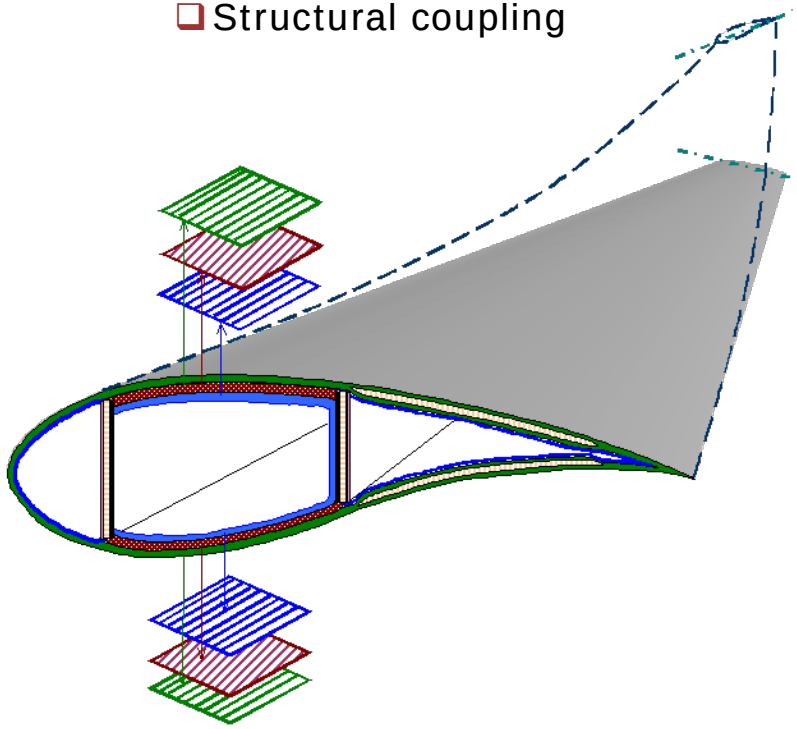

❑ Geometric coupling

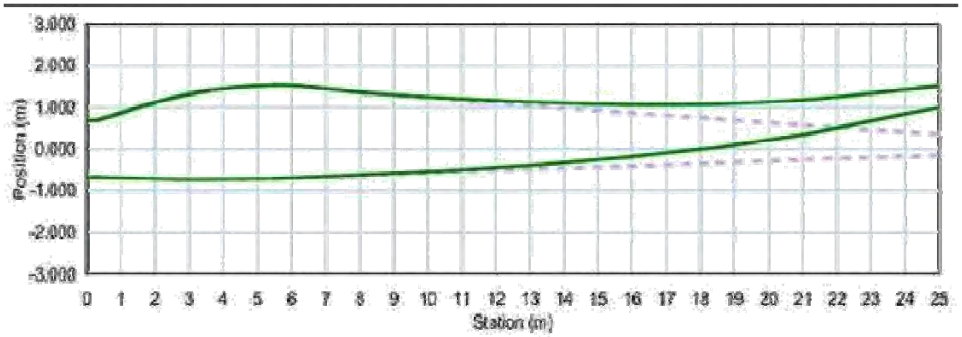

Objective & Method

- Objective
  - Developing a new beam element which can consider anisotropic characteristics
  - Implementing a new beam model into HAWC2
  - Investigating an effect of a structural coupling

- Method
  - General FEM approach
  - 2 nodes element, higher order of the polynomial shape function
  - Importing a cross-sectional stiffness and a mass information

New structural format

- New structural format (-st file format) is introduced for HAWC2 analysis
  - Old format

```
1 main data sets available
-------------------------------------------------------------------------------------------------------------------------------------------------------------------
#1  Main data set number 1
-------------------------------------------------------------------------------------------------------------------------------------------------------------------
r       m         x_cg     y_cg     ri_x     ri_y     x_sh     y_sh     E        G         I_x      I_y      I_p      k_x  k_y  A      pitch    x_e    y_e
[m]     [kg/m]    [m]      [m]      [m]      [m]      [m]      [m]      [N/m^2]  [N/m^2]   [N/m^4]  [N/m^4]  [N/m^4]  [-]  [-]  [m^2]  [deg]    [m]    [m]
```

  - New format

```
1 main data sets available
-------------------------------------------------------------------------------------------------------------------------------------------------------------------
#1  Main data set number 1
-------------------------------------------------------------------------------------------------------------------------------------------------------------------
r      m         x_cg     y_cg     ri_x     ri_y     E11   E12   E13   E14    E15    E16    E22   E23   E24    E25    E26    E33   E34    E35    E36    E44      E45      E46      E55      E56      E66
[m]    [kg/m]    [m]      [m]      [m]      [m]      [N]   [N]   [N]   [N-m]  [N-m]  [N-m]  [N]   [N]   [N-m]  [N-m]  [N-m]  [N]   [N-m]  [N-m]  [N-m]  [N-m^2]  [N-m^2]  [N-m^2]  [N-m^2]  [N-m^2]  [N-m^2]
```

  - Where Exx represents the sectional stiffness matrix element

Results (Case 1)

- Case 1: Blasques et al (2011)
  - $[0°]_T$ Solid square cross section with an arbitrary material

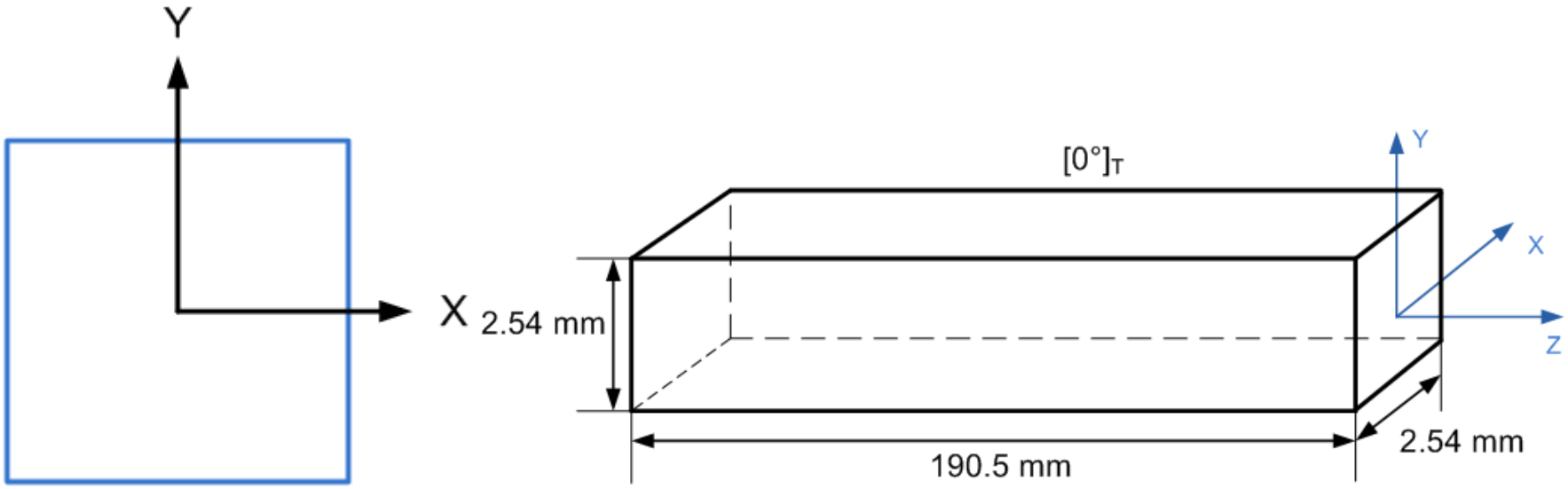

  - Purpose: validating whether the new beam model is correctly implemented into HAWC2 or not

Comparisons of the natural frequencies (Case 1)

Mode	New beam element [Hz]	HAWC2 [Hz]
1	2.87262×10^{-3}	2.87262×10^{-3}
2	2.87262×10^{-3}	2.87262×10^{-3}
3	1.80466×10^{-2}	1.80466×10^{-2}
4	1.80466×10^{-2}	1.80466×10^{-2}
5	5.09409×10^{-2}	5.09409×10^{-2}
6	5.09409×10^{-2}	5.09409×10^{-2}

- Results are exactly identical.

Results (Case 2)

- 5MW RWT
- Natural frequency comparisons
  - The new data format is obtained from the original structural data.
    - E11 = kxGA, E22 = kyGA, E33 = EA, ...

Whole turbine natural frequency (structure)			Blade natural frequency (body)		
	Old version	New version		Old version	New version
1	2.99499E-01	2.99489E-01	1	6.42915E-01	6.42126E-01
2	3.01766E-01	3.01745E-01	2	9.70733E-01	9.70323E-01
3	5.88521E-01	5.88366E-01	3	1.74780E+00	1.74320E+00
4	6.10445E-01	6.09750E-01	4	2.81604E+00	2.81413E+00
5	6.36840E-01	6.36079E-01	5	3.52602E+00	3.52027E+00
6	6.67130E-01	6.66403E-01	6	4.74572E+00	4.74129E+00
7	9.66966E-01	9.66564E-01	7	5.41973E+00	5.41629E+00
8	9.78581E-01	9.78093E-01	8	6.62254E+00	6.61381E+00
9	1.58169E+00	1.57891E+00	9	7.41935E+00	7.42257E+00
10	1.69090E+00	1.68696E+00	10	8.24123E+00	8.21291E+00

- Small discrepancies occur due to data converting process.

Results (Case 3)

- Objective
  - To check a load reduction potential with whole turbine configuration by considering the structural couplings
  - 5MW RWT

- Assumptions
  - Coupling effects are arbitrarily assigned (No real layup angles)
  - Other stiffness values, diagonal terms, are kept its own values while coupling effects are assigned.
  - Same amount of couplings along the blade span
  - Only flapwise bending – twist coupling is newly added.
  - Nothing changes !!

- Considered wind speed: 7 m/s

- Wind shear, Turbulence (TI: 0.217), Tower shadow

Results (Case 3)

- Producing bending-twist coupling
  - Coupling value

$$E_{BT} = \alpha\sqrt{EI_f \cdot GJ} \qquad -1 < \alpha < 1$$

Ref.: Lobitz and Veers, "Aeroelastic Behavior of Twist-Coupled HAWC Blades," AIAA-98-0029

  - Example

$$\begin{bmatrix} E_{11} & 0 & 0 & 0 & 0 & 0 \\ 0 & E_{22} & 0 & 0 & 0 & 0 \\ 0 & 0 & E_{33} & 0 & 0 & 0 \\ 0 & 0 & 0 & EI_f & 0 & \alpha\sqrt{EI_f GJ} \\ 0 & 0 & 0 & 0 & E_{55} & 0 \\ 0 & 0 & 0 & \alpha\sqrt{EI_f GJ} & 0 & GJ \end{bmatrix}$$

Results (Case 3)

- Two examples (1st example case)
  - ***α*=-0.05**: **1 m** flapwise bending (toward tower) results in approximately **0.3deg** twist (toward feather) at the blade tip
  - Static analysis with only a blade (cantilevered beam)

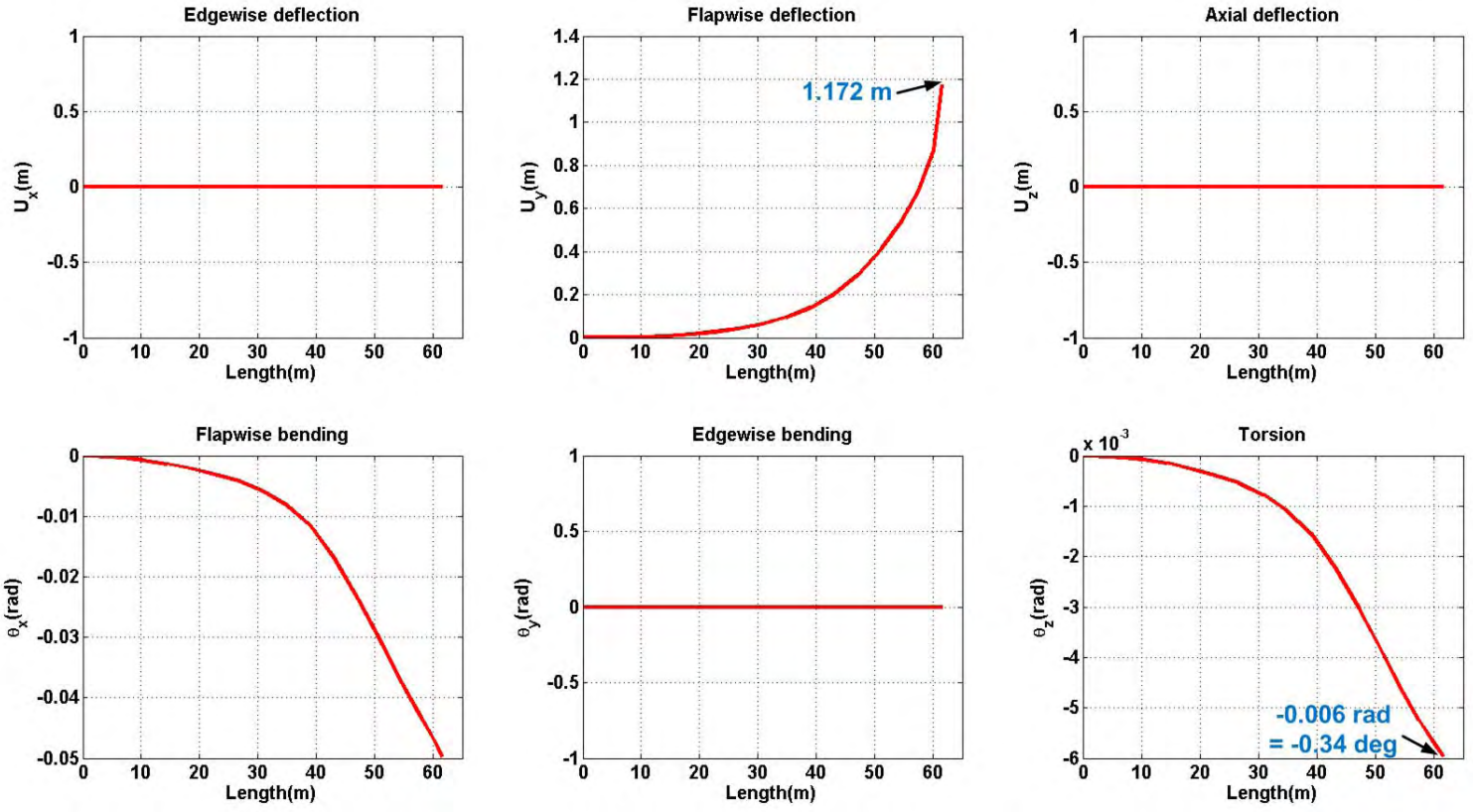

Results (Case 3)

- Two examples (2nd example case)
  - ***α*=-0.17**: **1 m** flapwise bending results in approximately **1deg** twist at the blade tip

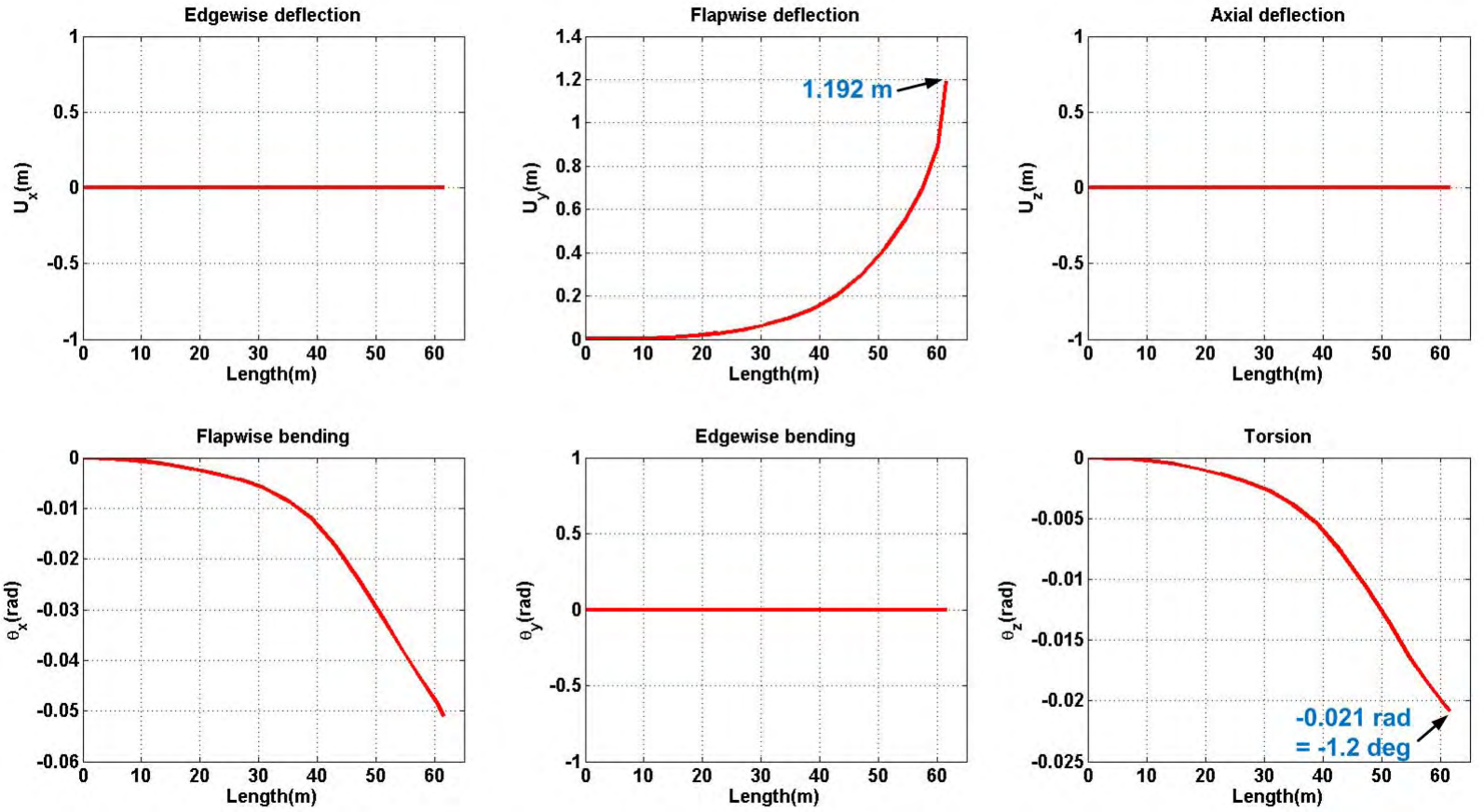

Results (Case 3)

- Blade equivalent fatigue loads comparison (flapwise and edgewise fatigue loads)
  - **Blue**: **-0.3deg** coupling case
  - **Red**: **-1 deg** coupling case

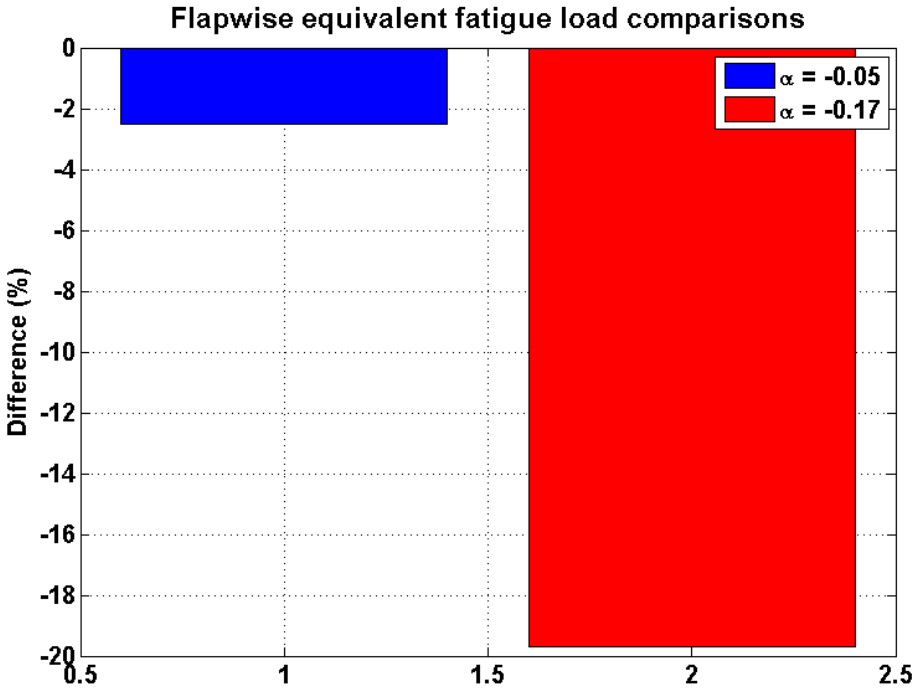

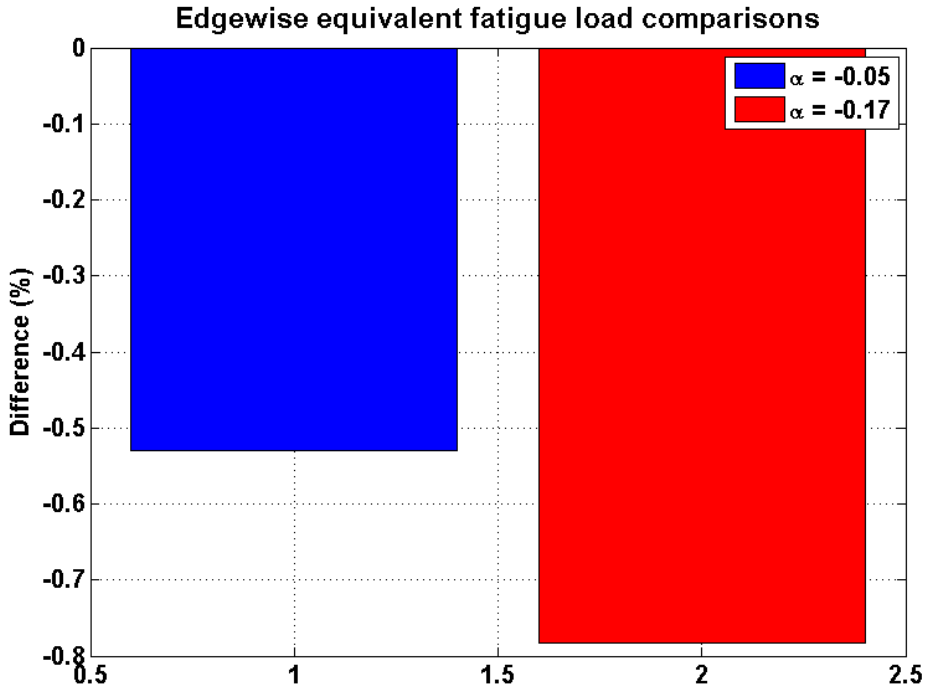

Results (Case 3)

- Blade torsional equivalent fatigue load measured from non-pitching axis and blade maximum tip deflection comparisons
  - **Blue**: **-0.3deg** coupling case
  - **Red**: **-1 deg** coupling case

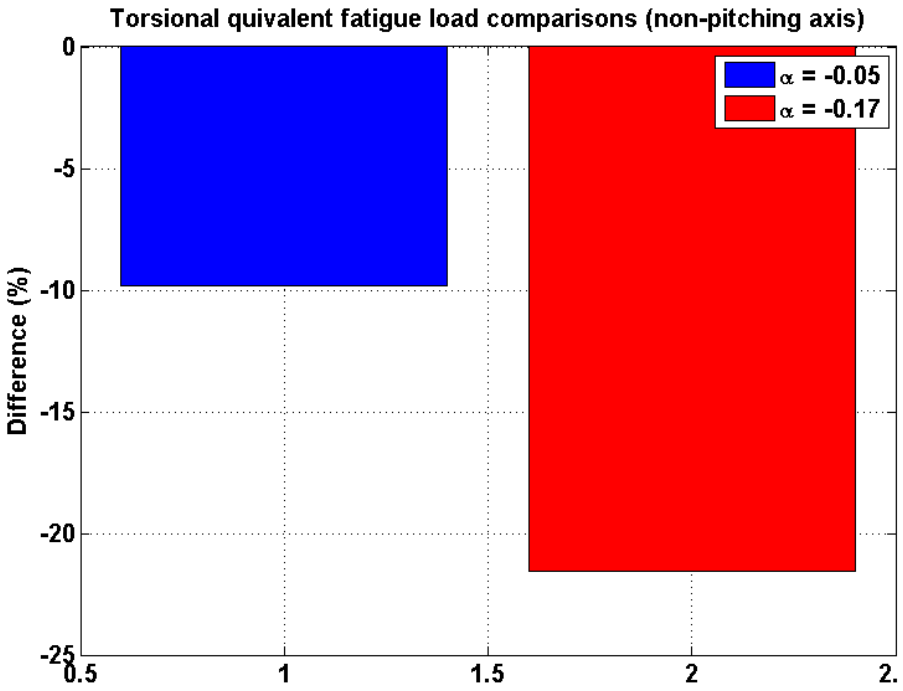

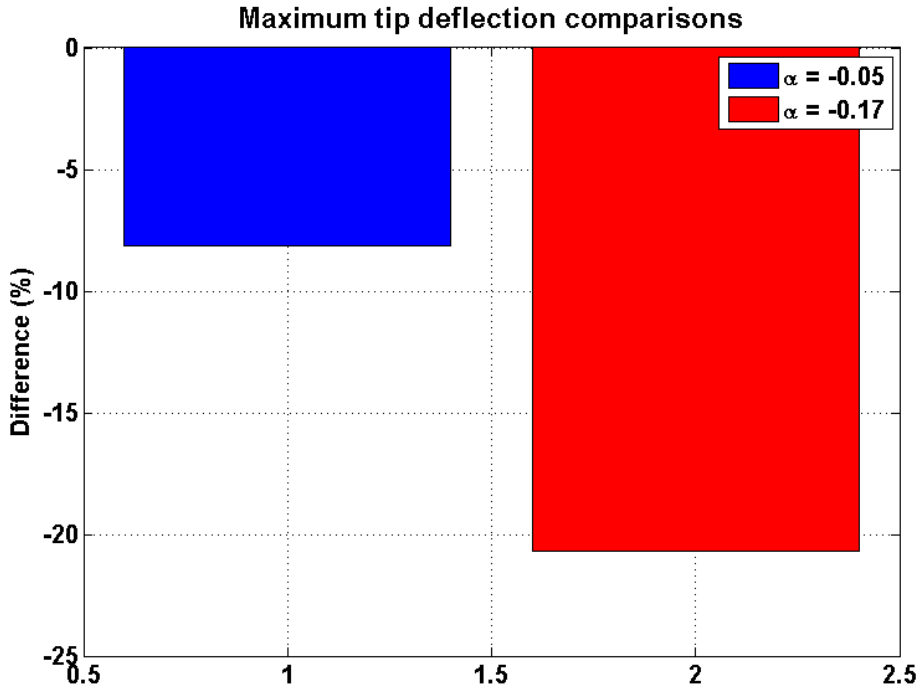

Results (Case 3)

- Mechanical power (mean value) comparisons
  - **Blue**: **-0.3deg** coupling case
  - **Red**: **-1 deg** coupling case

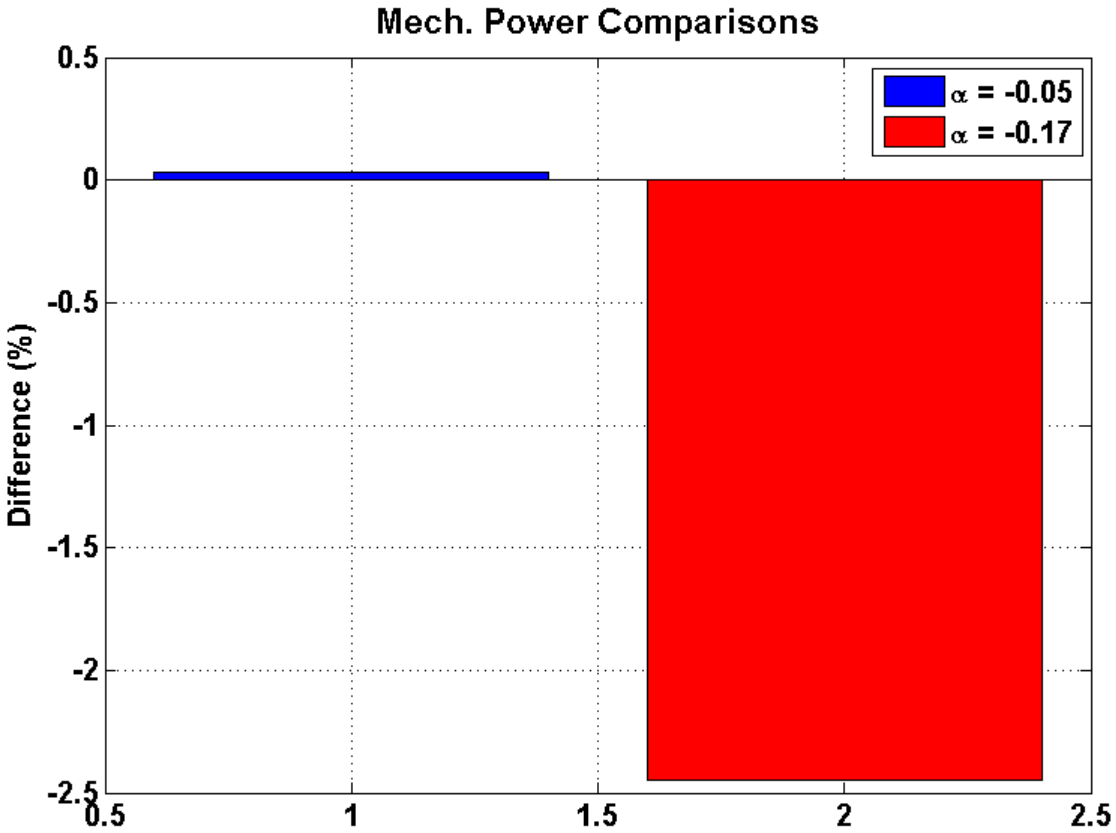

Results (Case 4)

- Tuned pre-twist
  - Objective: keep the same amount of power production
    check load reduction potential
  - Linear scaling manner

$$\theta_{new} = \theta_{PT} + \left(\theta_{PT} \times \beta_{SF}\right)$$

where *new*: new pre-twist, *PT*: given pre-twist, and *SF*: scaling factor (β_{SF}=0.35)

Results (Case 4)

- Tuned pre-twist

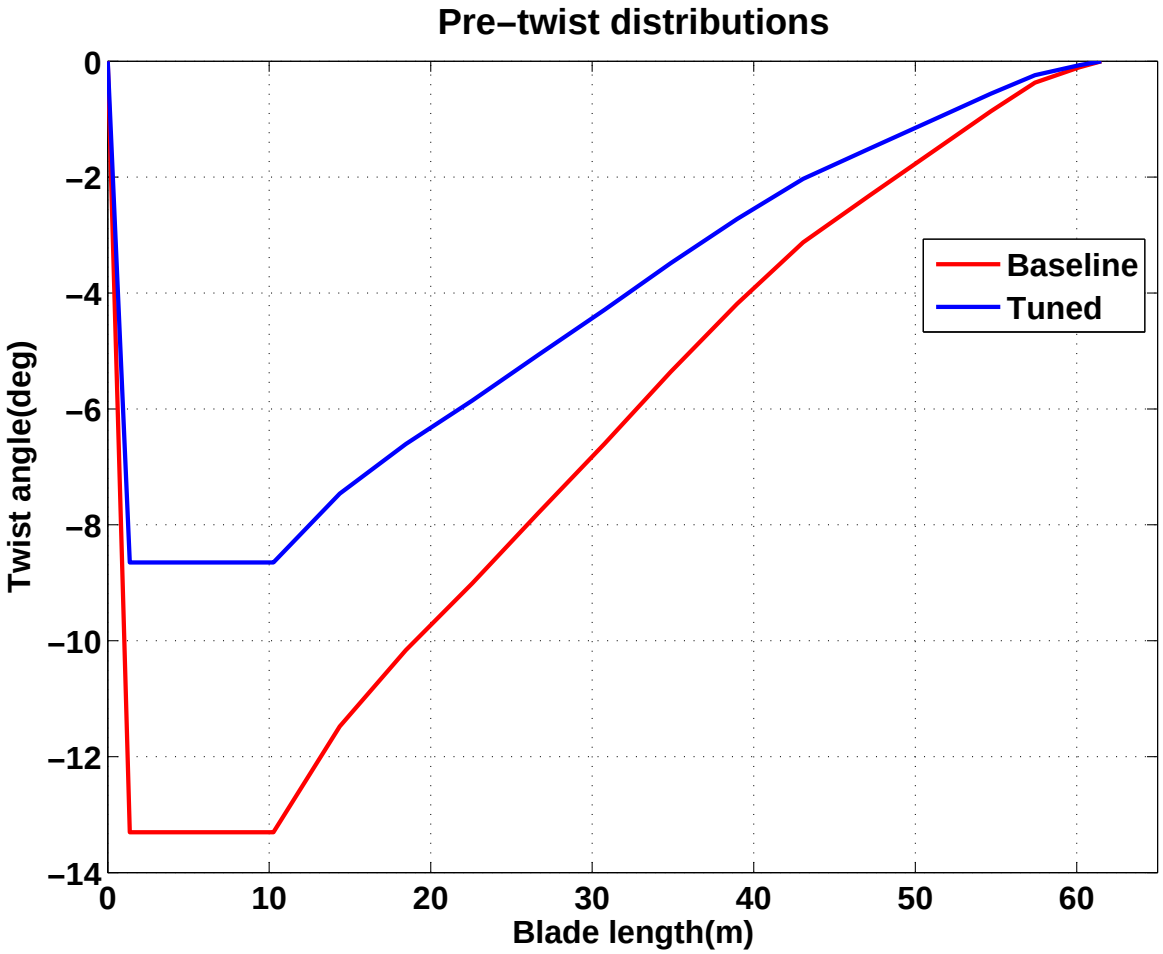

Results (Case 4)

- Mechanical power (mean value) comparisons
  - **Blue**: **-0.3deg** coupling case
  - **Red**: **-1 deg** coupling case ***before tuned***
  - **Green**: **-1 deg** coupling case ***after tuned***

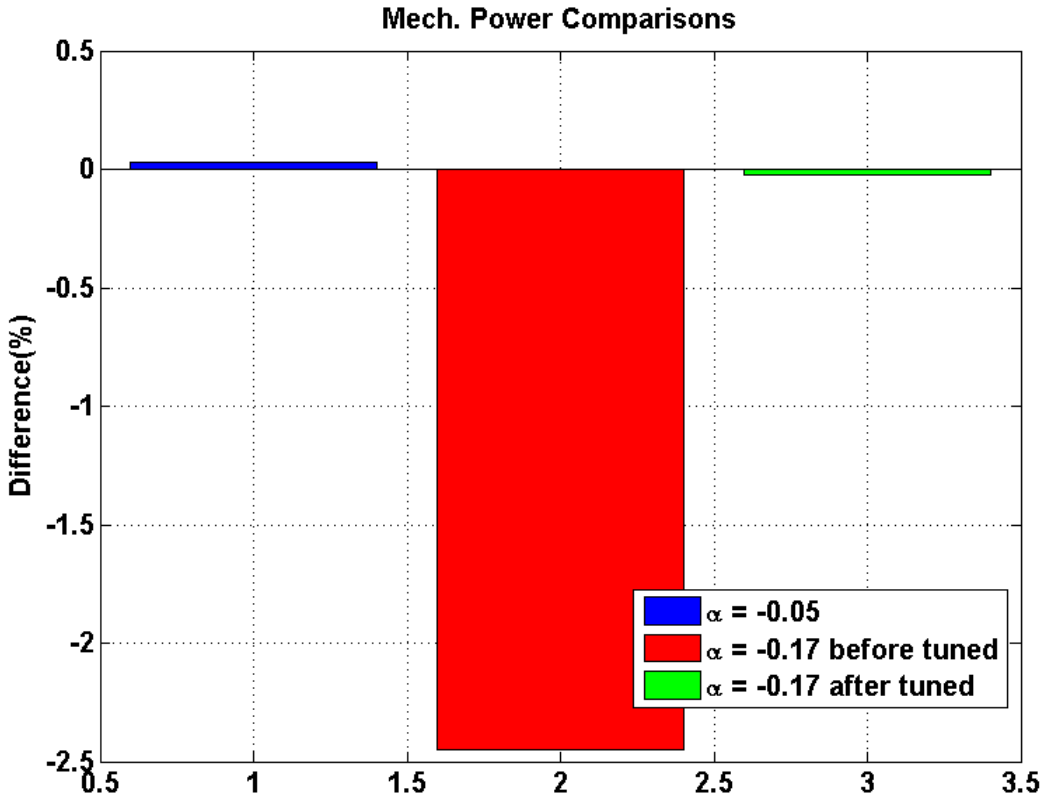

Results (Case 4)

- Blade equivalent fatigue loads comparison after pre-twist tuned (flapwise and edgewise fatigue loads)
  - **Blue**: **-0.3deg** coupling case
  - **Red**: **-1 deg** coupling case ***before tuned***
  - **Green**: **-1 deg** coupling case ***after tuned***

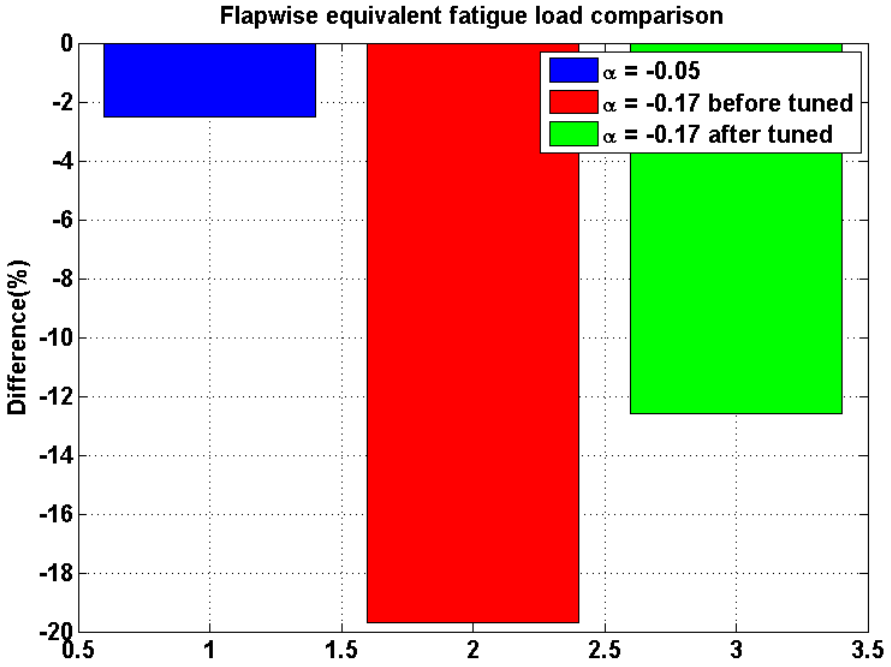

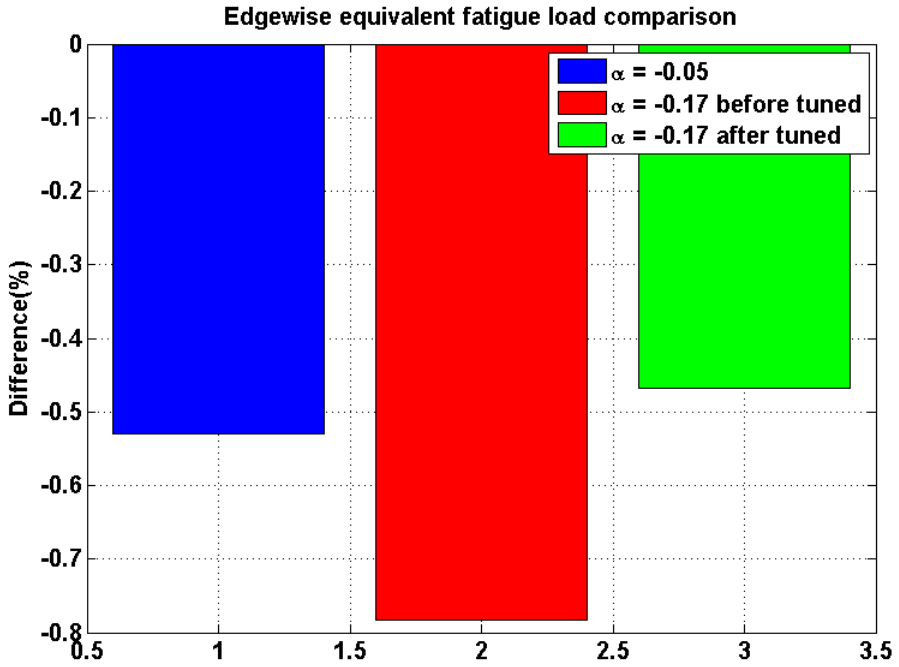

Results (Case 4)

- Blade torsional equivalent fatigue load measured from non-pitching axis and blade maximum tip deflection comparisons
  - **Blue**: **-0.3deg** coupling case
  - **Red**: **-1 deg** coupling case ***before tuned***
  - **Green**: **-1 deg** coupling case ***after tuned***

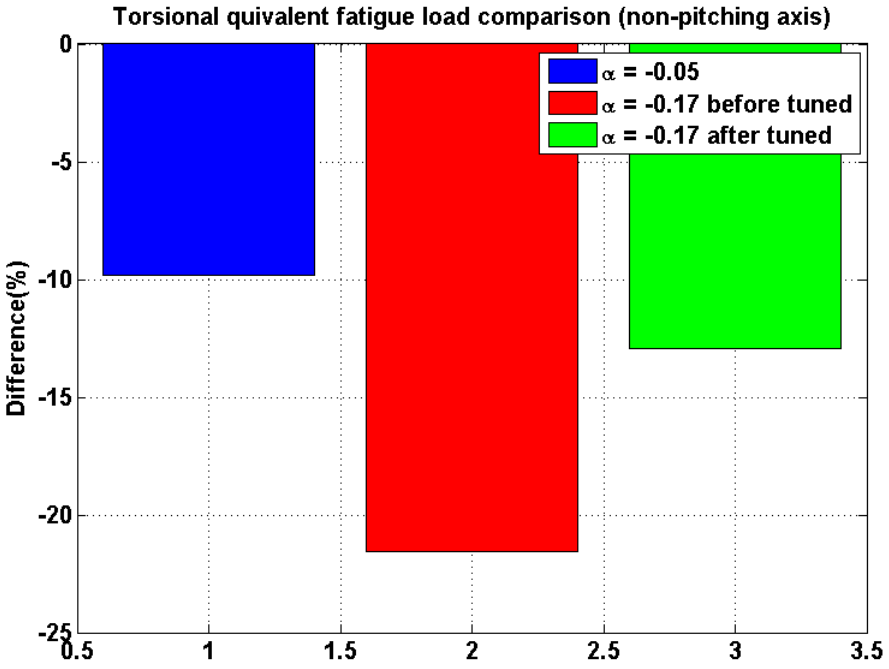

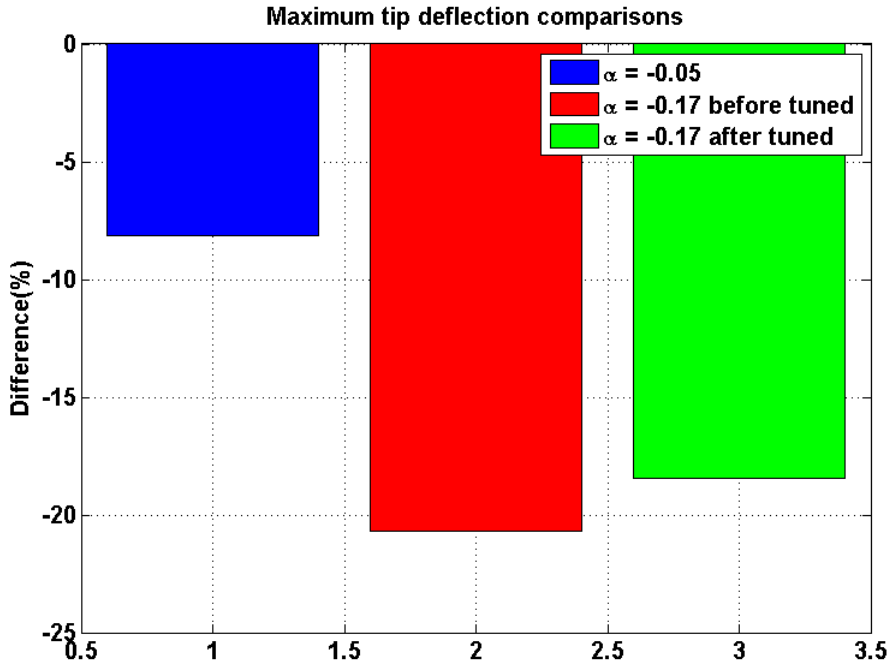

Conclusions

- A new beam element is successfully developed and implemented into HAWC2.
  - The beam element is validated before and after implementation.
    - Simple square beam model and 5MW RWT are used for the validations.
    - A new structural format is introduced for the new beam model.

- Bend-Twist coupling parametric studies are performed.
  - 5MW RWT
  - A good potential for load reduction is observed.
  - Higher couplings produce the reduction of the bending stiffness in the real world.
  - Blade re-design process is necessary in order for using bending-twist coupling blade such as pre-twist along the blade span.
  - The coupling effects may result in improving wind turbine performances
    - Increasing the life time of turbine.
    - Reduce materials for blade.
    - Etc.

Thank you for your attention

3 Q^3UIC – A new aerodynamic airfoil tool

Q3UIC – A new aerodynamic airfoil tool including rotational effects

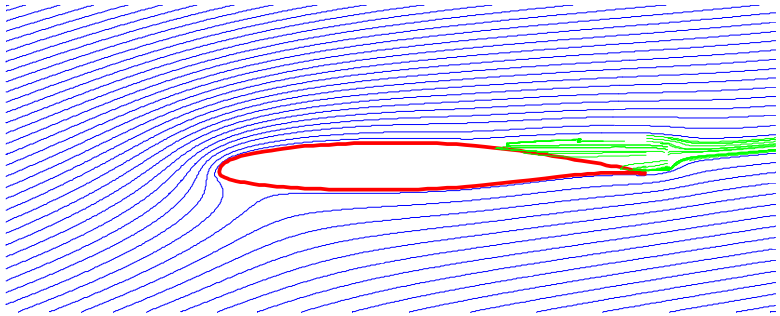

Néstor Ramos García
Jens Nørkær Sørensen
Wen Zhong Shen

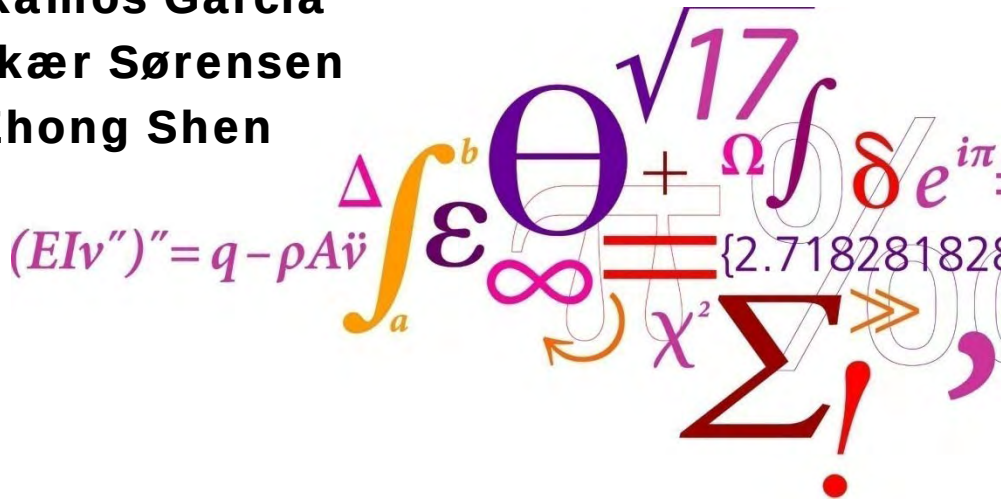

DTU Mekanik
Institut for Mekanisk Teknologi

PRESENTATION LAYOUT

- INTRODUCTION
- VISCOUS-INVISCID INTERACTION
- COMPUTATIONS AND BENCHMARKING
  - STEADY 2D.
  - UNSTEADY 2D.
  - STEADY 2D WITH VG.
  - STEADY QUASI3D
- POTENTIAL DOUBLE WAKE SOLVER
- CONCLUSIONS

INTRODUCTION

- Blade-Element Momentum theory is often used for the design of wind turbines. Required Input: Lift and Drag force coefficients.
- Computer resources are getting more powerful with the years, but it is still behind our limits to realize an active design of wind turbine blades using Navier-Stokes solvers. High cost in computational time.
- Blade Inboard regions are producing more power than predicted.
- Rotor is producing more power at high angles of attack due to secondary outward flow, caused by centrifugal pumping.

INTRODUCTION

- A code has been developed during the last three years that can fit our needs:
  - It has to compute accurately steady/unsteady airfoil forces.
  - It has to be fast in order to use it as a design method.
  - It has to take into account rotational effects. Centrifugal and Coriolis forces.

- The code uses the already known concept of UNSTEADY VISCOUS-INVISCID STRONG INTERACTION via transpiration velocity.

  - Inviscid flow → Unsteady potential flow, panel method.
  - Viscous flow → Quasi 3-D integral BL equations + Closures.

VISCOUS-INVISCID STRONG INTERACTION

- ASSUMPTION OF AN EQUIVALENT FLOW, where the effects of real flow can be added. Transpiration velocity will take into account the effects of the real flow in the potential flow solver.

$$v_T = \frac{d}{dx}\int_0^\infty (u_e - u)dz = \frac{d}{dx}(u_e \delta_1)$$

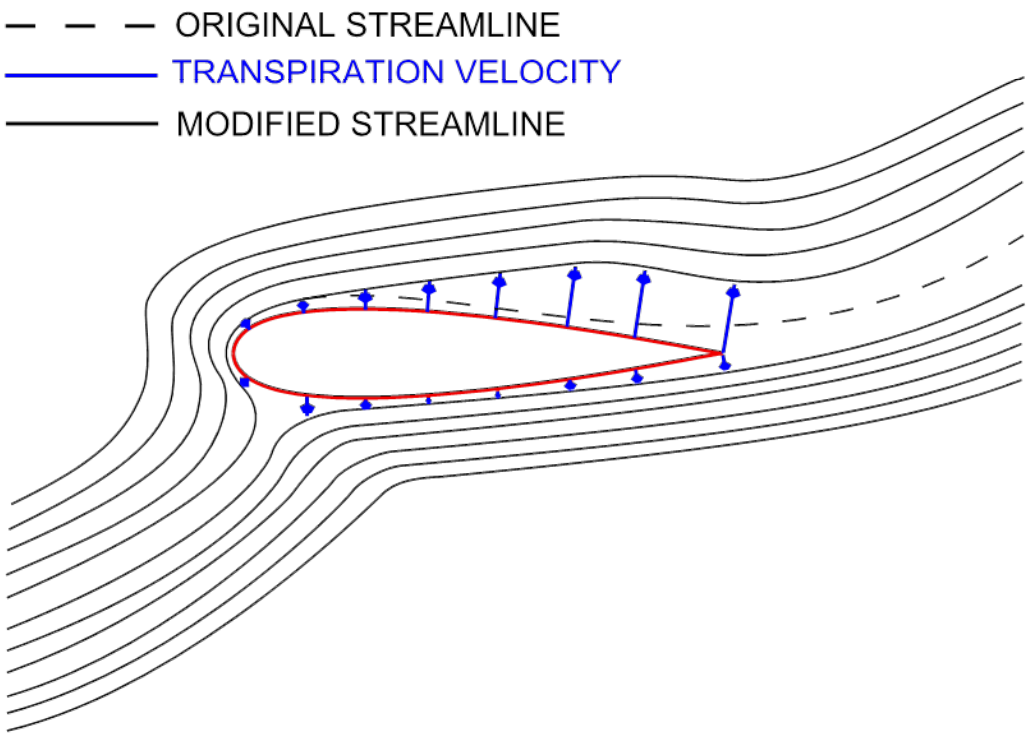

STEADY VISCOUS INVISCID SOLVER

STEADY VI COMPUTATIONS

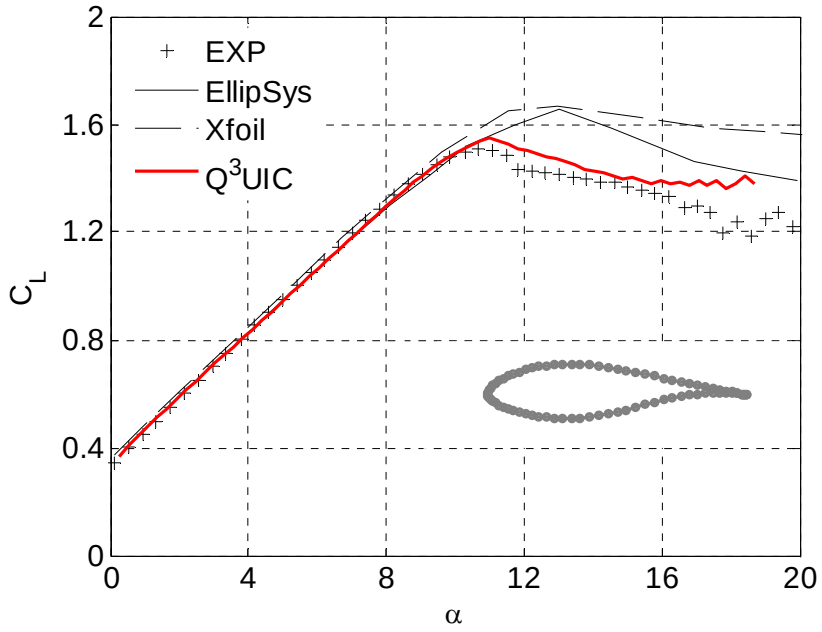

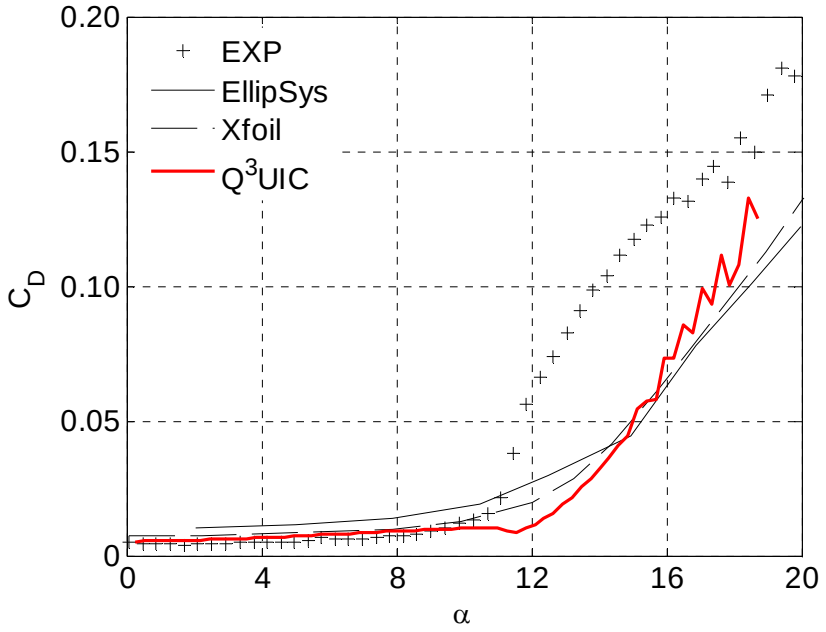

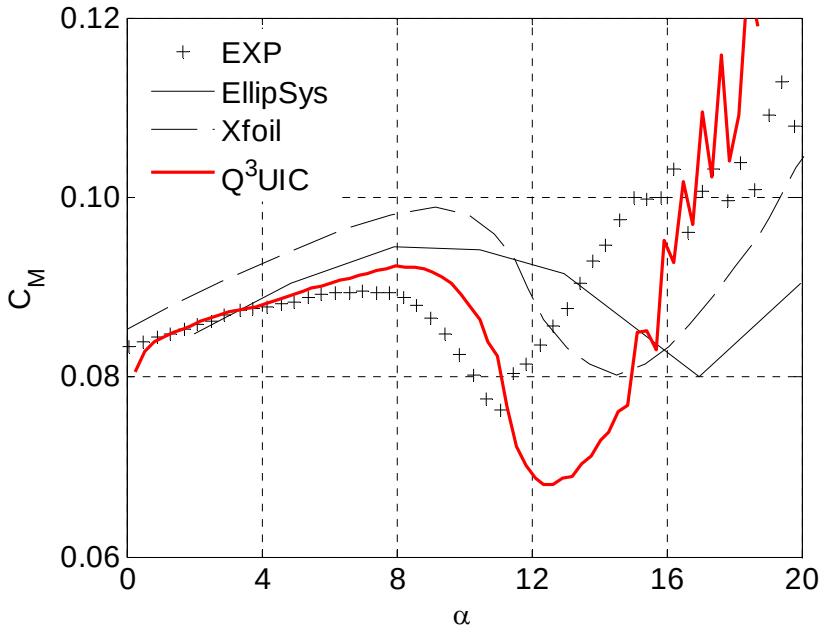

FFA-W3-211

Re = 1.8x10⁶

Low Speed Wind Tunnel L2000, KTH.

STEADY VI, THICKNESS VARIATION

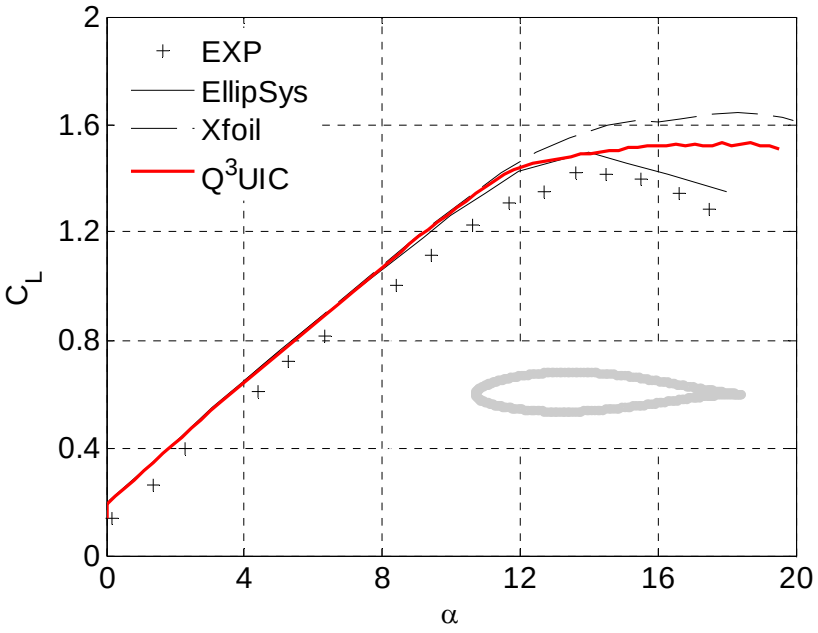

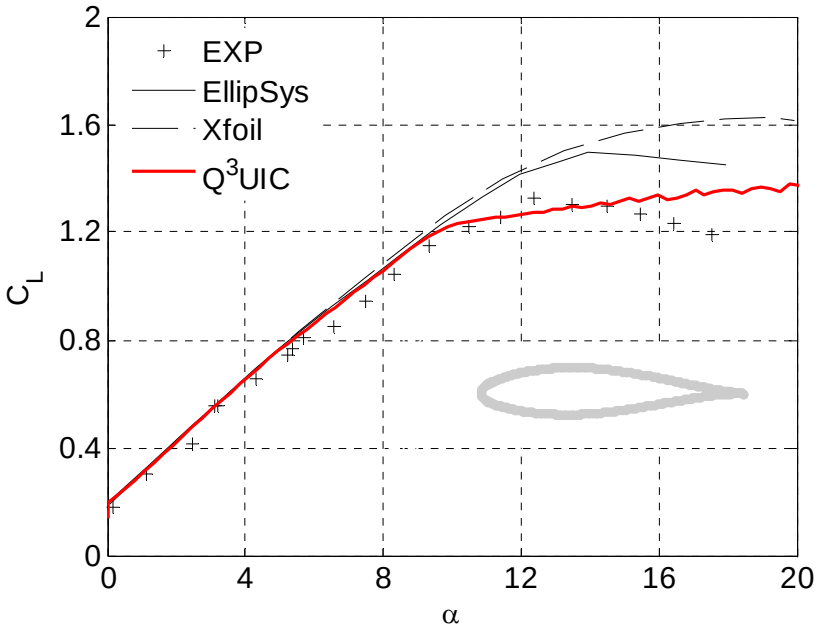

NACA 63-2xx: 15 %, 18 % and 21 % thickness

Re = 3.0x10^6

NASAs low-turbulence pressure tunnel.

Abbott and von Doenhoff, 1959.

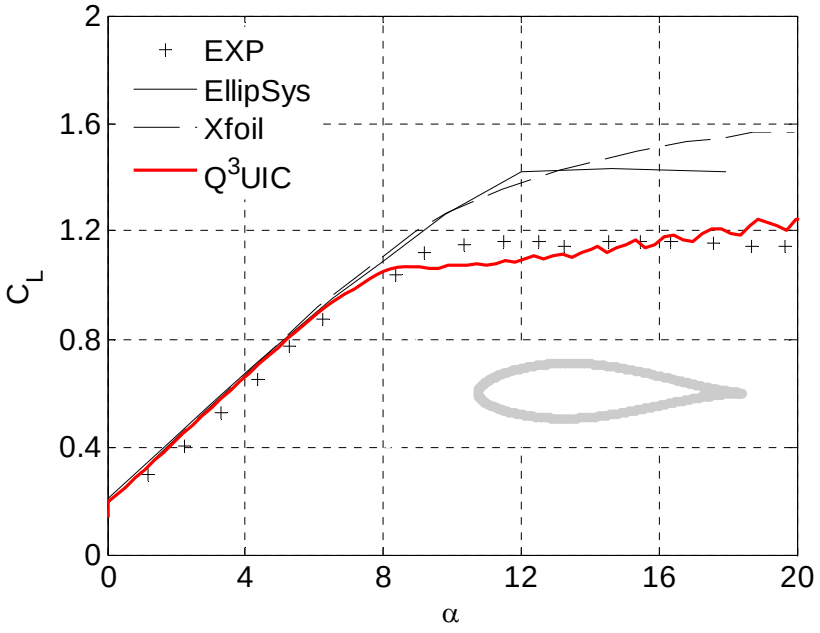

STEADY VI, REYNOLDS VARIATION

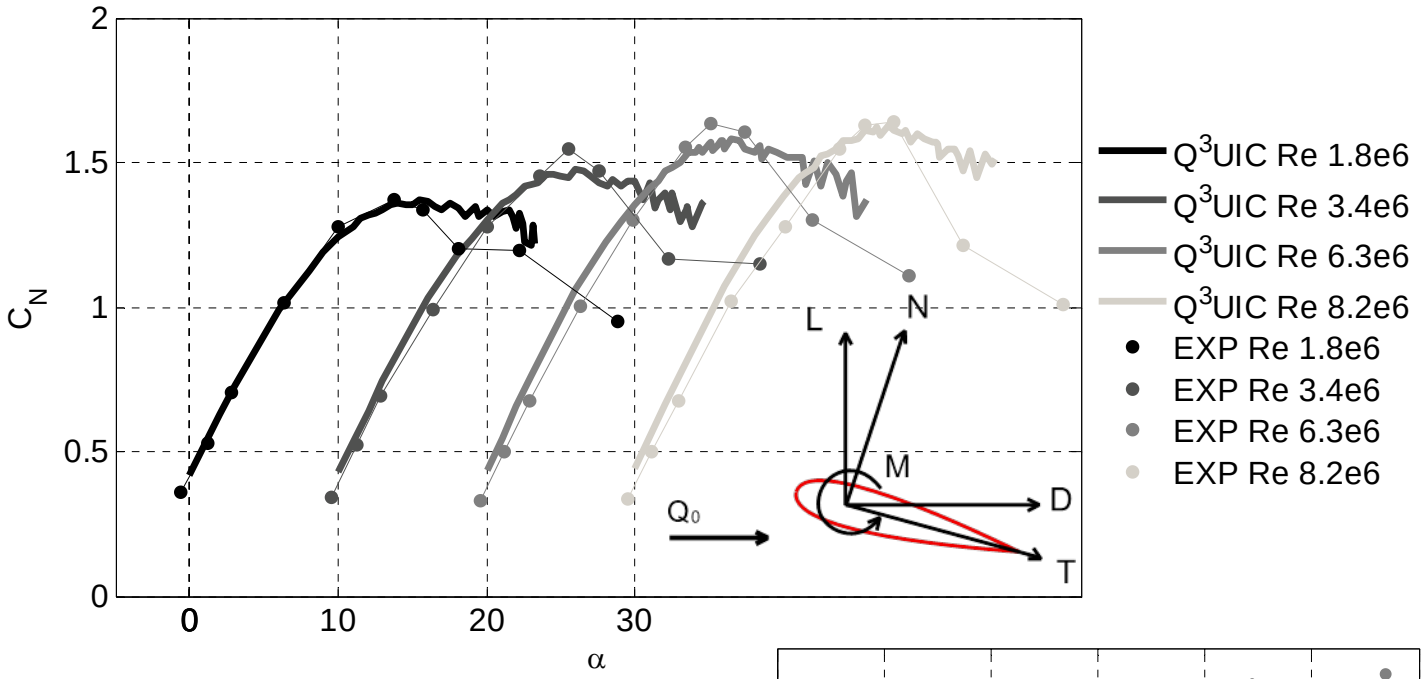

NACA 4412

N.A.C.A Variable-Density Wind Tunnel.

Pinkerton, 1938

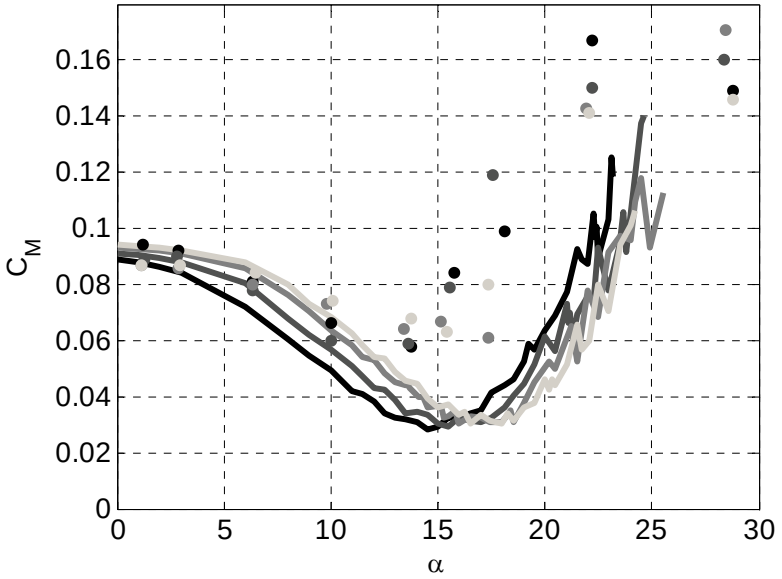

UNSTEADY VISCOUS INVISCID SOLVER SINGLE WAKE

UNSTEADY VISCOUS COMPUTATIONS, SINGLE WAKE

- **NACA 0015**
- **Re = 1.5x10^6**
- **k_A = 0.1**
- **α_m= 13.37˚ A = 7.55˚**

- ***University of Glasgow, G.U Aero Report 9221.***

- **Vorticity formulated NS running a Spallart Allmaras turbulent model. *J.N. Sørensen and P.J. Nygreen, Computers & Fluids 30 (2001).***

- **Unsteady Viscous-Inviscid strong coupling code.**

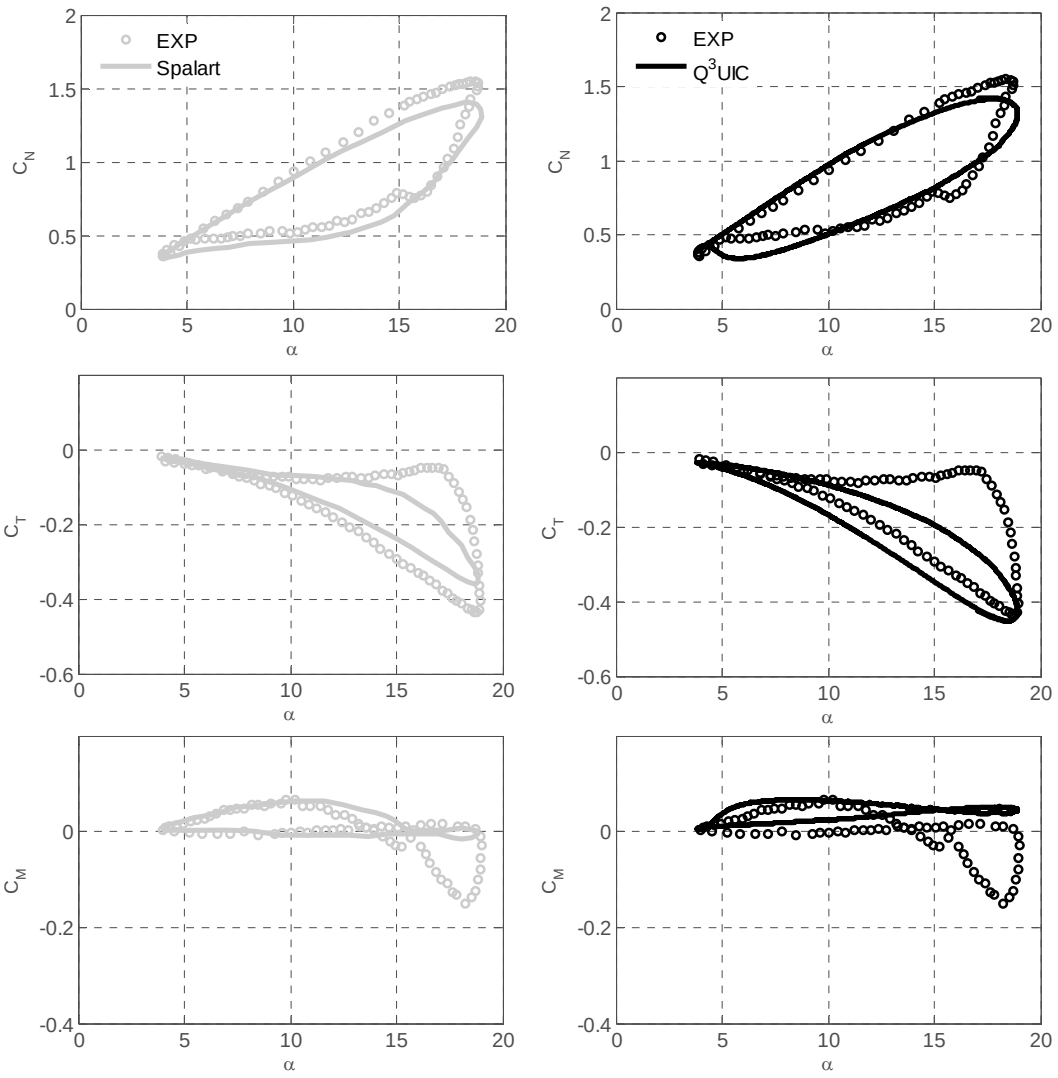

VG MODELLING

VG MODELLING WITH Q³UIC

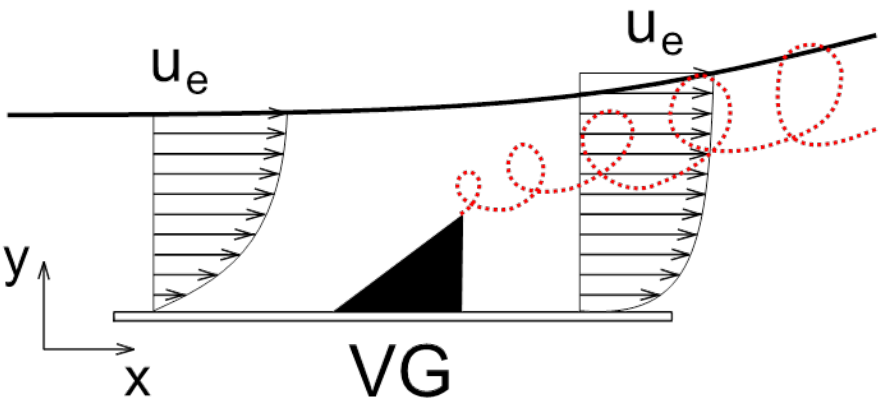

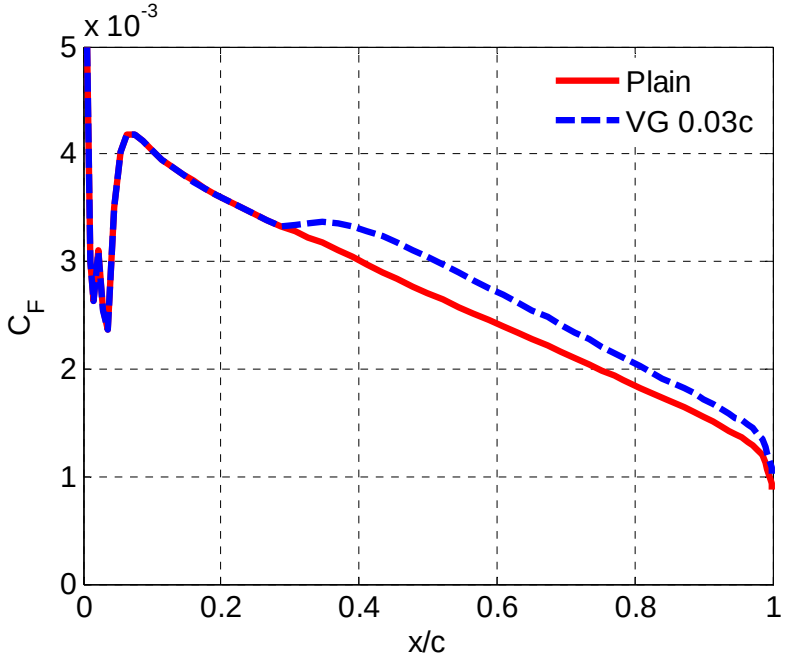

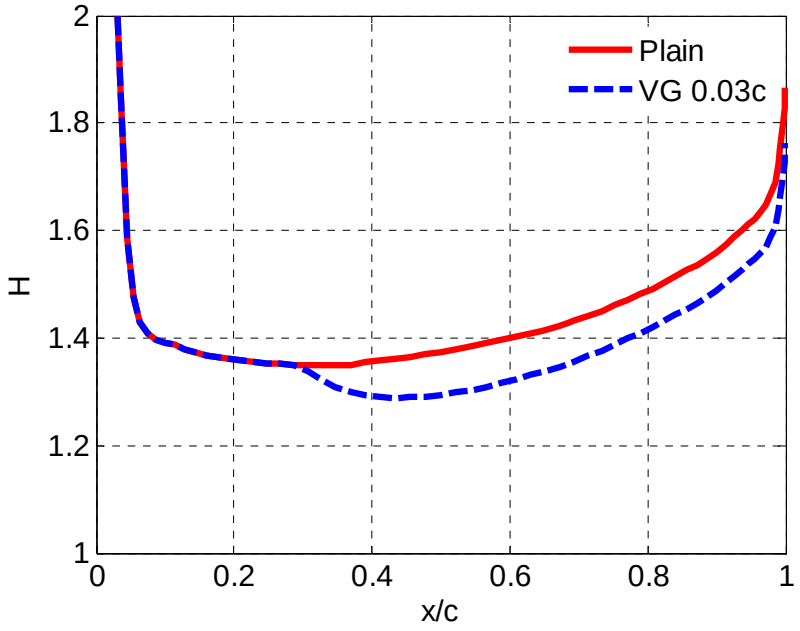

VG MODELLING WITH Q³UIC

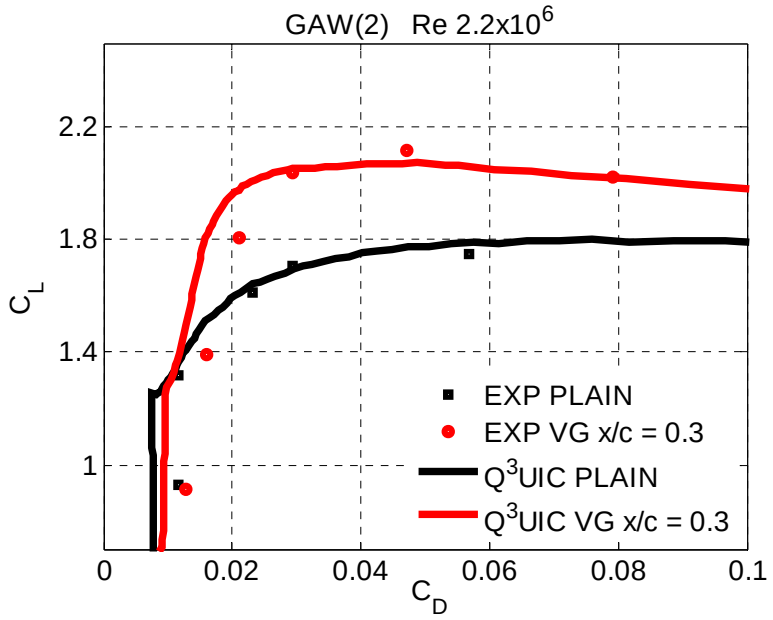

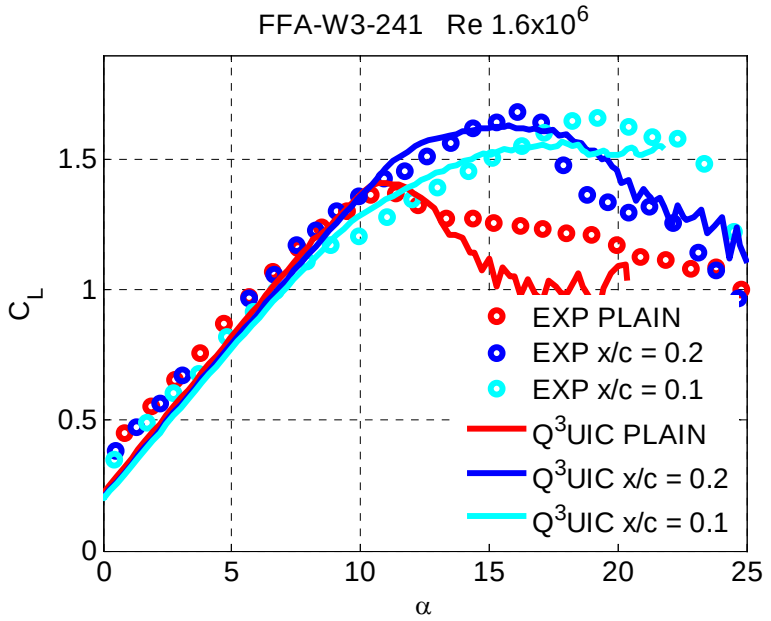

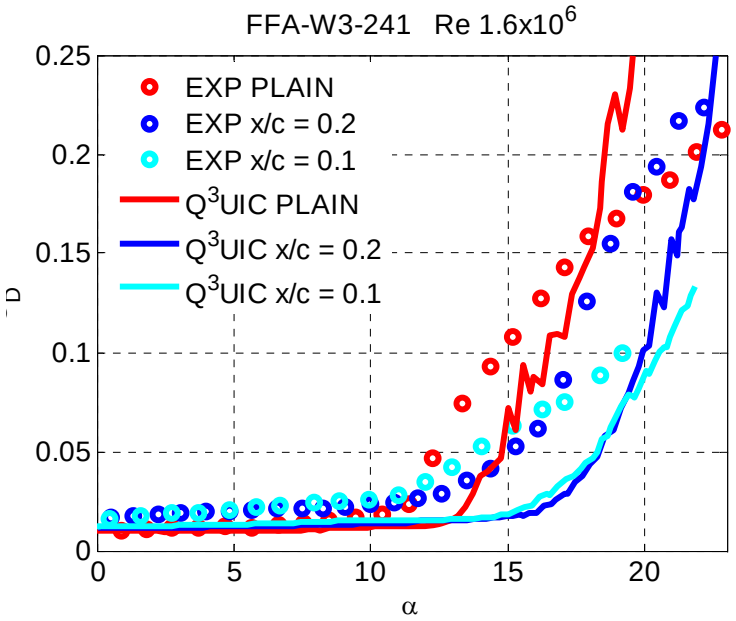

Q3D STEADY VISCOUS INVISCID SOLVER

QUASI-3D BOUNDARY LAYER EQUATIONS

- Dimensional variables of interest in rotational study: c, r, Ω , V_w

- In order to proceed with a parametric study of the rotational effects in a wind turbine blade, two variables are defined:

1. The ratio between the chord length and the radial position,

$$ls = \frac{c}{r}$$

2. The ratio between the rotational speed an the relative velocity,

$$RO = \frac{\Omega r}{U_{rel}}$$

Where Ω is the blade angular velocity, U_{rel} is defined typically,

$$U_{rel} = \sqrt{\left((1+a')\Omega r\right)^2 + \left((1-a)V_w\right)^2}$$

The four dimensional variables of interest are reduced to two adimensional parameters ls & RO, base for our parametric study.

QUASI-3D BOUNDARY LAYER

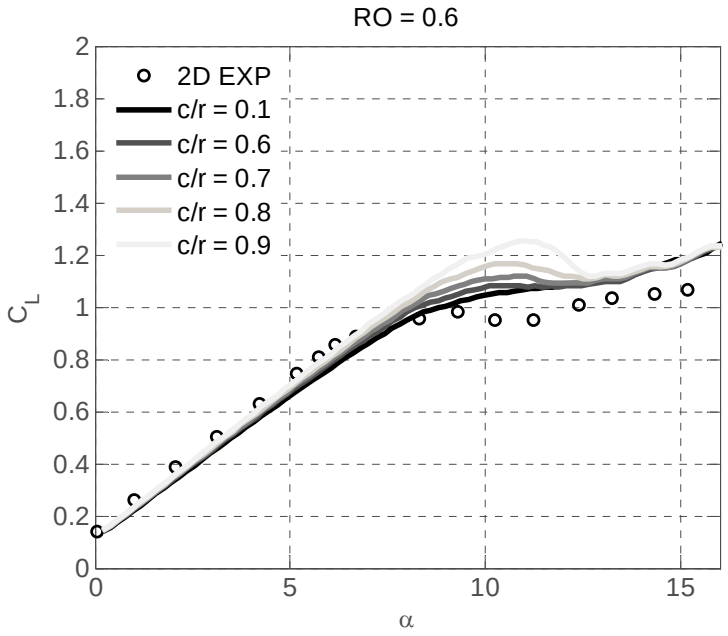

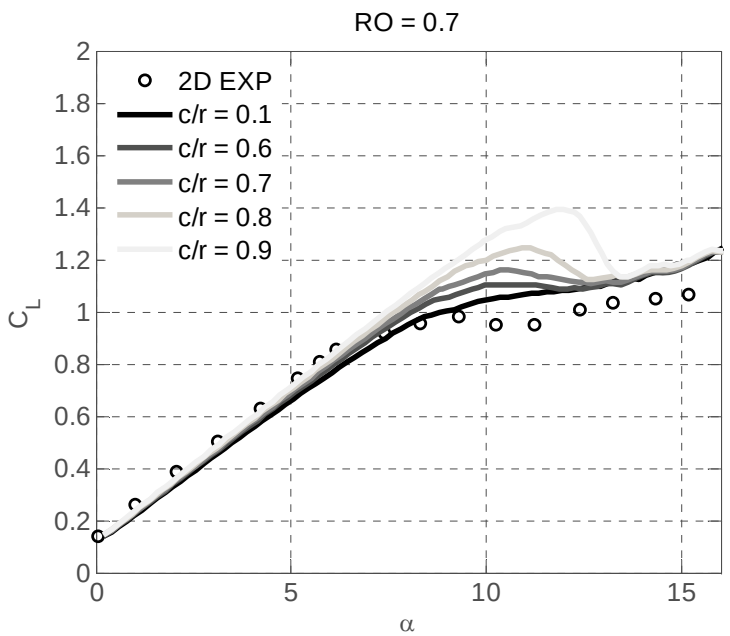

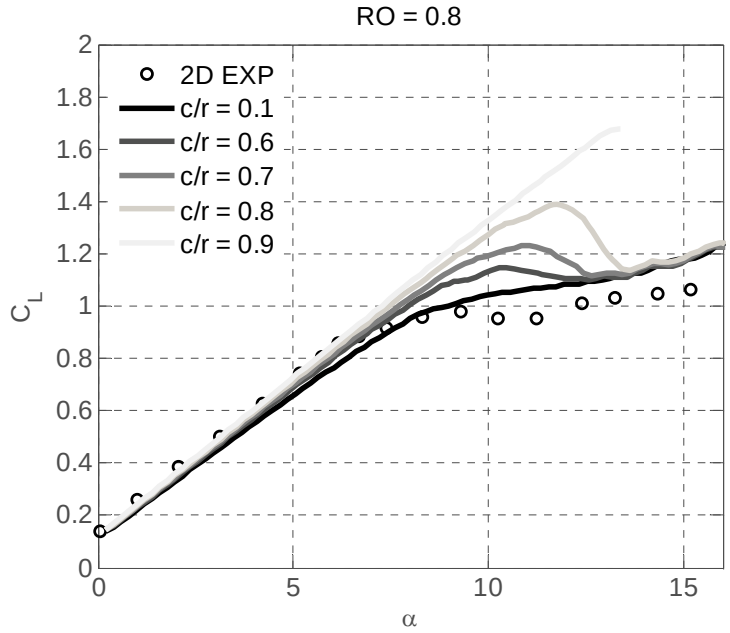

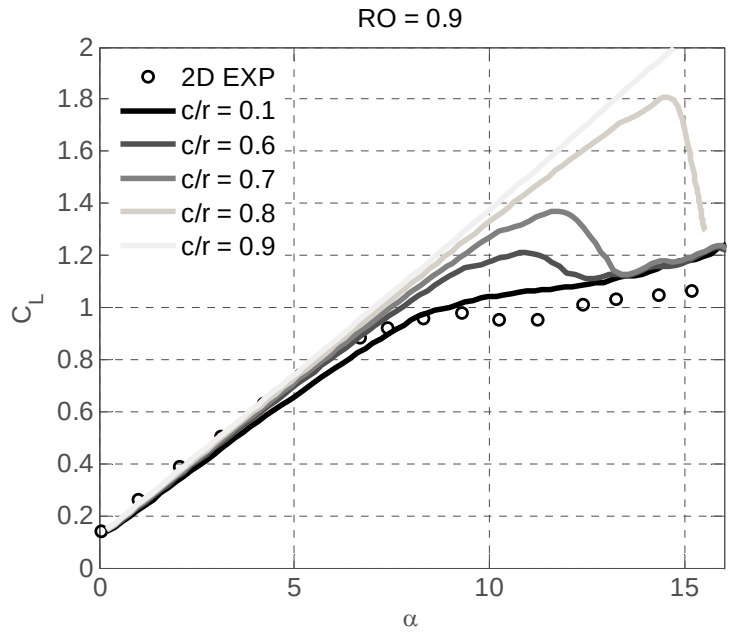

QUASI-3D BOUNDARY LAYER

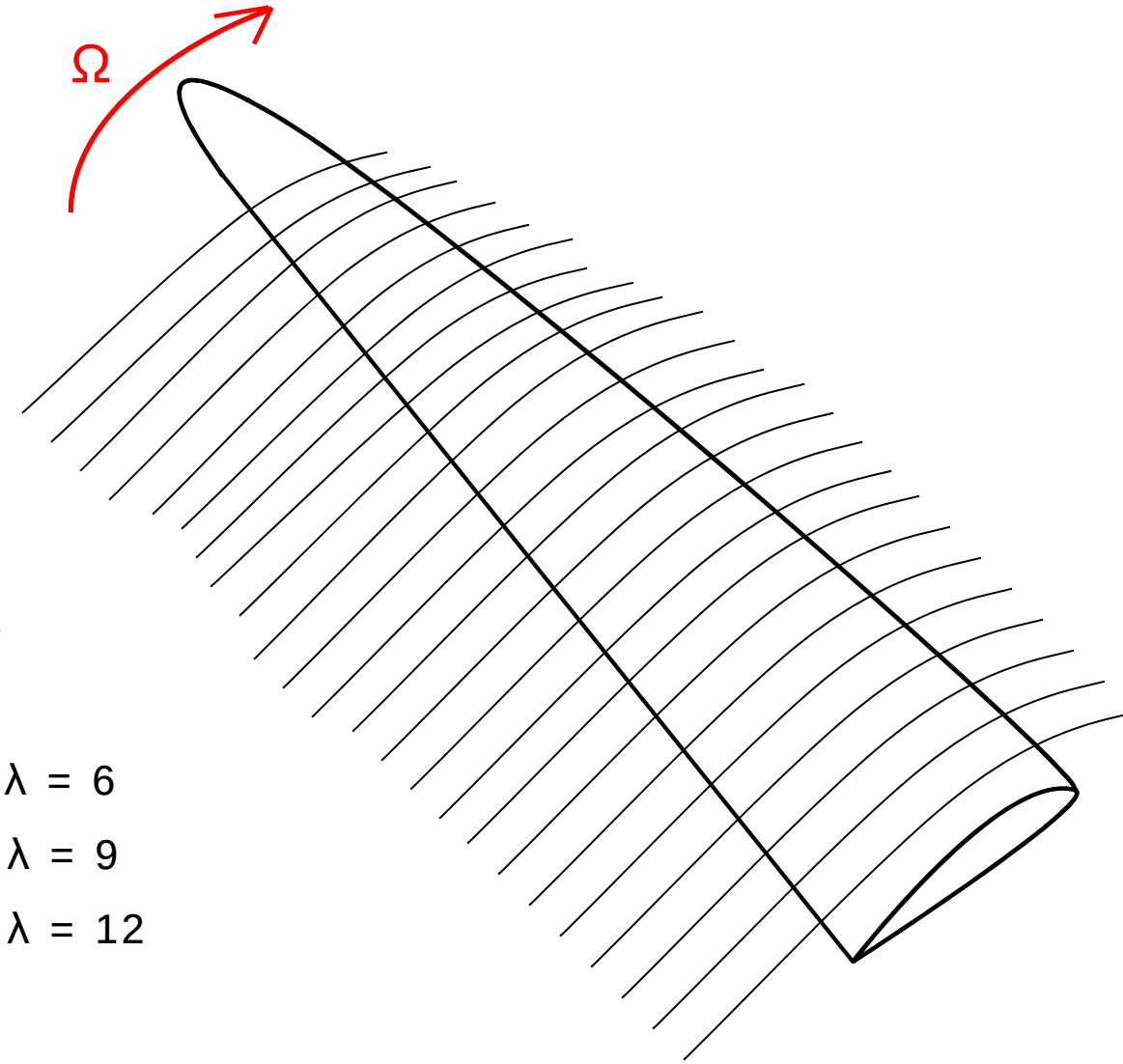

- Artificial rotor.
- S809 Airfoil.
- Re 1e6.
- R = 10 m.
- Ω = 70 rpm.

- Tip speed ratio, $\lambda = \frac{\Omega R}{Q_w}$

  - Q_W = 12.20 m/s → λ = 6
  - Q_W = 8.14 m/s → λ = 9
  - Q_W = 6.11 m/s → λ = 12

QUASI-3D BOUNDARY LAYER

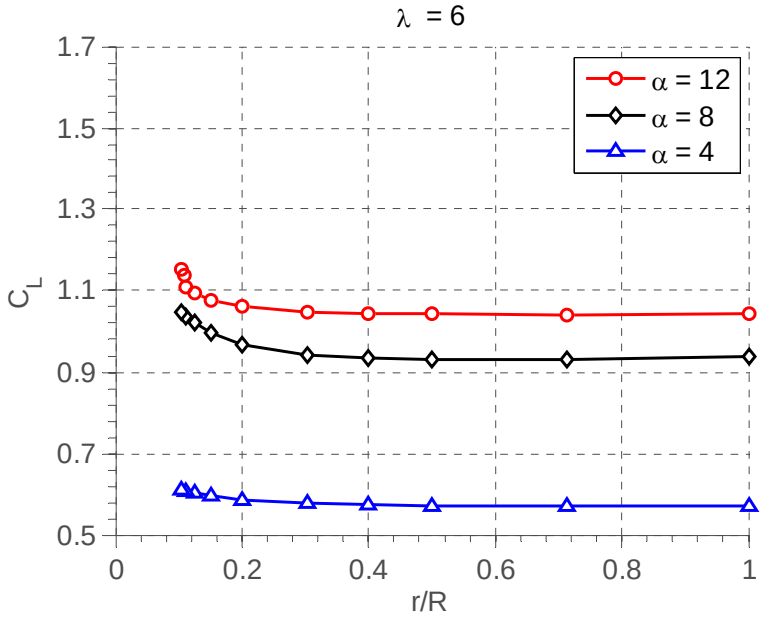

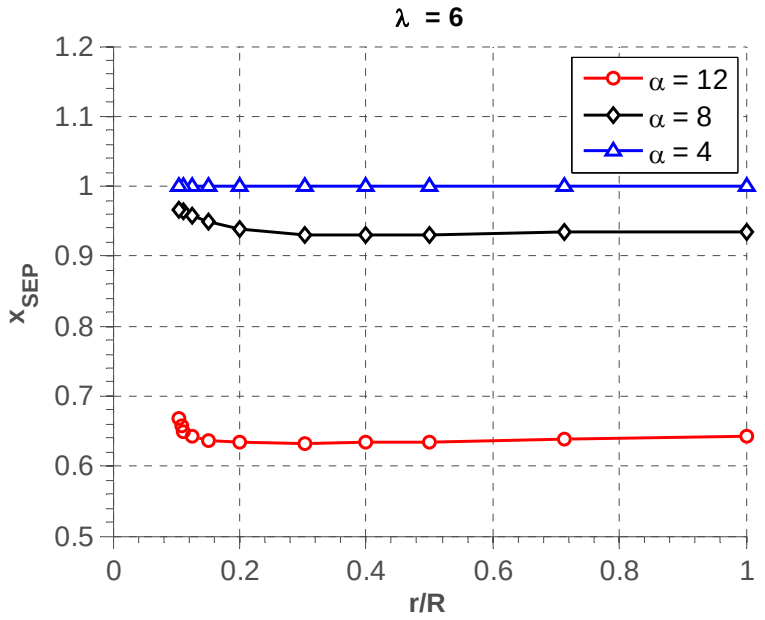

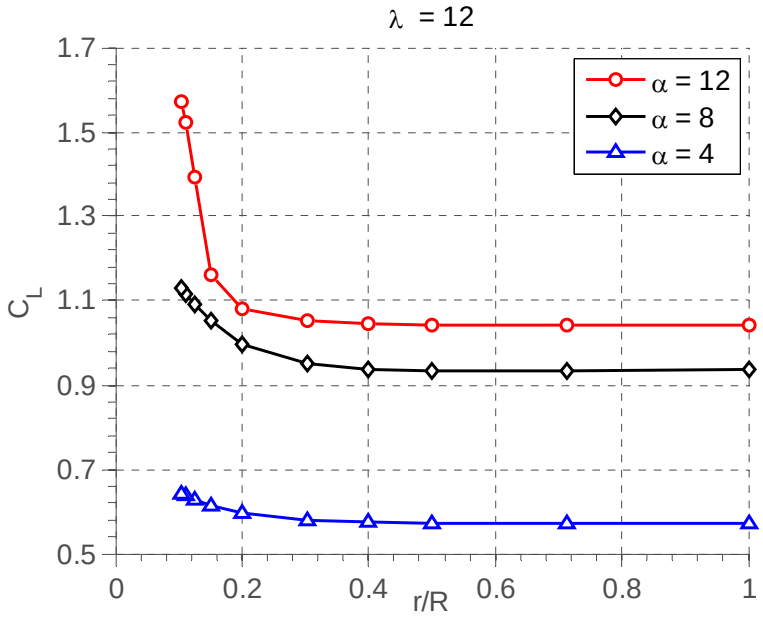

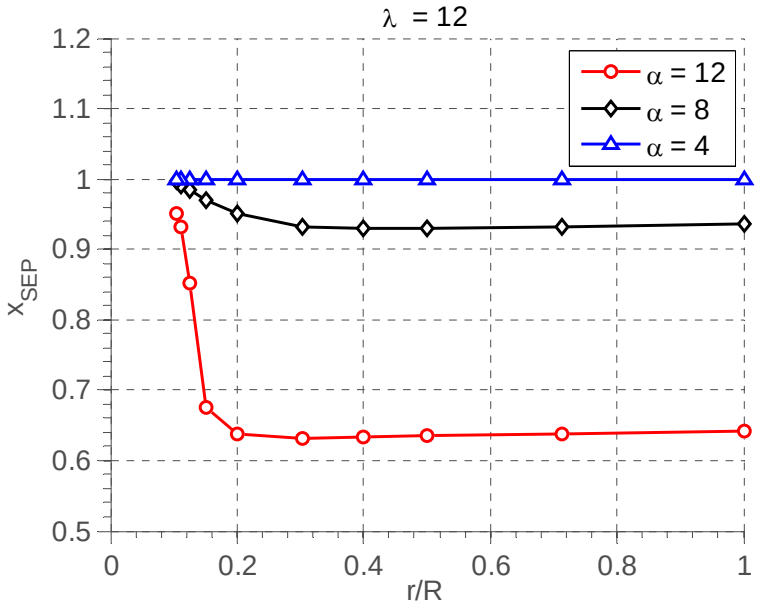

DOUBLE WAKE POTENTIAL SOLVER

DOUBLE WAKE MODEL

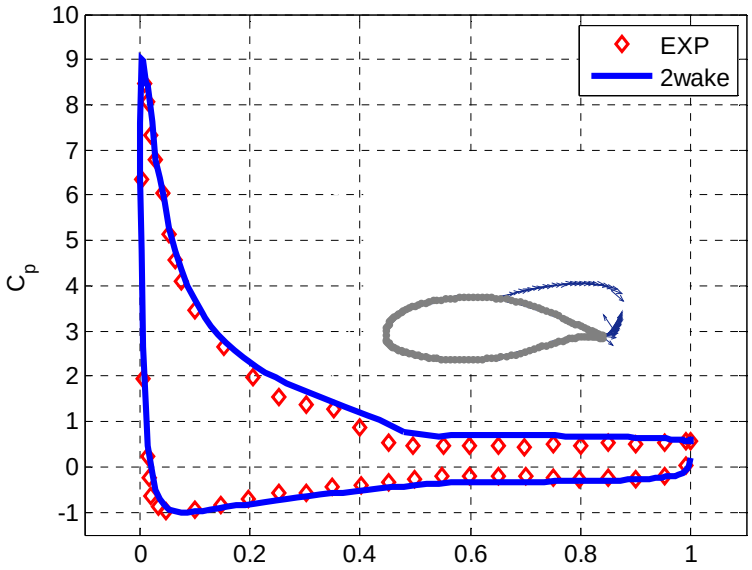

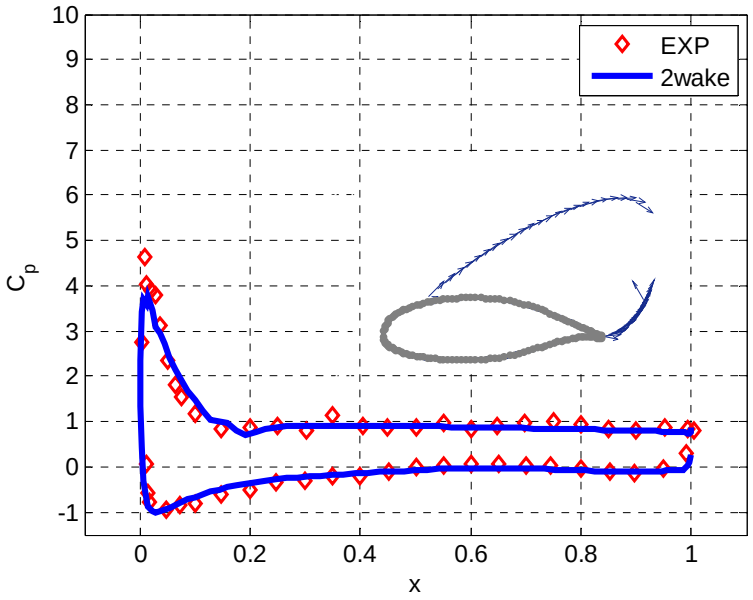

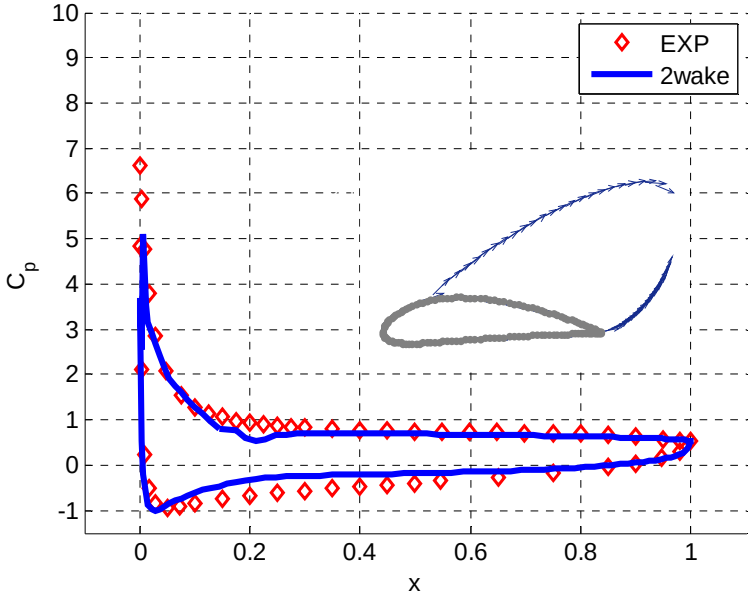

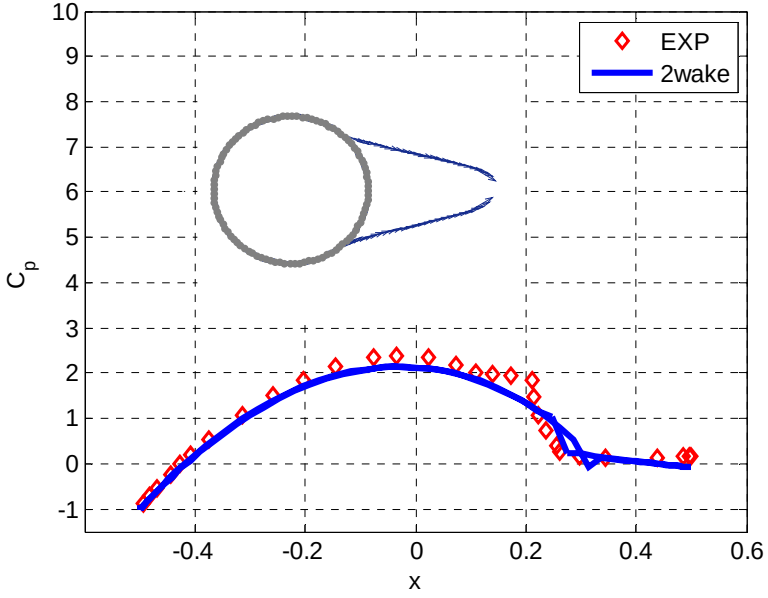

DOUBLE WAKE MODEL

SINGLE WAKE MODEL

- ATTACHED BL.

- LIGHT STALL

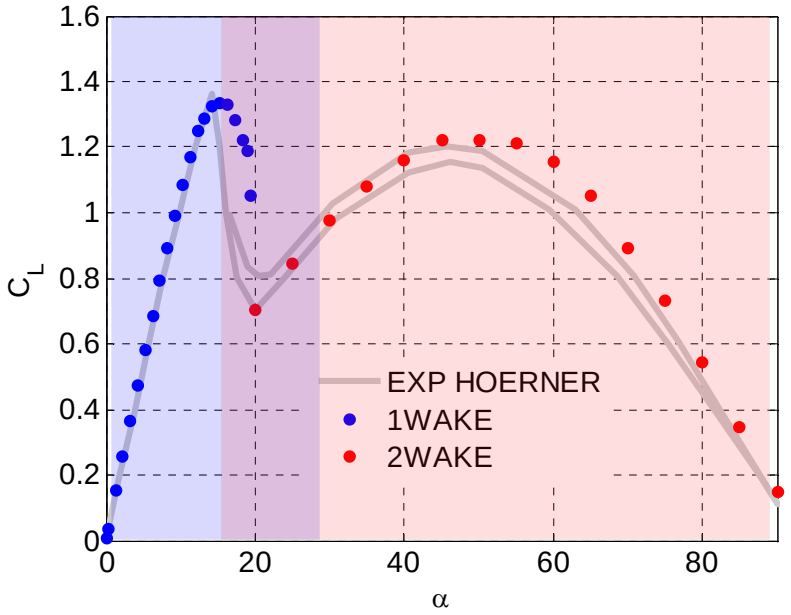

DOUBLE WAKE MODEL

- FULLY SEPARATED BL.

- DEEP STALL

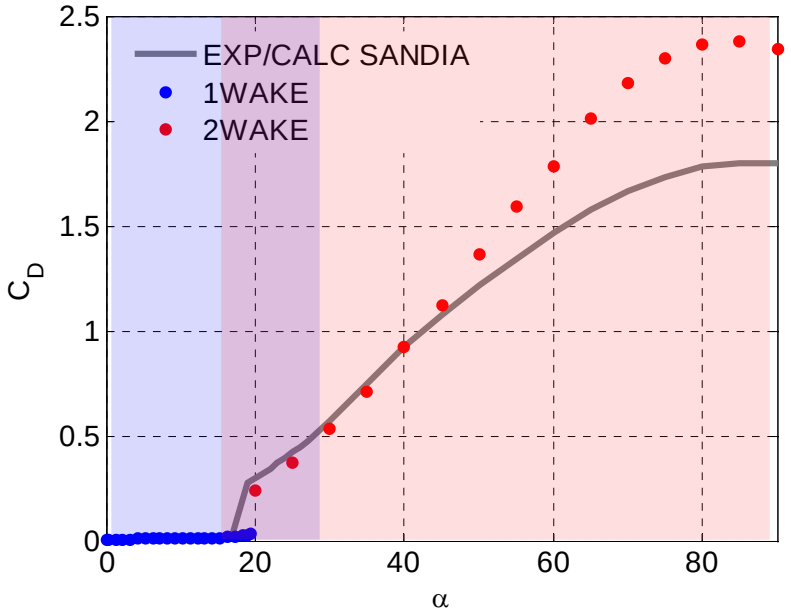

CONCLUSIONS

- **VISCOUS INVISCID SOLVER IMPLEMENTED**
  - **STEADY 2D**
  - **UNSTEADY 2D**
  - **STEADY 2D VG**
  - **STEADY Q3D**
- **DOUBLE WAKE POTENTIAL SOLVER IMPLEMENTED**
  - **DEEP STALL CONDITIONS**

THANK YOU FOR YOUR ATTENTION.

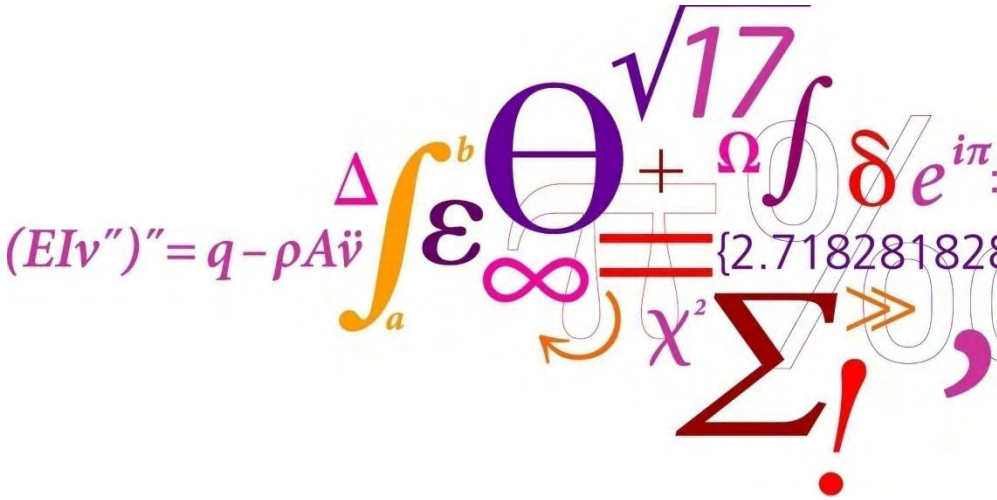

DTU Mekanik
Institut for Mekanisk Teknologi

4 Influence of up-scaling

Influence of up-scaling on loads, control and aerodynamic modeling

Loading from turbulence

Helge Aagaard Madsen
Flemming Rasmussen
Torben J. Larsen
Vasilis Riziotis (NTUA, Greece)

Wind Energy Division
Programme of Aeroelastic Design
Risø DTU

hama@risoe.dtu.dk

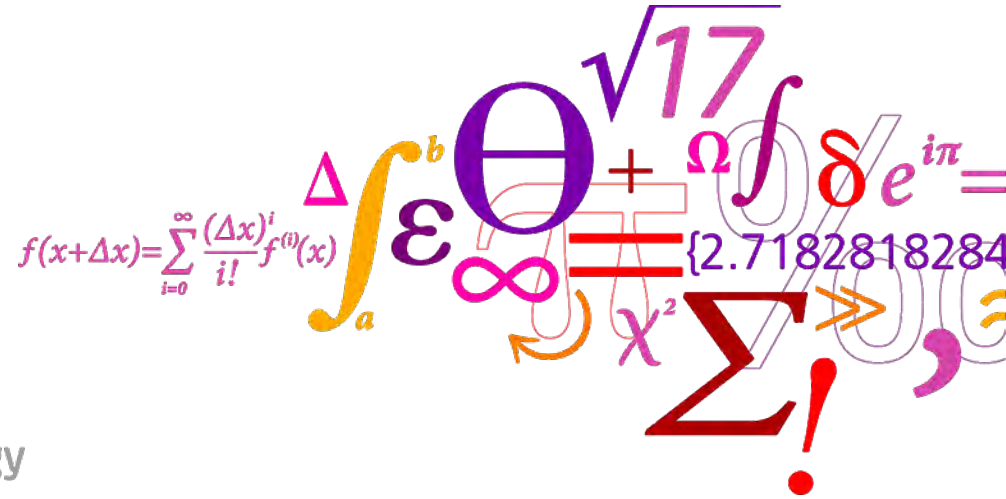

Risø DTU
National Laboratory for Sustainable Energy

The subject

Shear and turbulence in inflow

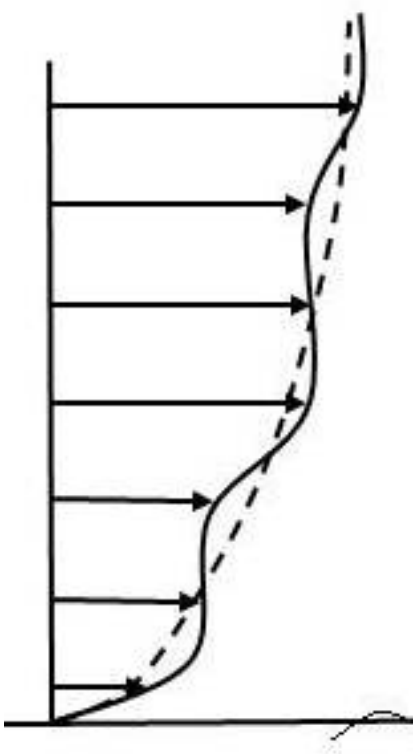

Ratio between rotor size and the atmospheric boundary layer height and turbulence scales increases

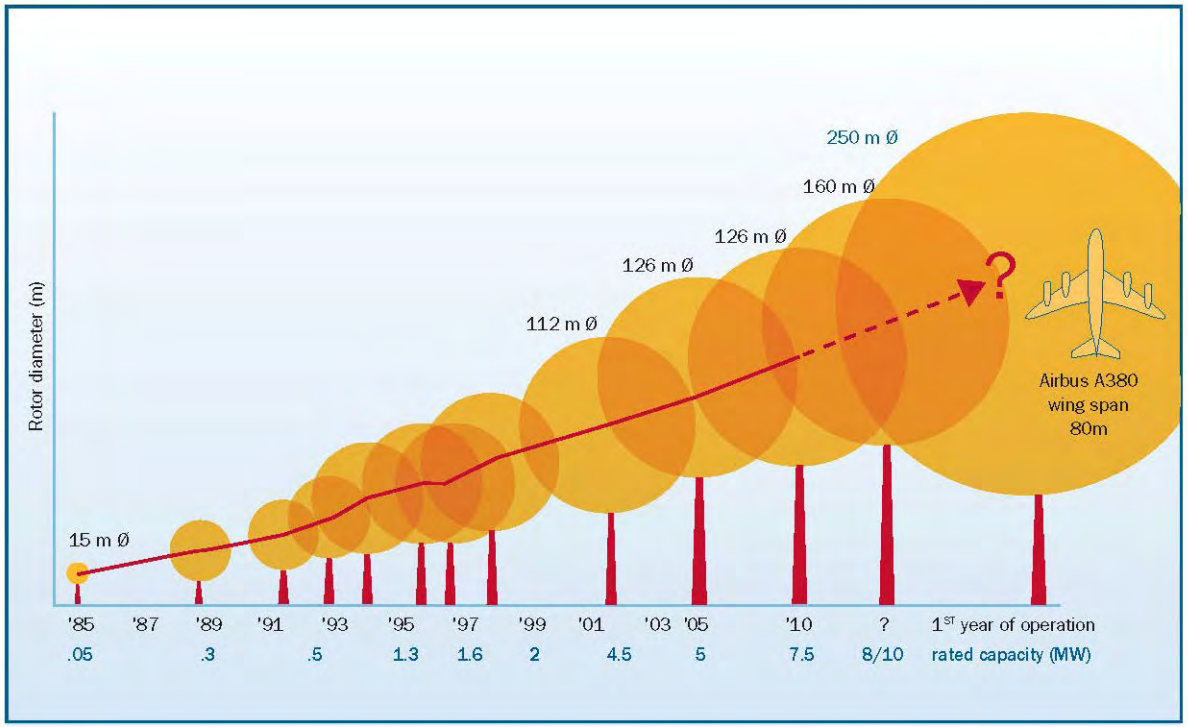

Rotational sampling of turbulence

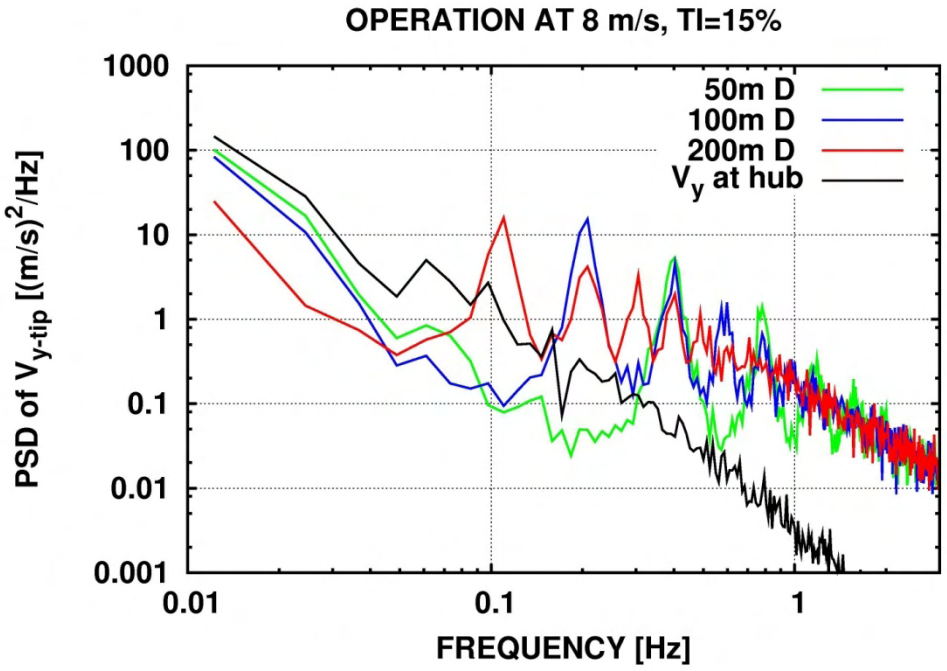

Do we model the 1p, 2p etc. aerodynamics accurately ?

- 1p, 2p … variations in induction not modeled in some BEM codes used by industry

The BEM model is based on the Galuert propeller theory - probably not originally intended to be used on rotors of 100m D or more in atmospheric turbulent flow

Rotational sampling of turbulence

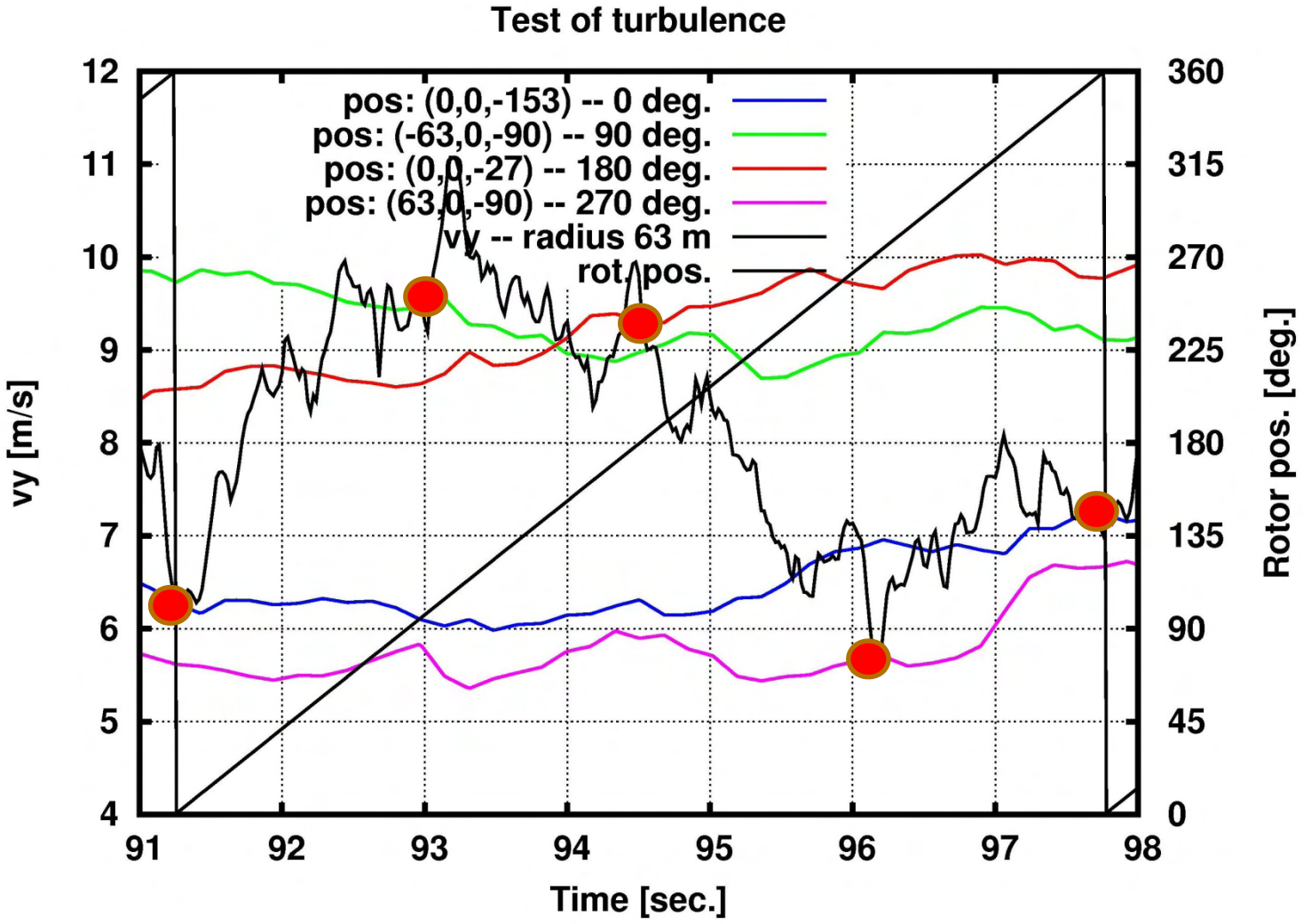

Objectives

Study the influence of up-scaling of rotors operating in turbulent inflow on:

- the aerodynamic loading characteristics
- control aspects
- aerodynamic and aeroelastic modeling requirements

Approach

- Four turbines with a rotor size of 25m, 50m, 100m and 200m were modeled in HAWC2aero (no structural dynamics) based on a direct scaling of the 5MW reference wind turbine rotor. The tip speed was kept constant at 60.5 m/s.
- A turbulence box with the dimension of 200m x 200m x 11200m was generated with number of points equal to 64 x 64 x 4096 and a wind speed of 8 m/s.
- A tower height of 120 m was used for all turbines and no wind shear.
- A simulation time of 1300 sec. was used and the first 100 sec. excluded.
- Only one wind speed at 8 m/s was simulated at a turbulence intensity of 15%.
- No turbine speed and pitch control was used.

Analysis

- Rotational sampling of turbulence
- Rotor thrust and power
- Flapwise blade root moment
- Control aspects
- Impact on model requirements

Results – rotational sampling

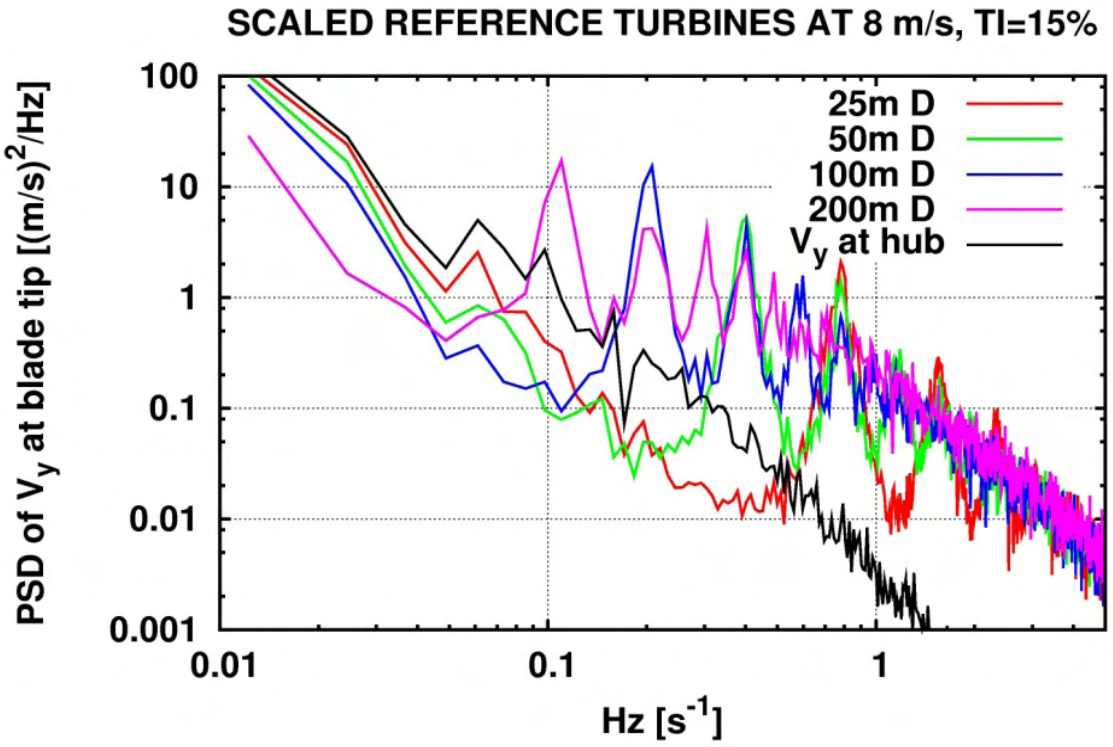

- The rotational sampling of the turbulence concentrates part of the turbulent energy on 1p, 2p etc.
- The contribution comes from frequencies below 1p due to the spatial averaging of the turbulence over the rotor area.
- The effect will thus increase with increasing rotor size and a considerable part of the total turbulent input for the 200 m rotor is now on 1p

Results - thrust

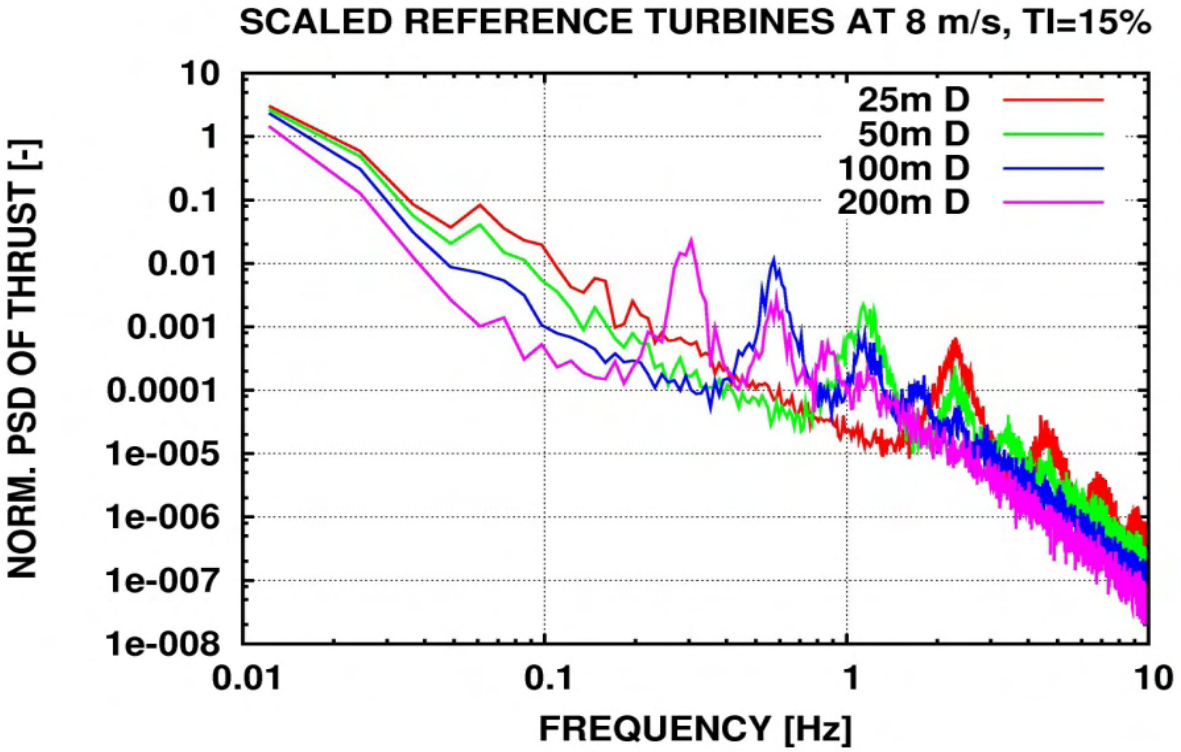

Spectra of thrust (normalized with their mean value squared) for the different rotors.

The thrust load input is found on 3p, 6p etc. and the concentrated energy is from frequencies below 3p.

Results – flapwise moment

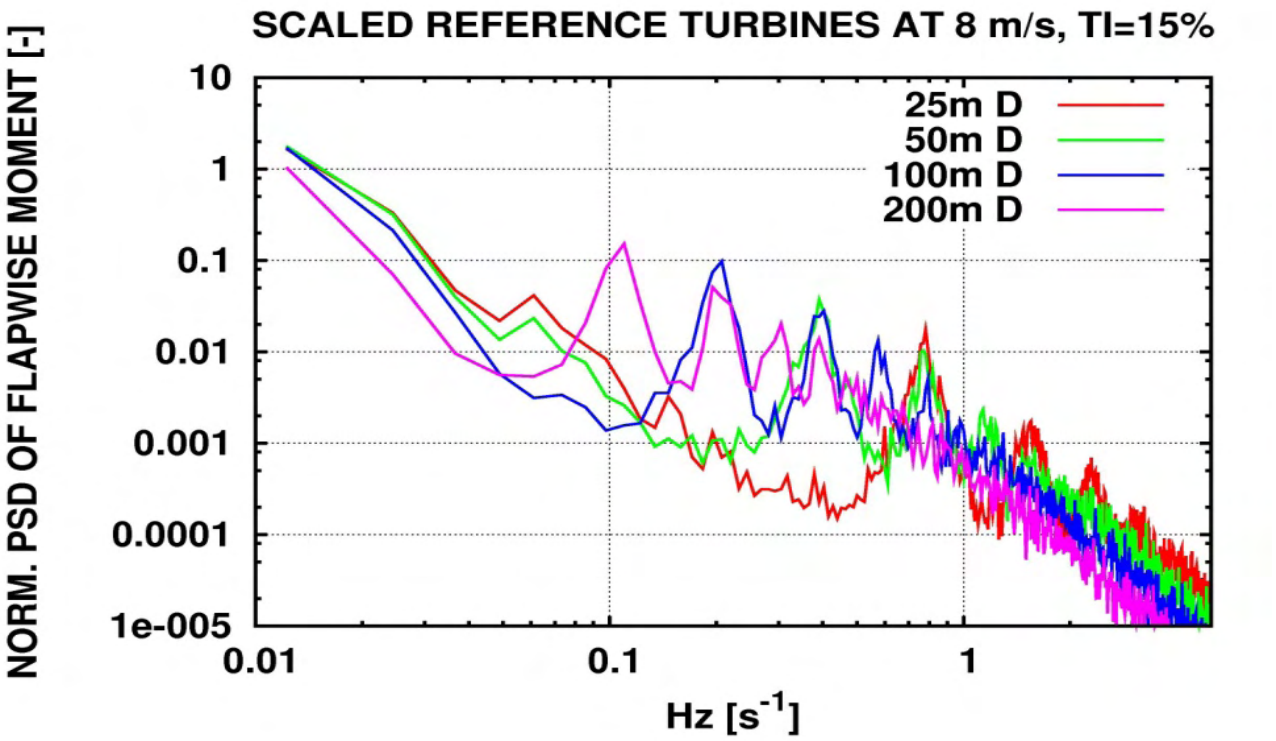

Spectra of flapwise moment (normalized with their mean value squared) for the different rotors.

The flapwise load input is found on 1p, 2p, 3p etc. and as for the wind speed the concentrated energy is from frequencies below 1p.

Results – ratio between std.dev. and mean

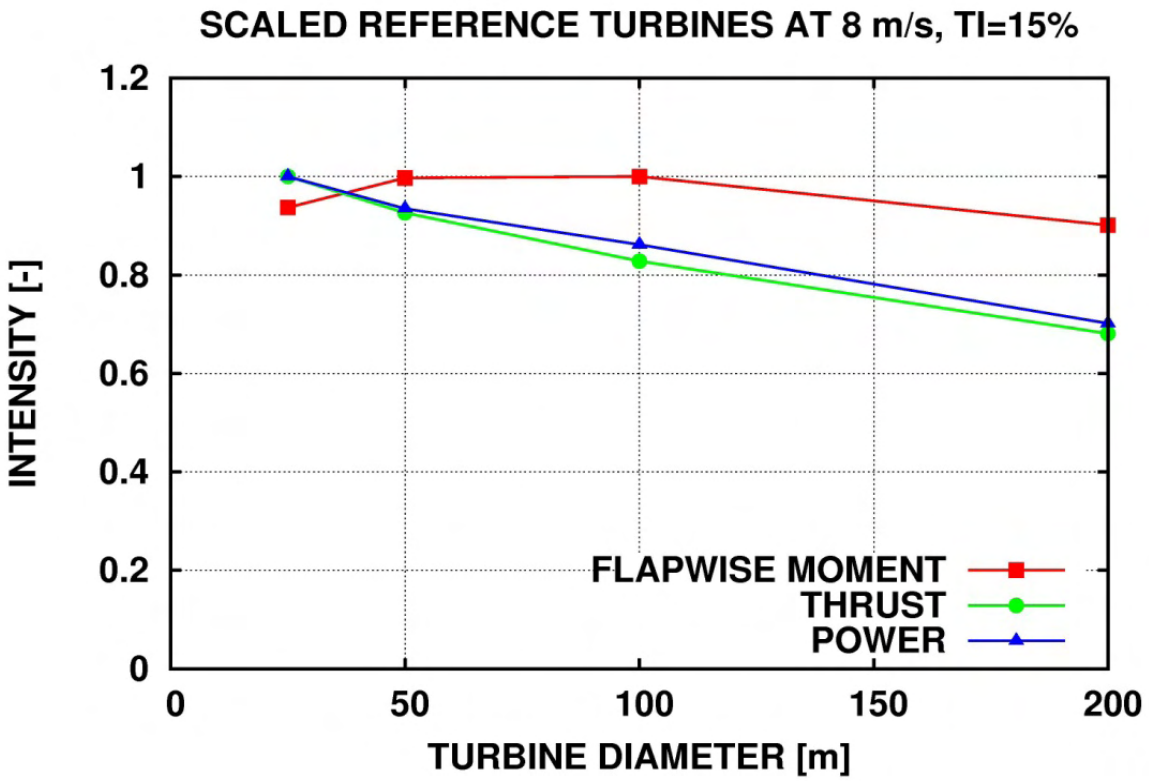

The ratio (std.dev./mean) denoted intensity is seen to decrease for the power and thrust and to some degree also for flapwise moment, due to the spatial averaging of the instantaneous forces over the swept area.

Results – time trace of thrust

200m rotor

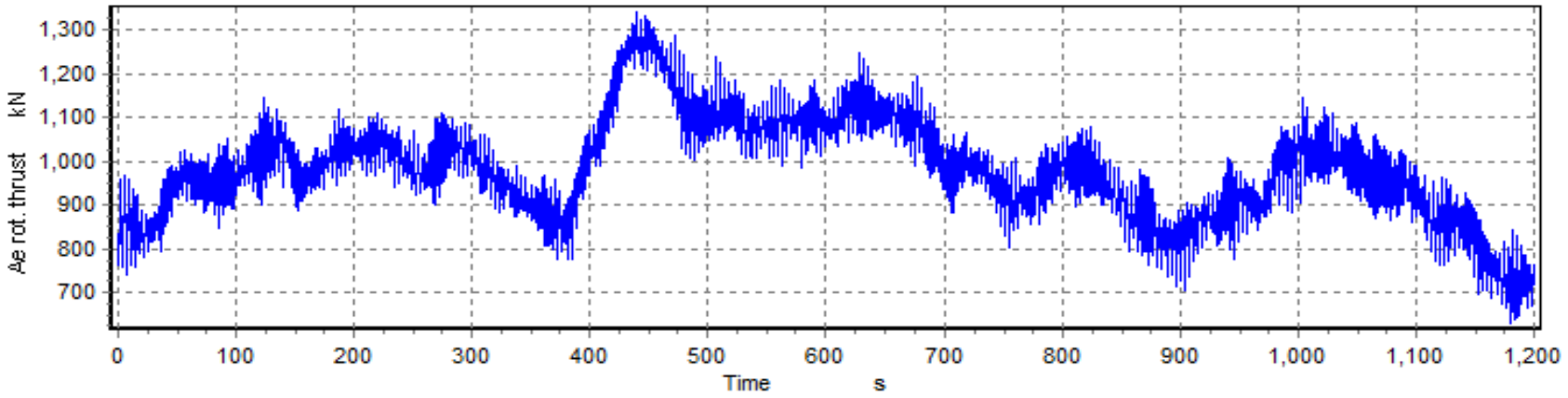

25m rotor

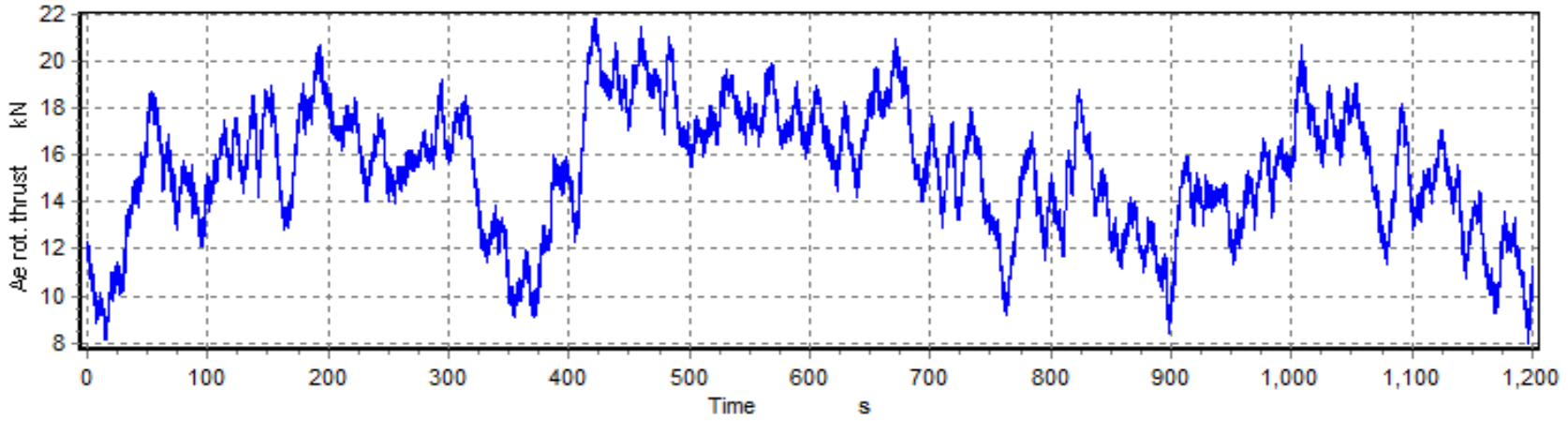

Results – rotor power

200m rotor

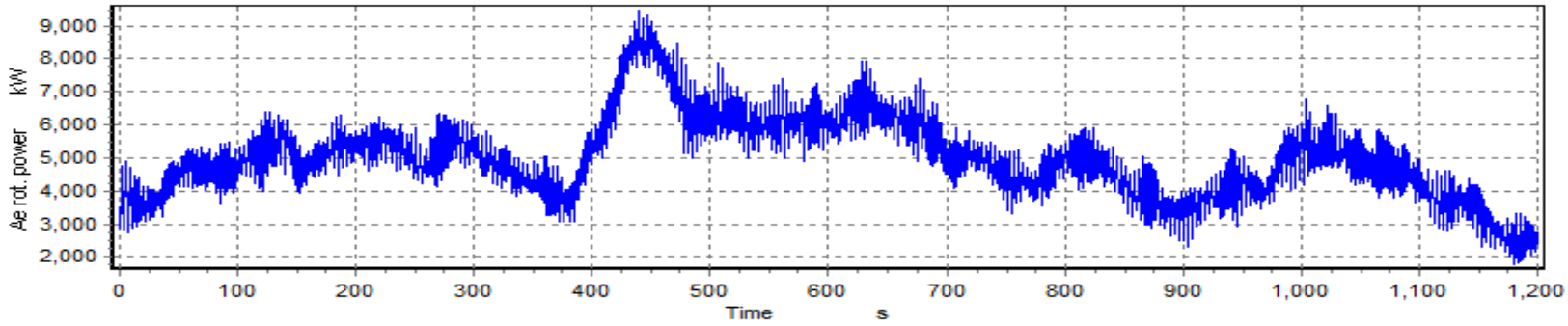

25m rotor

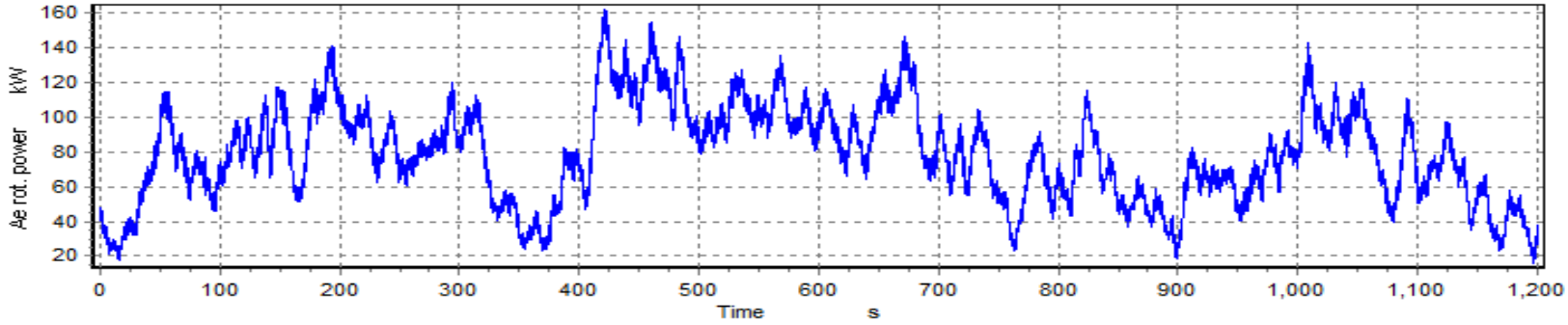

Results – flapwise moment

200m rotor

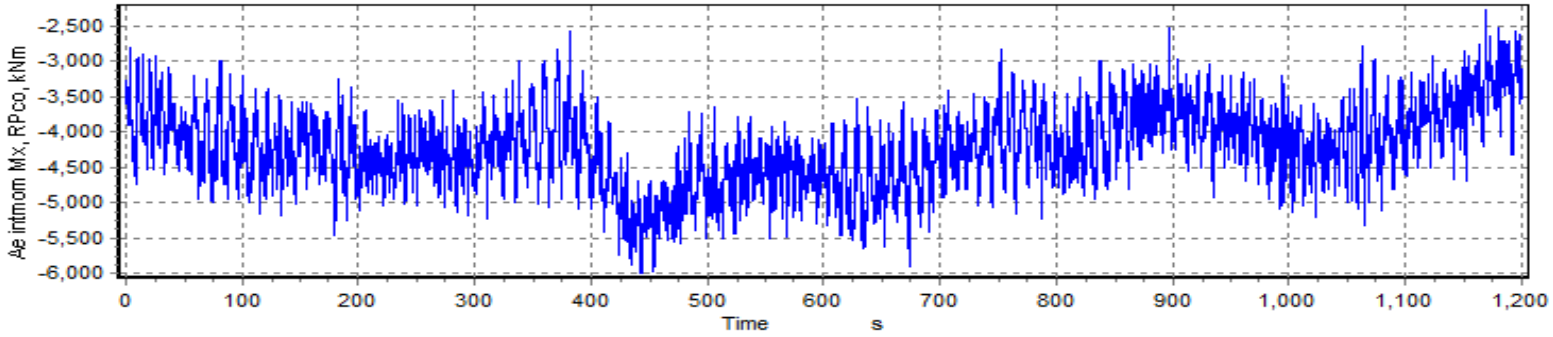

25m rotor

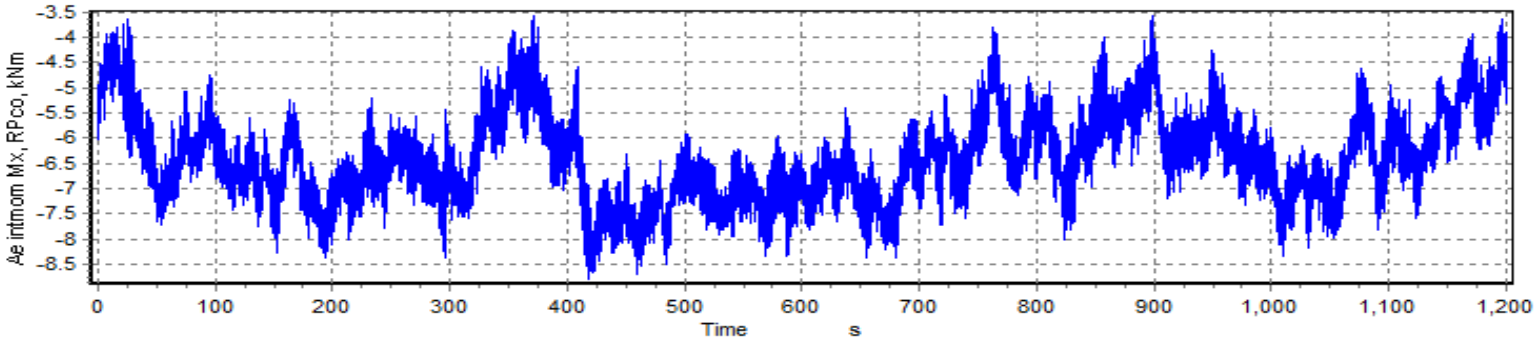

Loads on upscaled wind turbines – full aeroelastic simulations from NTUA

1Hz equivalent loads

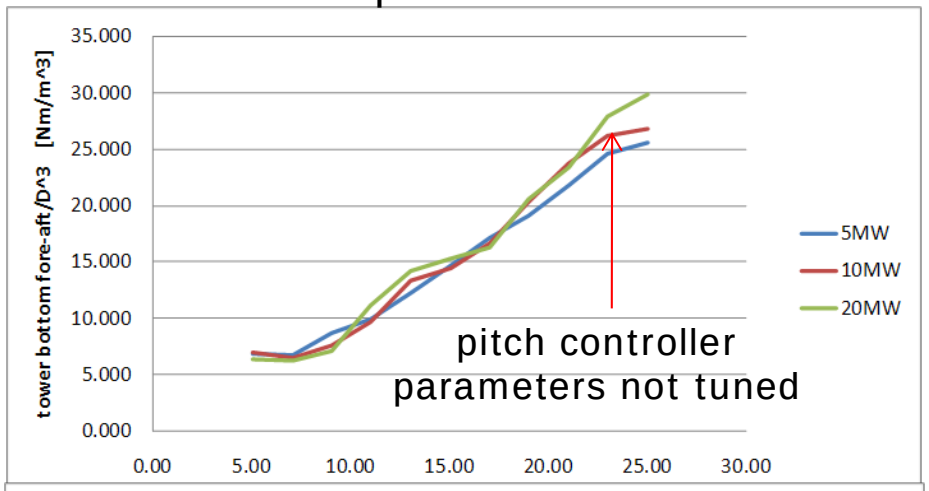

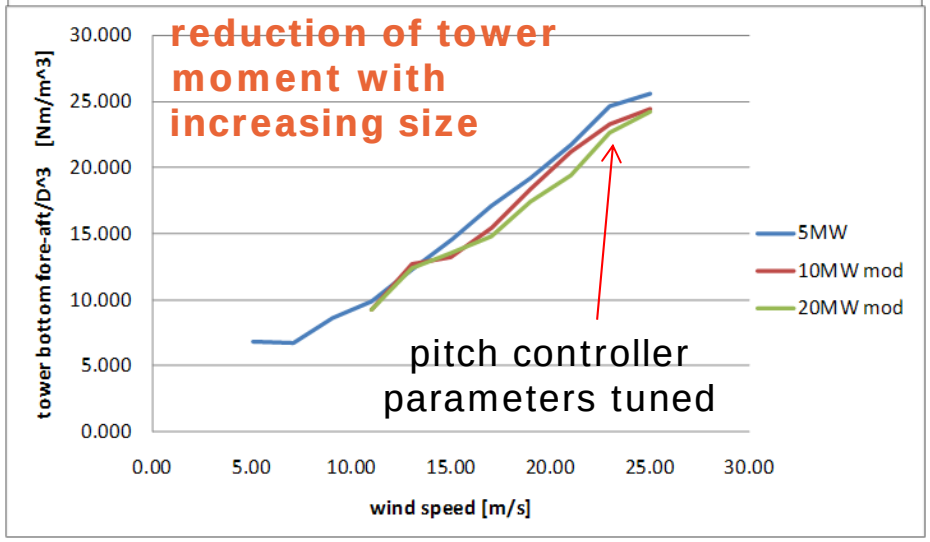

better power quality

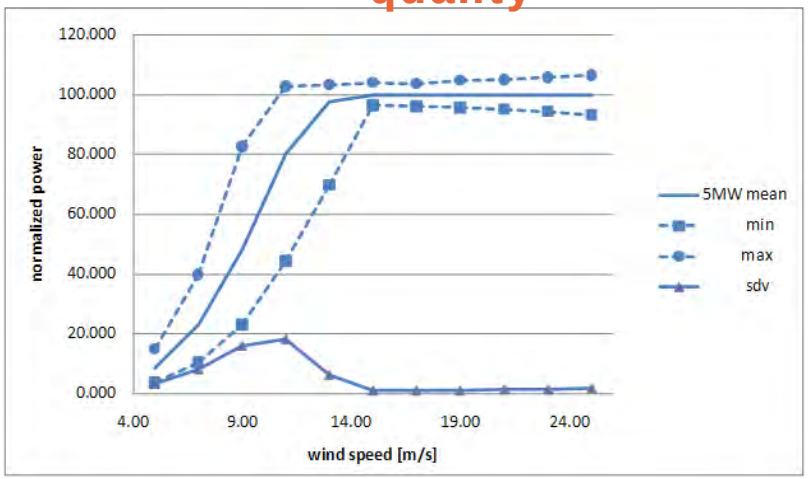

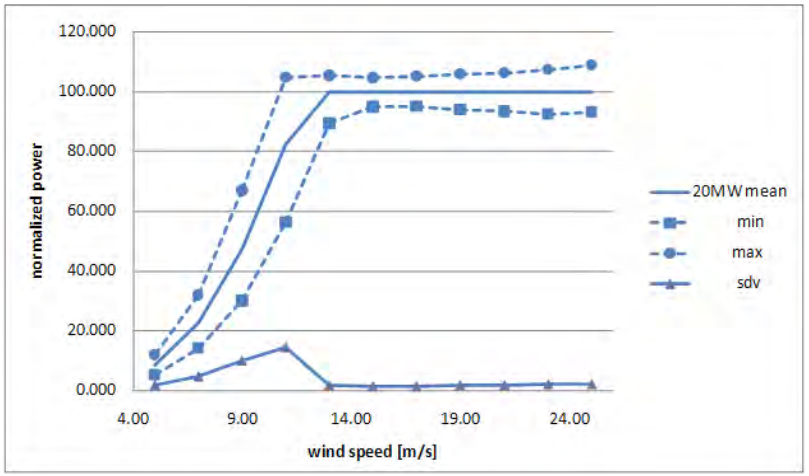

Results – control aspects

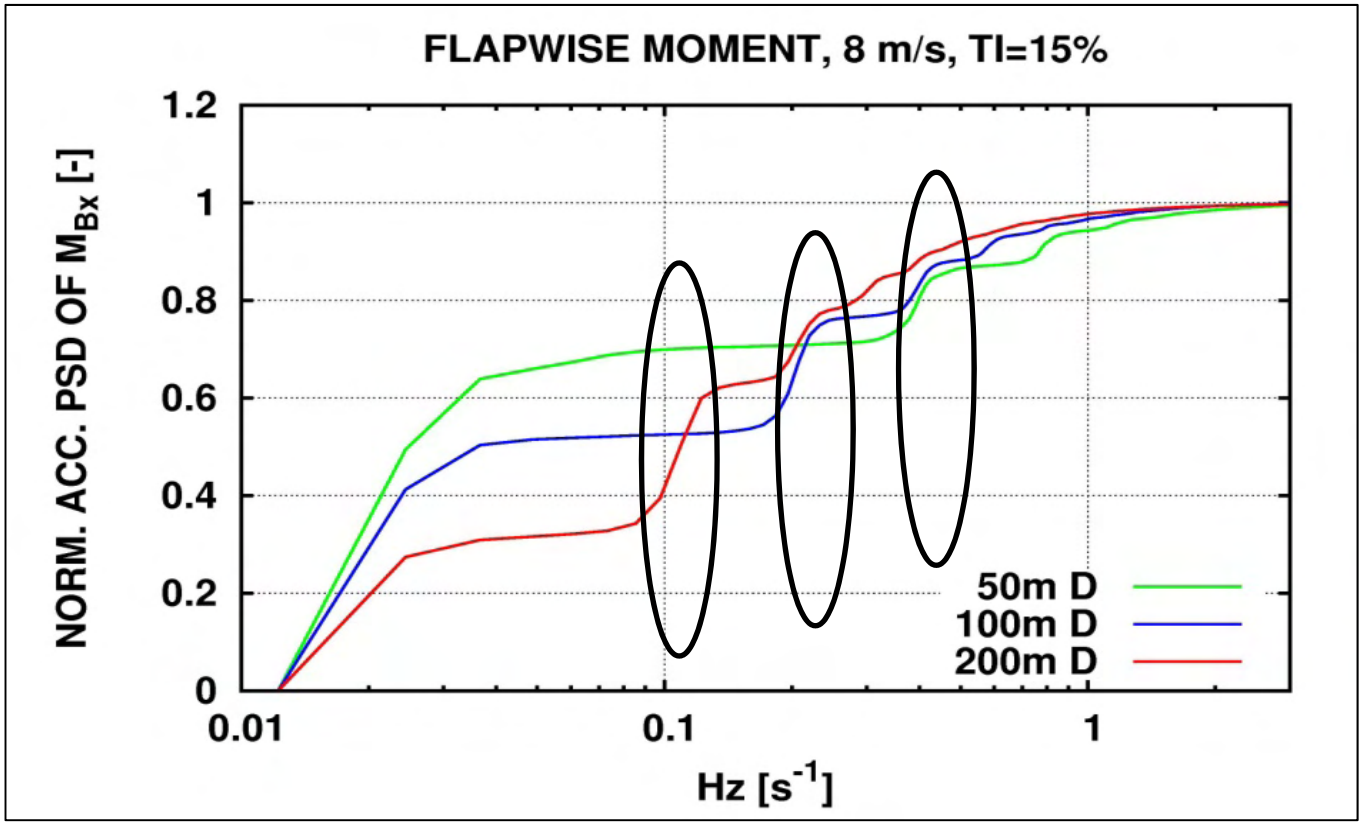

The influence on control is that a cyclic pitch control system, which alleviates 1p loads, will be relatively more efficient for increasing rotor size.

Results – impact on aerodynamic model requirements

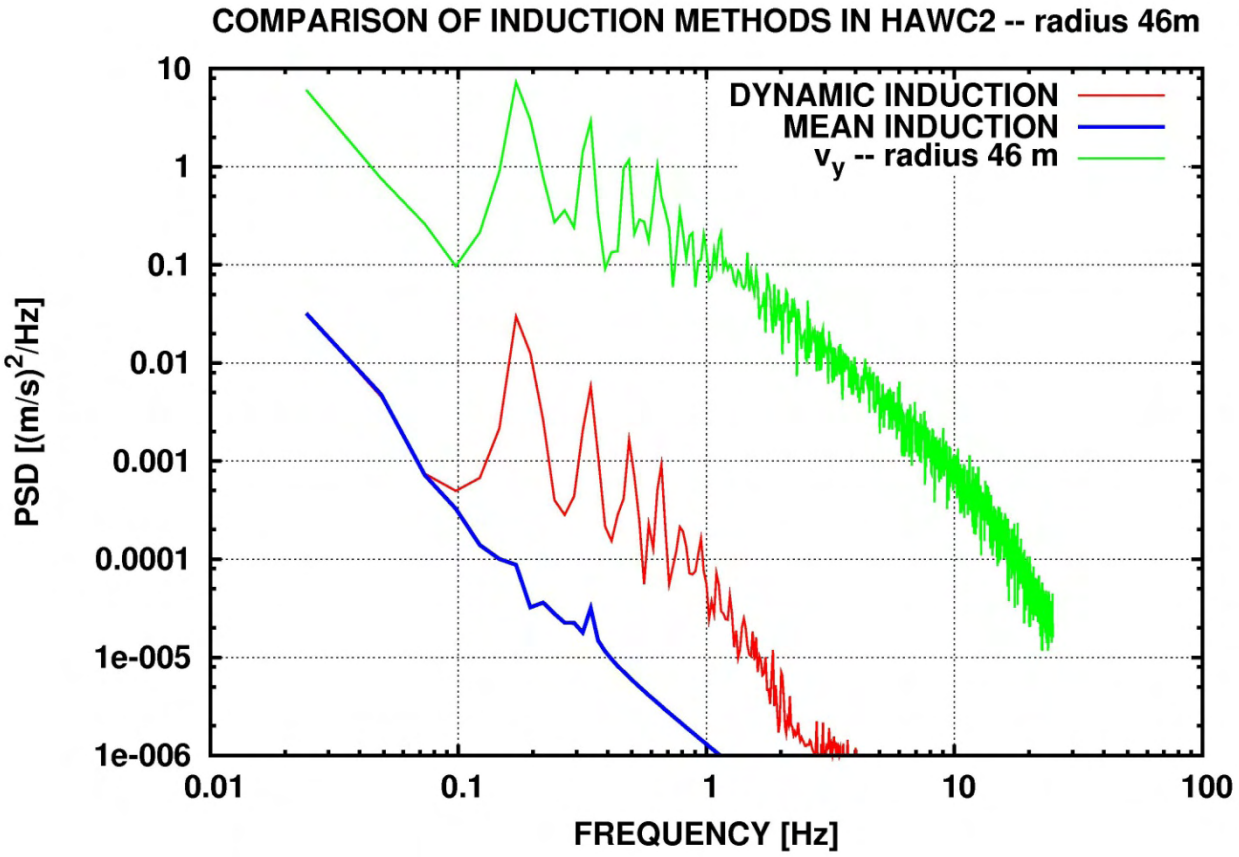

Results – impact on aerodynamic model requirements

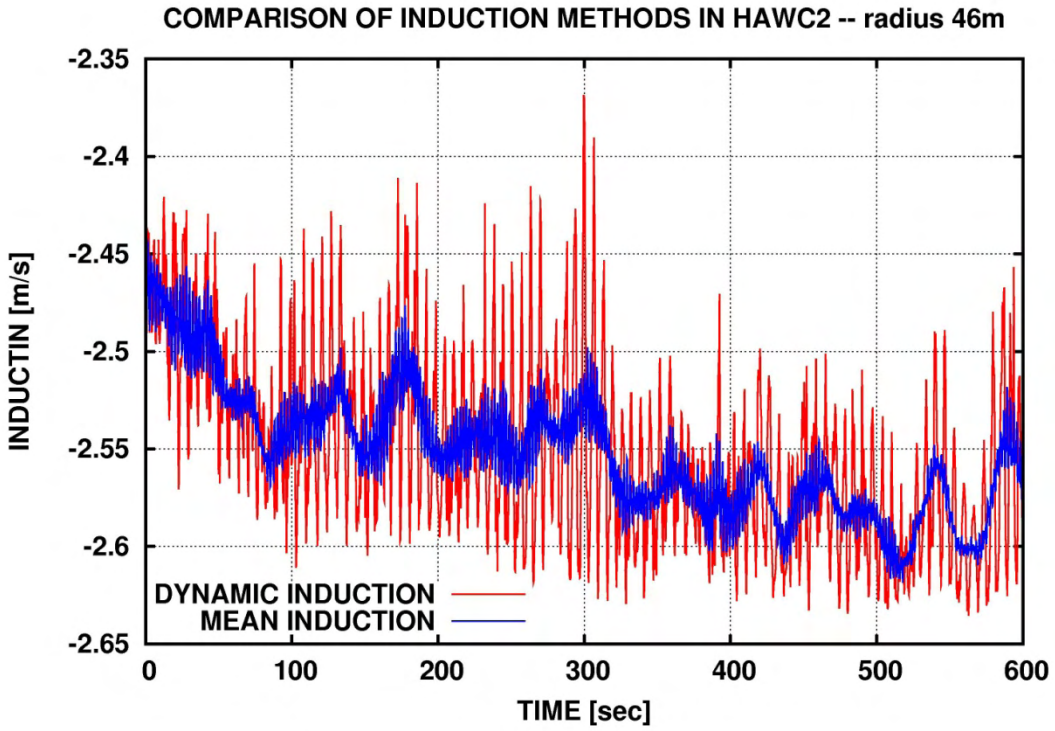

Impact on loading: slightly reduced fatt. loading with dynamic induction -- increased impact for e.g. half wake simulations with the Dynamic Wake Meandering model

Conclusions

- The upscaling of rotors has the influence that a bigger and bigger part of the turbulence is concentrated at 1p, 2p and 3p and the energy is taken from the spectrum at frequencies below 1p due to the spatial averaging effect of the rotor

- This means that it becomes more important to simulate more accurate the 1p, 2p variations of e.g. induced flow better as a bigger part of the total turbulence is centered on the p´s

- The quantities such as power and thrust which are integrated values over the rotor swept area show a decrease in dynamic content relative to the mean value as function of up-scaling due to this filtering effect

- Impact on control is that control algorithms directed to reduce 1p loads (cyclic pitch) should be better and better for increased rotor size

THANK YOU

5 Aerodynamic damping of tower vibrations

Aerodynamic damping of lateral tower vibrations

Bjarne S. Kallesøe
Niels N. Sørensen
Niels Troldborg

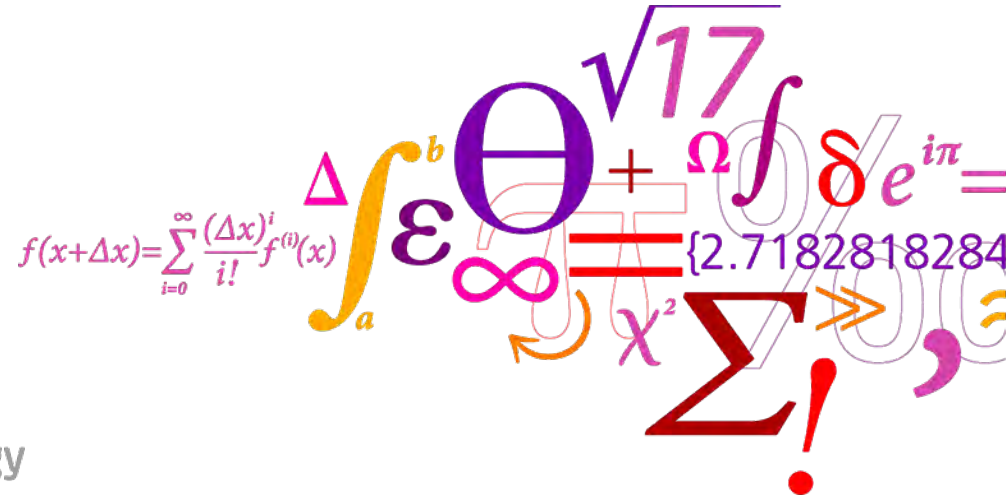

Risø DTU
National Laboratory for Sustainable Energy

Outline

- Motivation
- Aerodynamic damping of lateral rotor oscillations
- Aerodynamic damping of lateral tower mode

Motivation

- First lateral tower mode is excited by waves in some simulations cases leading to design giving loads
- Aeroelastic codes are based on BEM
- BEM predicted the aerodynamic damping of the lateral tower mode to be very low
- It has been questioned if BEM gives the correct aerodynamic forces for these lateral motions of the rotor
- **In this work** the aerodynamic work on lateral harmonic rotor motions are computed by both BEM and CFD (full rotor and actuator line)

Computational setup

- NREL 5 MW Reference turbine
- Pure lateral harmonic motion of the rotor
- 1 m amplitude, 0.3 Hz
- Three different wind speeds: 6 m/s, 12 m/s and 22 m/s
- Computational methods:
  - BEM, as implemented in HAWC2 (BEM)
  - Full rotor CFD in EllipSys3D (CFD)
  - Actuator line in EllipSys3D (AL)
- Integrating the lateral aerodynamic forces from each blade

Lateral aerodynamic forces

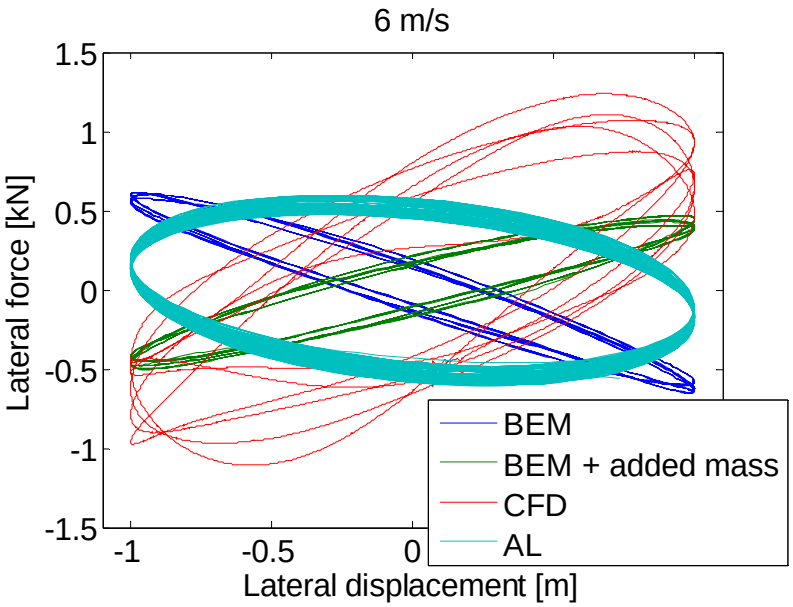

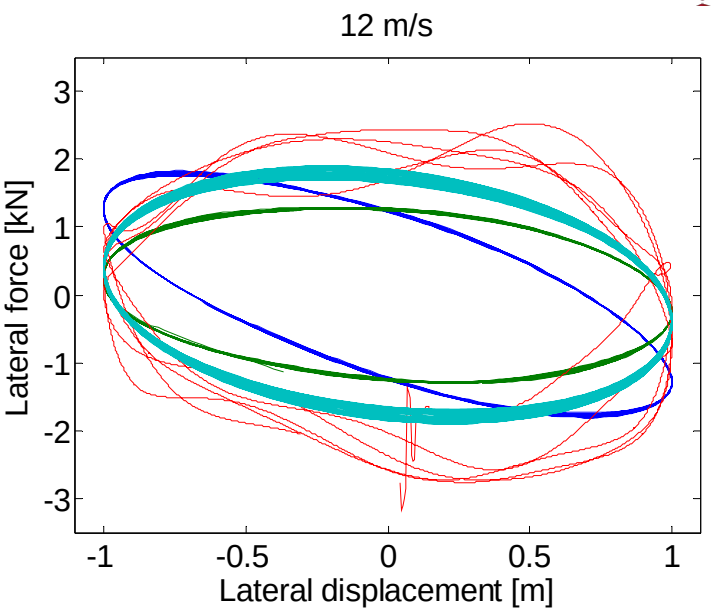

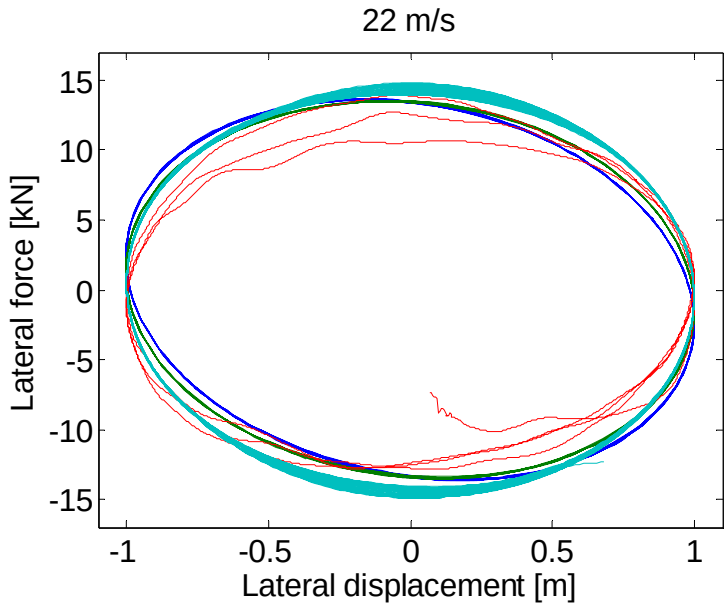

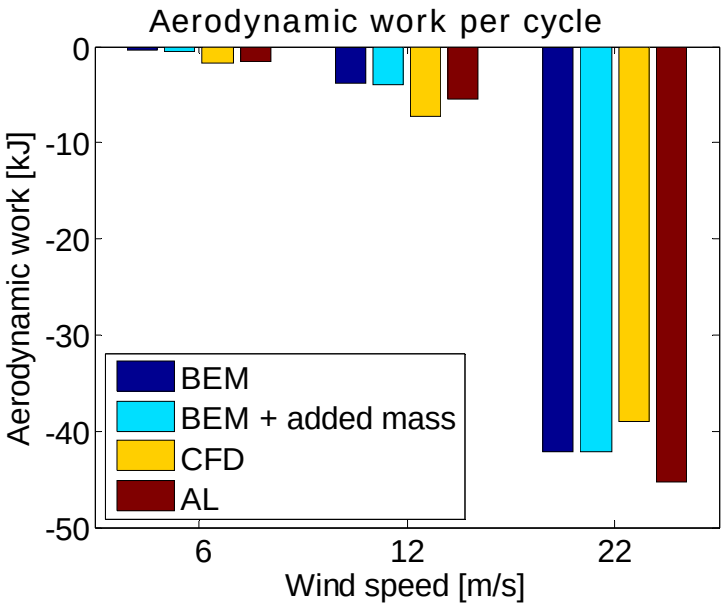

Aerodynamic work per cycle

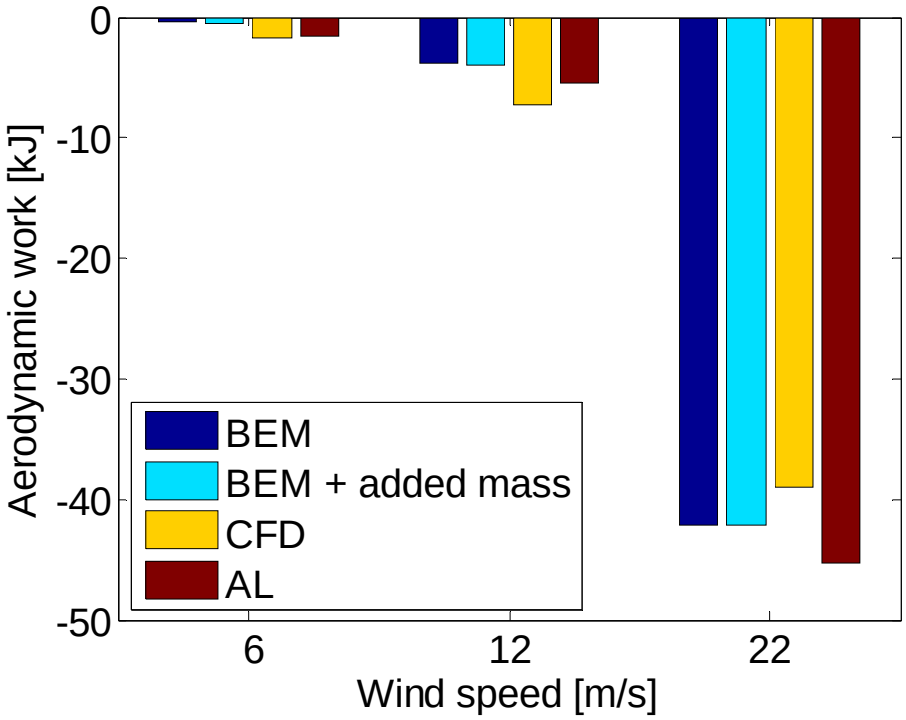

- Large relative differences for low wind speeds
- Good agreement for higher wind speeds
- Much smaller aerodynamic work for low wind speed than for high wind speed
- The added mass has no influence on the results!

Relating aerodynamic work to damping

Considering an one DOF modal description of the tower mode: $m\ddot{x} + c\dot{x} + kx = 0$

The aerodynamic work is given by: $W = \int_x^{x+x_T} c\dot{x}\mathrm{d}x$

Assuming harmonic oscillations: $x = A\sin(\omega t) \Rightarrow W = \int_t^{t+2\pi/\omega} cA^2\omega^2\cos^2(\omega t)\mathrm{d}t = A^2 c\omega^2\pi$

Whereby the relation between aerodynamic work and damping can be established: $\beta/W = 16A^2 f^3 m\pi^4 = A^2 C$

Tower top displacement at 22 m/s

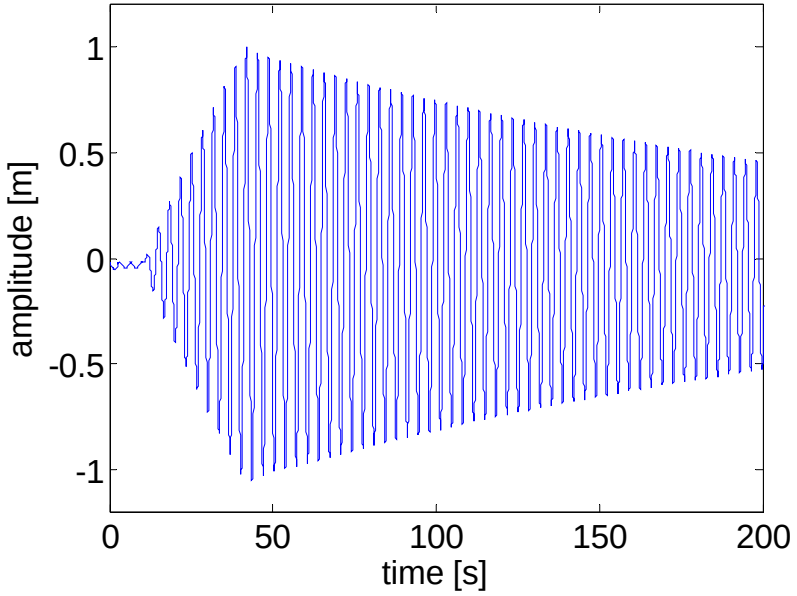

Relation between aero-work and damping

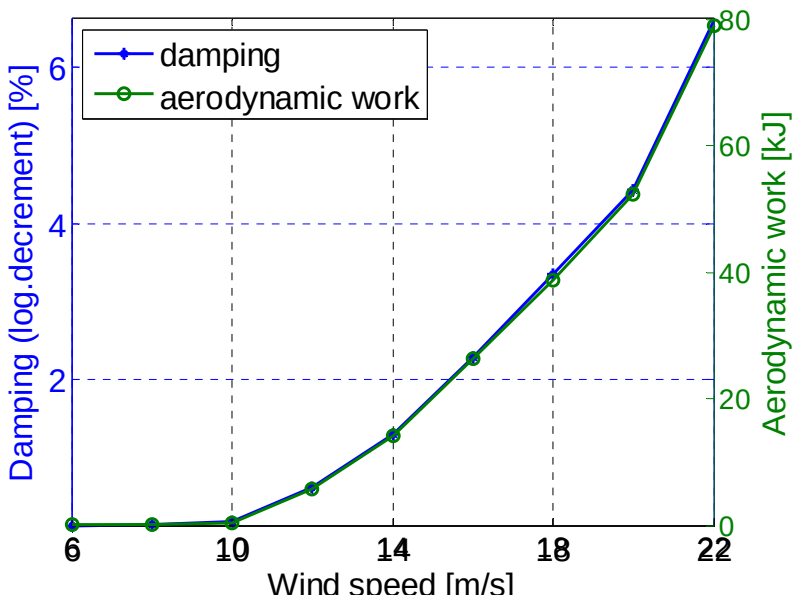

Aerodynamic damping of pure lateral tower mode

$$\beta = A^2 C W^{-1}$$

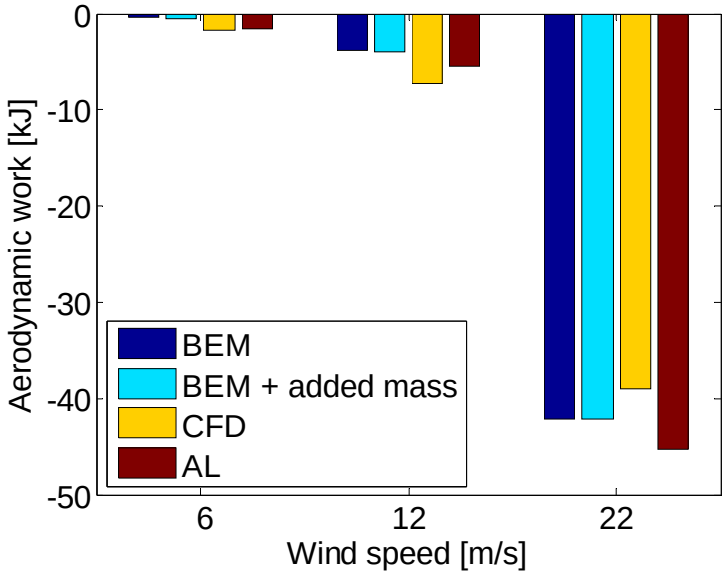

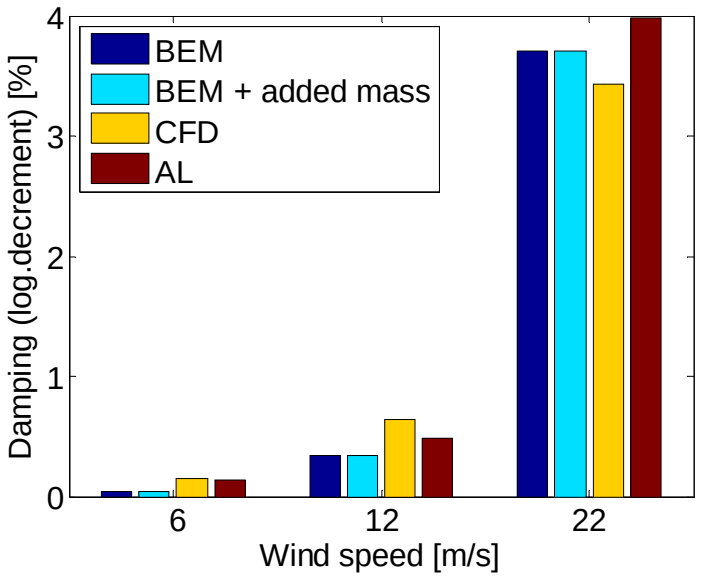

- The damping at 6 m/s is so small that the relative large difference between methods are of no particle interest

Aerodynamic damping of real lateral tower mode

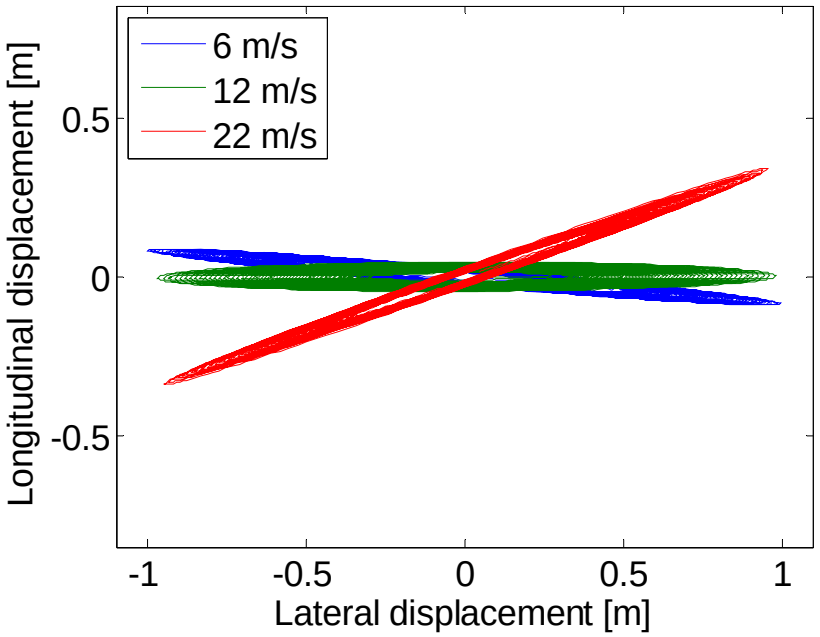

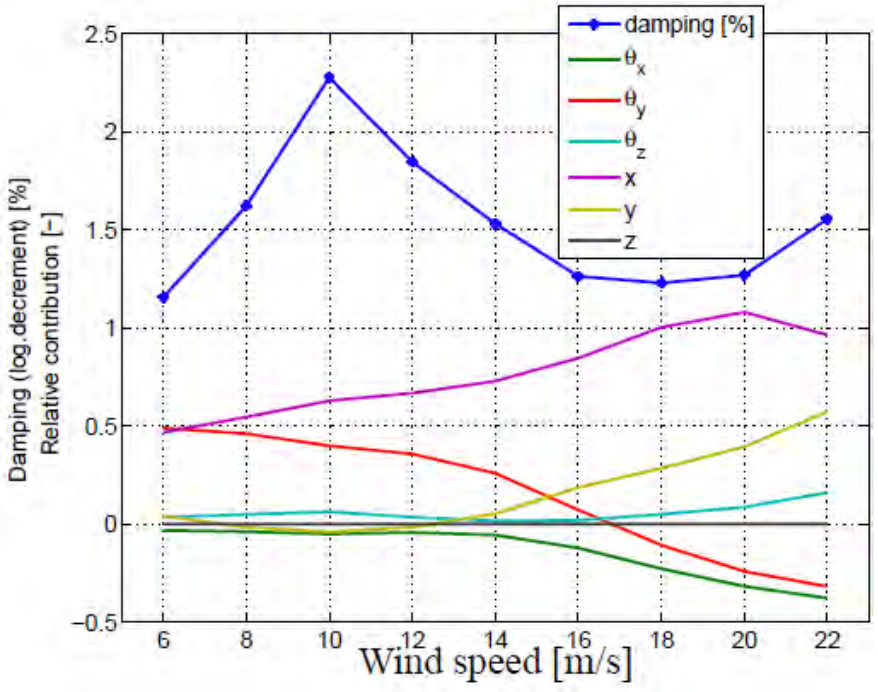

- Longitudinal component in the lateral tower mode
- Rotation of the rotor has a large contribution to the damping, this may be different with a free-free drive train model

Conclusion

- Some differences in lateral aerodynamic forces at low wind speeds
- But forces and damping is so low, so differences has no practical implications
- All computational method agree well for higher wind speeds, where force level is higher
- Aerodynamic damping of lateral tower vibrations are low (1-2 %)

6 Closed-loop aeroservoelastic analysis

Open- and closed-loop aero-servo-elastic analysis with HAWCStab2

Morten Hartvig Hansen and Ivan B. Sønderby

Outline:

- Aero-servo-elastic model in HAWCStab2
- Example: Tuning of collective and cyclic pitch controllers
- Reduced order models from HAWCStab2

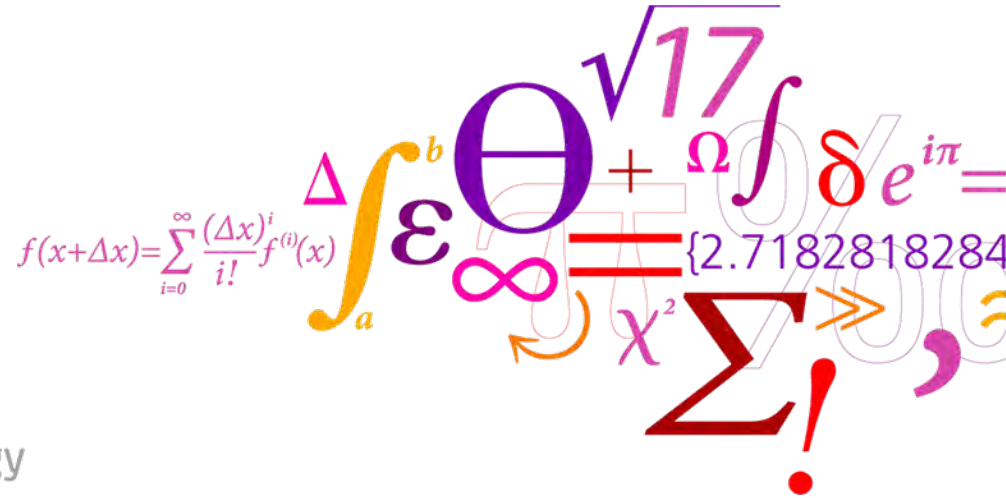

Risø DTU
National Laboratory for Sustainable Energy

Aeroelastic model

- Nonlinear kinematics based on co-rotational Timoshenko elements.
- Blade Element Momentum coupled with unsteady aerodynamics based on Leishman-Beddoes.
- Uniform inflow to give a stationary steady state that approximates the mean of the periodic steady state.
- Analytical linearization about the stationary steady state that include the linearized coupling terms from the geometrical nonlinearities.

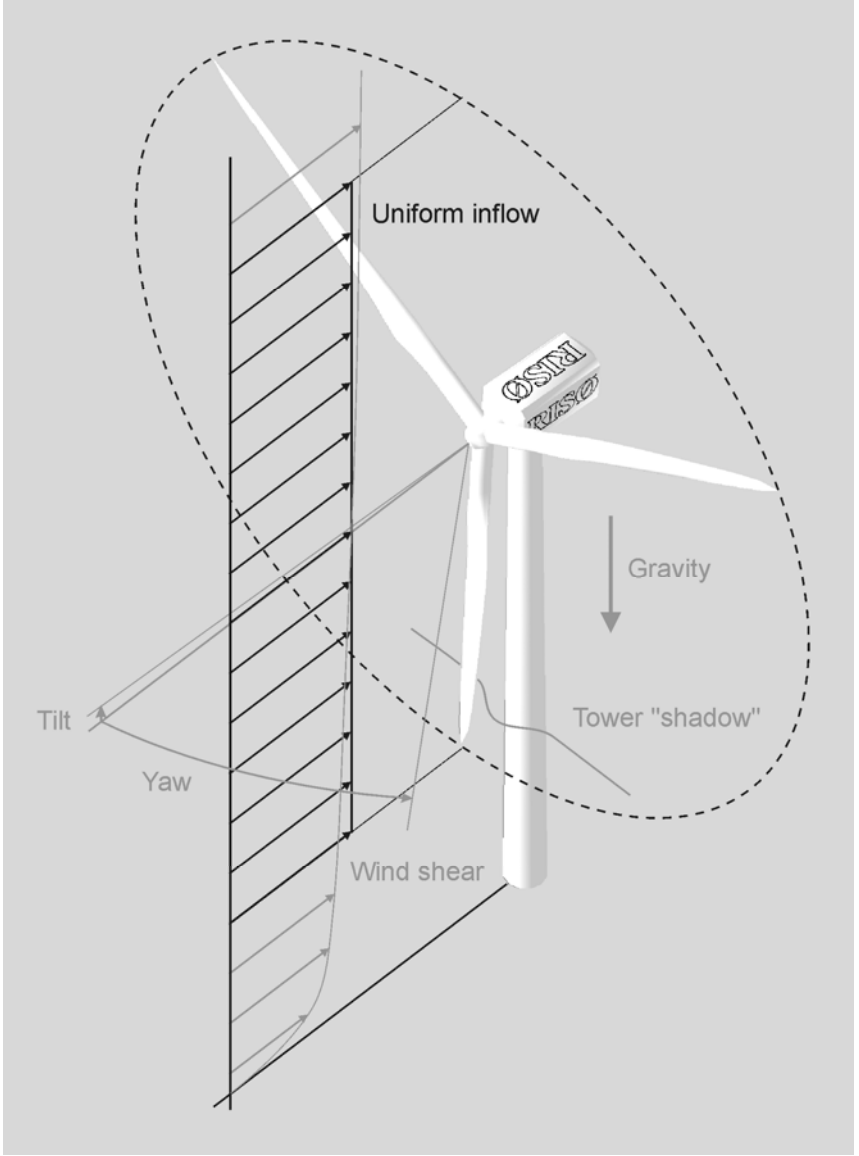

Linear open-loop aeroelastic equations

Structural mass
Structural damping
Gyroscopic forces
Aerodynamic damping
Elastic stiffness
Geometric stiffness of steady state force
Aerodynamic stiffness
Coupling to aerodynamic states

$$\mathbf{M}\ddot{\mathbf{x}}_s + (\mathbf{C} + \mathbf{G} + \mathbf{C}_a)\,\dot{\mathbf{x}}_s + (\mathbf{K} + \mathbf{K}_{sf} + \mathbf{K}_a)\,\mathbf{x}_s + \mathbf{A}_f\mathbf{x}_a = \mathbf{F}_s$$

$$\dot{\mathbf{x}}_a + \mathbf{A}_d\mathbf{x}_a + \mathbf{C}_{sa}\dot{\mathbf{x}}_s + \mathbf{K}_{sa}\mathbf{x}_s = \mathbf{F}_a$$

Time lags

Coupling to structural states

$\mathbf{x}_s$ = elastic and bearing degrees of freedom

$\mathbf{x}_a$ = aerodynamic state variables

$\mathbf{F}_s, \mathbf{F}_a$ = forces due to actuators and wind disturbance

Open-loop first order equations

$$\dot{\mathbf{x}} = \mathbf{A}\mathbf{x} + \mathbf{B}_{\text{act}}\mathbf{u} + \mathbf{B}_{\text{wind}} \begin{Bmatrix} v_{\text{mean}} \\ v_{\text{ver}} \\ v_{\text{hor}} \end{Bmatrix}$$

Closed-loop aero-servo-elastic equations

Additional output matrices

$$\dot{\mathbf{x}} = \mathbf{A}\mathbf{x} + \mathbf{B}_{\text{act}}\mathbf{u} + \mathbf{B}_{\text{wind}} \begin{Bmatrix} v_{\text{mean}} \\ v_{\text{ver}} \\ v_{\text{hor}} \end{Bmatrix}$$
$$\mathbf{y} = \mathbf{C}\mathbf{x} + \mathbf{D}\mathbf{u}$$

Additional (PID) controller states

$$\dot{\mathbf{x}}_c = \mathbf{A}_c\mathbf{x}_c + \mathbf{B}_c\mathbf{y}$$
$$\mathbf{u} = \mathbf{K}_g\mathbf{x}_c$$

Closed-loop equations

$$\begin{Bmatrix} \dot{\mathbf{x}} \\ \dot{\mathbf{x}}_c \end{Bmatrix} = \left[\begin{array}{c|c} \mathbf{A} & \mathbf{B}_{\text{act}}\mathbf{K}_g \\ \hline \mathbf{B}_c\mathbf{C} & \mathbf{A}_c + \mathbf{B}_c\mathbf{D}\mathbf{K}_g \end{array}\right] \begin{Bmatrix} \mathbf{x} \\ \mathbf{x}_c \end{Bmatrix} + \mathbf{B}_{\text{wind}} \begin{Bmatrix} v_{\text{mean}} \\ v_{\text{ver}} \\ v_{\text{hor}} \end{Bmatrix}$$
$$\mathbf{y} = \mathbf{C}\mathbf{x} + \mathbf{D}\mathbf{K}_g\mathbf{x}_c$$

Example: Collective and cyclic pitch controllers

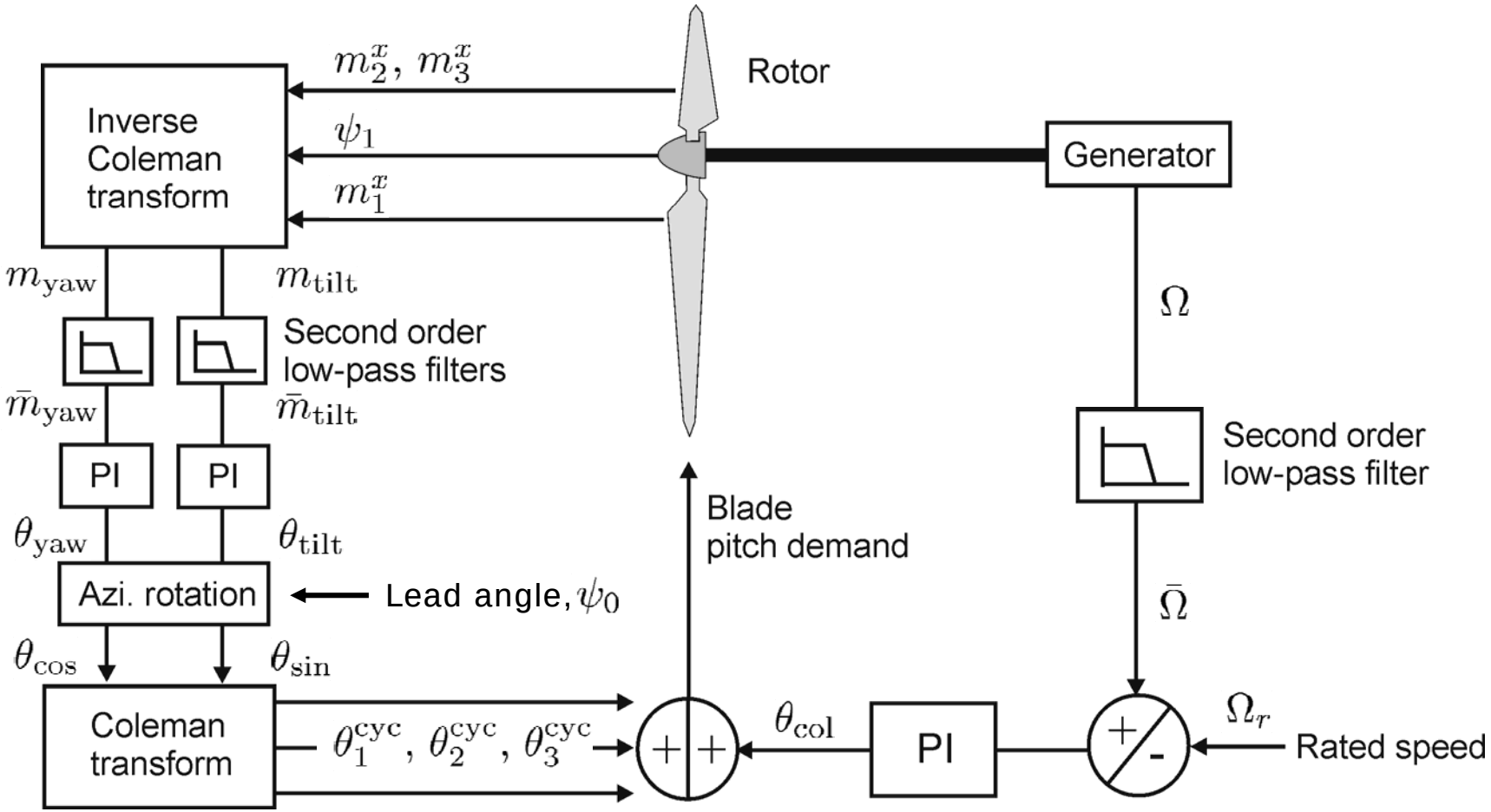

Closed-loop aero-servo-elastic equations

$$\dot{\mathbf{x}} = \mathbf{A}\mathbf{x} + \mathbf{B}_{\text{act}} \begin{Bmatrix} Q_{\text{gen}} \\ \theta_{\text{col}} \\ \theta_{\cos} \\ \theta_{\sin} \end{Bmatrix} + \mathbf{B}_{\text{wind}} \begin{Bmatrix} v_{\text{mean}} \\ v_{\text{ver}} \\ v_{\text{hor}} \end{Bmatrix}$$

$$\underbrace{\dot{\mathbf{x}}_c = \mathbf{A}_c\mathbf{x}_c + \mathbf{B}_c\mathbf{y}}_{\text{Filters and integrators}} \qquad \mathbf{y} = \begin{Bmatrix} \Delta\Omega \\ m_{\text{tilt}} \\ m_{\text{yaw}} \end{Bmatrix} = \mathbf{C}\mathbf{x}$$

Tuning parameters

P-gain on speed	k_P
I-gain on speed	k_I
Lead angle	ψ_0
P-gain on cyclic	k_P^{c}
I-gain on cyclic	k_I^{c}
Filter frequencies	
Filter damping ratios	

$$\mathbf{x}_c = \left\{ \Delta\bar{\Omega} \quad \Delta\dot{\bar{\Omega}} \quad \phi \quad \bar{m}_{\text{tilt}} \quad \dot{\bar{m}}_{\text{tilt}} \quad M_{\text{tilt}} \quad \bar{m}_{\text{yaw}} \quad \dot{\bar{m}}_{\text{yaw}} \quad M_{\text{yaw}} \right\}^T$$

$$\begin{Bmatrix} Q_{\text{gen}} \\ \theta_{\text{col}} \\ \theta_{\cos} \\ \theta_{\sin} \end{Bmatrix} = \begin{bmatrix} 0 & 0 & 0 & 0 & 0 & 0 & 0 & 0 & 0 \\ k_P & 0 & k_I & 0 & 0 & 0 & 0 & 0 & 0 \\ 0 & 0 & 0 & k_P^{\text{c}} \cos\psi_0 & 0 & k_I^{\text{c}} \cos\psi_0 & k_P^{\text{c}} \sin\psi_0 & 0 & k_I^{\text{c}} \sin\psi_0 \\ 0 & 0 & 0 & -k_P^{\text{c}} \sin\psi_0 & 0 & -k_I^{\text{c}} \sin\psi_0 & k_P^{\text{c}} \cos\psi_0 & 0 & k_I^{\text{c}} \cos\psi_0 \end{bmatrix} \mathbf{x}_c$$

Lead angle from open-loop analysis

$$\theta_{\cos} \rightarrow \begin{Bmatrix} m_{\text{tilt}} \\ m_{\text{yaw}} \end{Bmatrix}$$

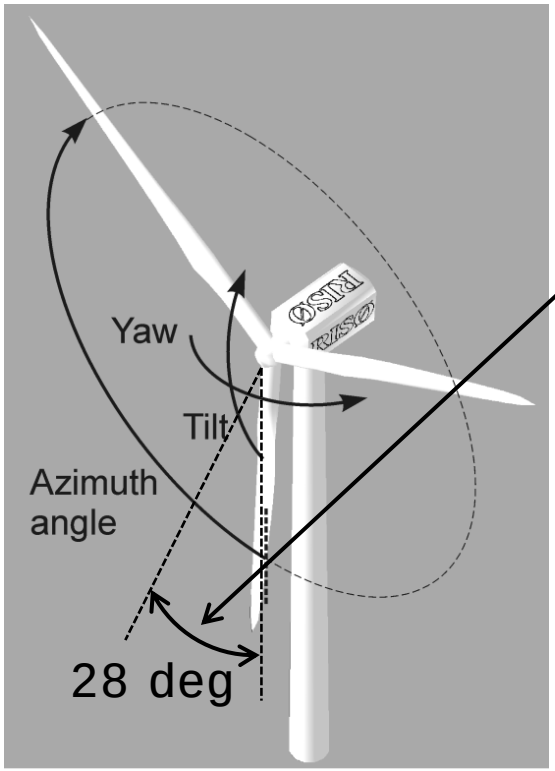

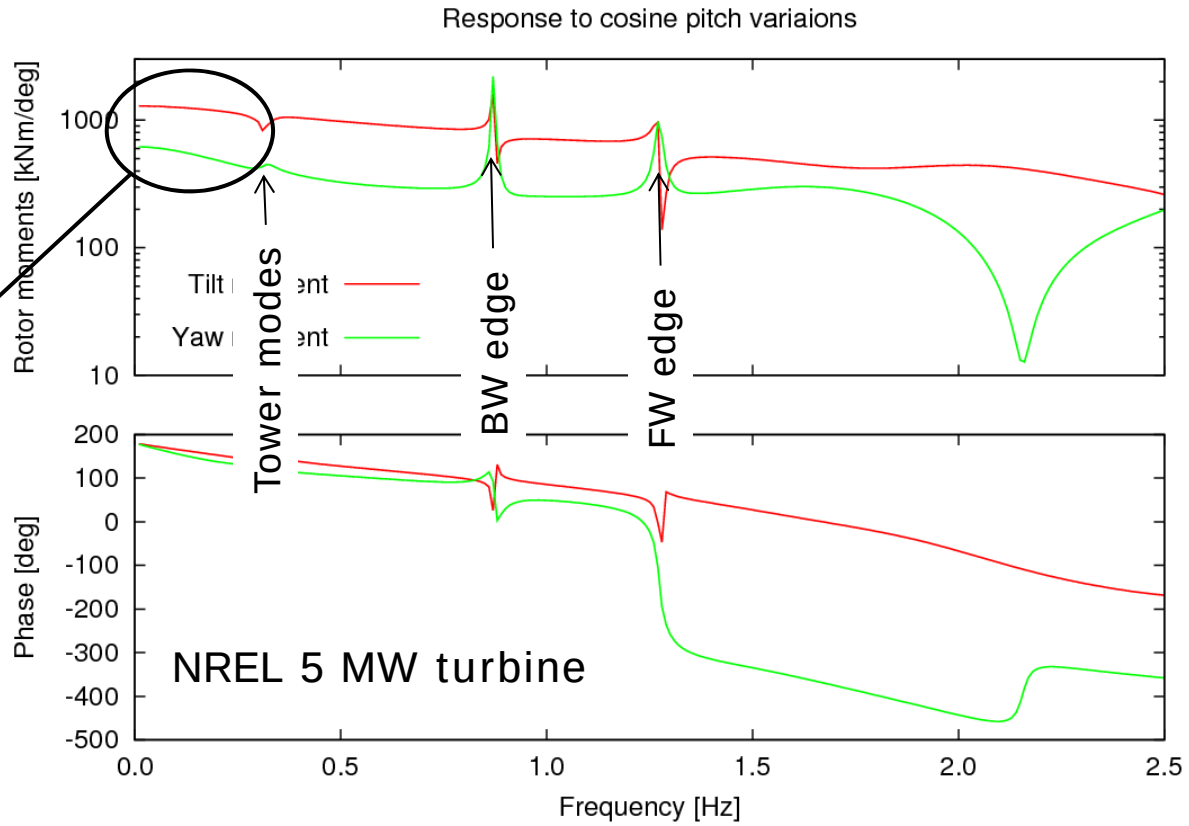

Open and closed-loop wind shear response

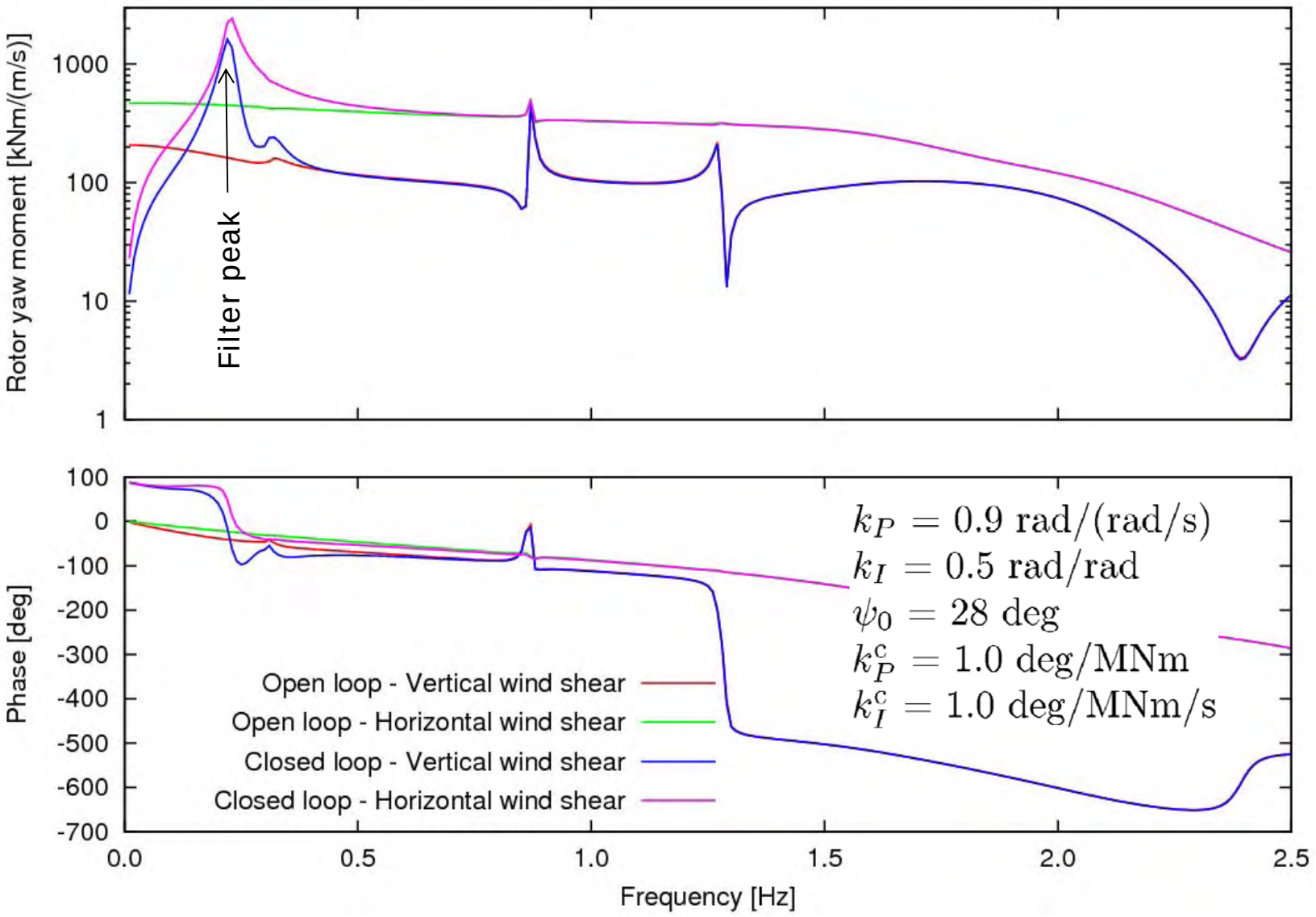

Aero-servo-elastic modes and damping

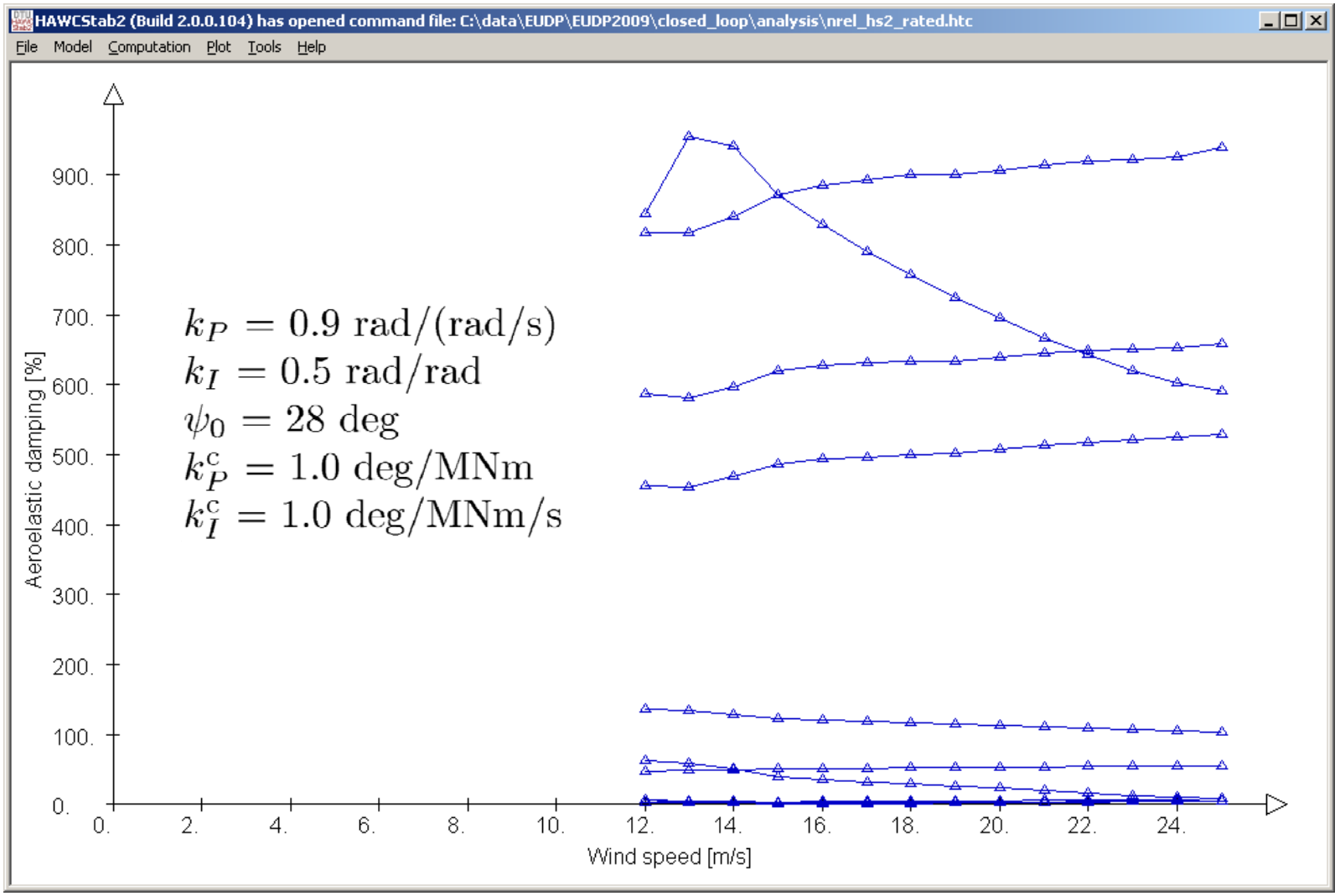

HAWC2 simulations at 17 m/s with NTM

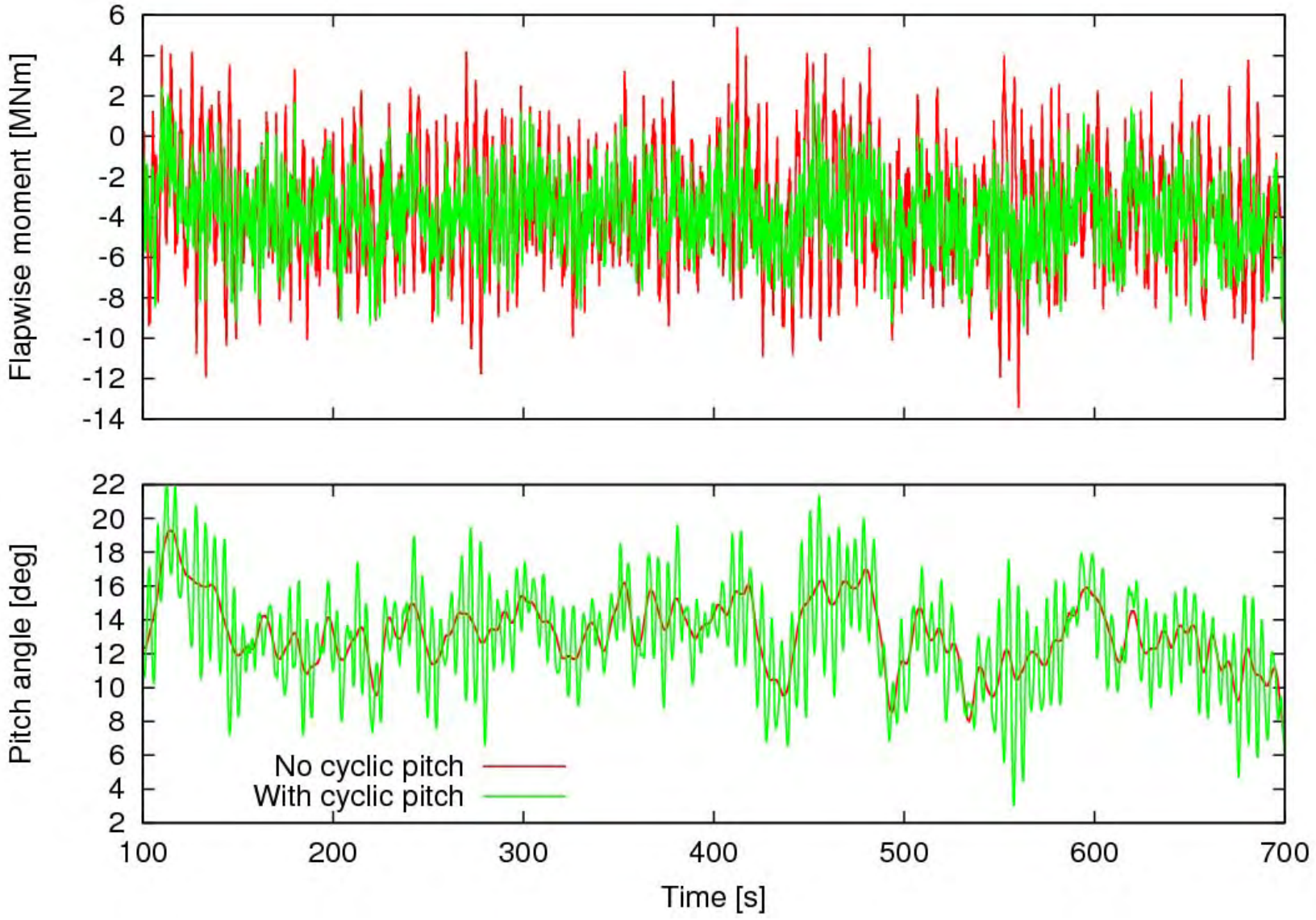

Cyclic controller induced instability

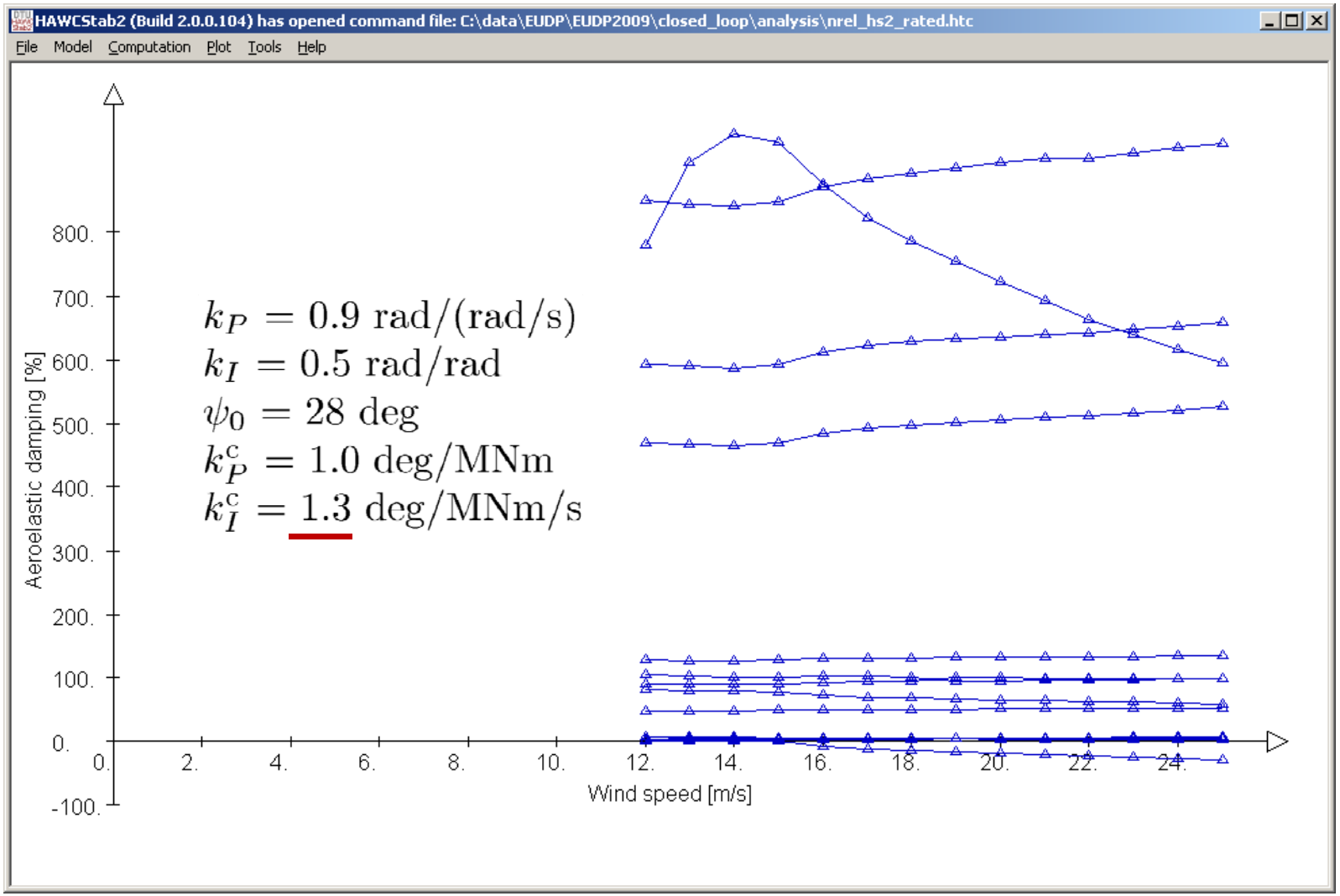

Validation of transfer functions with HAWC2

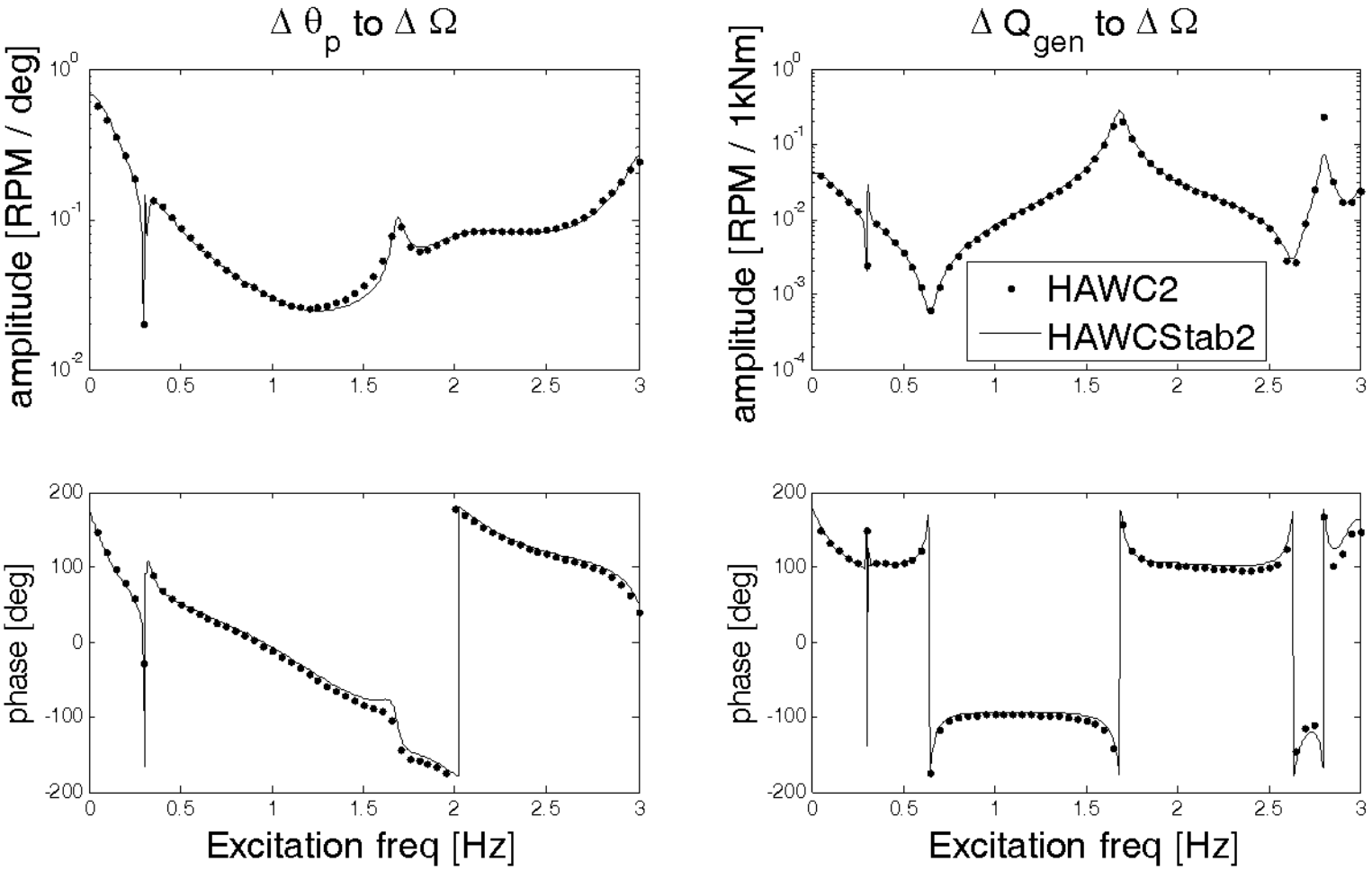

Validation of low order models

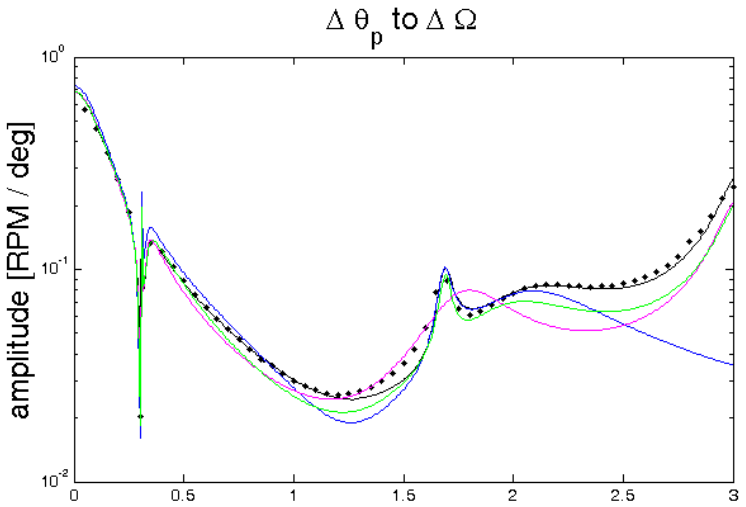

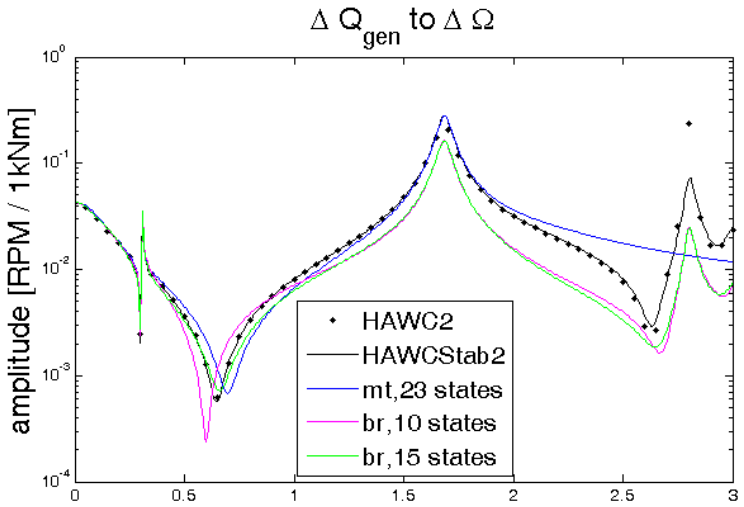

Methods: “mt” = Modal truncation and “br” = Balanced residualization

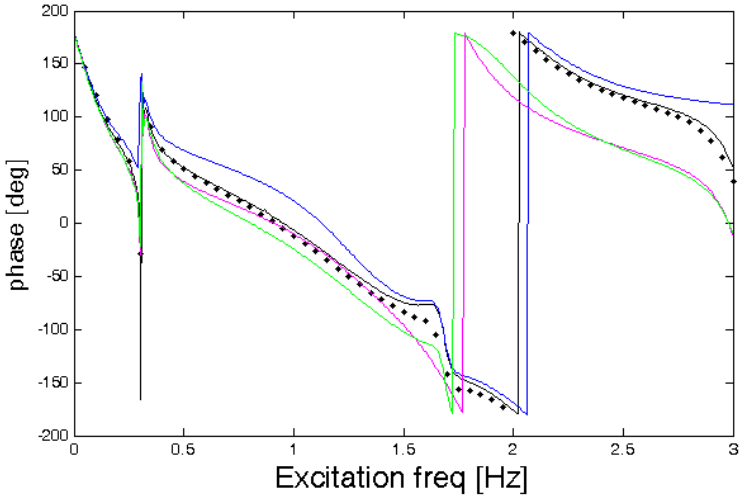

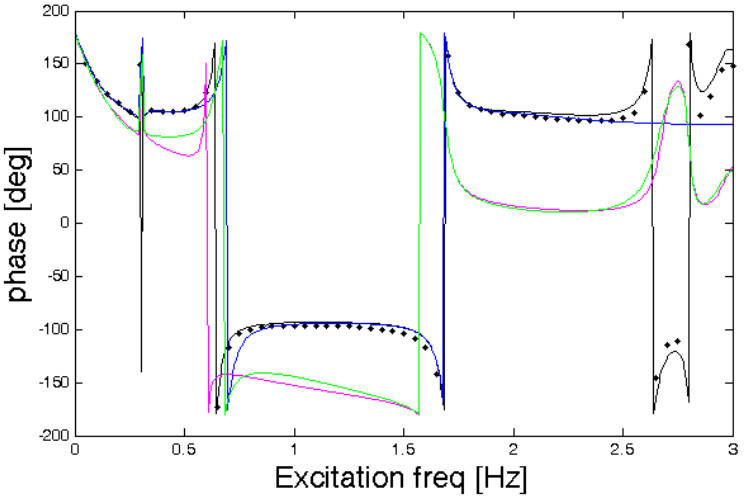

Summary

- HAWCStab2 can be used for performing open-loop and closed-loop eigenvalue and frequency-domain analysis of three-bladed turbines:
  - Controller equations are still hardcoded. A suitable interface is under consideration, for example based on DLLs as in HAWC2.
  - Full order analyses can be performed both inside or outside HAWCStab2 by writing out system matrices for each operation point.
  - Reduced order modelling capabilities are currently performed outside HAWCStab2. Automated procedures for obtaining models with desired details will be implemented in HAWCStab2, or in Matlab scripts.
- HAWCStab2 is a common tool for both control engineers and mechanical engineers:
  - It can provide first-principle models for model-based controllers.
  - It can explain phenomena observed in load simulations.

7 Thick, flatback, high-lift multi-element airfoil

Design and test of a thick, flatback, high-lift multi-element airfoil

Frederik Zahle, Mac Gaunaa, Christian Bak, Niels N. Sørensen

Wind Energy Division · Risø DTU

27 October 2011

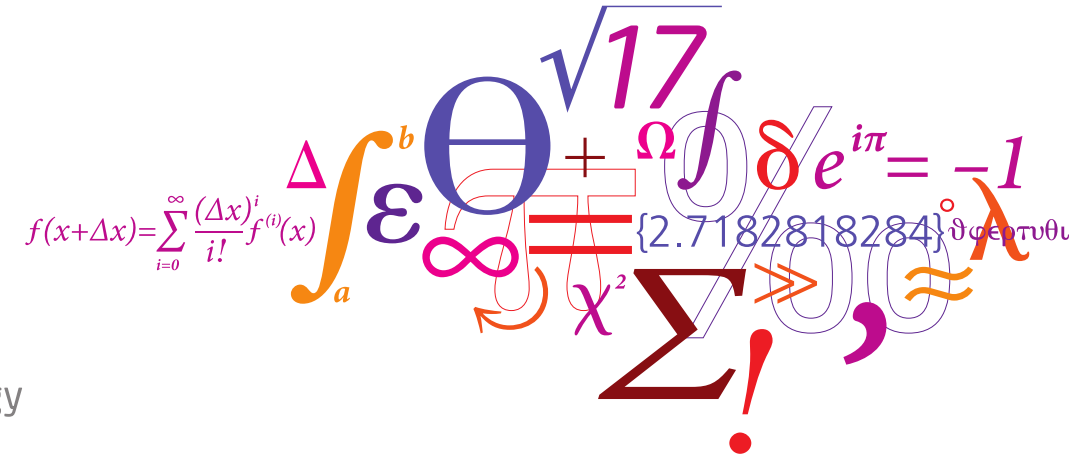

Risø DTU
National Laboratory for Sustainable Energy

Introduction

The aim of this work has been to design and test a high lift airfoil for validation of numerical codes.

Airfoil properties

- Two elements: Main airfoil and a slat.
- 40% thick main element, flatback.
- 30% chord slat.
- Lift coefficient > 3

This presentation

- Numerical optimization method used to design the multi-element airfoil.
- Final design and predicted performance of the multi-element airfoil.
- Wind tunnel setup.
- Preliminary comparisons of numerical results and wind tunnel measurements.
- Flow visualization.

Why are we interested in high-lift airfoils for the root?

- Madsen et al. showed that the neglection of the rotational effects in standard BEM formulations could potentially lead to designs with a less than optimal power production, since the root was not loaded sufficiently.
- Johansen et al. designed a rotor for maximum power production where a C_P of 0.515 was achieved.
- This rotor had significantly higher loading towards the root than conventional rotors.
- Main drawback: Very large root chords.
- Gaunaa et al. explore the subject of high root loading further and show that at 20% radius the loading should be approx. 1.7 times that of the reference rotor used.

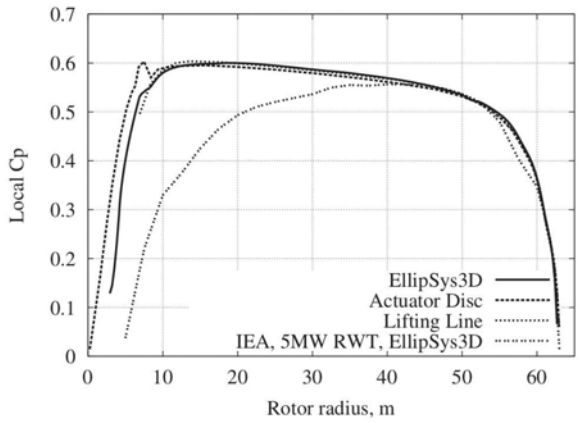

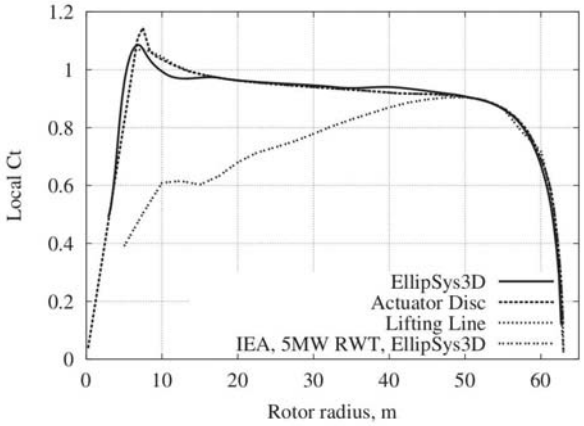

Why multi-element airfoils?

Motivation

- One way to achieve high loading is to increase the chord.
- This is not desirable for many reasons: e.g. increased extreme loads, limitations on transport height, material costs.
- Multi-element airfoils can produce high lift coefficients even with thick airfoil sections.
- With very high lift coefficients the chord can be reduced even further, reducing extreme loads.

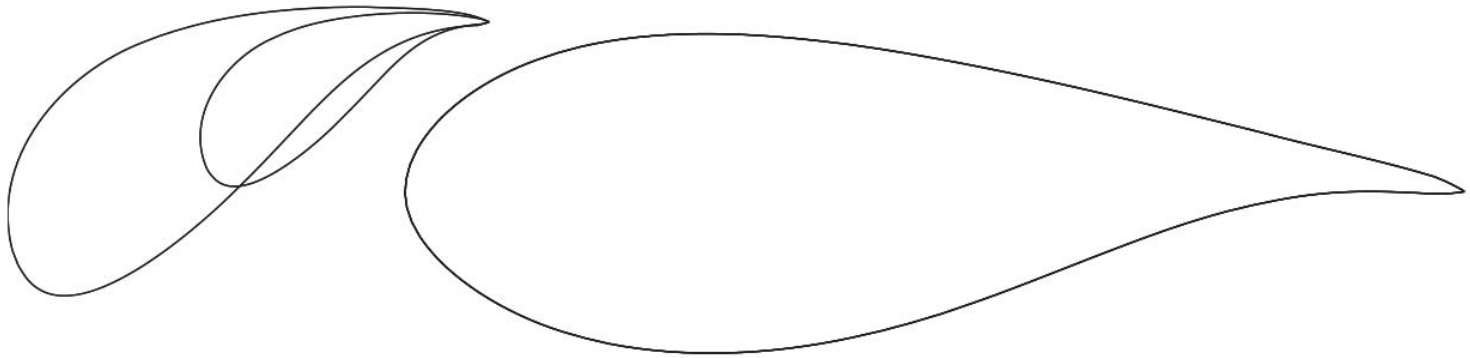

How to design a multiple element airfoil?

Challenge

- Current in-house airfoil design codes were not adapted to handle multiple elements.
- Gaunaa et al. used a panel code to optimize the shape of a slatted airfoil.
- Performance subsequently evaluated using 2D CFD.
- Problem: panel code not sufficiently accurate.
- Our choice: Optimization code coupled with the 2D CFD solver Ellipsys2D.

Design Method

Optimization

- The optimization method developed for this work was programmed in Matlab.
- Bounded Nelder-Mead Simplex (`fminsearchbnd`).
- Ellipsys2D is used to evaluate the cost function.

Cost function

Composed of three factors:

- The function A_1 which evaluates the lift-to-drag ratio at the target angle of attack.
- The function A_2, which seeks to maximize the lift coefficient at some angle of attack, which the optimizer is free to tune.
- A penalty function which forces the optimizer towards achieving the desired lift coefficient, $C_{l,target}$, at the specified target angle of attack, α_{target}.

Design Method

Cost function

$$CostFun = -Penalty\,(A_1 + A_2) \tag{1}$$

$$A_1 = \frac{C_l(\alpha_{target})}{C_d(\alpha_{target})} \cdot \frac{1}{(C_l/C_d)_{target,ref}} \cdot K_{optim} \tag{2}$$

$$A_2 = \frac{C_l(\alpha)}{C_{l,maxref}} \cdot (1 - K_{optim}) \tag{3}$$

$$Penalty = exp\left(-\frac{(C_l(\alpha_{target}) - C_{l,target}))^2}{2\sigma_{penalty}}\right) \tag{4}$$

K_{optim} is a factor which biases the cost function towards either the target lift coefficient or lift-to-drag ratio.

- In this work there is no target angle of attack. C_l was maximized while ensuring high lift-to-drag ratio at $\alpha_{C_{l-max}}$ -5 deg.
- For each optimization iteration two design evaluations were thus needed.

Design variables

- Angle of attack,
- Position of slat trailing edge measured as:
  - Surface distance along main aerofoil surface from leading edge,
  - Normal distance from main aerofoil surface to slat trailing edge.
- Slat angle relative to main aerofoil.
- Slat camber (parabolic curve).

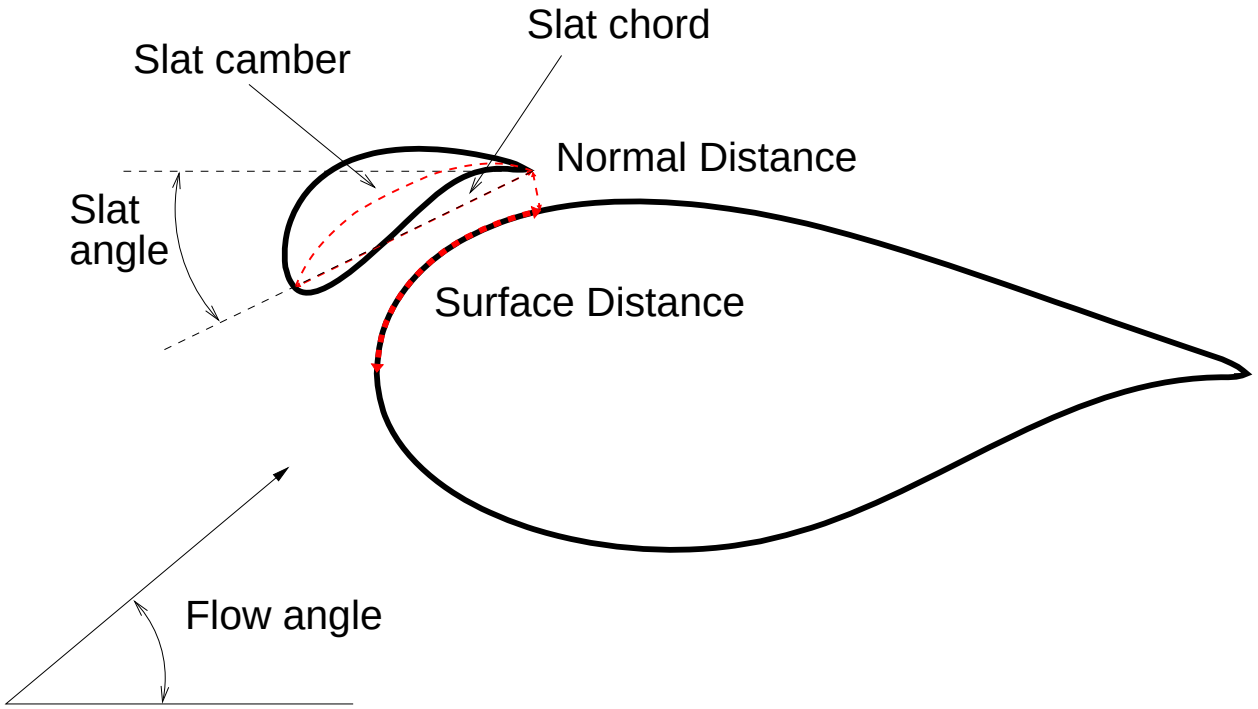

Design evaluation using EllipSys2D

Mesh generation of multi-elements has been automized using Bash/fortran/HypGrid2D.

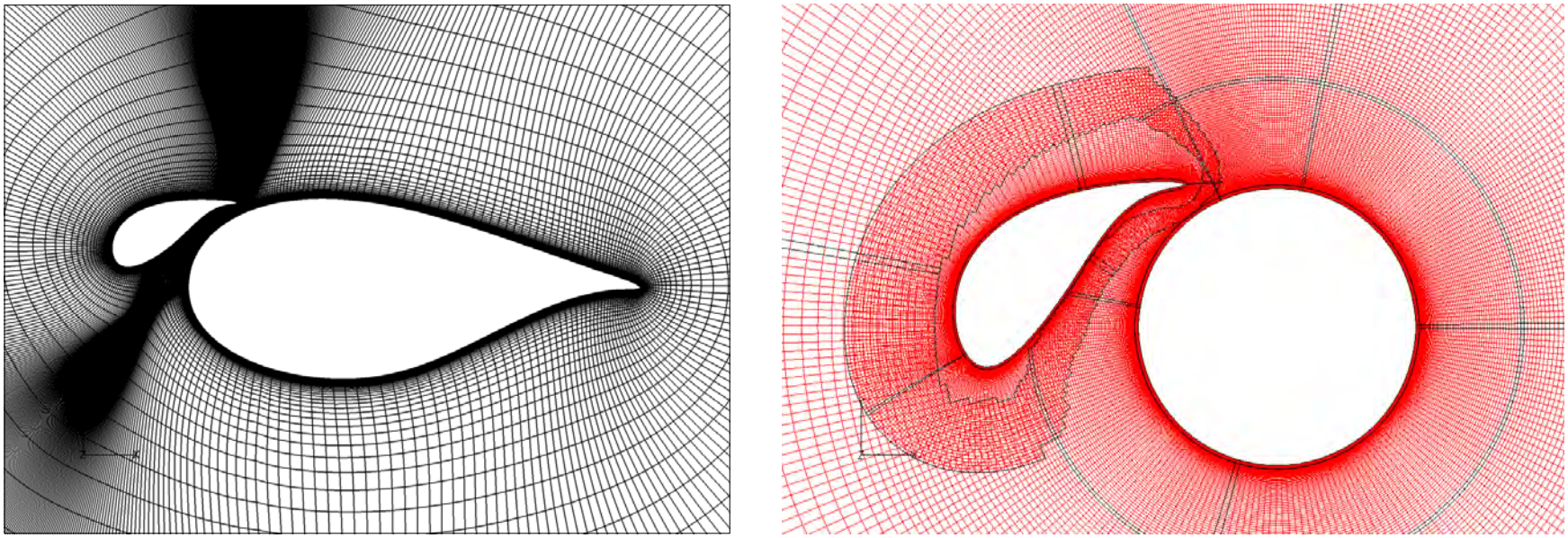

Figure: Typical meshes generated using the automated meshing scripts, left: standard patched grid, right: overset grid.

Optimization Flowchart

- Communication between Matlab and EllipSys2D was handled from a series of Bash scripts that read files written by each code.
- Matlab ran in the background, outputting for each optimization step a file containing the coordinates of the slat as well as the required angle of attack.
- EllipSys was executed in parallel for maximum speed, and subsequently returned values of C_l and C_d for the given configuration.
- Optimization was converged in approximately 100 optimization iterations, i.e. 200 EllipSys2D evaluations. $\approx$ 10 hours on 19 CPUs.

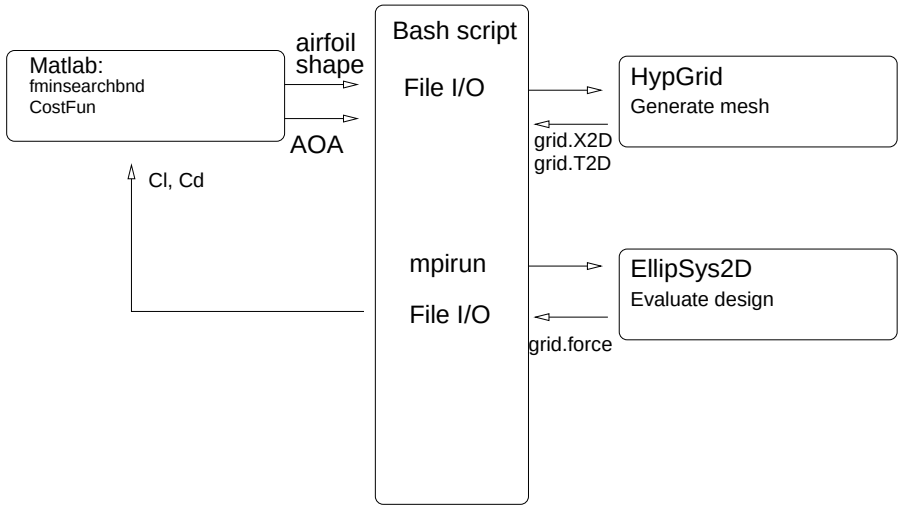

Flaback Airfoil

The present study is based on the FFA-W3-360 aerofoil which was modified in the following manner:

- Increased thickness from 36% chord to 40% chord,
- Opening of trailing edge from 3.6% chord to 5.6% chord.

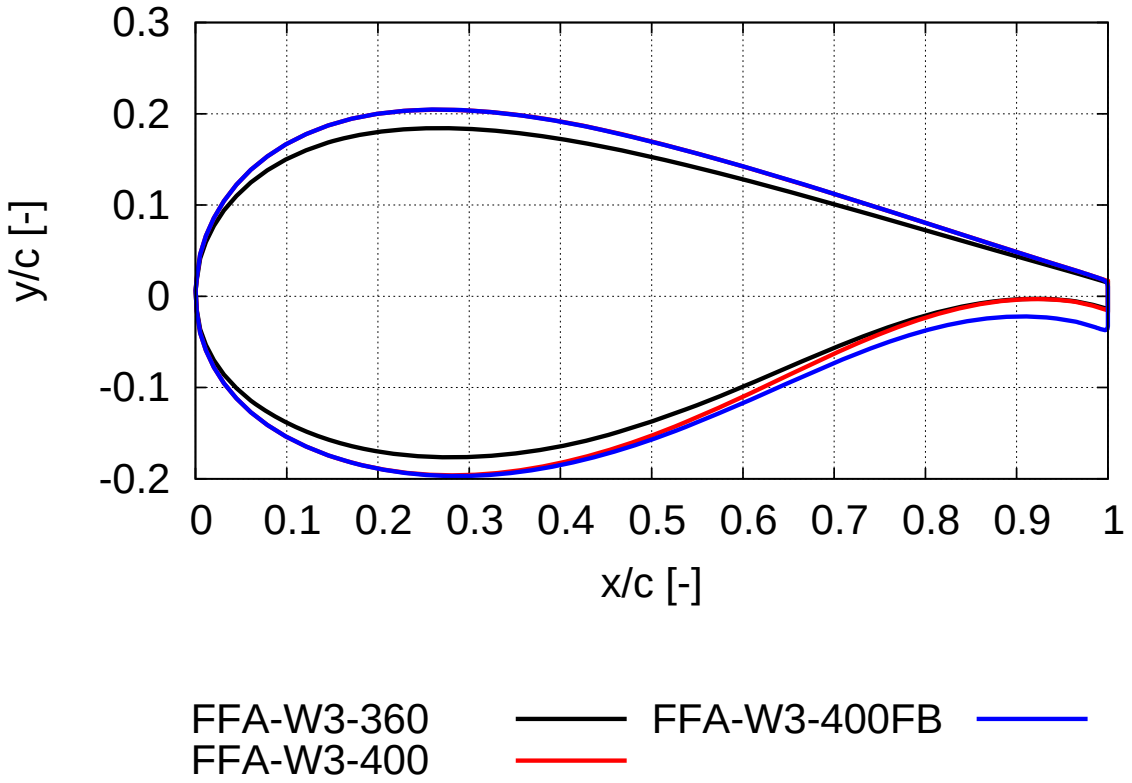

Flaback Airfoil Performance

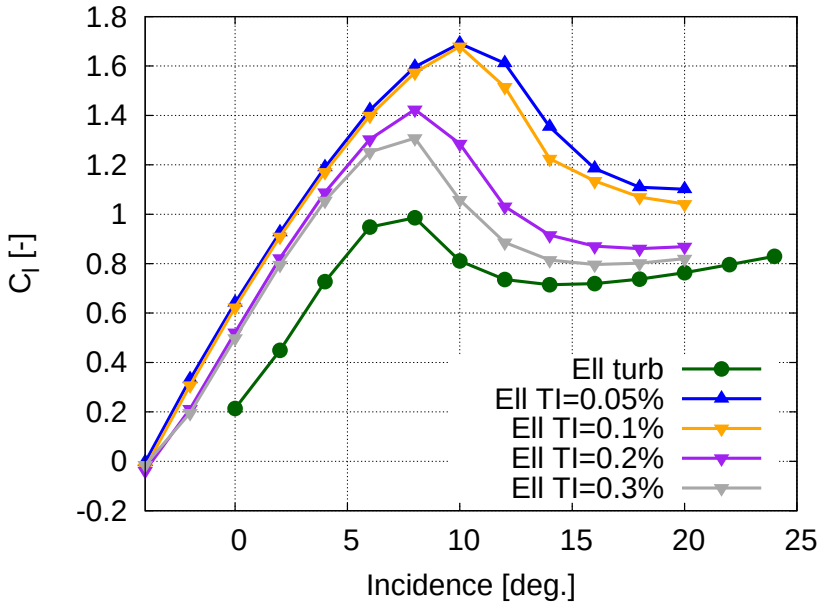

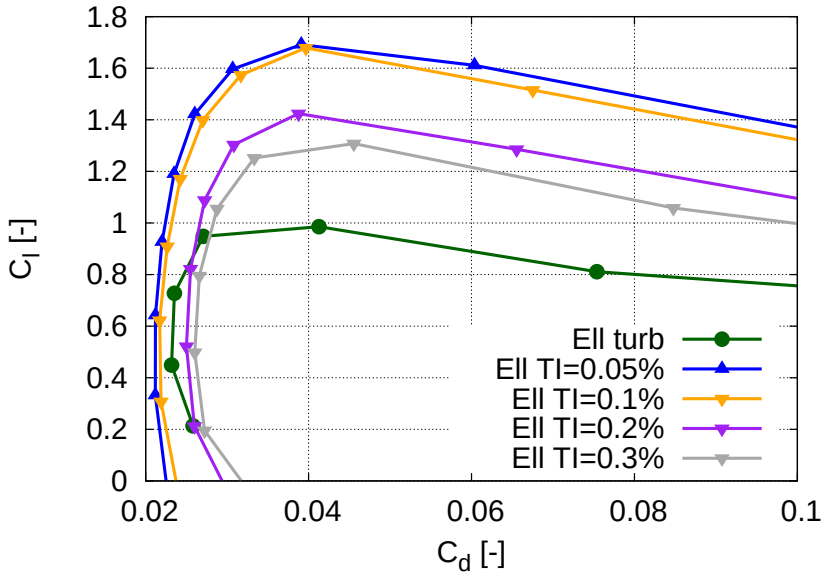

Slat Optimization

- Chosen slat baseline airfoil: FFA-W3-360.
- Chord length relative to main airfoil: 30%.

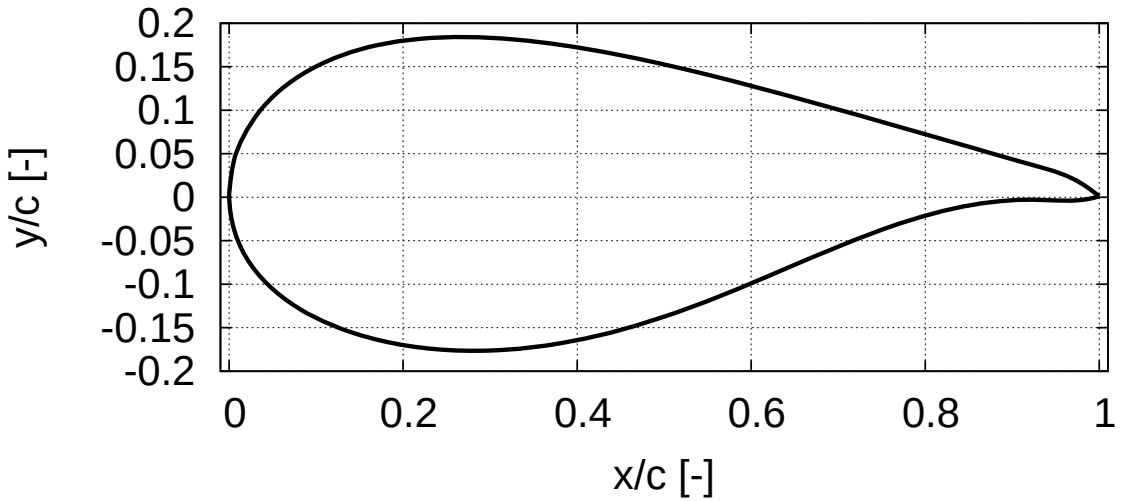

Slat Optimization

- Four optimizations with different values of k_{optim} were carried out.

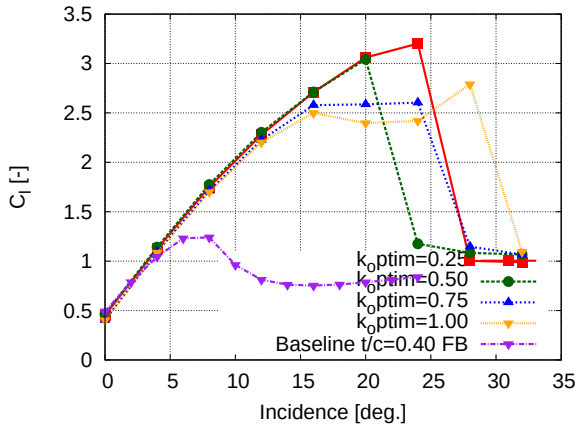

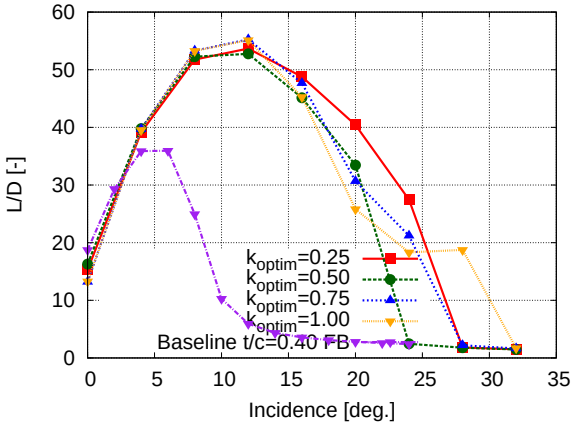

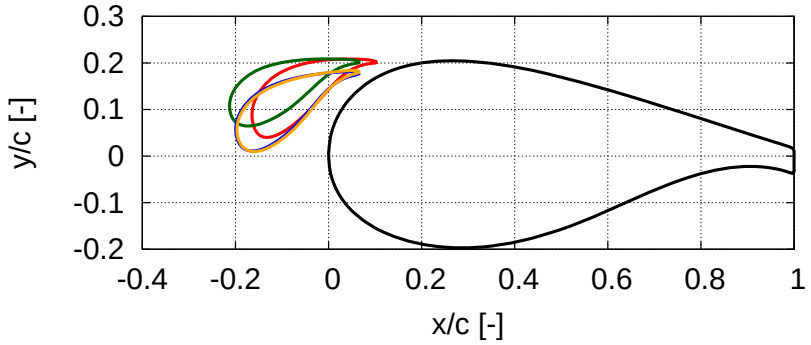

koptim=0.25
koptim=0.50
koptim=0.75
koptim=1.00

Frederik Zahle et al.
Risø DTU

Slat Optimization - final design

K_{optim}=0.25 optimization yielded the best overall results.

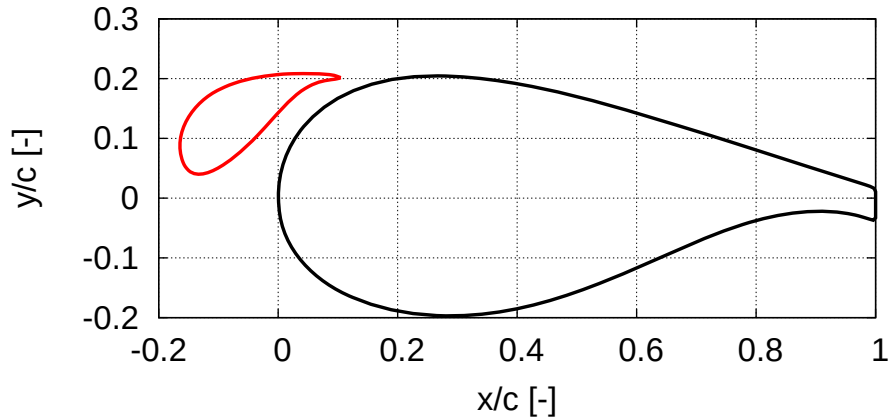

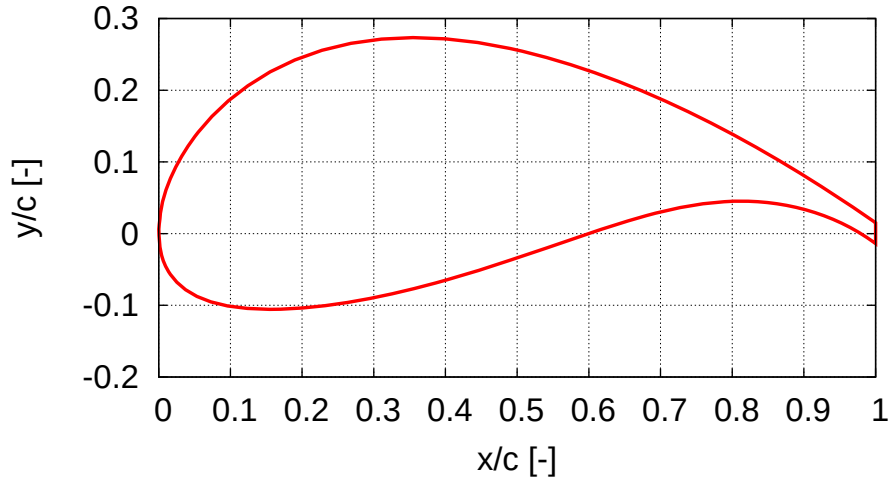

Predicted Slat Performance

2D lift coefficielt and lift to drag ratio as function of incidence for fully turbulent and transitional boundary layers.

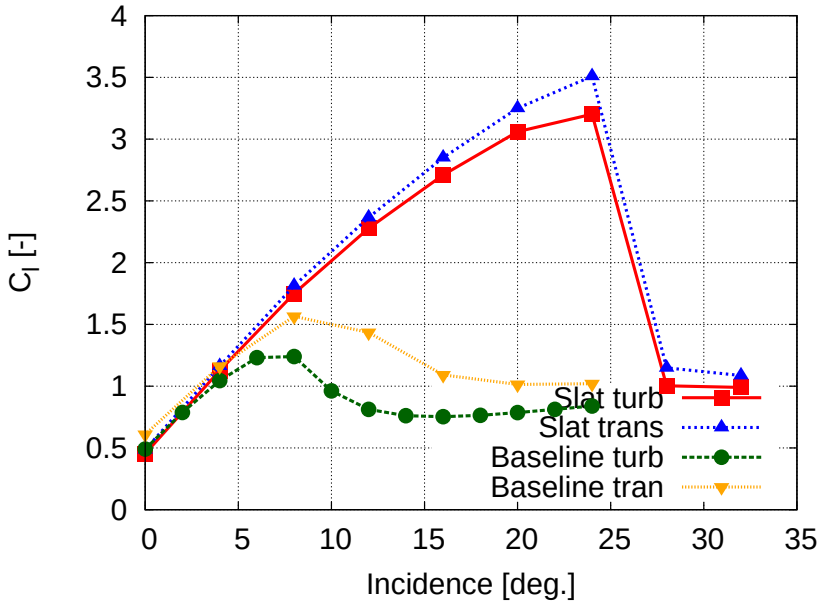

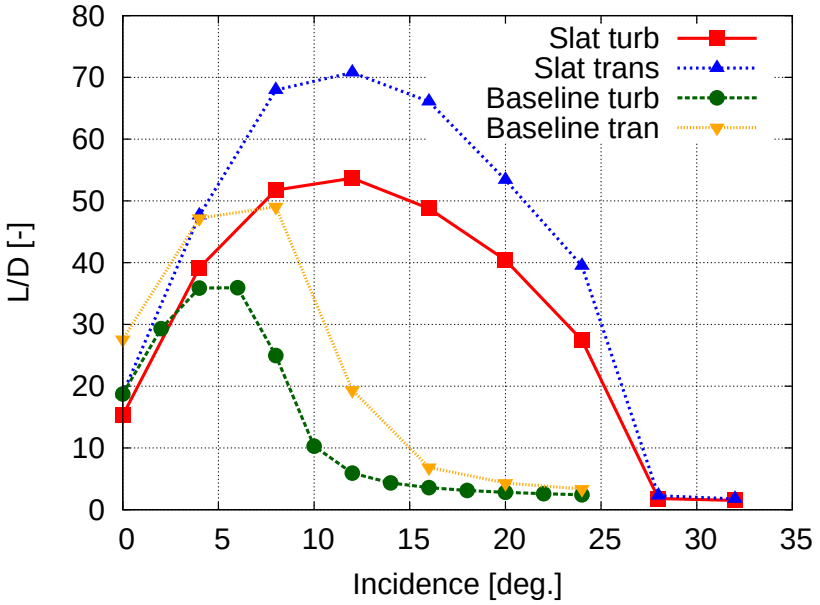

Predicted Slat Performance

Parameter study

- Using the optimized slat shape a parameter study was carried out to determine the performance of the slat within the grid shown below.
- For each grid position the slat angle was optimized to minimize the cost function.
- $42 \times 60 = 2520$ EllipSys2D simulations.
- All carried out using a coarser grid than for the actual optimization (grid level 2).

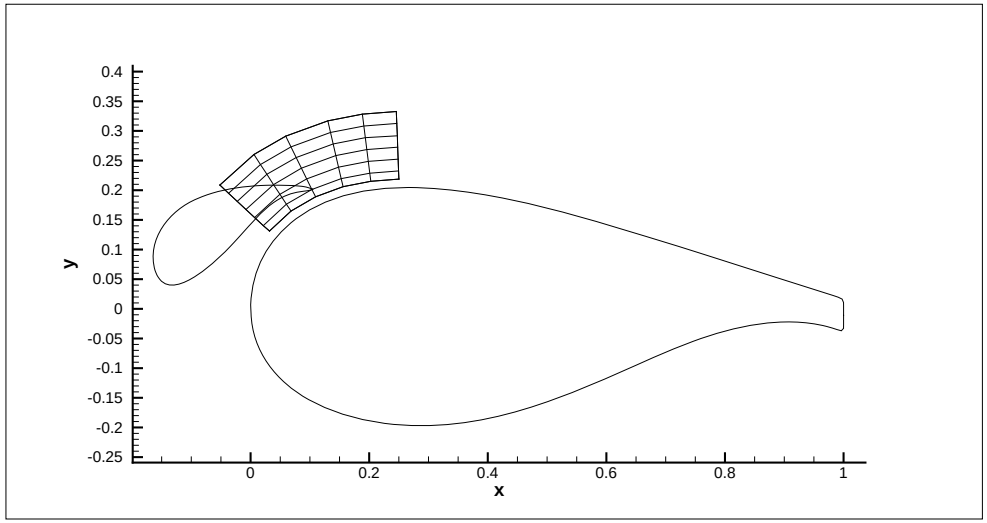

Predicted Slat Performance

Contours of maximum lift coefficient.

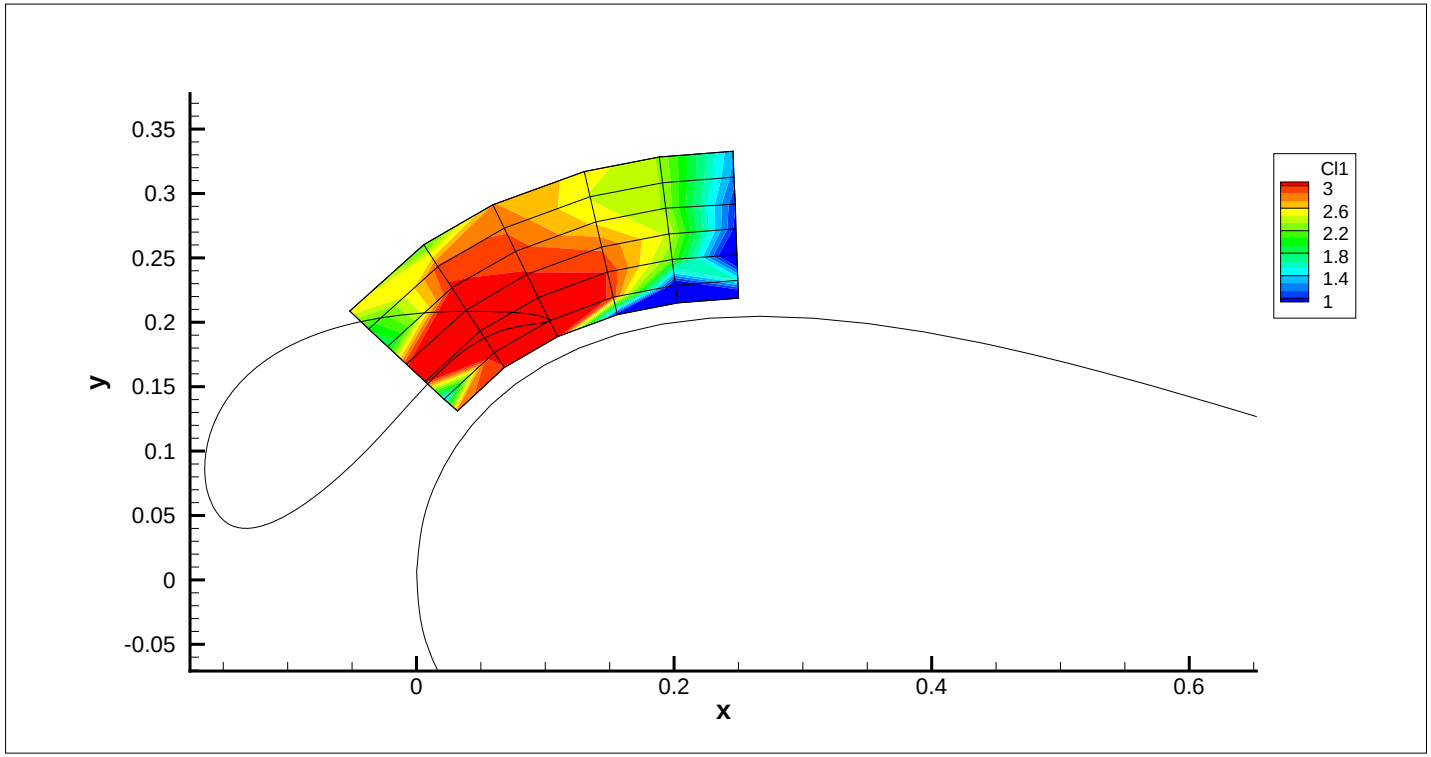

Predicted Slat Performance

Contours of L/D at $\alpha_{C_{lmax}}$.

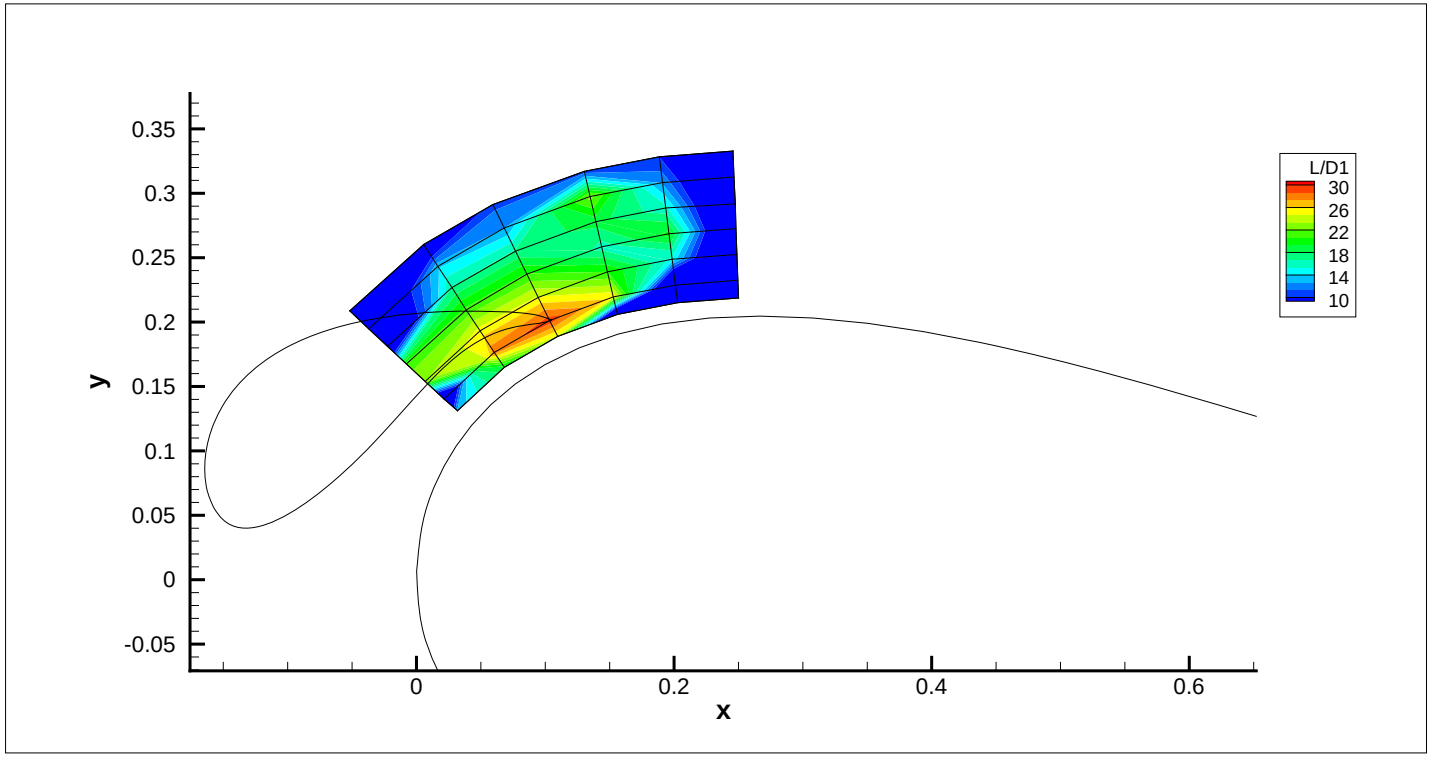

Predicted Slat Performance

Contours of lift coefficient at $\alpha_{C_{lmax}}$ -5 deg.

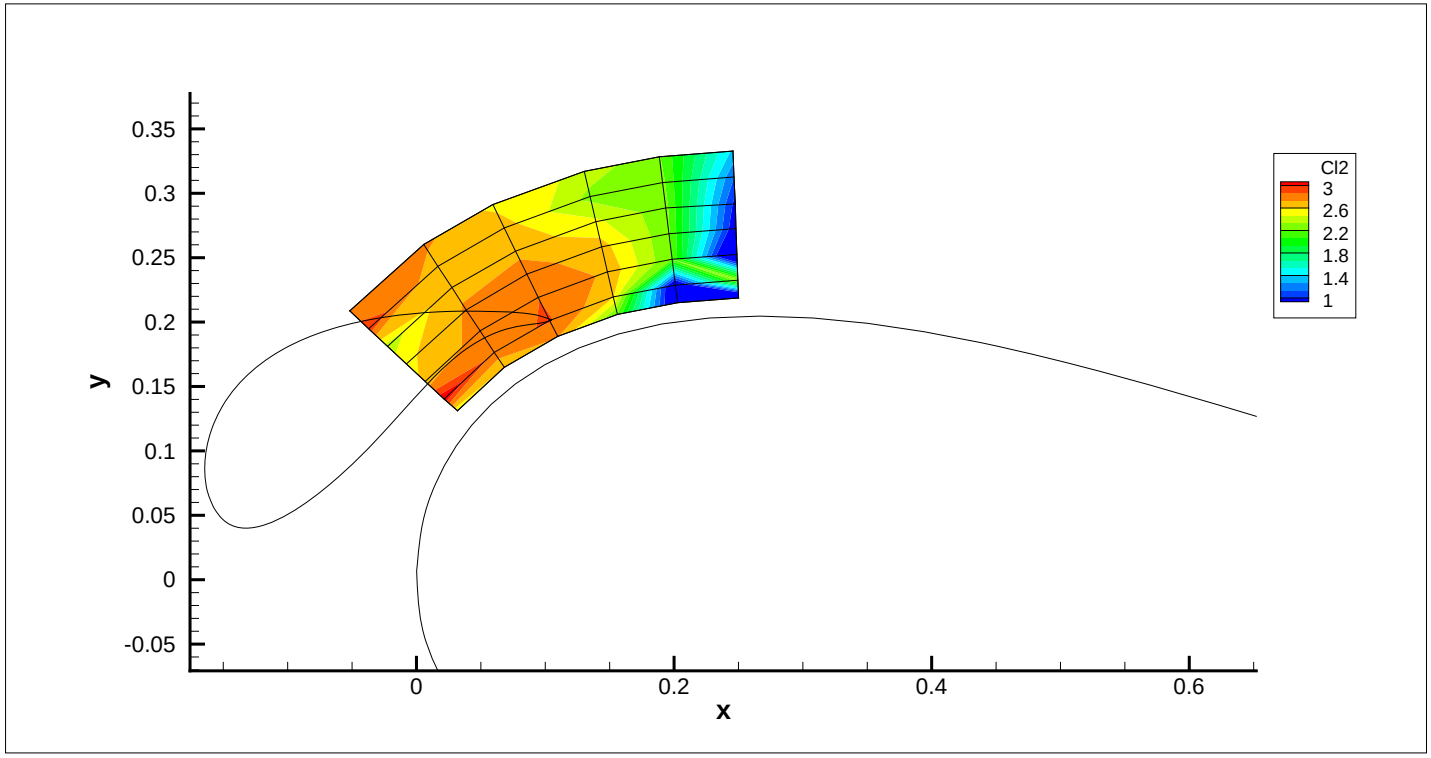

Frederik Zahle et al.
Risø DTU

Predicted Slat Performance

Contours of L/D at $\alpha_{C_{lmax}}$ -5 deg.

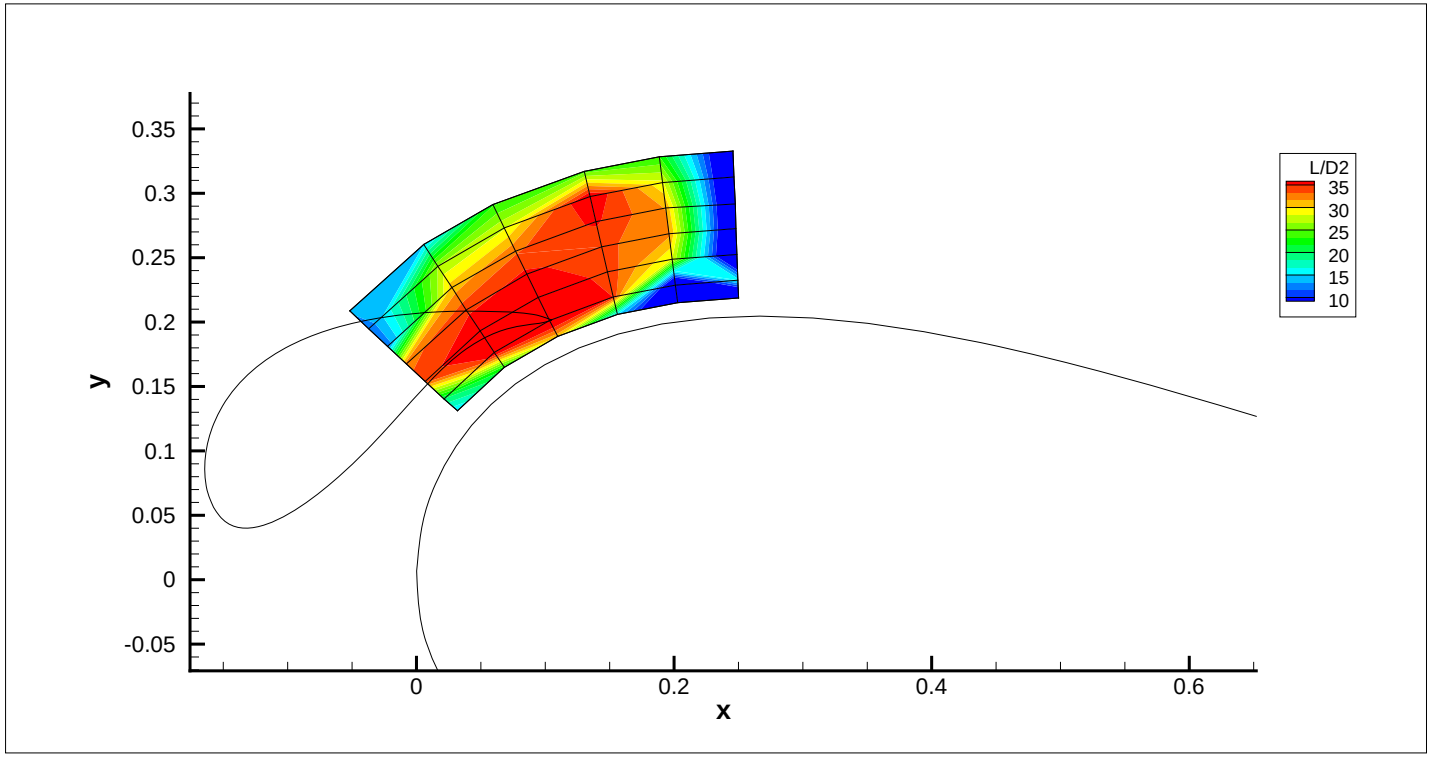

Predicted Slat Performance

Contours of velocity magnitude over the isolated main airfoil at 16 deg. AOA.

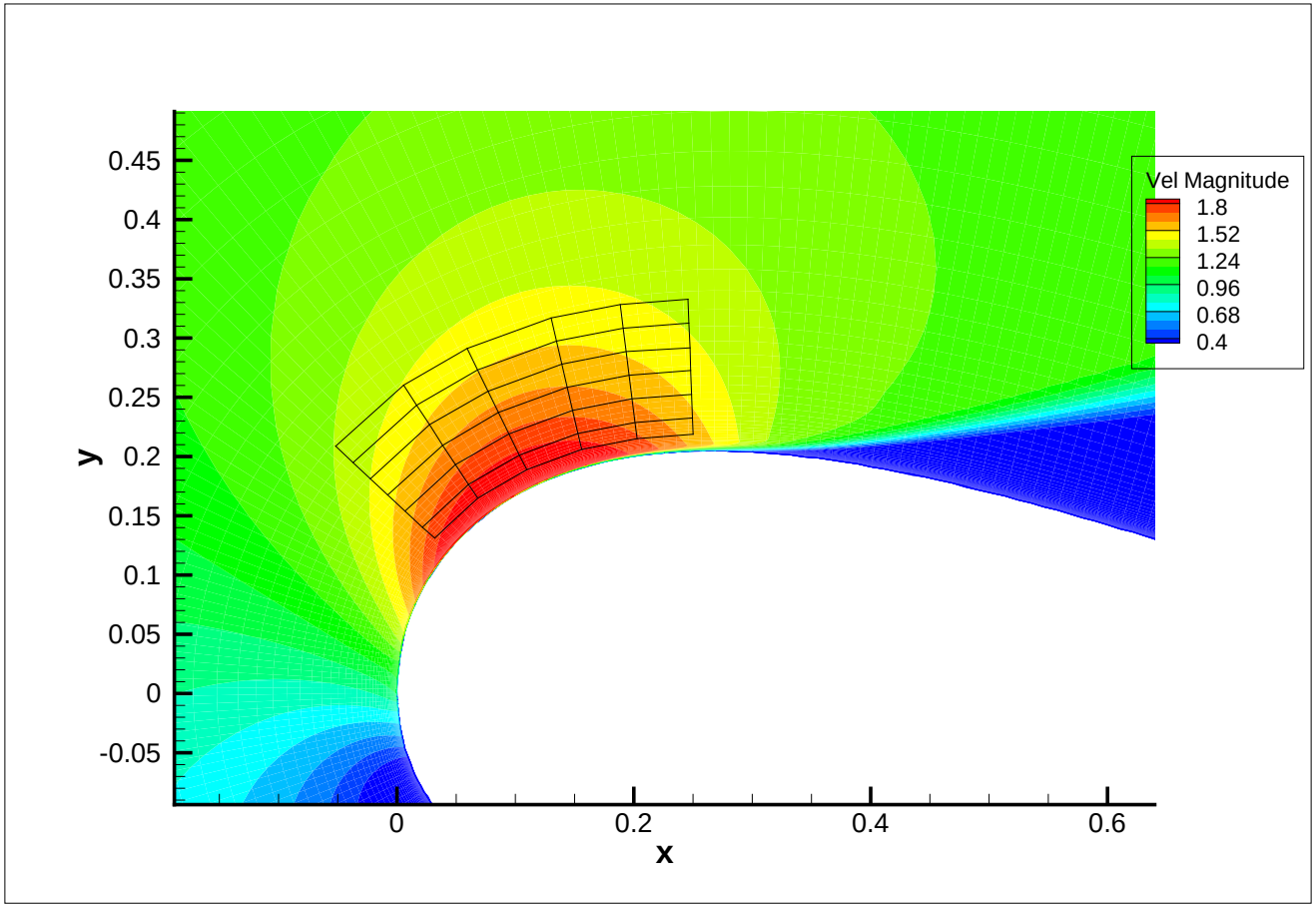

Frederik Zahle et al.
Risø DTU

What makes the slat work so well?

- Best performance of the slat was found to be in the region where the flow acceleration over the suction side of the main airfoil was greatest.
- The flow disturbance at the slat TE results in a camber effect or modification of the local kutta condition, increasing the obtainable lift.
- The low pressure at the slat TE reduces the needed pressure recovery of the flow over the slat, allowing for much greater suction peaks than on conventional airfoils.
- The suction peak on the main airfoil is completely removed, requiring only a small pressure recovery for the flow on the main element.
- The airfoil can thus maintain attached flow up to much greater angles of attack due to these effects and hence produce very high lift.
- The positioning of the slat can thus be narrowed down considerably by studying the flow over the isolated main airfoil.

Wind Tunnel Setup

Test setup designed by LM Wind Power.

- The slat was hinged at it's leading edge.
- Could be moved within limits of a grid with 8×8 holes with 10 mm spacing.
- Slat angle β could be changed steplessly.

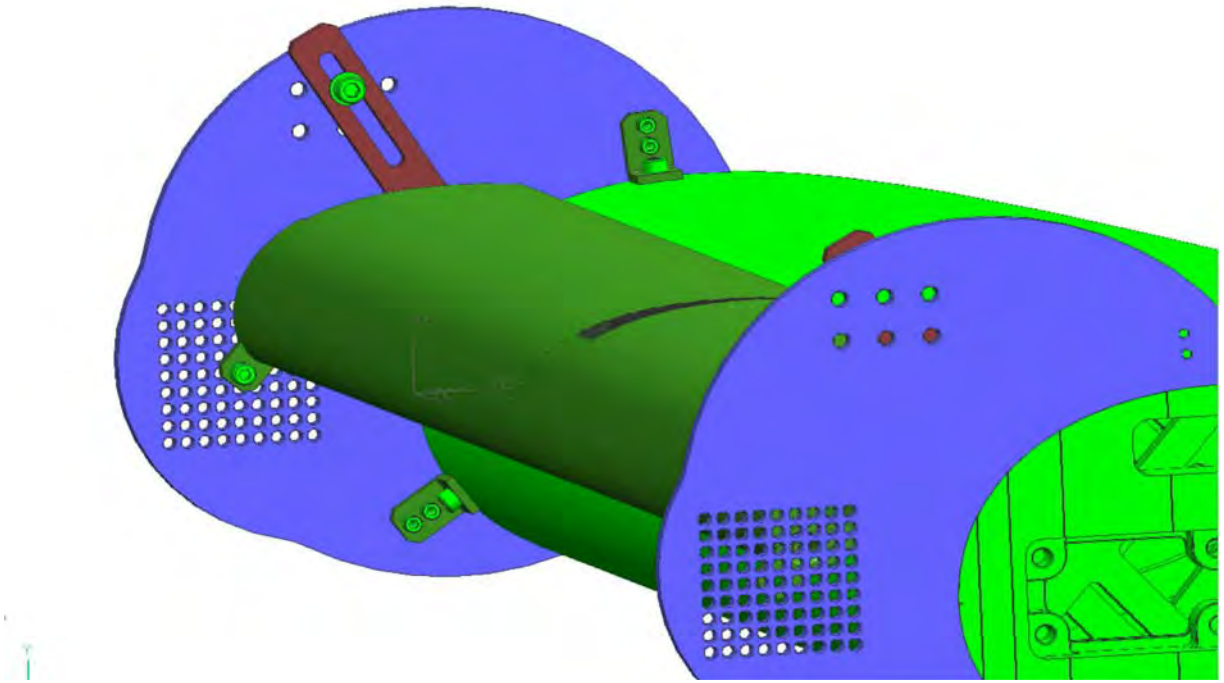

Wind Tunnel Experiment Plan

Parameter study

- Another parameter study was carried out to determine the performance of the slat within the test setup grid.
- For each grid position the slat angle was optimized to minimize the cost function.
- $81 \times 60 = 4860$ EllipSys2D simulations.
- All carried out using a coarser grid than for the actual optimization (grid level 2).

Wind Tunnel Experiment Plan

Parameter study

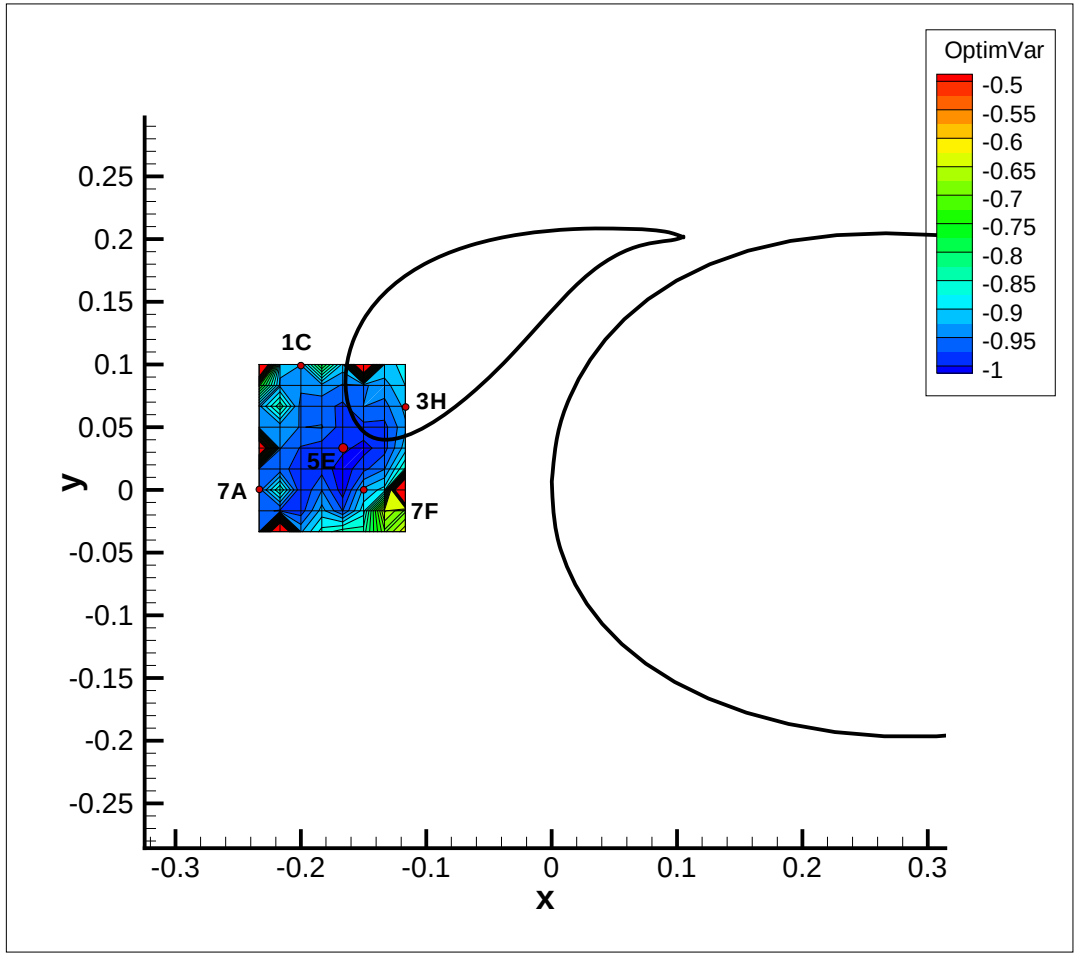

Frederik Zahle et al.
Risø DTU

Wind Tunnel Experiment Plan

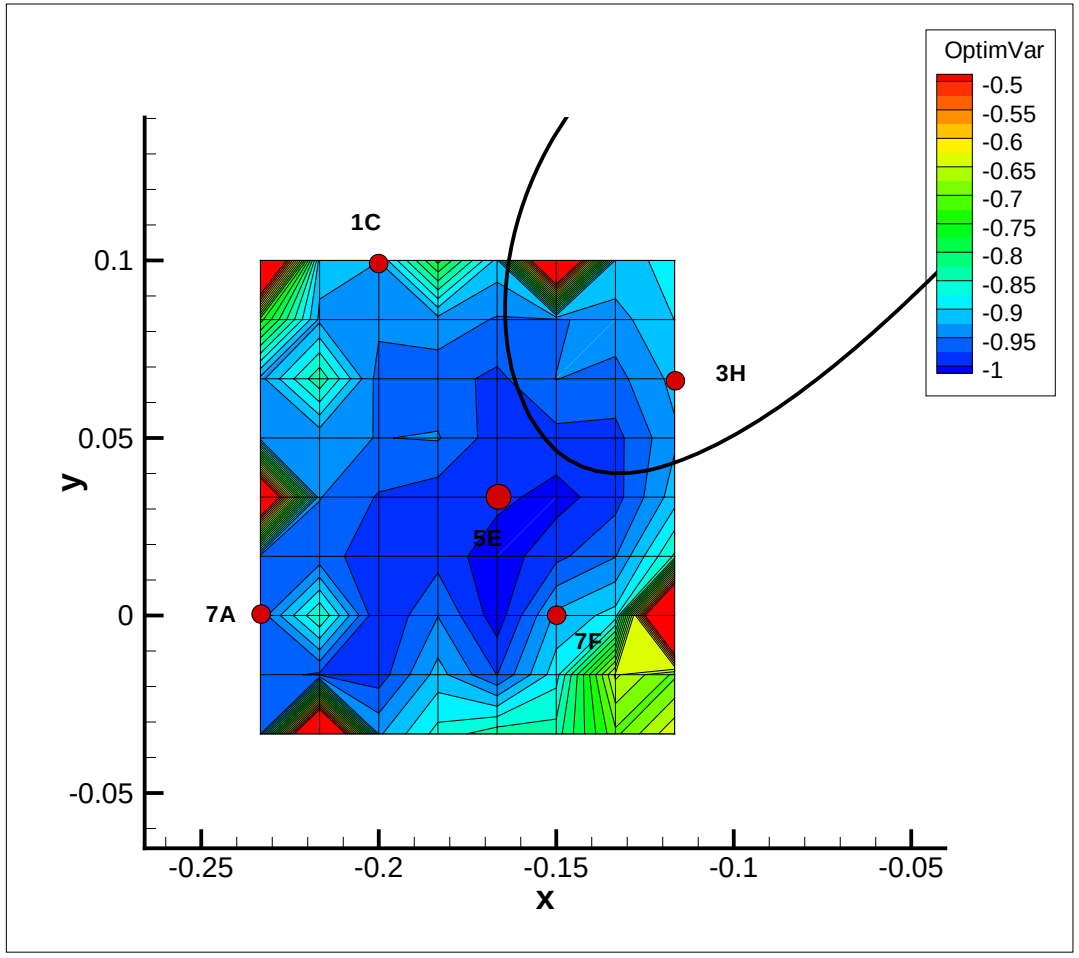

Frederik Zahle et al.
Risø DTU

Wind Tunnel Experiment Plan

A comprehensive test plan

- The wind tunnel campaign was split into two parts:
- Flatback airfoil:
  - Clean, four Reynolds numbers: 1, 2, 3 and 4×10^6,
  - Roughness, Vortex generators, Gurney flaps.
- Slatted airfoil:
  - Clean, four Reynolds numbers: 1, 2, 3 and 4×10^6,
  - Seven slat positions,
  - Slat angle variations at five positions,
  - Roughness, Vortex generators, Gurney flaps at slat one position.
  - Flow visualization using wool tufts.

Data

Preliminary data!

- The data from the experiment presented here are preliminary and not corrected for tunnel effects.
- Only selected data will be shown.
- Profile geometries as well as all data will be published and available to the public.

Wind Tunnel Results
Isolated flatback airfoil

Measurement sources - lift coefficient

- To measure the lift either the airfoil pressure (AP), the load cell (LC) or the wall pressure (WP) was used.
- Good agreement up to 5 deg. AOA (except for LC offset).

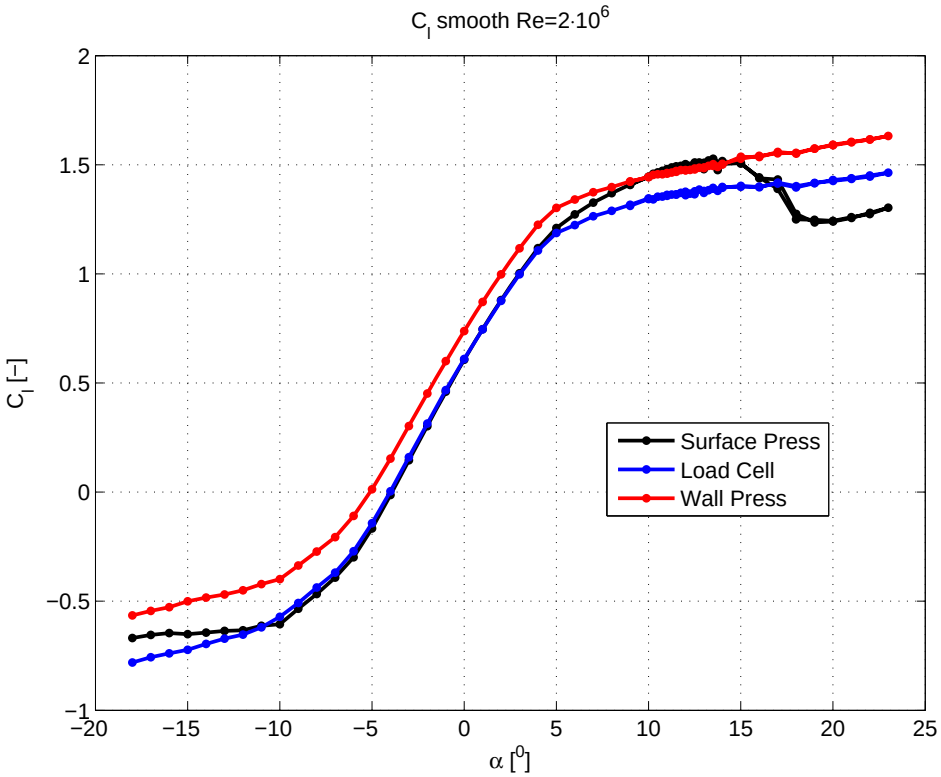

Wind Tunnel Results
Isolated flatback airfoil

Measurement sources - drag coefficient

- To measure the drag either the airfoil pressure (AP), the load cell (LC) or the wake rake (WR) was used.
- Drag behaves as expected for AOA < 5 deg.: $C_{D-AP} < C_{D-WR}$
- For AOA > 5 deg. AP and LC drag increase drastically.

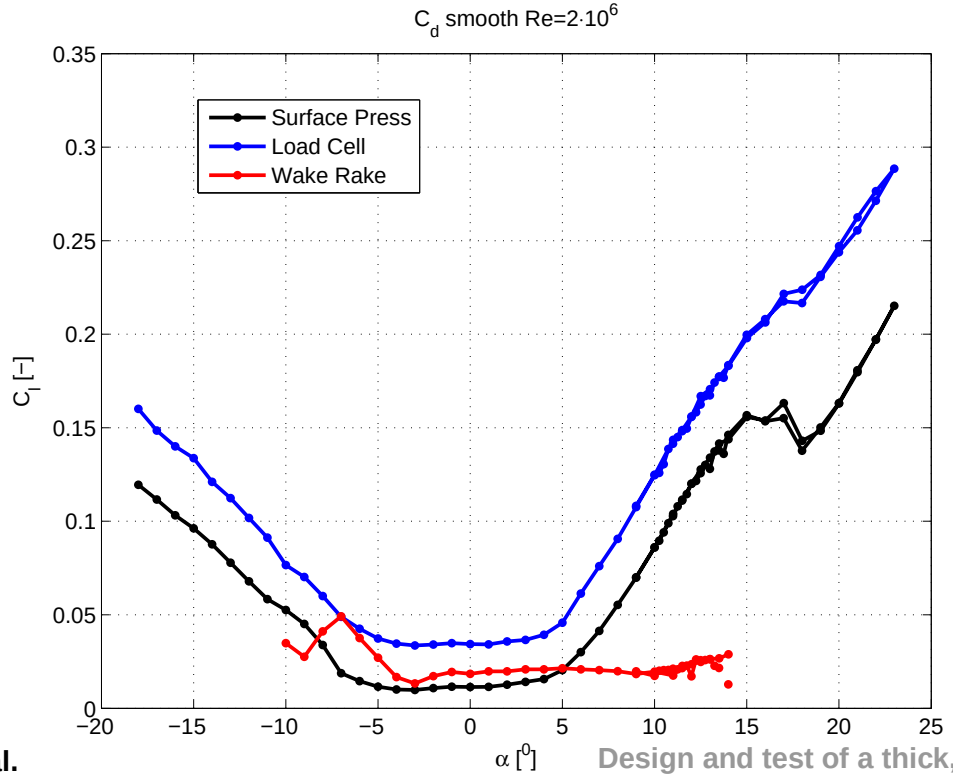

Wind Tunnel Results
Isolated flatback airfoil

Comparison to EllipSys2D

- Variation of TI in EllipSys2D simulations: low TI simulations agree well with experiment for AOA $<$ 5 deg.
- For AOA $>$ 5 deg. TI$>$0.2% apper to be in better agreement.

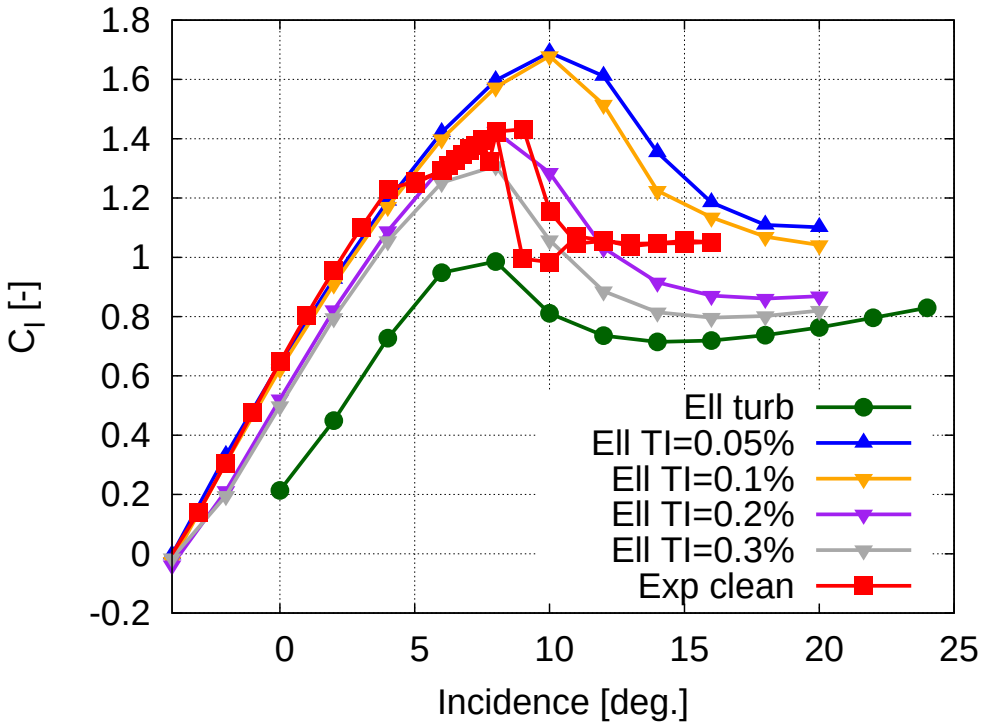

Wind Tunnel Results
Isolated flatback airfoil

Comparison to EllipSys2D

- Variation of TI in EllipSys2D simulations: low TI simulations agree well with experiment for AOA $<$ 5 deg.
- For AOA $>$ 5 deg. TI$>$0.2% apper to be in better agreement.

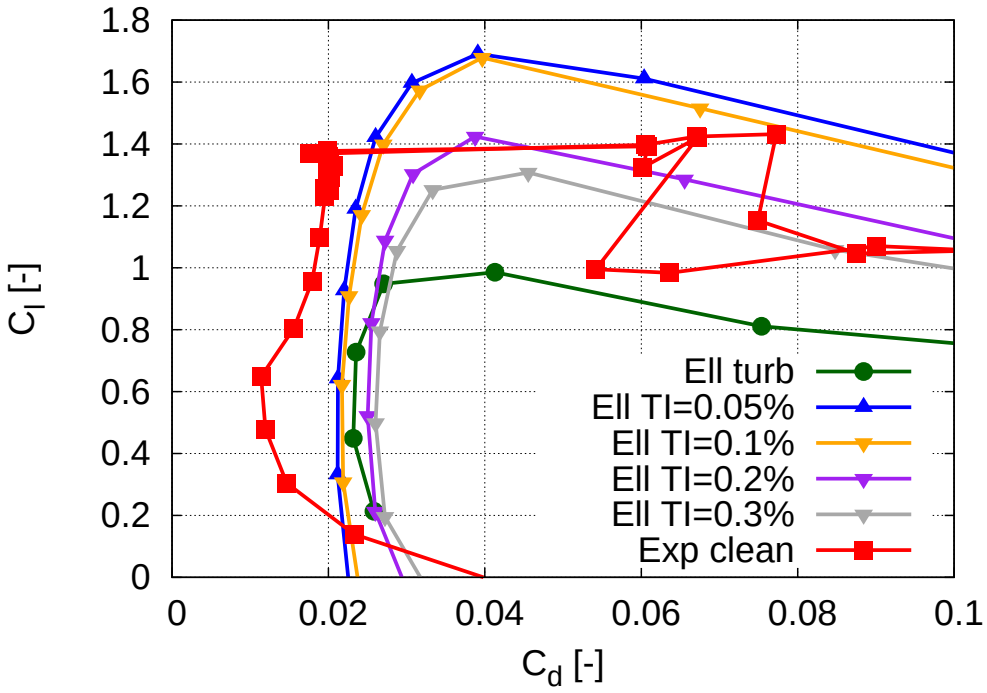

Wind Tunnel Results
Isolated flatback airfoil

Variation of Reynolds number - Experimental results only

- Increasing Re reduces C_{l-max}.

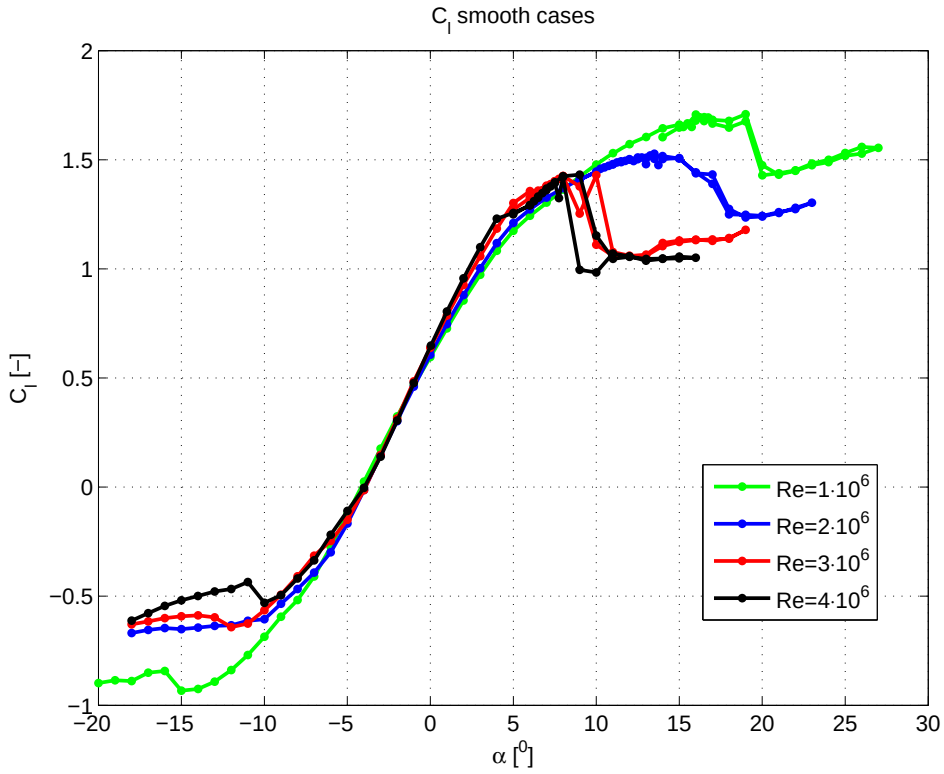

Wind Tunnel Results
Isolated flatback airfoil

Roughness

- Roughness tape was mounted at various chordwise positions.

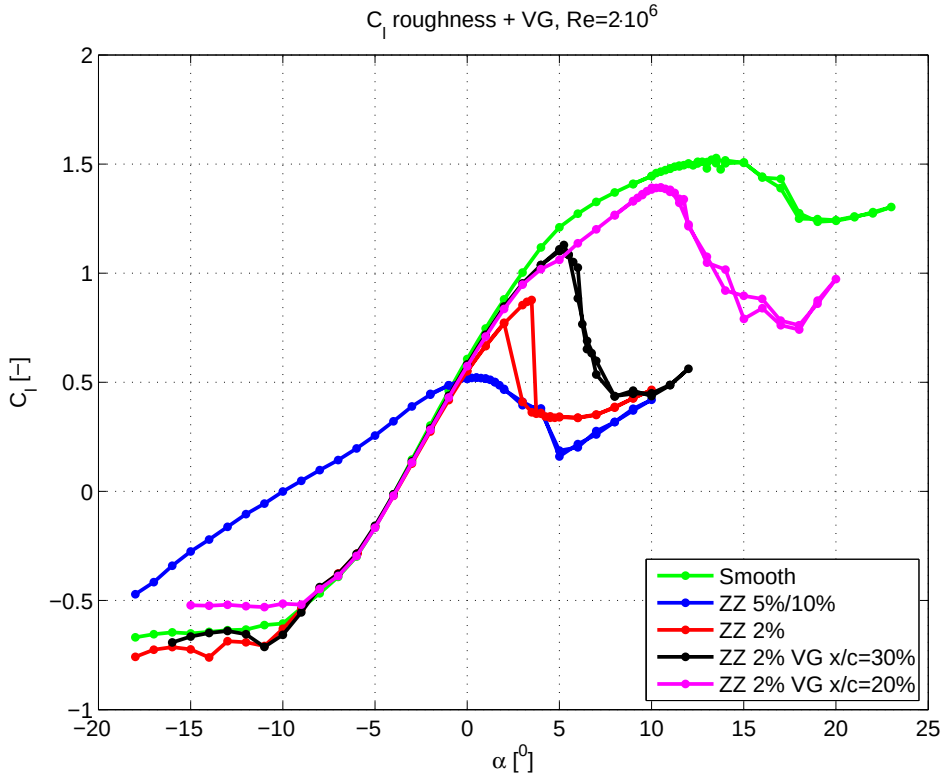

Frederik Zahle et al.
Risø DTU

Wind Tunnel Results
Isolated flatback airfoil

Devices

- The flatback airfoil was tested with vortex generators and Gurney flaps.

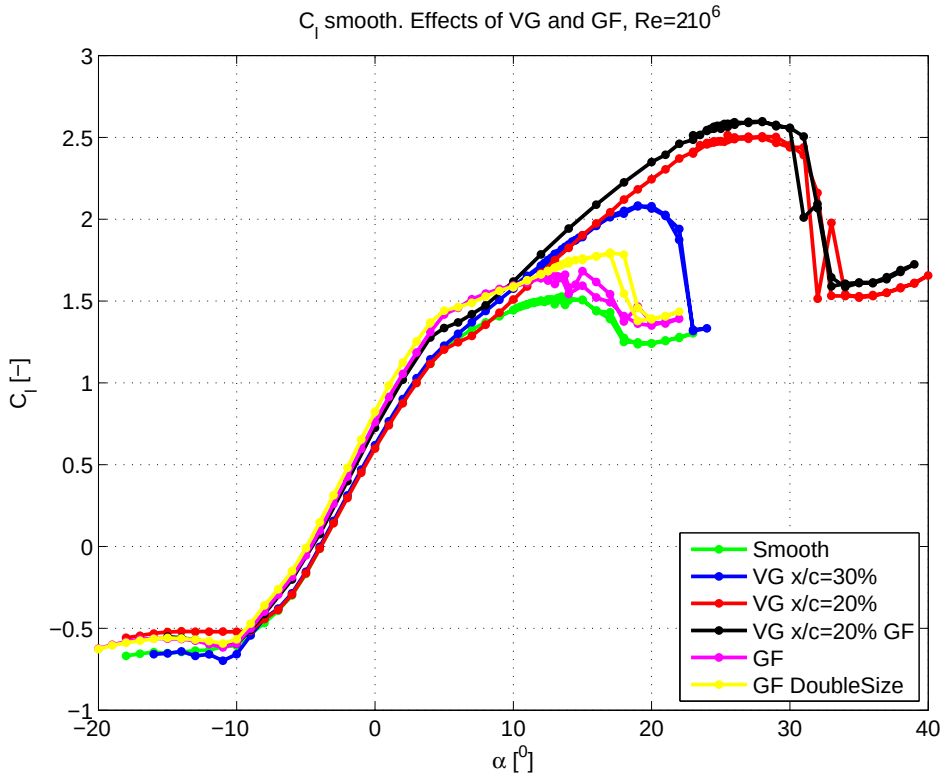

Frederik Zahle et al.
Risø DTU

Wind Tunnel Results
Flatback with slat airfoil

Reference position 5E

- Variation of TI in EllipSys2D simulations: Lift coefficient vs angle of attack at the reference position 5E with reference β=-29.35 deg.
- All simulations show on the following slides were carried out with TI=0.2%.

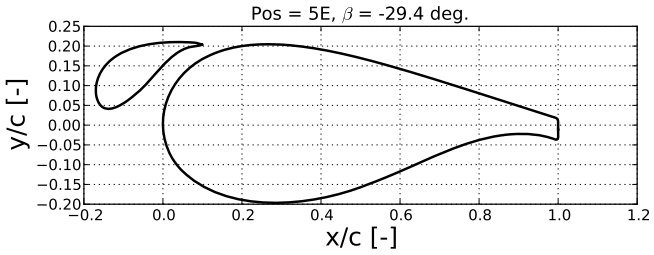

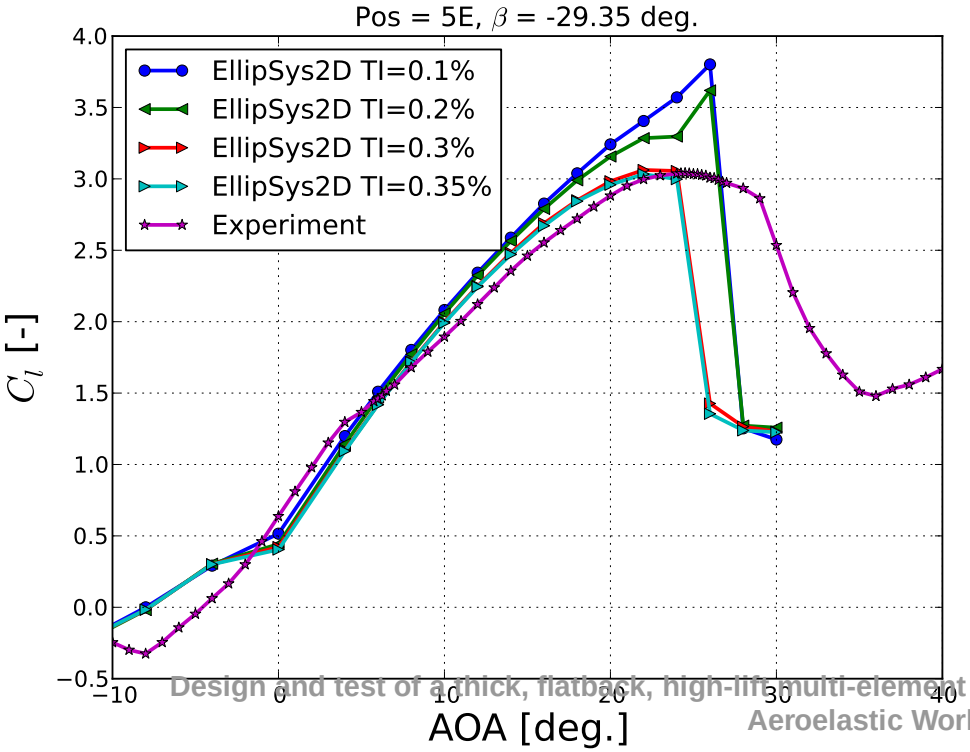

Wind Tunnel Results
Flatback with slat airfoil

Reference position 5E

Position 5E with reference β=-29.35 deg. showing contributions from main, slat and total.

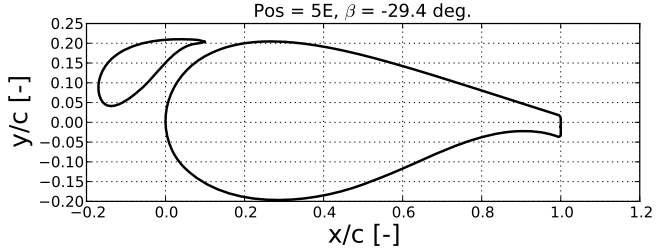

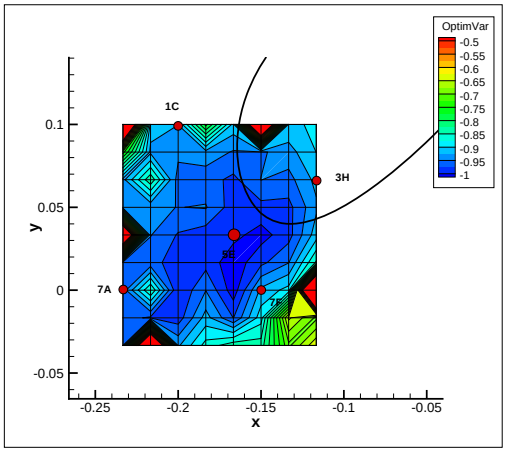

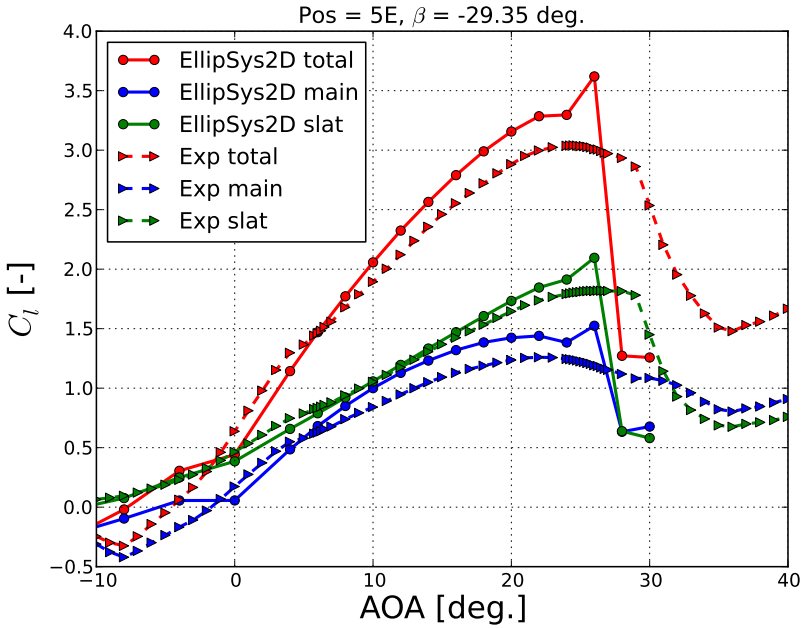

Wind Tunnel Results
Flatback with slat airfoil

Reference position 5E

Position 5E with reference β=-29.35 deg. showing contributions from main, slat and total.

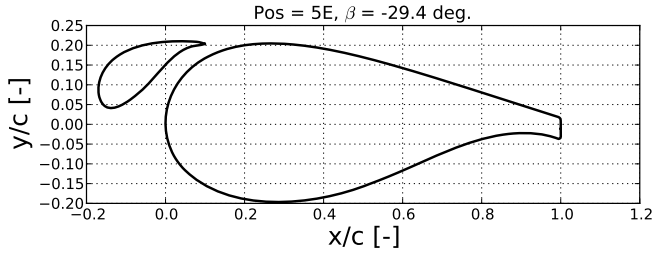

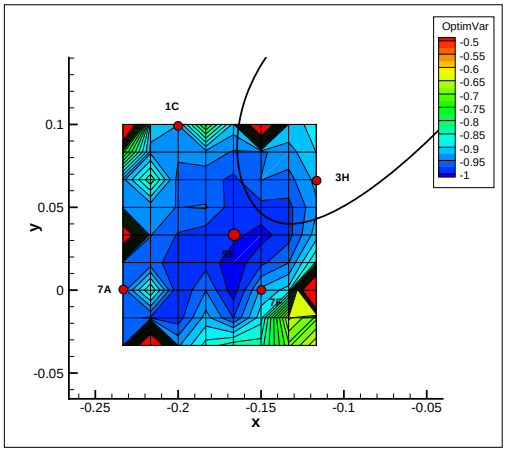

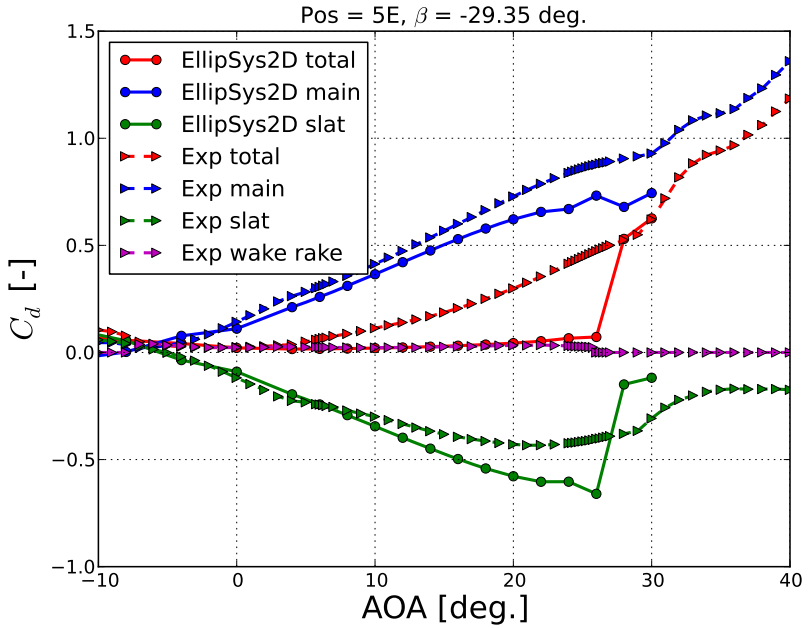

Wind Tunnel Results
Flatback with slat airfoil

Reference position 5E

Position 5E with reference β=-29.35 deg. showing contributions from main, slat and total.

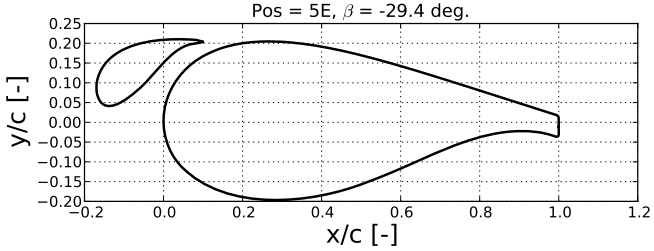

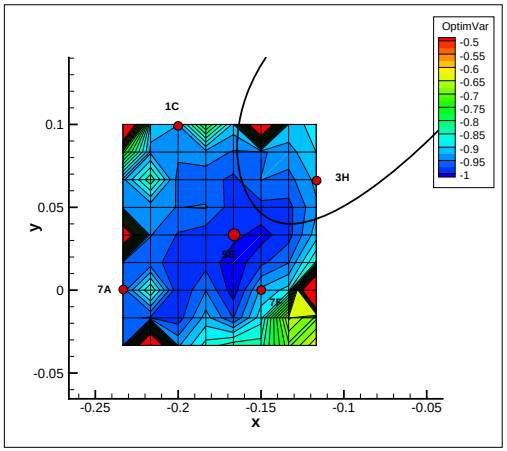

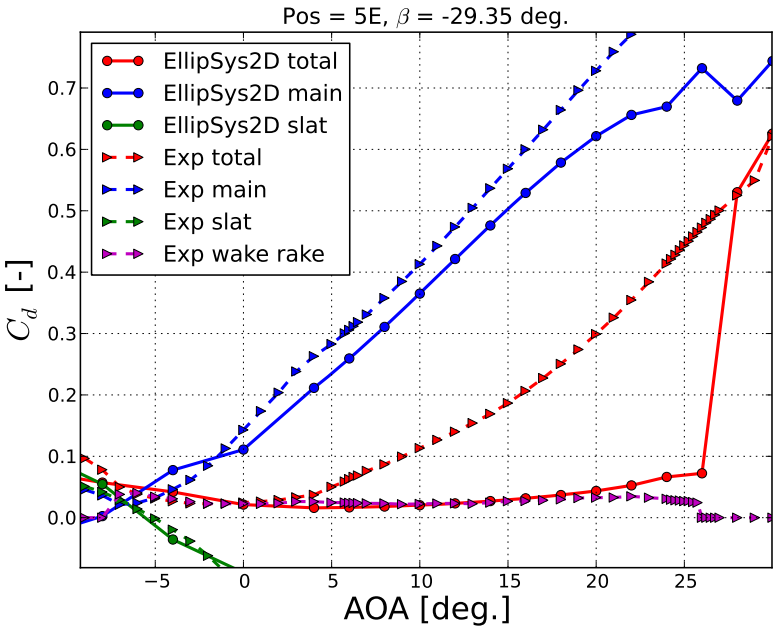

Wind Tunnel Results
Flatback with slat airfoil

Reference position 5E

Position 5E with reference β=-29.35 deg. showing contributions from main, slat and total.

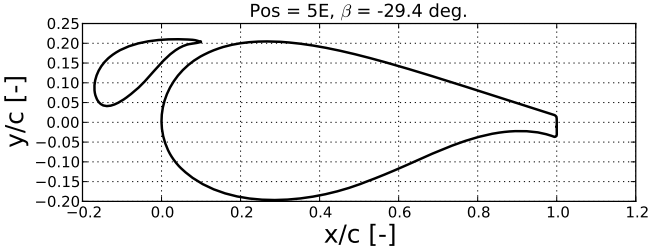

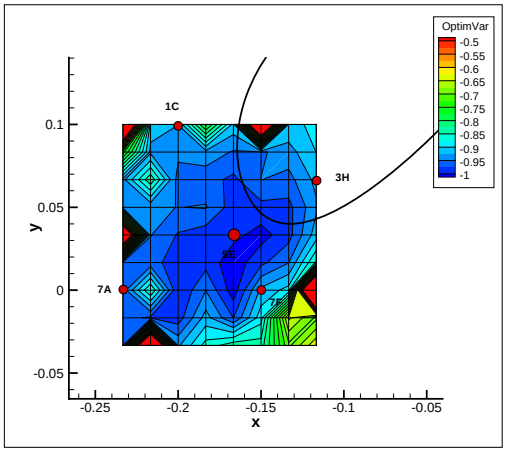

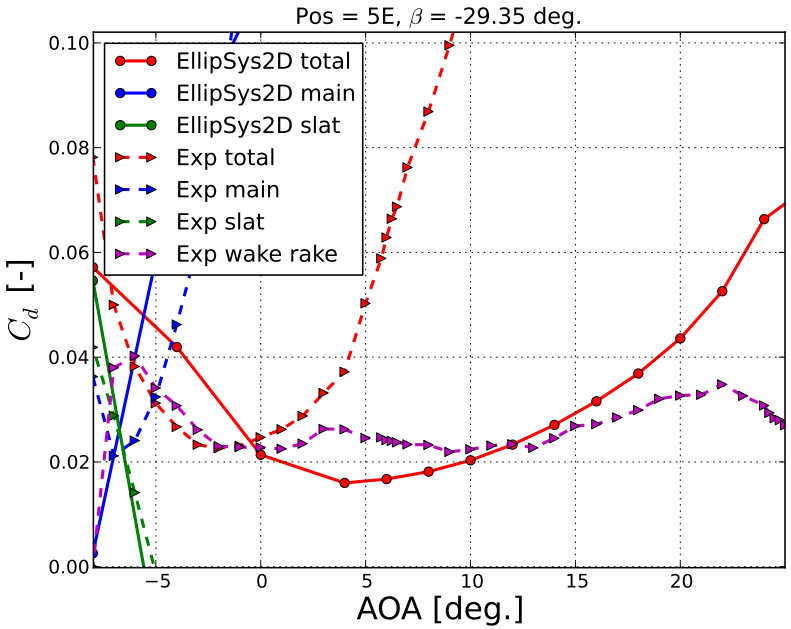

Wind Tunnel Results
Flatback with slat airfoil

Reference position 5E

Position 5E with reference β=-29.35 deg. showing contributions from main, slat and total.

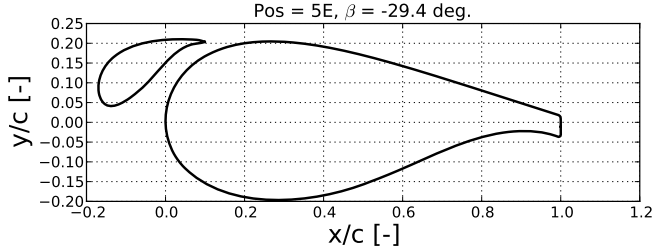

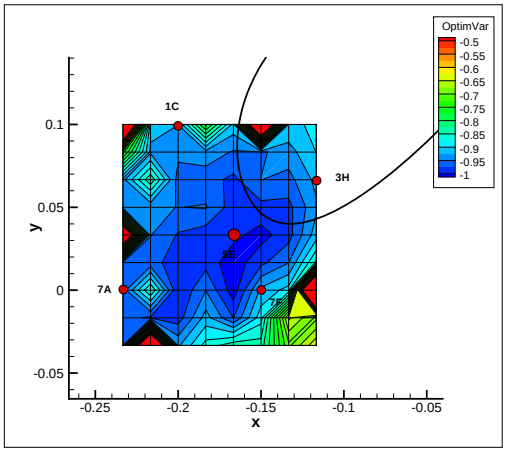

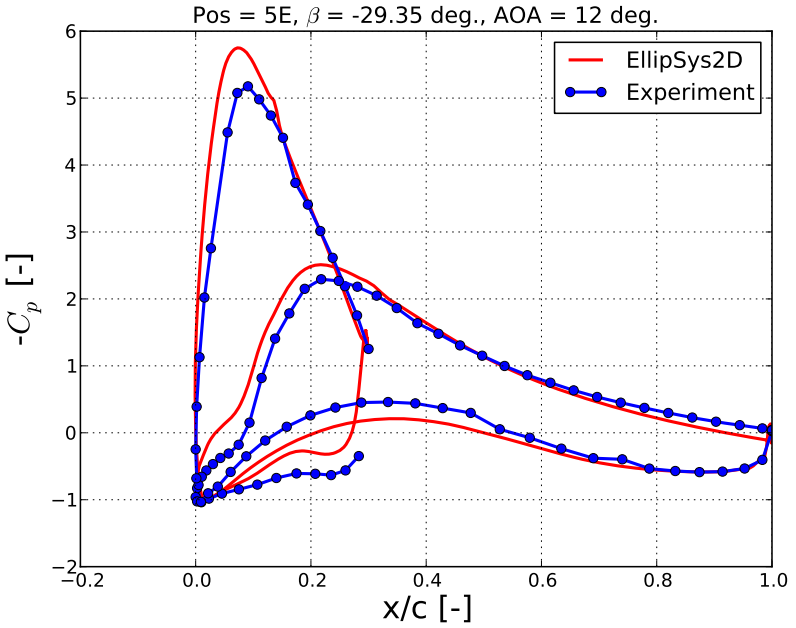

Frederik Zahle et al.
Risø DTU

Wind Tunnel Results
Flatback with slat airfoil

Reference position 5E

Position 5E with reference β=-29.35 deg. showing contributions from main, slat and total.

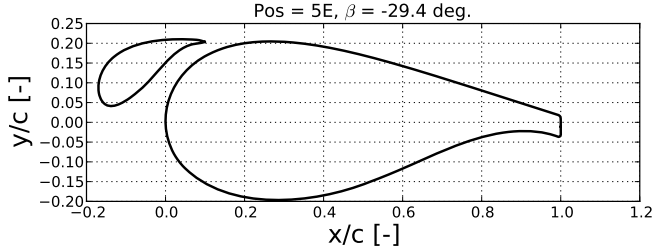

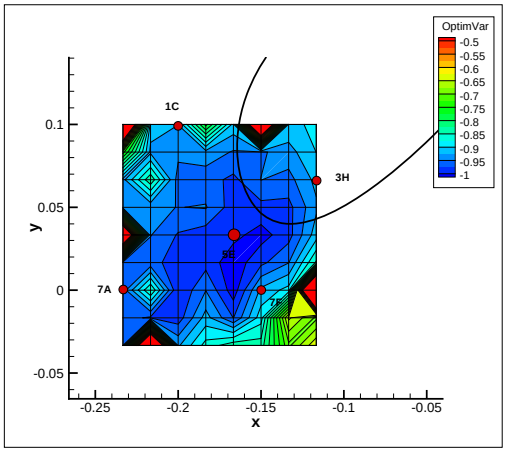

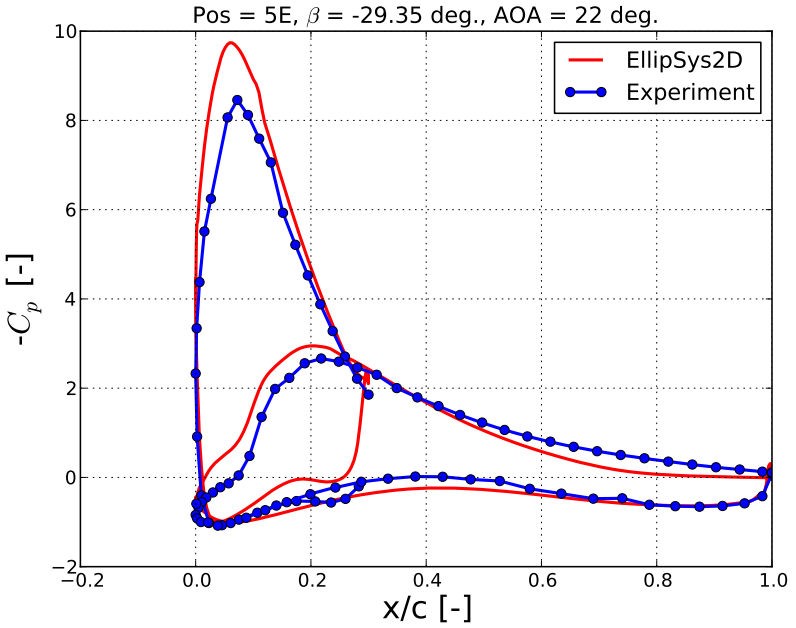

Flatback with slat airfoil

Position 7F

Position 7F with reference β=-34.2 deg. showing contributions from main, slat and total.

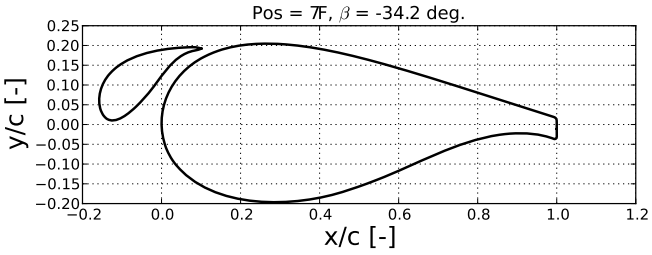

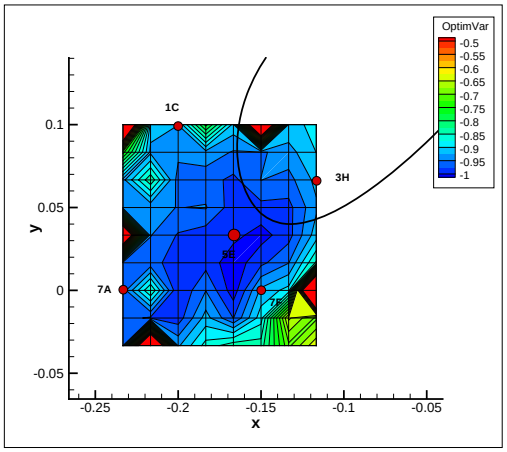

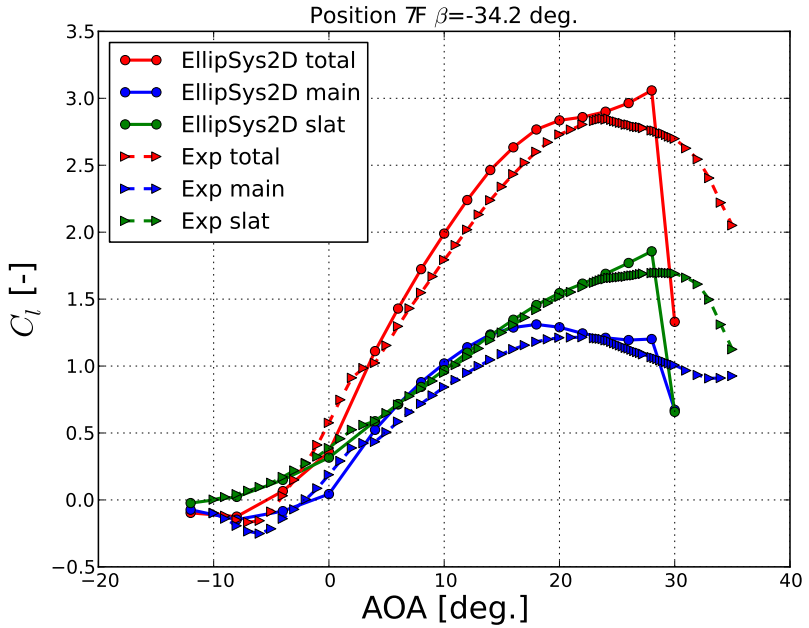

Wind Tunnel Results
Flatback with slat airfoil

Position 7F

Position 7F with reference β=-34.2 deg. showing contributions from main, slat and total.

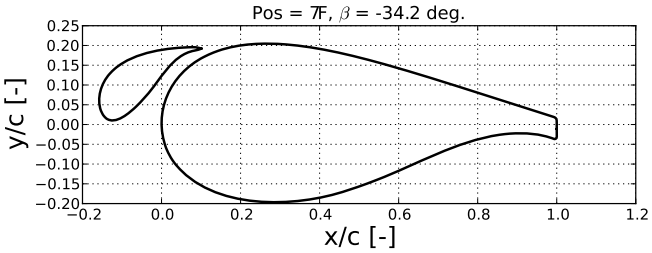

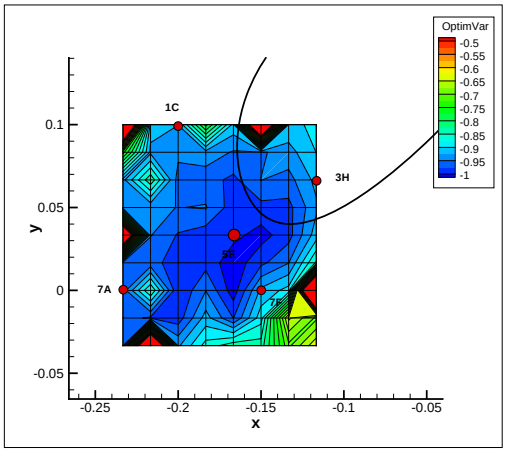

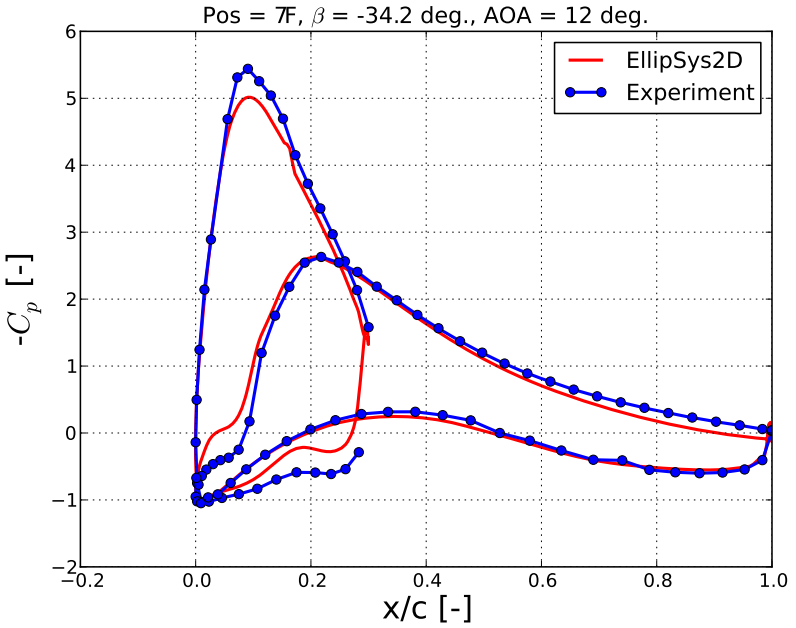

Frederik Zahle et al.
Risø DTU

Wind Tunnel Results
Flatback with slat airfoil

Position 7F

Position 7F with reference β=-34.2 deg. showing contributions from main, slat and total.

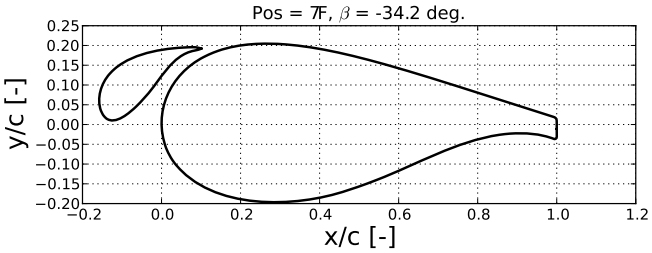

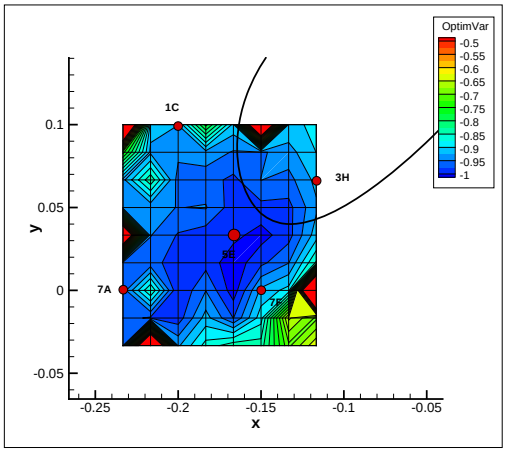

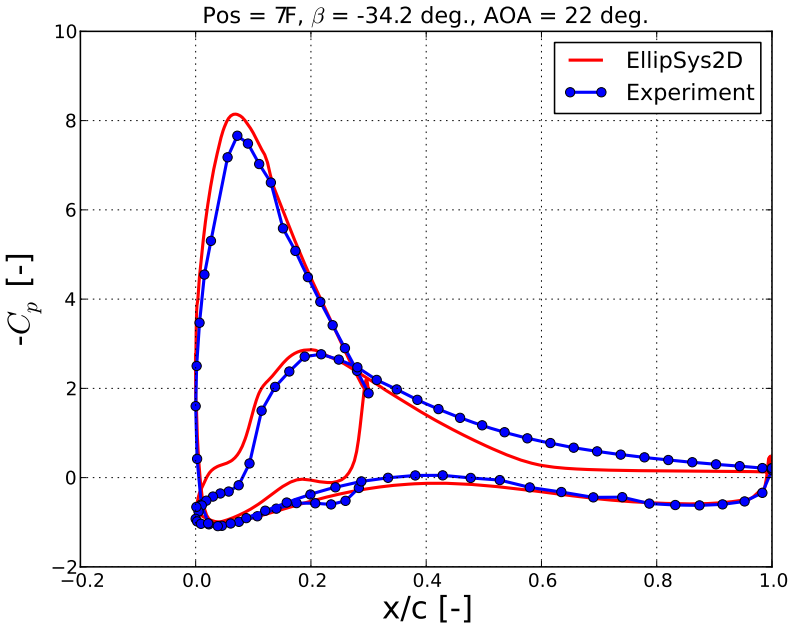

Frederik Zahle et al.
Risø DTU

Wind Tunnel Results
Flatback with slat airfoil

Position 7A

Position 7A with reference β=-29.4 deg. showing contributions from main, slat and total.

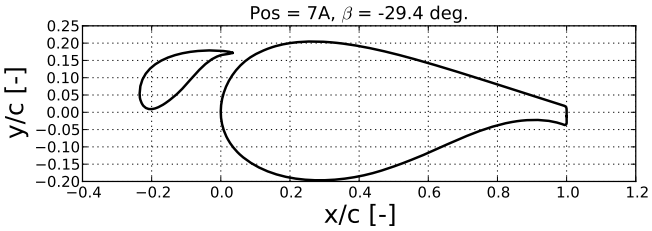

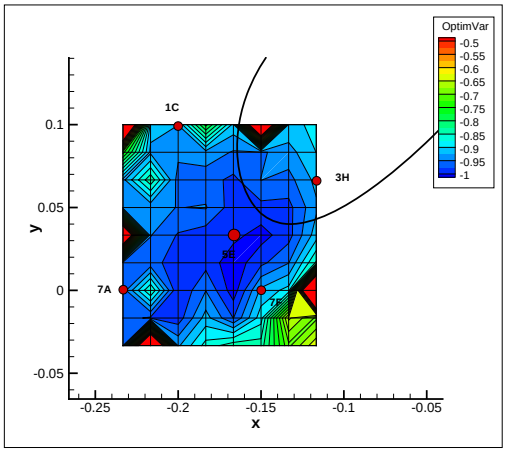

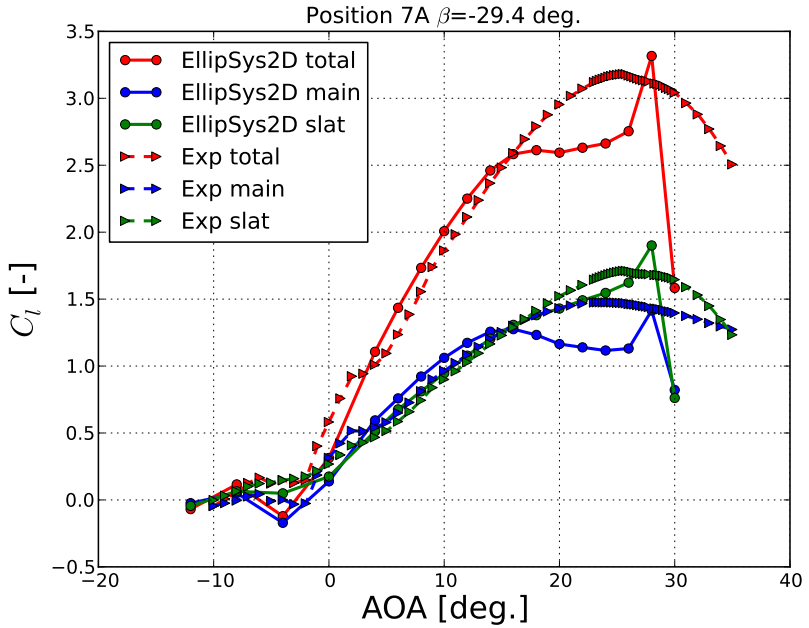

Wind Tunnel Results
Flatback with slat airfoil

Position 7A

Position 7A with reference β=-29.4 deg. showing contributions from main, slat and total.

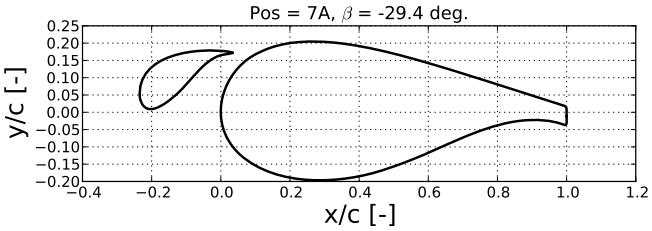

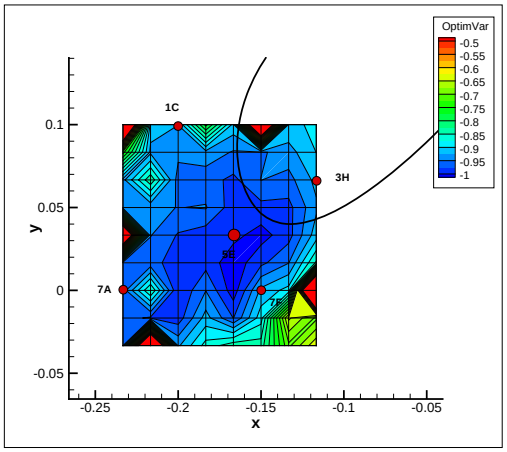

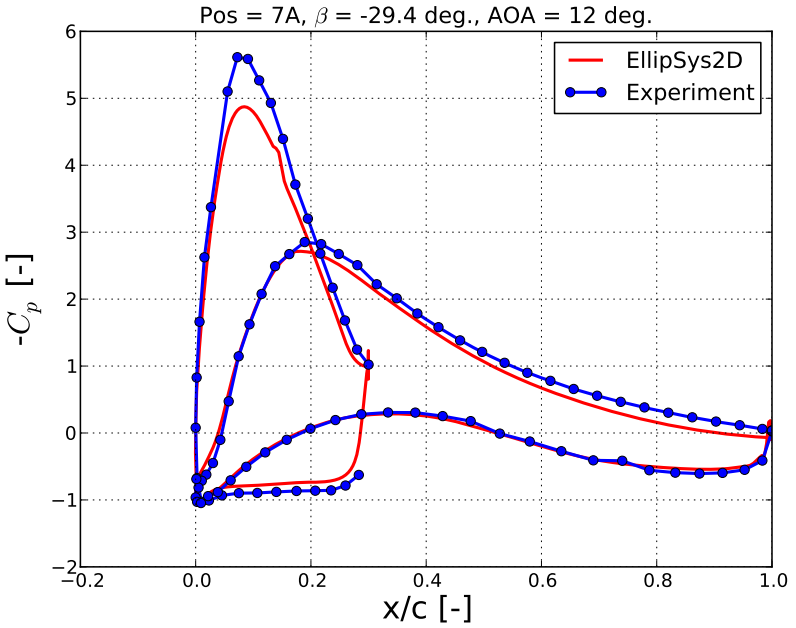

Wind Tunnel Results
Flatback with slat airfoil

Position 7A

Position 7A with reference β=-29.4 deg. showing contributions from main, slat and total.

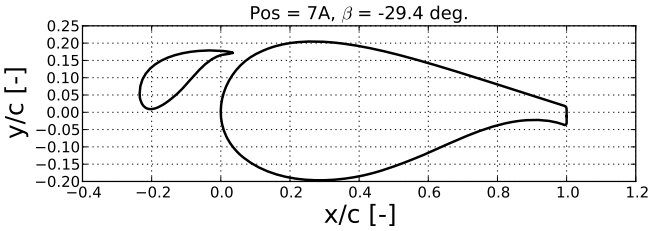

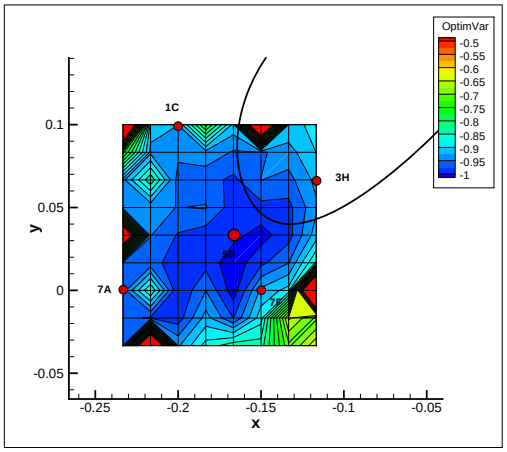

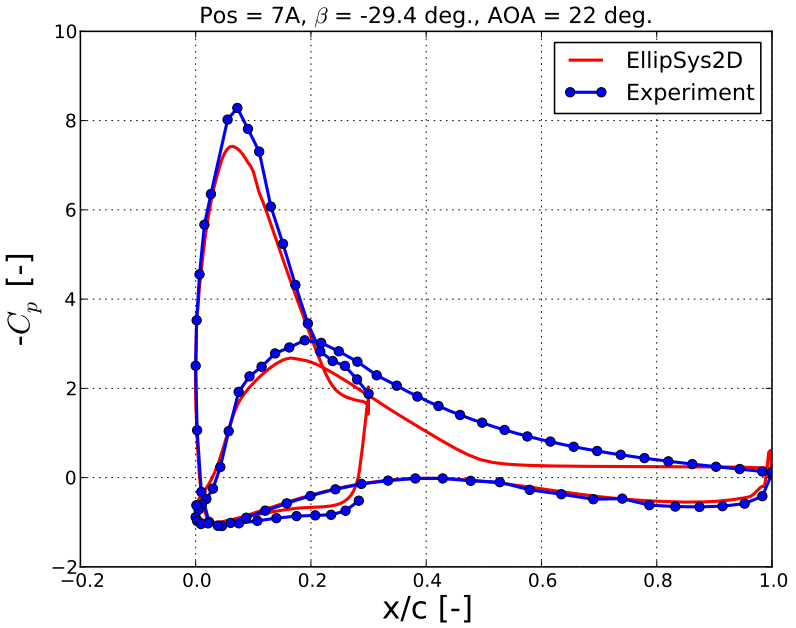

Wind Tunnel Results
Flatback with slat airfoil

Position 1C

Position 1C with reference β=-23.7 deg. showing contributions from main, slat and total.

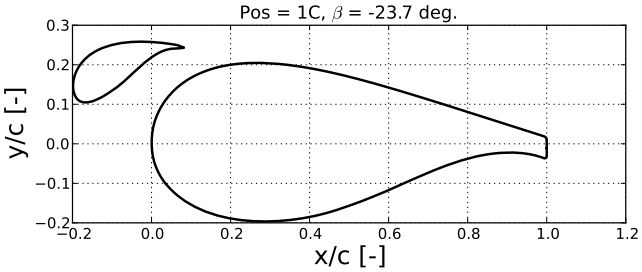

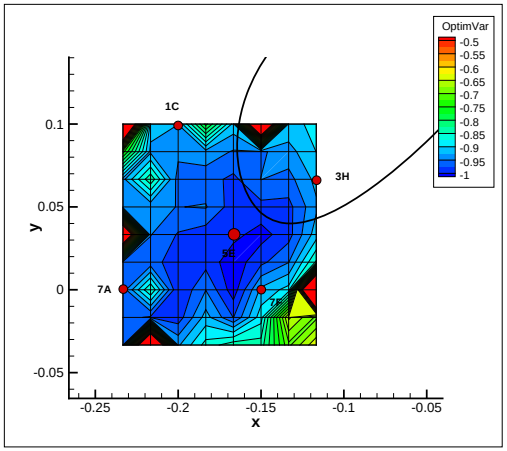

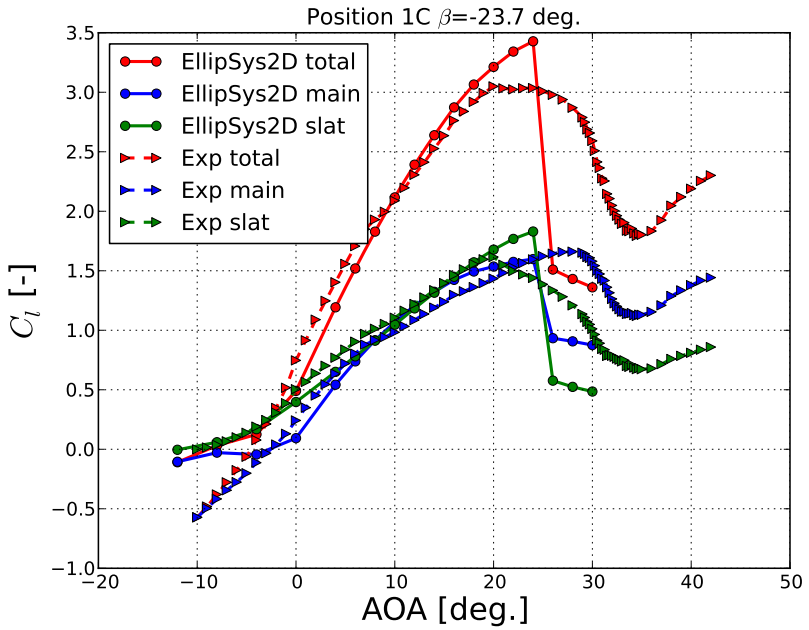

Wind Tunnel Results
Flatback with slat airfoil

Position 1C

Position 1C with reference β=-23.7 deg. showing contributions from main, slat and total.

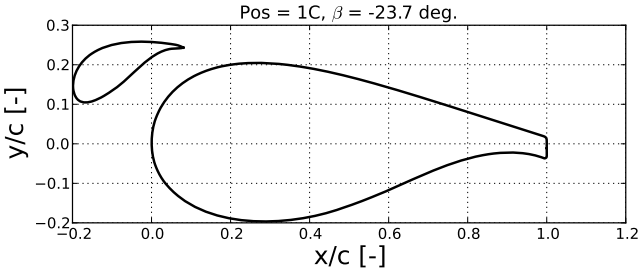

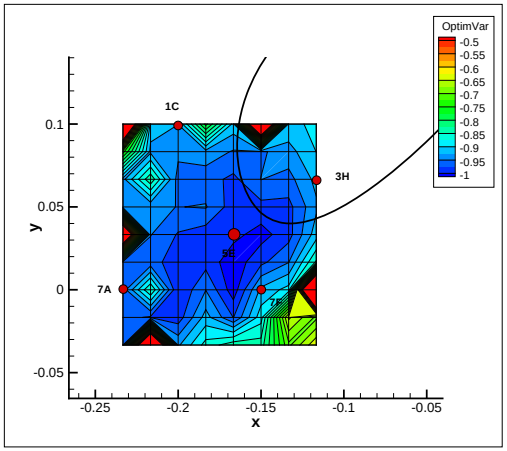

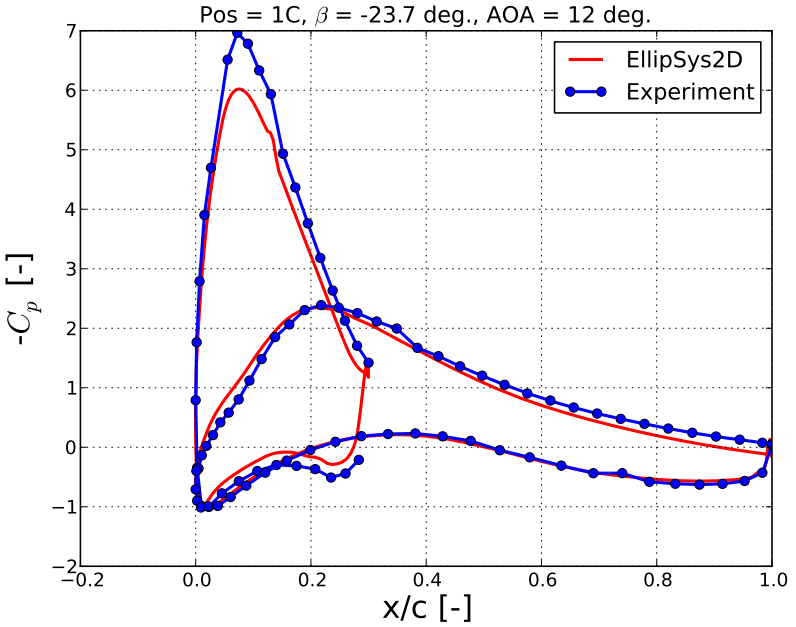

Wind Tunnel Results
Flatback with slat airfoil

Position 1C

Position 1C with reference β=-23.7 deg. showing contributions from main, slat and total.

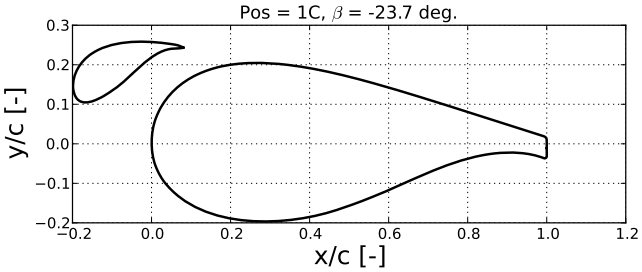

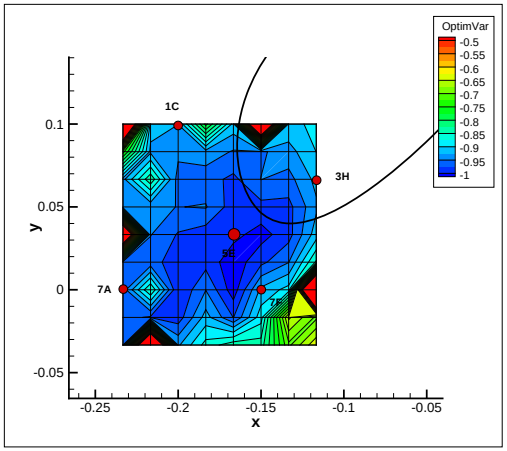

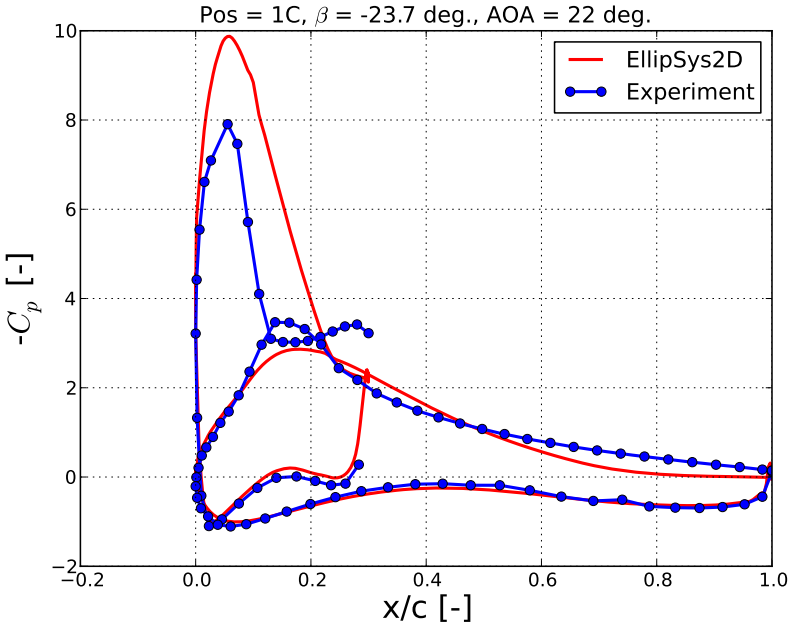

Wind Tunnel Results
Flatback with slat airfoil

Position 3H

Position 3H with reference β=-29.4 deg. showing contributions from main, slat and total.

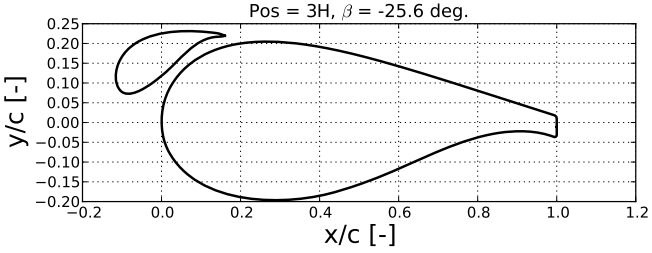

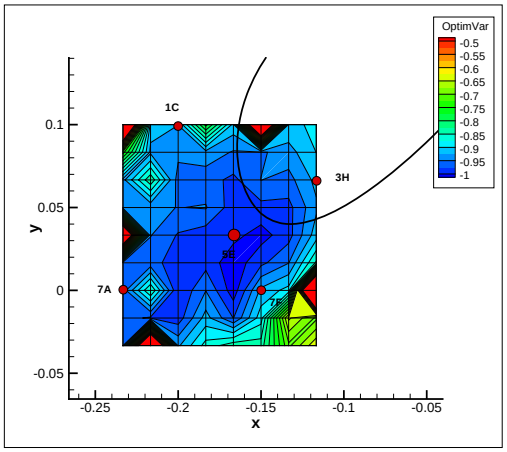

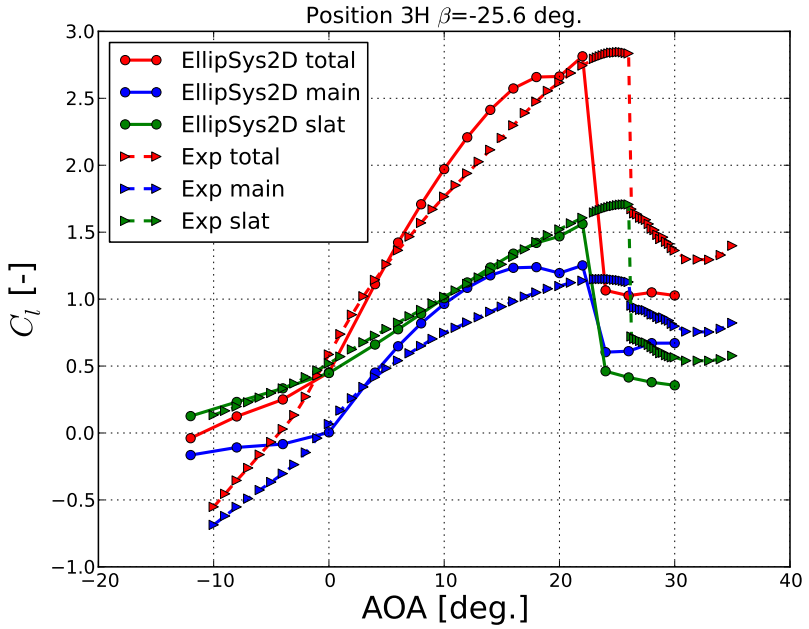

Wind Tunnel Results
Flatback with slat airfoil

Position 3H

Position 3H with reference β=-29.4 deg. showing contributions from main, slat and total.

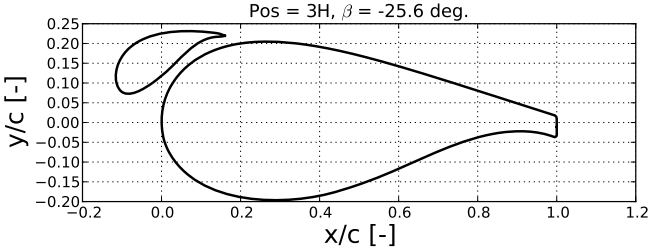

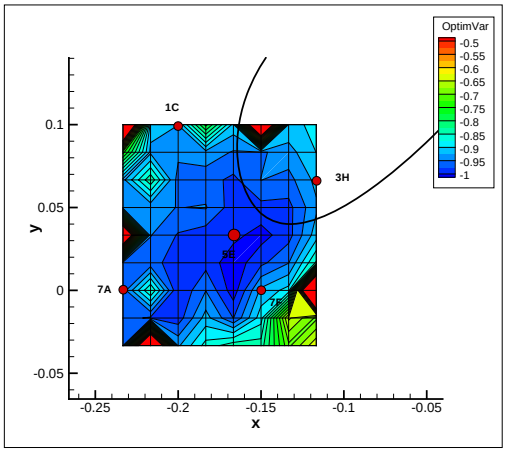

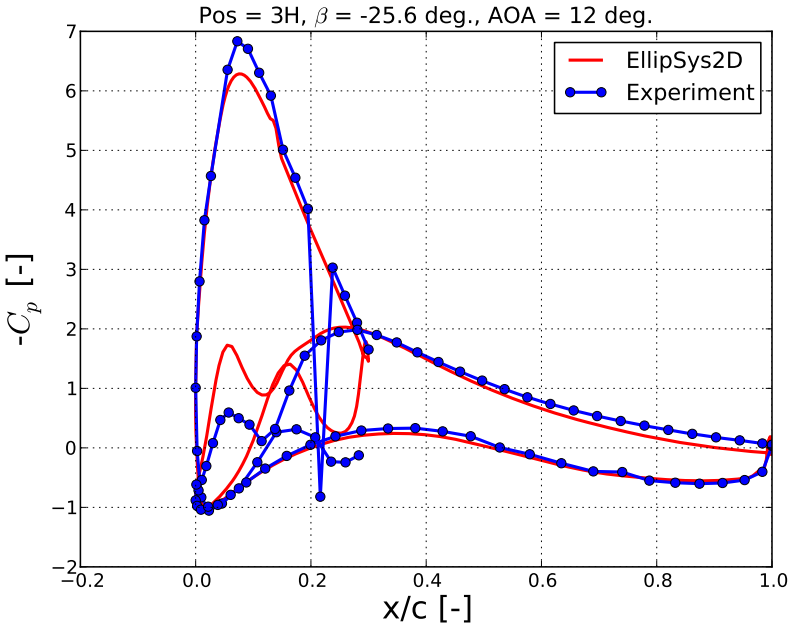

Wind Tunnel Results
Flatback with slat airfoil

Position 3H

Position 3H with reference β=-29.4 deg. showing contributions from main, slat and total.

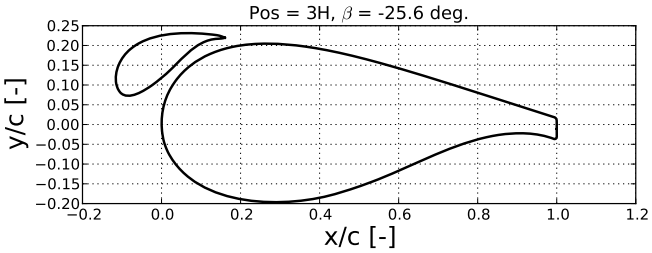

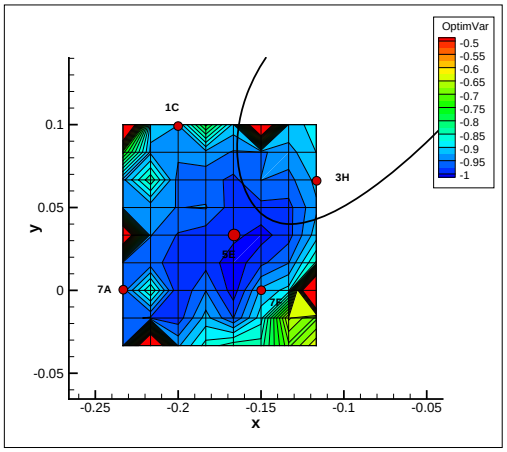

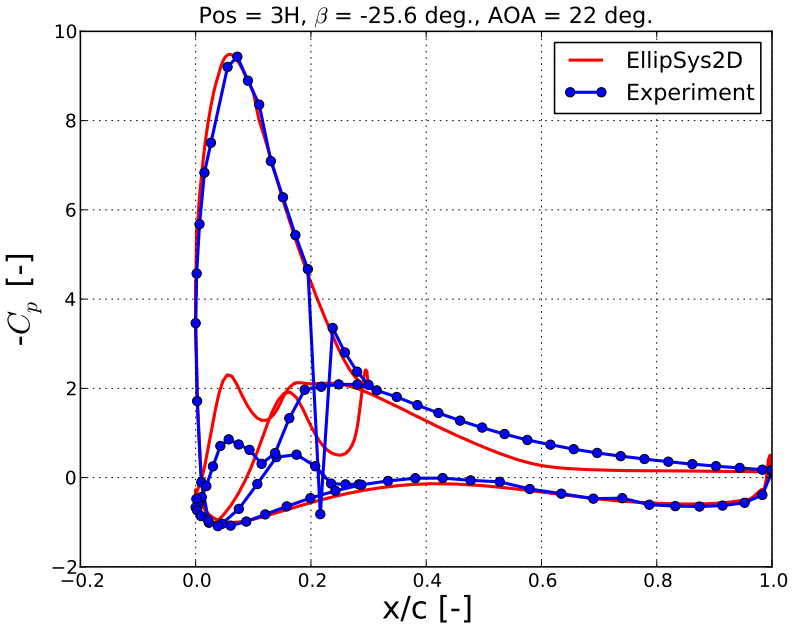

Wind Tunnel Results
Flatback with slat airfoil

Position 5E changing the slat angle β.

- 2D CFD predicts best performance for β=-29.35 deg.

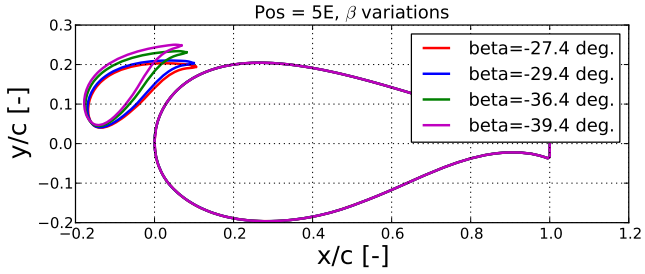

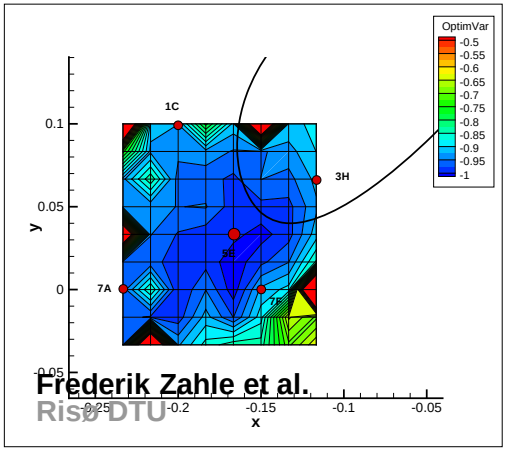

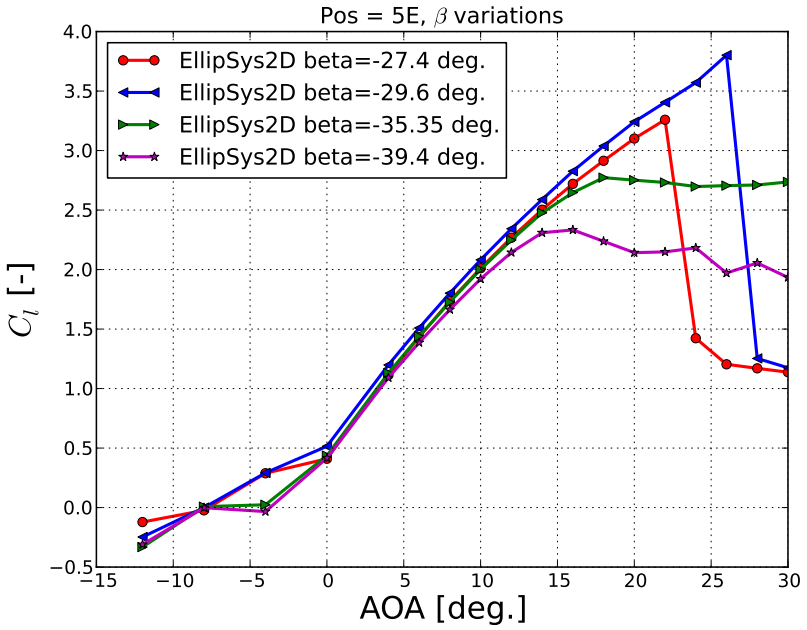

Wind Tunnel Results
Flatback with slat airfoil

Position 5E changing the slat angle β.

- 2D CFD predicts best performance for β=-29.35 deg.
- Experimental results show an increasing maximum lift coefficient for decreasing β.

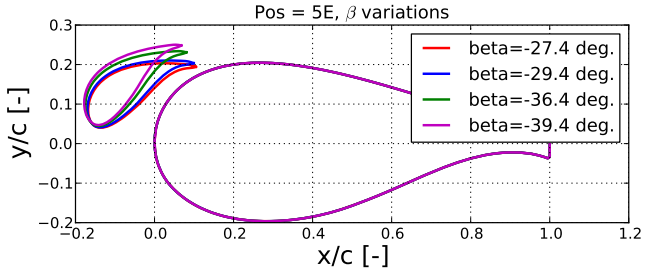

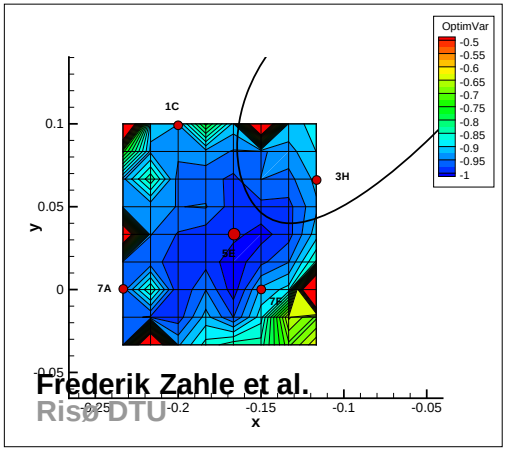

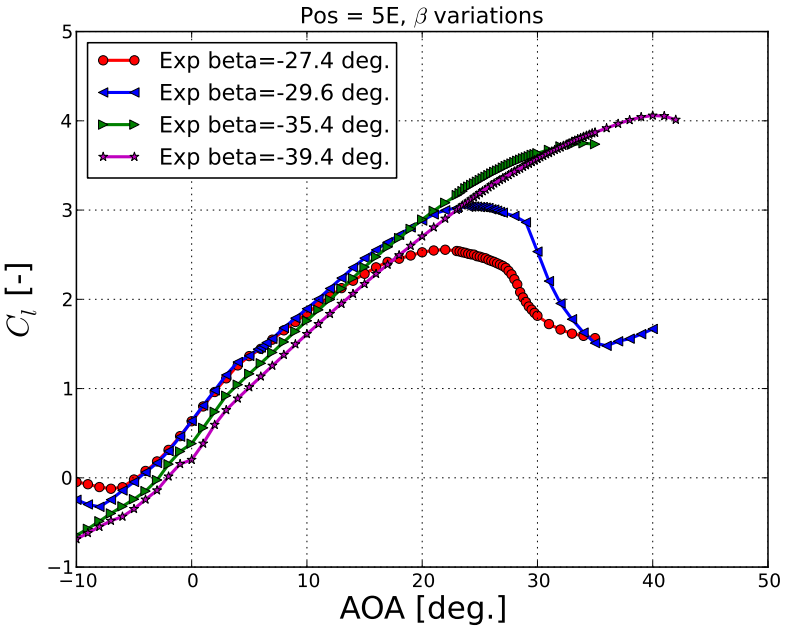

Wind Tunnel Results
Flatback with slat airfoil

Position 5E changing the slat angle β.

- 2D CFD predicts best performance for β=-29.35 deg.
- Experimental results show an increasing maximum lift coefficient for decreasing β.

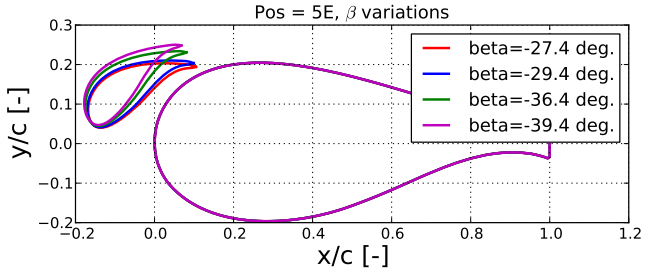

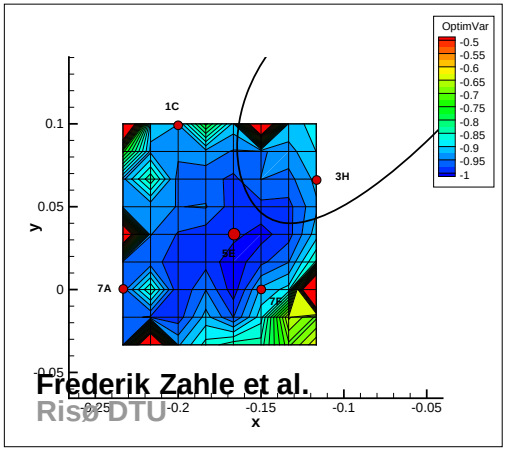

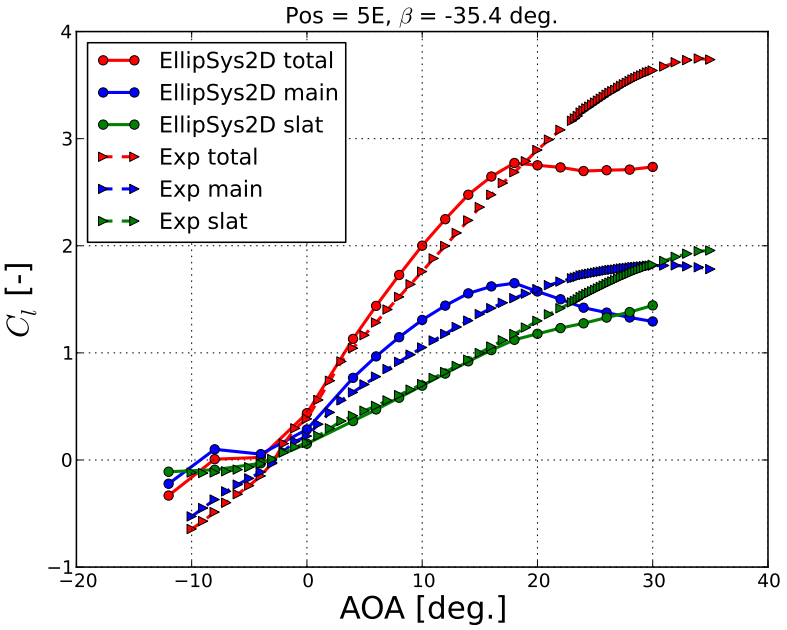

Wind Tunnel Results
Flatback with slat airfoil

Position 5E changing the slat angle β.

- 2D CFD predicts best performance for β=-29.35 deg.
- Experimental results show an increasing maximum lift coefficient for decreasing β.

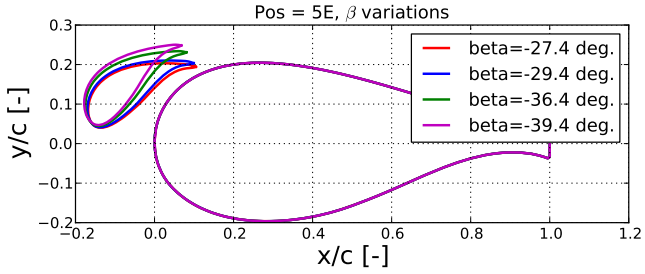

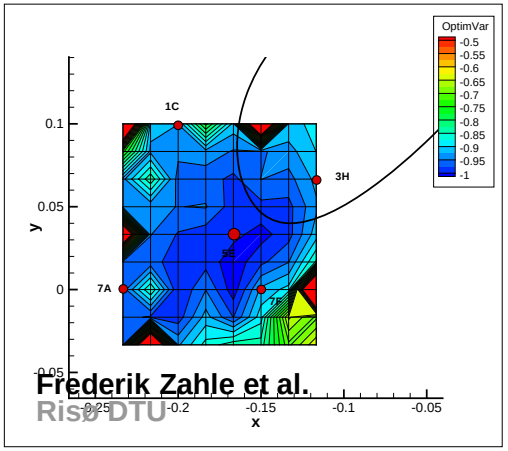

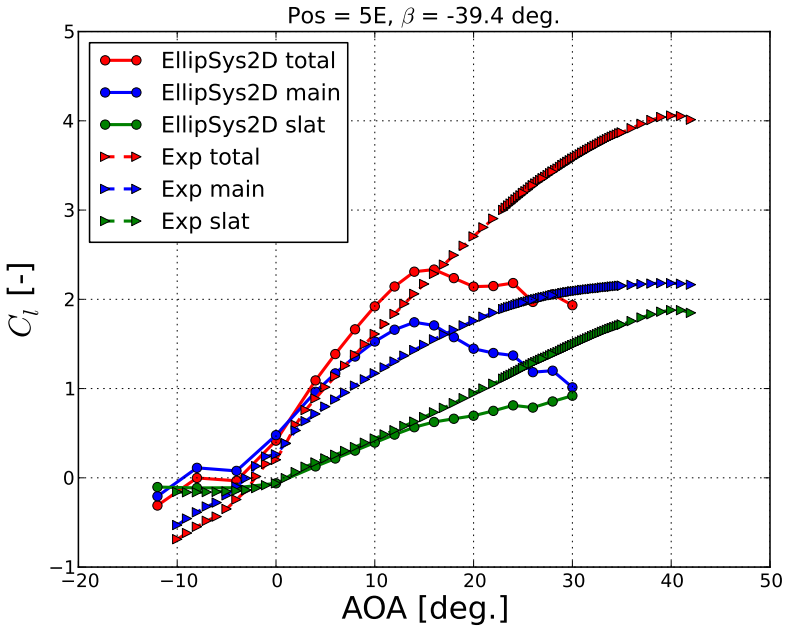

Wind Tunnel Results
Flatback with slat airfoil

2D Tunnel Effects

- 2D simulations were carried out using a wind tunnel setup with symmetry conditions on top and bottom walls.
- 2D simulations with same airfoil grids but with outer mesh boundaries placed 30c away from airfoil made for comparison.

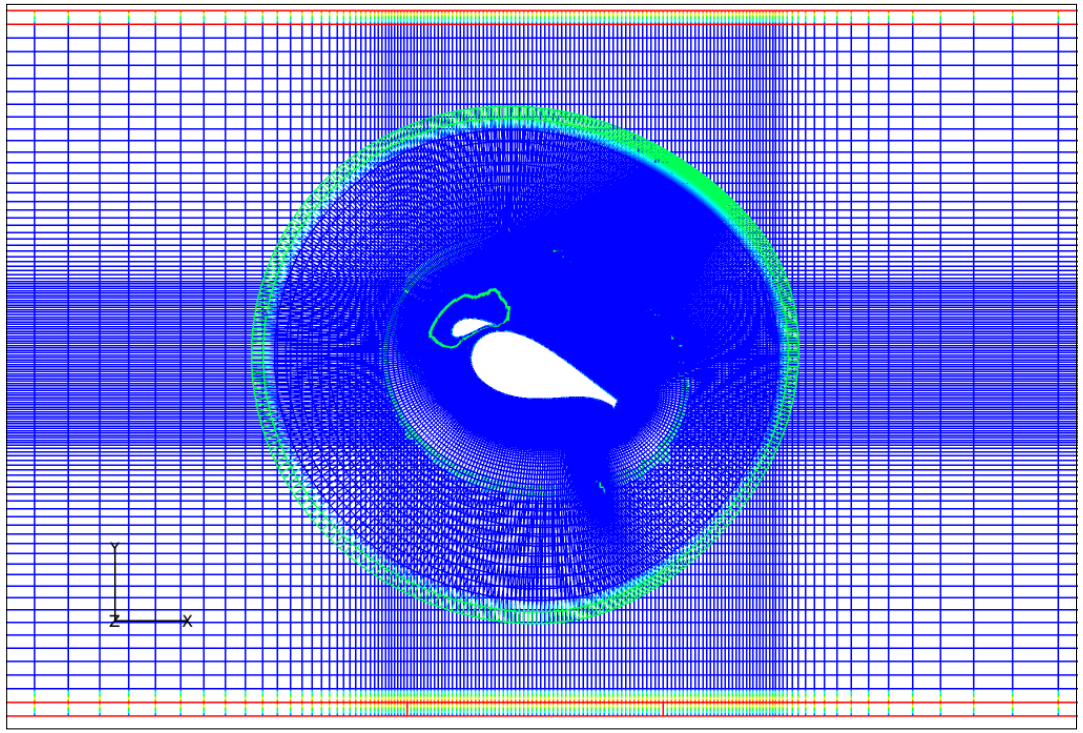

Flatback with slat airfoil

2D Tunnel Effects

- 2D simulations were carried out using a wind tunnel setup with symmetry conditions on top and bottom walls.
- 2D simulations with same airfoil grids but with outer mesh boundaries placed 30c away from airfoil made for comparison.

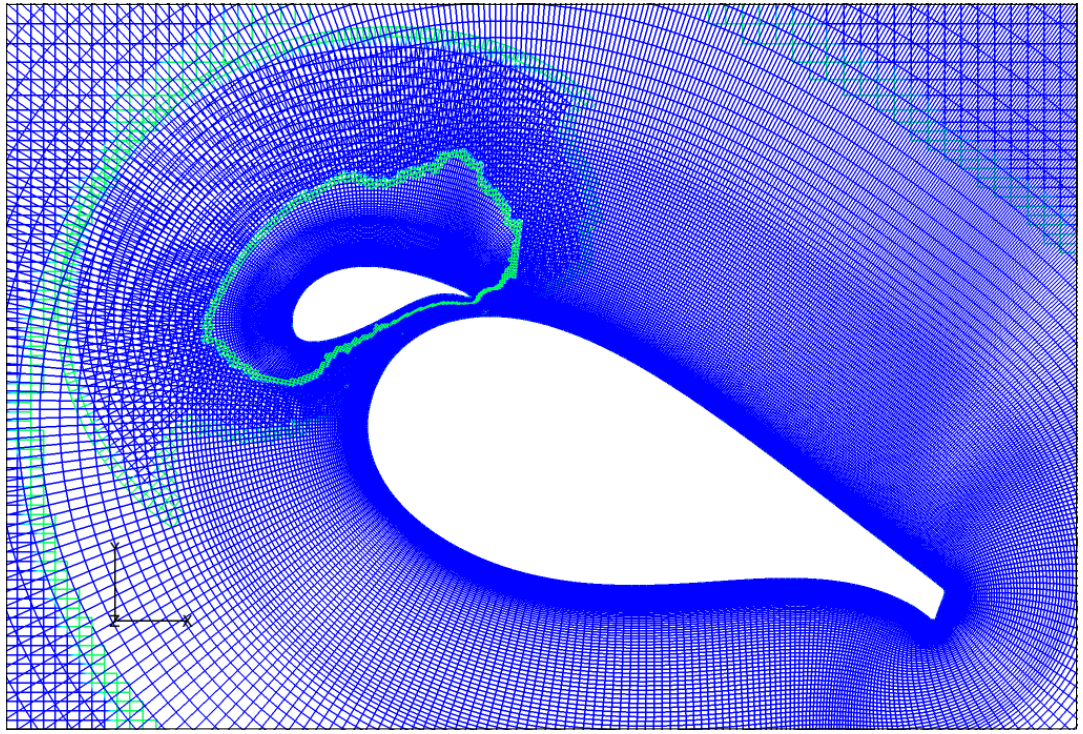

Wind Tunnel Results
Flatback with slat airfoil

2D Tunnel Effects

- 2D simulations were carried out using a wind tunnel setup with symmetry conditions on top and bottom walls.
- 2D simulations with same airfoil grids but with outer mesh boundaries placed 30c away from airfoil made for comparison.

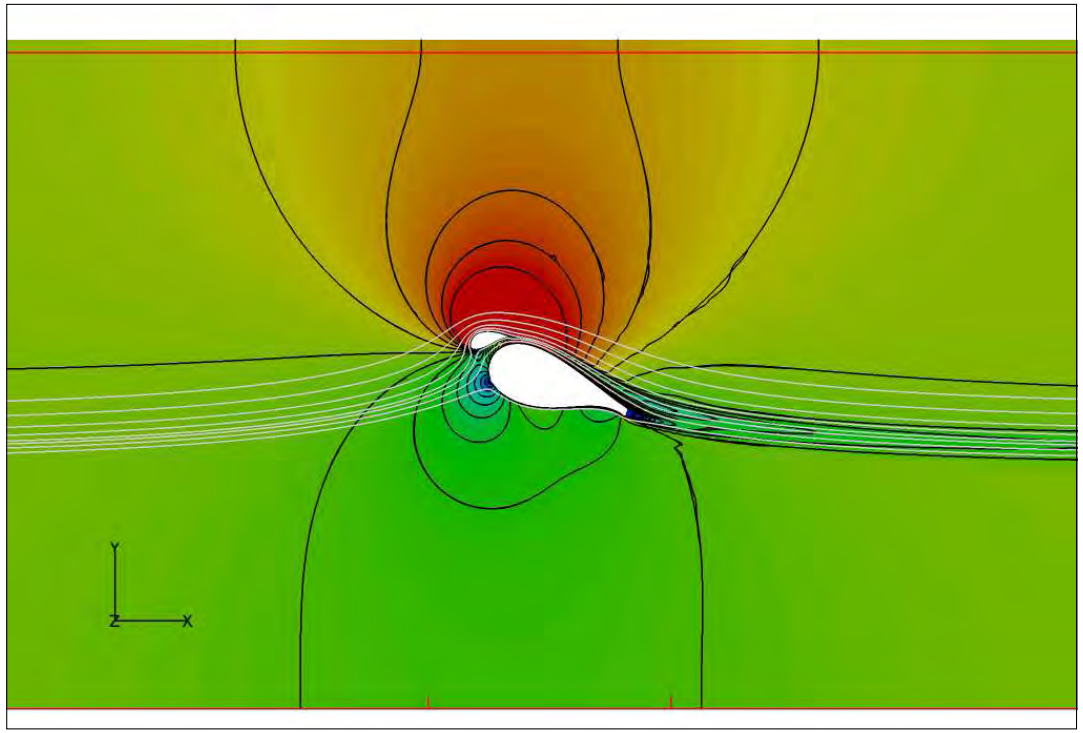

Wind Tunnel Results
Flatback with slat airfoil

2D Tunnel Effects

- Lift coefficient increases in a tunnel configurations.
- Drag coefficient is largely unchanged.
- 2D tunnel effects cannot explain the discrepancies seen between simulations and measurements.

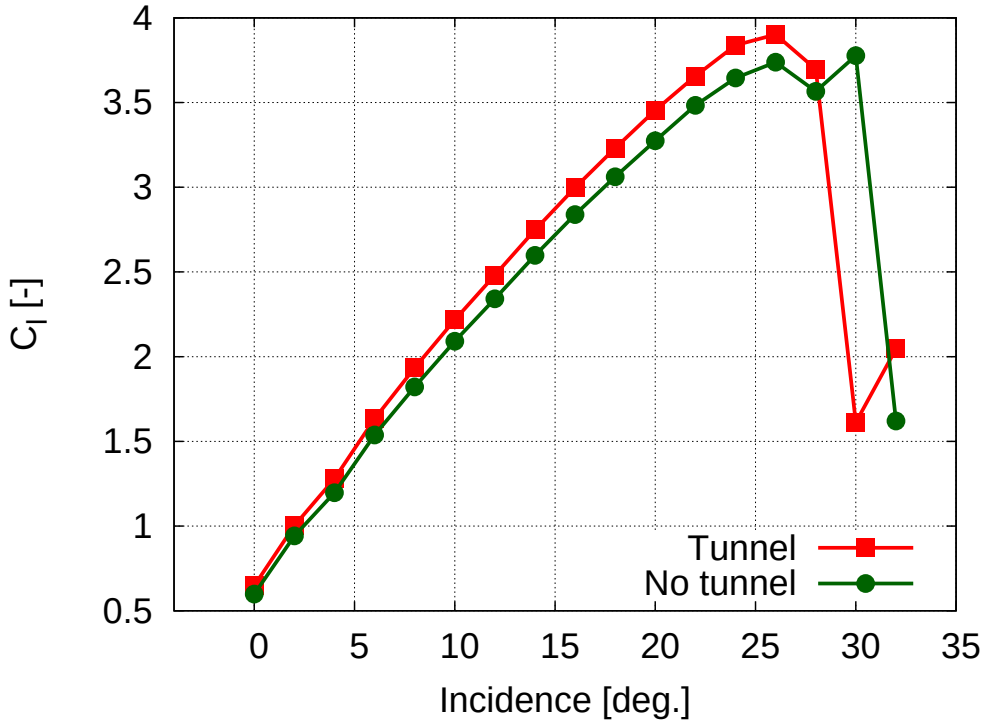

Wind Tunnel Results
Flatback with slat airfoil

2D Tunnel Effects

- Lift coefficient increases in a tunnel configurations.
- Drag coefficient is largely unchanged.
- 2D tunnel effects cannot explain the discrepancies seen between simulations and measurements.

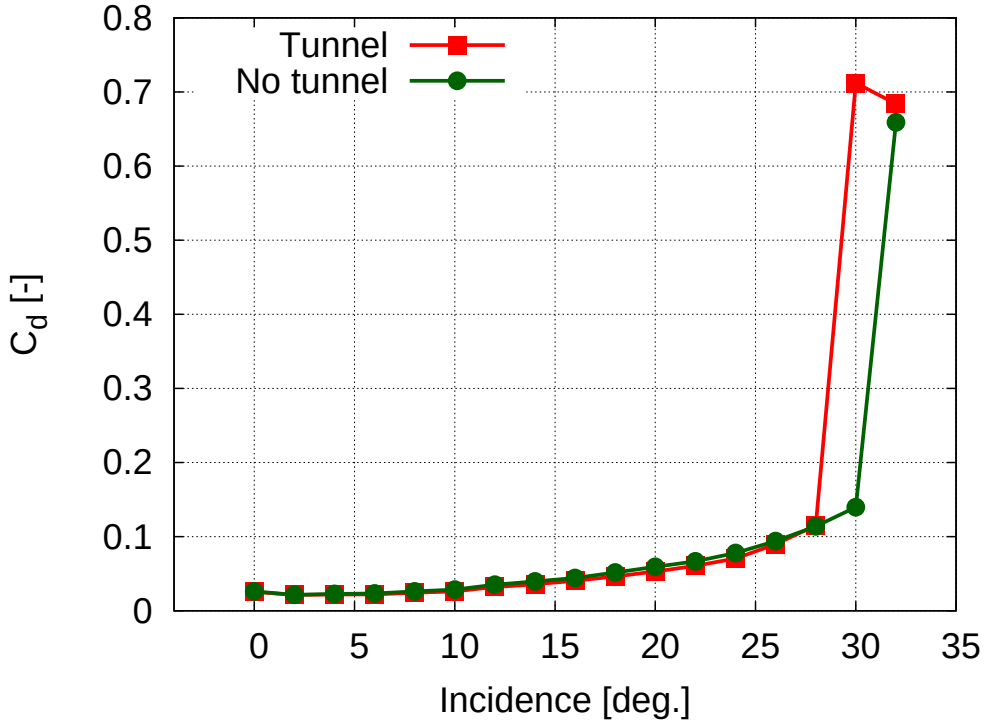

Wind Tunnel Results
Flow Visualization

3D surface flow

- Flow visualization using tufts revealed 3D effects caused by wall effects even at low AOA.
- Below picture is from AOA=22 deg.

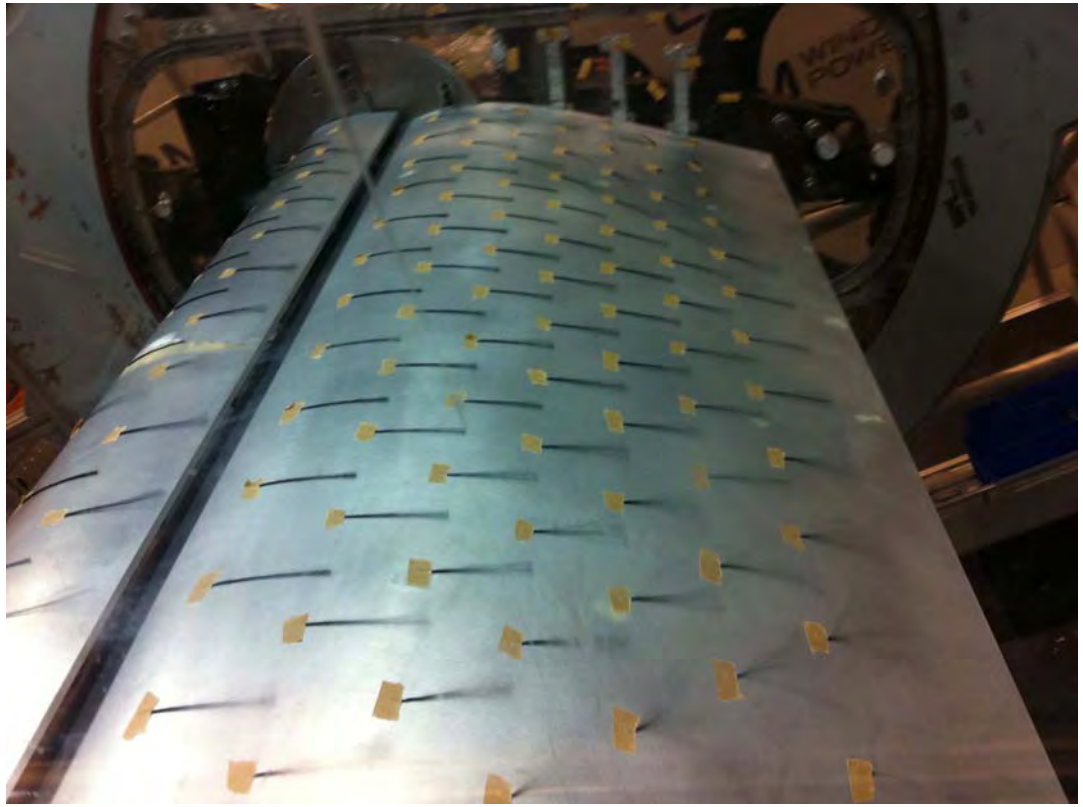

Wind Tunnel Results
Flow Visualization

3D surface flow

- 3D CFD simulations by Niels N. Sørensen on an FB-3500-1750 flatback airfoil show similar trends when comparing simulations with and without walls.
- Below picture is from AOA=19 deg.

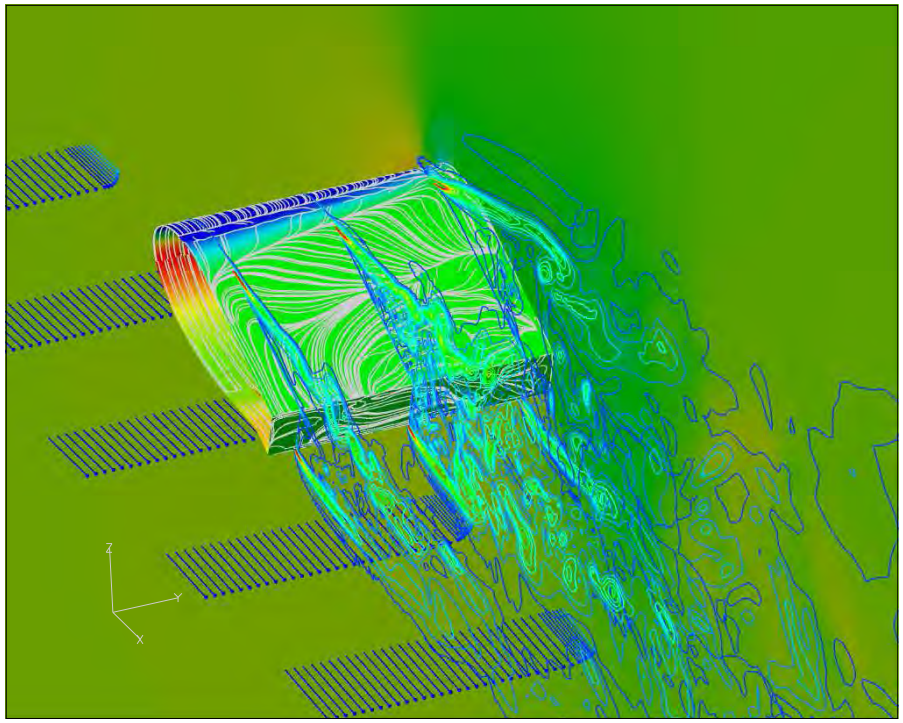

Wind Tunnel Results
Flow Visualization

3D surface flow

- 3D CFD simulations by Niels N. Sørensen on an FB-3500-1750 flatback airfoil show similar trends when comparing simulations with and without walls.
- Below picture is from AOA=19 deg.

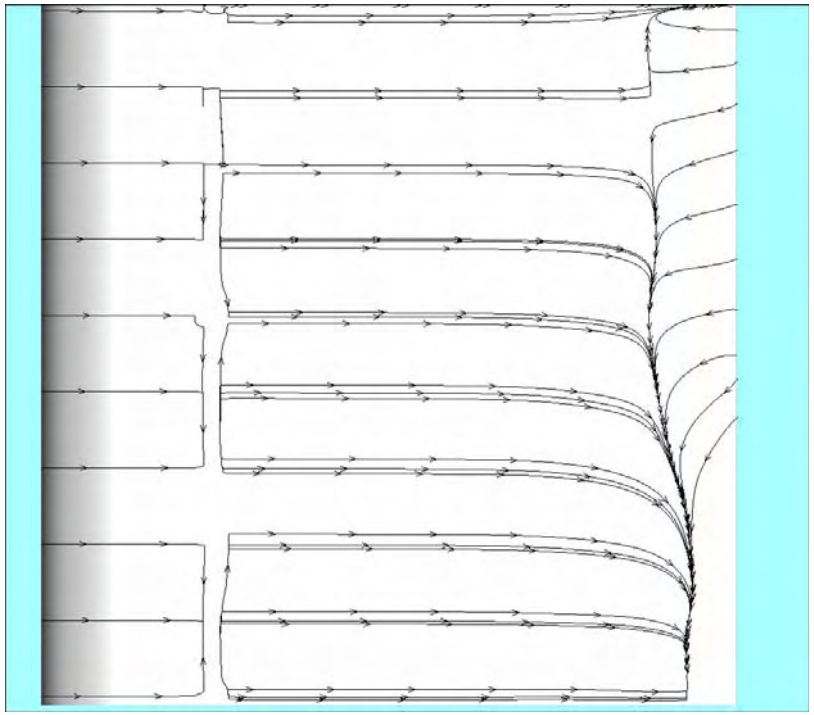

Wind Tunnel Results
Flow Visualization

3D surface flow

- 3D CFD simulations by Niels N. Sørensen on an FB-3500-1750 flatback airfoil show similar trends when comparing simulations with and without walls.
- Below picture is from AOA=19 deg.

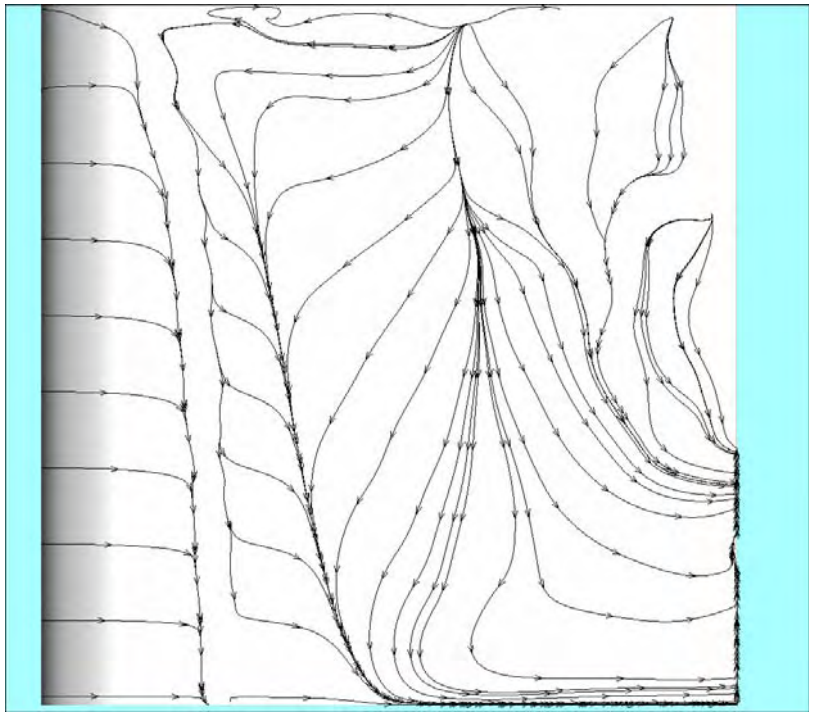

Wind Tunnel Results
Flow Visualization

Wind Tunnel Condensation Trails

- Running the wind tunnel at 100 m/s (Re = 4e6) resulted in condensation trails forming on the suction surface of the slat and main element.
- The very low pressure coefficients (C_p=-9) resulted in the vapour condensation threshold being reached.

Flow Visualization

High angle of attack flow re-attachment

- Using wool tufts to visualize the surface flow patterns we observed that the flow seemingly did not separate on the mail airfoil even for angles of attack up to 50 deg.
- We knew the flow was stalled, but why did it appear to be attached?

<animation: not included>

Wind Tunnel Results
Flow Visualization

2D CFD particle tracking simulation

- A 2D CFD simulation was carried out at 40 deg. incidence with particles seeded upstream of the airfoil.
- In the animation it is clearly seen that particles remain attached to the surface of the main airfoil.

<animation: http://www.youtube.com/watch?v=3oal5Mohq9g>

Conclusions

Optimization method for multi-element airfoils

- Method has been implemented to optimize the shape of a multi-element airfoil.
- Mesh generation has shown to be very robust.
- On a cluster, optimization with 5 design variables required approx. 10 hrs.

Conclusions

Optimization method for multi-element airfoils

Design of a high lift, thick, flatback, multi-element airfoil

- A 40% flatback and 30% slat airfoil was designed that was predicted to have a C_{l-max}=3.4.
- Less roughness sensitivity than flatback airfoil alone.
- Extensive parameter study carried out to map the performance of the slat at different positions.

Conclusions

Optimization method for multi-element airfoils

Design of a high lift, thick, flatback, multi-element airfoil

Wind Tunnel Campaign

- The multi-element airfoil was tested in the LM Wind Power wind tunnel.
- Comprehensive test matrix, data still being processed.
- Generally good agreement for lift (AP) and drag (WR).
- Comparison of AP and WP revealed what is believed to be severe 3D effects.
- Flow visualization confirmed this.
- The AP drag and WR drag were in very poor agreement.

Future Work

EUDP application in collaboration with Siemens and LM

- WP1: Design and validation of new thick airfoils.
- WP2: Identification of 2D/3D thick airfoil data.
- WP3: Identification of the standstill problem using aeroelastic 3D CFD.
- WP4: Identification of the importance of elastic couplings in the aeroelatic behaviour of wind turbine blades

EUDP application in collaboration with Siemens and LM

- WP1: Design and validation of new thick airfoils.
- WP2: Identification of 2D/3D thick airfoil data.
- WP3: Identification of the standstill problem using aeroelastic 3D CFD.
- WP4: Identification of the importance of elastic couplings in the aeroelatic behaviour of wind turbine blades

Thank you for listening :-)

Risø DTU is the National Laboratory for Sustainable Energy. Our research focuses on development of energy technologies and systems with minimal effect on climate, and contributes to innovation, education and policy. Risø has large experimental facilities and interdisciplinary research environments, and includes the national centre for nuclear technologies.

Risø DTU
National Laboratory for Sustainable Energy
Technical University of Denmark

Frederiksborgvej 399
PO Box 49
DK-4000 Roskilde
Denmark
Phone +45 4677 4677
Fax +45 4677 5688

www.risoe.dtu.dk